2004

Heat transfer and pressure drop of refrigerant R404A at near-critical and supercritical pressures

Yirong Jiang
Iowa State University

Heat transfer and pressure drop of refrigerant R404A at near-critical and supercritical pressures

by

Yirong Jiang

A dissertation submitted to the graduate faculty

in partial fulfillment of the requirements for the degree of

DOCTOR OF PHILOSOPHY

Major: Mechanical Engineering

Program of Study Committee:
Srinivas Garimella, Major Professor
Ron M. Nelson
Michael B. Pate
Richard H. Pletcher
Brent H. Shanks

Iowa State University

Ames, Iowa

2004

Graduate College
Iowa State University

This is to certify that the doctoral dissertation of

Yirong Jiang

has met the dissertation requirements of Iowa State University

Signature was redacted for privacy.

Major Professor

Signature was redacted for privacy.

For the Major Program

To my husband—Yongjun Hou

For his love and support.

TABLE OF CONTENTS

LIST OF FIGURES

LIST OF TABLES

NOMENCLATURE

Symbols

A	area
Cp	specific heat (kJ/kg-K)
d	derivative operator
D	diameter (m)
D^+	non-dimensional tube diameter
E	specific work of thermal expansion
f	friction factor
F	function of liquid Prandtl and Reynolds numbers in Traviss et al. (1973)
Fr	Froude number
g	gravitational constant 9.81 m/s^2
G	mass flux (kg/m^2-s)
Ga	Galileo number
h	enthalpy (kJ/kg), condensation heat transfer coefficient (W/m^2-K), height (m)
I.D.	tube inner diameter (m)
j	superficial velocity (m/s)
Ja	Jakob number
k	thermal conductivity (W/m-K)
L	length
LMTD	log-mean temperature difference (K)
$\dot{m}$	mass flow rate (kg/s)
n	Reynolds number constant in friction factor calculation
N	number
Nu	Nusselt number
O.D.	tube outer diameter (m)
P	pressure (kPa), wetted perimeter (m)
Pr	Prandtl number
Q	heat duty (W)
r	radial direction
r^*	tube to annulus diameter ratio
R	heat transfer resistance (K/W)
Re	Reynolds number
T	temperature (°)
U	absolute uncertainty
UA	overall heat transfer conductance (W/K)
V	velocity (m/s)
Vol	volumetric flow rate (m^3/s)
w	width (m)
W	power (W)
We	Weber number
x	quality

X	Martinelli parameter
Y	Chisholm Y coefficient (Chisholm 1973)
β	coefficient of thermal expansion (1/K)
∂	partial derivative operator
δ	film thickness
Δ	change, difference
ε	void fraction, tube roughness (m),
η	efficiency
ϕ	two-phase multiplier
λ	ratio of interface and film velocities
μ	dynamic viscosity (kg/m-s)
ρ	density (kg/m^3)
σ	surface tension (N/m)
θ	angle subtended from the top of the tube to the liquid pool level in stratified flow (rad)
τ	torque (N-m), shear stress (kPa)
ω	angular speed (rad/s)

Subscripts and Superscripts

+	dimensional turbulent parameter
∞	ambient, infinity
actual	actual diameter in present study
air	ambient property
ambient	ambient
annular	annular flow
annulus	annulus-side
avg	average
b	bulk
conf	confinement
conv	convection
crit	critical
DB	Dittus-Boelter
eff	effective
equivalent	equivalent length
f	friction, force
fg	latent heat
film	film
flowmeter	flowmeter
fluid	fluid temperature
forced	forced convection
frictional	frictional
G	gas phase
GO	vapor only phase
h	hydraulic

ideal	ideal
in	in
inner	inner
l	liquid phase
L	tube length, liquid phase
liquid	liquid pool
LO	liquid only phase
nc	natural convection
out	out
outer	outer
primary	primary loop
pump	pump
rad	radiation
refg	refrigerant
sat	saturation
sec	secondary loop
shaft	pump shaft input
shell	shell side of the shell-and-tube heat exchanger
surface	at the surface
total	total
test	test section
top	laminar film condensation region in stratified flow
tt	turbulent-turbulent
tube	tube
turb	turbulent
v	vapor phase
w	water-side
wall	at the wall, wall
water	water-side
wavy	wavy flow

ACKNOWLEDGEMENTS

I would like to take this opportunity to thank the people for their contribution to this work. Above all of those whom I would like to thank is my major professor, Dr. Srinivas Garimella, for his commitment to education and willingness to lend his guidance and support to me throughout the course of this study. I would like to thank my committee members—Drs. Ron M. Nelson, Michael B. Pate, Richard H. Pletcher, Brent H. Shanks, for their considerate guidance and constructive suggestions to this study. I also thank Air-Conditioning and Refrigeration Technology Institute for funding this project. Special thanks to Biswajit Mitra, for his help finishing the tests; to Leo Mincks, Matt Determan, and Tim Ernst, for their help constructing the test facility. Thanks to Jesse Killion and Mark Meacham for watching my test loop during class. Finally, my heartfelt appreciation goes to my beloved husband, Yongjun Hou, who made it possible to begin and to complete this journey. Without him, my life would have been totally different.

ABSTRACT

A comprehensive study of heat transfer and pressure drop of refrigerant R404A during condensation and supercritical cooling at near-critical pressures inside a 9.4 mm tube was conducted. Investigations were carried out at five nominal pressures: 0.8, 0.9, 1.0, 1.1 and $1.2\times P_{crit}$. Heat transfer coefficients were measured using a thermal amplification technique that measures heat duty accurately while also providing refrigerant heat transfer coefficients with low uncertainties. For condensation tests, local heat transfer coefficients and pressure drops were measured for the mass flux range $200 < G < 800 kg/m^2$-s in small quality increments over entire vapor-liquid region. For supercritical tests, local heat transfer coefficients and pressure drops were measured for the same mass flux range as in the condensation tests for temperatures ranging from 30 – 110°C. For both phase-change condensation and supercritical cooling, frictional pressure gradients were calculated by separating the deceleration component due to momentum change from the measured pressure gradients.

During condensation, the effect of reduced pressure in heat transfer is not very significant, while this effect is more pronounced in the pressure gradient. Flow regime transition criteria by Coleman and Garimella (2003) were used to designate the prevailing flow regimes for a given combination of mass flux and quality. The condensation data collected in the present study were primary in the wavy and annular flow regimes. For supercritical cooling, the sharp variations in thermophysical properties in the vicinity of the critical temperature were found to have substantial effect on heat transfer coefficients and pressure drop. Based on the characteristics of the specific work of thermal expansion (contraction), the data from the supercritical tests were grouped into three regimes: liquid-like, pseudo-critical transition and gas-like regimes.

Flow regime-based heat transfer and pressure drop models were developed for both condensation and supercritical cooling. For condensation, the overall heat transfer model predicts 89% of the data within ±15% while the overall pressure drop model predicts 96% of the data within ±15%. For supercritical cooling, the heat transfer model predicted 73% of the data within ±25% while the pressure gradient model predicts 90% of the data within ±15%.

CHAPTER 1. INTRODUCTION

CFC and HCFC-based refrigerants are being phased out because of their contribution to the ozone depletion and global warming problems (ASHRAE 1997). The ozone layer in the stratosphere acts as a shield to protect us from the harmful effects of ultraviolet light by absorbing much of it. Ozone is created by collisions of oxygen molecules (O_2) and oxygen atoms (O) and destructed by similar collisions of O_3 molecules and O atoms, resulting in pairs of O_2 molecules. It is believed that, due to the extraordinary stability of CFC compounds, CFCs are contributing to the deterioration of the ozone layer. CFC (Chlorofluorocarbon) molecules are made of chlorine, fluorine, and carbon, while HCFC (Hydrochlorofluorocarbon) molecules also have hydrogen atoms attached. These compounds do not break down in the lower atmosphere. Furthermore, although heavier than air, traces of CFCs have been found in the upper atmosphere (stratosphere) and predicted to last for 100 years or more due to their high stability. However, once affected by ultraviolet radiation, these CFC traces slowly decompose and release chlorine (Cl_2). Since ozone is an oxidizer, with the presence of sunlight, chlorine catalytically decomposes ozone, and forms chlorine oxide (which is unstable) and oxygen. The unstable chlorine oxide then breaks down to again form chlorine and oxygen. This process keeps repeatedly attacking the ozone and causes ozone destruction to happen faster than ozone creation.

Refrigerant R404A is a near azeotropic blend (an azeotropic blend is a mixture of two or more refrigerants with similar boiling points and acts like a single fluid. Azeotropic blends do not have a temperature glide: the temperature difference between the vapor and liquid state during evaporation or condensation at constant pressure. Near-azeotropic mixtures have small temperature glides while zeotropic mixtures have larger temperature glides than 5°C) of hydrofluorocarbons (HFCs) instead of CFCs or HCFCs. It is a mixture of HFC refrigerants R125 (CHF2CF3, pentafluoroethane), R143a (CF3CH3-1,1,1, trifluoroethane), and R134a (CF3CH2F-1,1,1,2, tetrafluoroethane) with mass fractions of 44%, 52% and 4%, respectively. Hydrofluorocarbons (HFCs) are made of hydrogen, fluorine, and carbon atoms. Because they have no chlorine, they do not interact with the ozone layer once it breaks down. Therefore, R404A is benign to the ozone layer.

R404A has a low critical temperature and pressure: 72.046°C and 3729 kPa, respectively, whereas the critical temperature and pressure for R22 are 96.145°C and 4990 kPa, respectively (Lemmon *et al.* 2002). Table 1 shows the liquid and vapor phase properties of R404A and R22 at saturation temperatures of 35 and 50°C. The recent interest in using vapor compression cycles without CFCs and HCFCs for high temperature-lift space-conditioning and water heating applications has created an urgent need for the understanding of refrigerant blend behavior at high operating pressures. To achieve the desired heat rejection temperatures for these applications, refrigerant blends such as R404A must either operate as condensers at pressures close to their critical pressure, or as gas coolers exceeding the critical pressure. Phase change at such near-critical pressures, and non-isothermal heat rejection above critical pressure in these refrigerant blends are not well understood. While it is known that heat transfer coefficients and pressure drop in convective condensation are strong functions of vapor quality, few predictive methods are reported in the literature for refrigerant blends at near-critical pressures. When cooling at or above critical pressure, phase-change does not take place. However, near the critical point, as shown in Figure 1, the thermophysical properties of the fluid change drastically as the temperature changes (Lemmon *et al.* 2002). The fluid experiences a gas-like to liquid-like transition in fluid properties. These effects are crucial in determining the variation in heat transfer coefficients along the length of the heat exchanger. In addition, fluid property variations from the bulk temperature to the tube surface temperature assume much greater significance. As reported by Shitsman (1963), Krasnoshchekov *et al.* (1970) and Tanaka *et al.* (1971), in supercritical

Table 1. Phase-Change Properties of R404A and R22

Fluid	h_{fg} kJ/kg	ρ_l kg/m^3	ρ_v kg/m^3	$\mu_l \times 10^6$ kg/m-s	$\mu_v \times 10^6$ kg/m-s	$C_{p,l}$ kJ/kg-K	$C_{p,v}$ kJ/kg-K	k_l W/m-K	k_v W/m-K
$T_{sat} = 35°C$									
R404A	127.5	993.07	88.97	111.70	15.40	1.649	1.382	61.024	19.933
R22	172.3	1150.07	57.99	146.92	13.01	1.308	0.949	78.914	12.281
$T_{sat} = 50°C$									
R404A	103.4	899.07	139.94	88.87	17.38	1.959	1.866	55.740	24.366
R22	154.2	1082.30	85.95	122.96	13.95	1.419	1.113	71.900	14.165

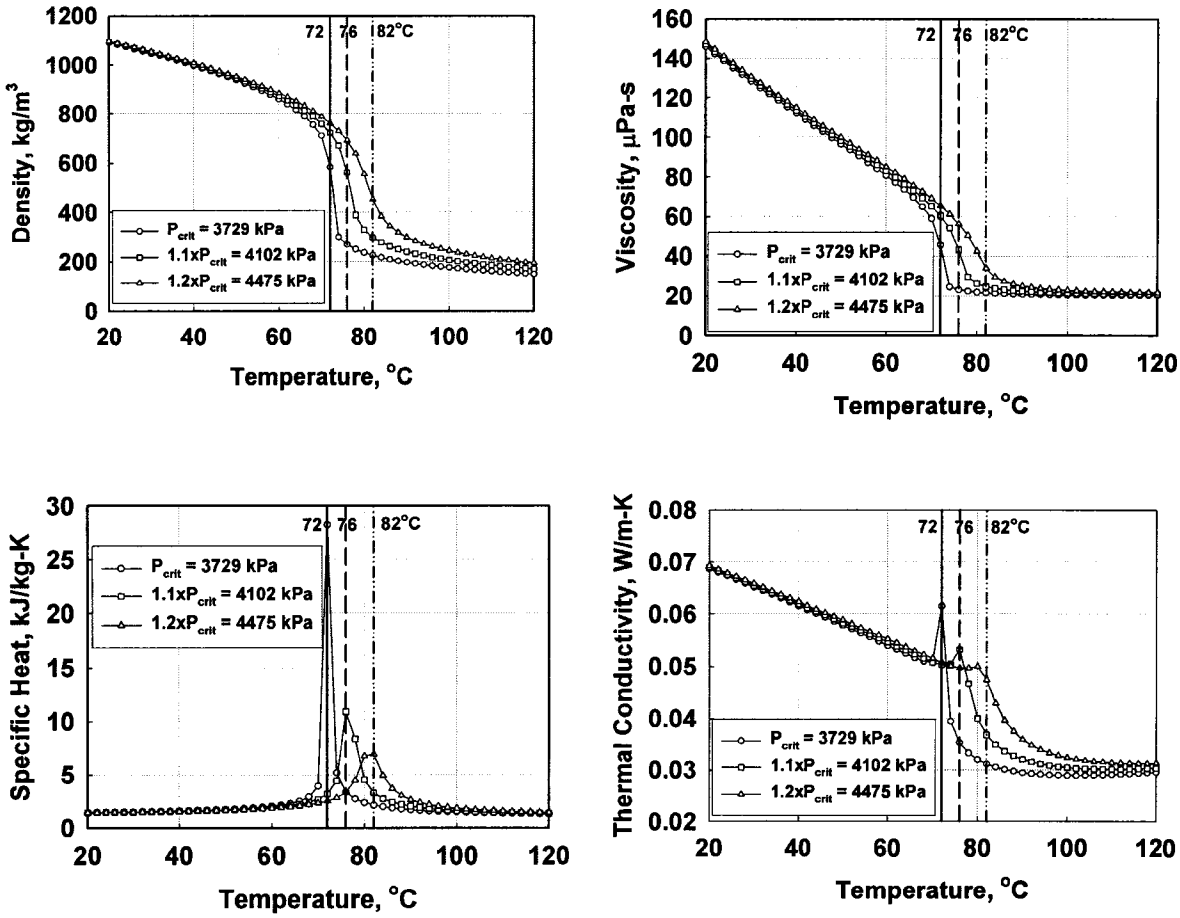

Figure 1 R404A Properties at and above Critical Pressure

cooling of carbon dioxide, when the bulk fluid is above the critical temperature, and the tube wall temperature is below the critical point, there was an improvement in the heat transfer coefficient. Krasnoshchekov *et al.* (1970) attributed the improvement in heat transfer to the formation of a lower-temperature, liquid-like layer near the wall of the tube. This liquid-like layer has a higher thermal conductivity. Although much research has been done to investigate condensation heat transfer and pressure drop in pure refrigerant and refrigerant blends, there is little literature available on in-tube gas cooling and pressure drop of a supercritical fluid. Furthermore, much of the available literature on supercritical heat transfer and pressure drop has focused on carbon dioxide or steam, but not refrigerant blends.

The focus of the present research is to experimentally investigate the heat transfer and pressure drop during condensation near the critical pressure, and supercritical cooling above the critical pressure of refrigerant R404A. To accomplish this task, the present study is divided into two parts. The first part is to investigate the condensation heat transfer and pressure drop for R404A at near critical pressures. The second part is to investigate the quasi single-phase gas cooling and pressure drop for R404A above critical pressures. The overall objectives of the proposed study are as follows:

1. Conduct condensation heat transfer and pressure drop experiments at near-critical pressures in horizontal condenser tubes over the range of mass fluxes and qualities of interest (defined below).
2. Conduct quasi single-phase heat transfer and pressure drop experiments at supercritical pressures in horizontal condenser tubes over the range of mass fluxes and temperatures of interest.
3. Compare experimental data with the limited local condensation and supercritical heat transfer correlations in the literature.
4. Develop flow mechanism-based condensation and quasi single-phase heat transfer and pressure drop models from these data.

The tube to be studied is a 9.4 mm-I.D. circular tube, as this is the tube most commonly used by industry. The tests are conducted at five pressures:

- Phase-change tests: $0.8\times P_{crit}$ (2983 kPa) and $0.9\times P_{crit}$ (3356 kPa)
- Critical pressure tests : P_{crit} = 3729 kPa, and
- Supercritical tests: $1.1\times P_{crit}$ (4102 kPa), and $1.2\times P_{crit}$ (4475 kPa)

The first two pressures are phase-change (condensation) tests, while the remaining three pressures are quasi single-phase (gas cooling) tests. For each pressure, tests are conducted at seven different mass fluxes ranging between 200 and 800 kg/m^2-s. For each mass flux of the phase change tests, experiments are conducted with nominal local test-section qualities from 0.9 to 0.1. For quasi single-phase tests, at each mass flux, data points are taken with nominal test-section inlet temperatures from 30 to 110°C in nominally 10°C increments.

The thesis is organized as follows. Chapter 2 provides a review of the literature on condensation and supercritical heat transfer and pressure drop, and identifies the deficiencies in the understanding of these phenomena. These identified deficiencies are used to formulate the details of the research project. The experimental set-up and procedures for determining the condensation and supercritical cooling heat transfer coefficients are described in Chapter 3. The data analyses techniques and uncertainty analyses are discussed in Chapter 4. Chapter 5 presents the results of the experiments. This chapter also contains a discussion of the comparisons between the literature and the experimental data from this study, and a presentation of the flow regime-based heat transfer and pressure drop correlations for condensation and supercritical cooling. Chapter 6 summarizes the conclusions from this study and also presents recommendations for further research in this area.

CHAPTER 2. LITERATURE REVIEW

The discussion of the relevant literature is divided into two parts: research on in-tube condensation and on supercritical heat transfer and pressure drop. For in-tube condensation, numerous studies have been conducted by previous investigators on condensation of a variety of fluids in different orientations. The literature review presented here will focus primarily on studies with condensation of pure and refrigerant blends in horizontal tubes. For supercritical heat transfer, most of the available literature is on carbon dioxide (R744) and steam under supercritical heating conditions.

Prior Investigations of In-Tube Condensation

Heat transfer

Condensation inside horizontal tubes is governed by a combination of gravity forces and interfacial shear stresses, the relative contributions of which change with the geometry and fluid conditions (for smaller diameter tubes, surface tension forces also play an increasing role, as demonstrated by Coleman and Garimella (2000; 2003). While the annular flow pattern is associated with high vapor shear stresses, stratified and wavy flows appear when gravity forces dominate.

Many of the widely used condensation heat transfer correlations were developed for annular flow. Traviss et al. (1973) proposed an annular flow model by applying the momentum and heat transfer analogy using the von Karman universal velocity distribution to describe the liquid film. Assuming the liquid film was thin over the tube length, a flat plate approximation could be used for the liquid film. The interfacial shear stress was assumed to be approximately equal to the wall shear stress. By assuming the turbulent Prandtl number was unity and the heat flux at the interface was approximately equal to the wall heat flux, the heat transfer equation was represented as a function of turbulent film thickness, which in turn is a function of liquid Reynolds number. The results were compared with experimental data on R12 and R22 in an 8 mm ID tube. The experiments were conducted at mass fluxes ranging from 161 – 1532 kg/m^2-s, and at saturation temperatures between 25 and 58°C. They found good agreement between the predictions and the data for qualities as low as 0.1. For

qualities less than 0.1, a linear extrapolation between the model and a single-phase heat transfer correlation was found to yield good results.

Shah (1979) developed a dimensionless correlation for film condensation inside pipes based on his previous work on evaporative heat transfer (Shah 1976). He argued that, as long as the entire pipe surface remains wetted, the mechanisms for heat transfer during film condensation were similar to evaporation without nucleate boiling. Similar to his evaporation correlation, the author developed a new two-phase multiplier using a large set of condensation data (473 data points from 21 independent experimental studies). The fluids included R-11, R-12, R-22, R-113, water, methanol, ethanol, benzene, toluene, and trichloroethylene condensing inside tubes as well as an annulus with various tube orientations. The mass fluxes ranged from 11 – 211 kg/m^2-s for tube diameters between 7 and 40 mm. The reduced pressure of the data ranged from 0.002 to 0.44. The author noted that the application of this model should be restricted to the operating ranges of the data considered, and for $1 < Pr_l < 13$. The model is also restricted to $Re_l > 350$ due to limited data at lower Re_l values. This correlation was found to predict all data with a mean deviation of 17%.

Kosky and Staub (1971) studied annular flow condensation of steam inside a horizontal 12.57 mm copper tube at 20 – 152 kPa. The mass flux range covered was 2.712 – 149.2 kg/s-m^2. Assuming the film was thin and smooth, and entrainment was negligible, the author proposed an analytical model based on the modified Martinelli analogy (Martinelli 1947) between heat and momentum transfer in turbulent flow to calculate the thermal resistance of a flowing film of condensate. They suggested that the annular flow heat transfer coefficient could be related to the frictional pressure gradient through the shear velocity. In their study, an empirical pressure drop relation was used to fit their own data, and data from an independent investigation. The model was developed for annular flow. Therefore, tube orientation is irrelevant, provided that there is sufficient vapor shear at the liquid-vapor interface to maintain annular flow.

Jaster and Kosky (1976) used data from Kosky and Staub (1971) supplemented by additional measurements in the annular-stratified transition and fully stratified flow regime. For the mass flux range 12.6 – 145 kg/s-m^2, they observed three different flow regimes:

annular, annular-stratified transition and stratified. They suggested that the annular-to-stratified transition was a function of the ratio of axial shear force to gravitational body force F. Thus, for $F < 5$, the flow was considered as stratified flow. For $F > 29$, the flow was considered annular. A transition region between annular and stratified flow was defined as $5 < F < 29$. They also presented heat transfer correlations for annular and stratified flow. For fully annular flow, the heat transfer was governed by boundary layers whose thermal resistance could be found using the Martinelli analogy as modified in Kosky and Staub (1971). Assuming the heat transfer in the liquid pool is negligible, a simplified model from Rufer and Kezios (1966) was suggested for the fully stratified flow. For the transition region between fully annular and stratified flow, the authors suggested that a linear interpolation was a good approximation. The comparison between the experiments and predictions showed that the errors were of the same order magnitude as those of the annular and stratified models.

More recent attempts at modeling condensation heat transfer in pure fluids and blends have yielded correlations that are based on the specific flow pattern that exists for the applicable conditions. Dobson and Chato (1998) conducted flow visualization and heat transfer experiments for R12, R22, R134a and R32/R125 condensing at saturation temperatures between 35 and 45°C in smooth tubes for the diameter range $3.14 < d < 7.04$ mm. Stratified, wavy, wavy-annular, annular, annular-mist and slug flow regimes were observed. They found that mass flux and quality are the dominant factors in establishing the relevant flow regime. They also reported that, at low mass fluxes (25 and 75 kg/m^2-s), the flow regime was not affected by tube diameter or refrigerant type, while at 150 and 300 kg/m^2-s, these parameters must be taken into account. They proposed a heat transfer correlation for annular and wavy flow, treating them as shear-dominated and gravity-dominated flow regimes, respectively. For the gravity driven correlation, they argued that the heat transfer in the liquid pool might not be negligible at high mass flux and low quality situations due to the convective heat transfer in the bottom part of the tube, resulting in a correlation that accounted for both film condensation and liquid pool forced convection. The shear driven correlation was based on a two-phase multiplier approach, and agreed well with data from the literature. They suggested that for $G > 500$ kg/m^2-s, the annular flow

correlation should be used; whereas for $G < 500$ kg/m^2-s, the annular flow correlation should be used for modified Froude numbers (as defined by Soliman (1982)), $Fr > 20$, and the wavy-stratified flow correlation should be used for $Fr < 20$. The applicability of this model by Dobson and Chato (1998) was extended for use with R407C by Sweeney (1996), who proposed simple mass flux-based modifications to Dobson and Chato's annular and wavy Nusselt numbers.

Boissieux et al. (2000) investigated condensation heat transfer for R404A, R407C, and Isceon 59 in a smooth horizontal tube ($D = 9.5$ mm), for $150 < G < 400$ kg/m^2-s, at saturation temperatures between 15°C and 35°C. They concluded that their test results were in good agreement with the correlations from Dobson and Chato (1998) and Shah (1979), and recommended that the Dobson and Chato correlation could be used for the near-azeotropic mixture, R404A.

Ebisu and Torikoshi (1998), Han and Lee (2001) and Cavallini et al. (2001; 2002b) investigated condensation heat transfer characteristics of the refrigerant blend R410A. For $150 < G < 300$ kg/m^2-s, a saturation temperature of 50°C, and $0.2 < x < 0.8$, Ebisu and Torikoshi (1998) found that the pressure drops for R410A were about 30% lower than those for R22. In addition, the heat transfer coefficients for R410A were also found to be lower than those for R22, particularly in the low quality region. They stated that the heat transfer coefficients for $x > 0.4$ were in good agreement with the correlation developed by Haraguchi et al. (1994). Han and Lee (2001) conducted tests on R410A and R22 in 7 and 9.52 mm O.D. smooth and microfin tubes, and found that the heat transfer coefficients are slightly larger, and the pressure drops are slightly lower, for R410A than R22. They stated that their data for the 7 mm smooth tube were within ±30% of the values predicted by the correlations of Shah (1979), Traviss et al. (1973), and Cavallini and Zecchin (1974).

Cavallini et al. (2001) measured heat transfer coefficients and pressure drops during condensation inside an 8 mm I.D. smooth tube with pure and nearly azeotropic HFC refrigerants for $30 < T_{sat} < 50$°C, $100 < G < 750$ kg/m^2-s, and $0.15 < x < 0.85$. The tests also covered a wide range of operating pressures as determined by the saturation conditions: low pressure (R236ea), mid-pressure (R134a, R22) and high pressure (R32, R125, R410A). In general, they found that at the same mass flux and quality, the high pressure fluids had lower

pressure drops, and they recommended that the Friedel (1980) correlation should be used to compute the pressure drop, even though this correlation was found to slightly over predict the pressure drop for high pressure fluids. They found that the model by Kosky and Staub (1971) should be used for heat transfer in the annular flow regime, while the correlation proposed by Jaster and Kosky (1976) should be used for the stratified flow regime for R32, R125, and R410A. In a follow up paper (Cavallini *et al.* 2002b) they compared their experimental heat transfer coefficients and other independent experimental data collected by different researchers with several theoretical or semi-empirical condensation heat transfer models for annular and gravity dominated flows (Akers et al. (1959), Akers and Rosson (1960), Dobson and Chato (1998), Jaster and Kosky (1976), Haraguchi et al. (1994), Tang (1997), Shah (1979)). This comparison showed that quite a few of their data were outside the validity ranges for these models, especially for the high-pressure refrigerants such as R125, R32 and R410A. The correlation by Akers et al. (1959) was found to underestimate the heat transfer coefficient, while the subsequent model by Akers and Rosson (1960) overestimated the data for 3 mm tubes. For the most part, they found that the conditions of interest for high-pressure refrigerants fall outside the ranges of validity of the Cavallini and Zecchin (1974) equation and the Haraguchi et al. (1994) models. The Dobson and Chato (1998) model was found to strongly over-predict the heat transfer coefficients for the high-pressure fluids, particularly at the higher values, although the predictions under wavy-stratified conditions were found to be better. Similarly, the Shah (1979) correlation also over-predicted the data for high-pressure fluids, whereas the Tang (1997) model yielded better predictions. Cavallini et al. (2002b) noted, however, that Shah (1979) and Tang (1997) models could only be applied to annular flow, and would not be appropriate for stratified, wavy-stratified and slug flow. Their overall conclusion, therefore, was that either the available models and correlations did not address the conditions of interest for high-pressure refrigerants, or, even if the stated range of applicability is adequate, the resulting predictions were considerably different from the measured values for these fluids.

Based on the above observations, Cavallini et al. (2002b) proposed a new flow regime-based model for condensation heat transfer and pressure drop for pure fluids and refrigerant blends, notably including the high-pressure fluids. They used their own data and

those of other researchers to develop three submodels to include annular flow, annular-stratified transition and stratified flow, and stratified-slug transition and slug flow. The transition criteria between different flow regimes were based on dimensionless vapor velocity J_G and Martinelli parameter X_{tt}. Thus, for $J_G > 2.5$, they suggested that the annular flow model be used. For $J_G < 2.5$, when $X_{tt} < 1.6$, the annular-stratified flow transition and stratified flow model was applicable, while for $X_{tt} > 1.6$, the stratified-slug and slug flow model was recommended. The annular flow model was based on the theoretical model of Kosky and Staub (1971), in which the heat transfer coefficient was related to the frictional pressure gradient (based on the Friedel (1979) correlation) through the interfacial shear stress. The stratified model accounted for the Nusselt type condensation in the upper region, and a convective term at the bottom that computed the liquid pool heat transfer at the bottom of the tube. The heat transfer coefficient for slug flow was calculated with a two-phase multiplier applied to the corresponding single-phase heat transfer coefficient. The model yielded excellent agreement with their own data as well as those of many other investigators, and was recommended for halogenated refrigerants in tubes with $3 < D < 21$ mm, reduced pressure $p_r < 0.75$, and liquid/vapor density ratio $\rho_L/\rho_G > 4$.

However, as pointed out in Cavallini et al. (2002a), the slug flow model did not smoothly approach to the heat transfer coefficient calculated from the annular-stratified flow transition and stratified flow model, resulting in some cases in abrupt jumps in the predicted heat transfer coefficients as vapor quality varies. Cavallini *et al.* (2002a) suggested that, when $J_G < 2.5$ and $X_{tt} > 1.6$, the heat transfer coefficient should be calculated as a linear interpolation between the coefficient calculated at $X_{tt} = 1.6$ and the coefficient obtained if the entire flow was liquid flow only.

Hajal *et al.* (2003) proposed a two-phase flow pattern map for condensation inside horizontal plain tubes based on the Kattan *et al.* (1998) flow regime map for flow boiling. Their map incorporated a newly defined logarithmic mean void fraction (LMε) method for void fraction calculations from low to near-critical pressures. At pressures close to critical pressure, a homogeneous void fraction was applicable:

$$\varepsilon_h = \left[1 + \left(\frac{1-x}{x}\right)\left(\frac{\rho_v}{\rho_l}\right)\right]^{-1} \tag{1}$$

At low-to-medium pressures, a horizontal tube version (Steiner 1993) of the Rouhani-Axelsson expression for vertical tubes (Rouhani and Axelsson 1970) was used to calculated the void fraction.

$$\varepsilon_{ra} = \frac{x}{\rho_v}\left[\left[1+0.12(1-x)\right]\left(\frac{x}{\rho_v}+\frac{1-x}{\rho}\right)+\frac{1.18(1-x)[g\sigma(\rho_l-\rho_v)]^{0.25}}{G\rho_l^{0.5}}\right]^{-1} \quad (2)$$

However, this void fraction did not approach the limit of the homogeneous void fraction as the pressure approaches the critical point. The authors suggested the use of a simple logarithmic mean void fraction between ε_h and ε_{ra} for void fractions from low to near-critical pressures.

$$\varepsilon = \frac{\varepsilon_h - \varepsilon_{ra}}{\ln\left(\frac{\varepsilon_h}{\varepsilon_{ra}}\right)} \quad (3)$$

This LMε model was validated indirectly by the authors for reduced pressures from 0.02 to 0.8 through an evaluation of heat transfer data. The new flow regime map based on LMε model was also compared with some recent flow pattern observations and showed qualitative agreement. For instance, two flow pattern observations from Dobson and Chato (1998) in the transition of wavy to wavy-annular flow agreed well with the LMε-based flow regime map, while two wavy-annular flow to annular flow transition observations from Dobson and Chato (1998) were near the corresponding flow transition in the new map. The authors also compared the proposed flow regime map with six flow pattern observations reported by Shao and Granryd (2000) for R134a, R22 and R502 inside a 6-mm bore sight glass. 83% (5 out of 6) observations were correctly identified while the sixth one was in the vicinity of the transition. The proposed flow regime map also showed qualitative agreement with other flow regime maps, i.e. Breber *et al.* (1980), Tandon *et al.* (1982), Sardesai *et al.* (1981), and Cavallini *et al.* (2002b).

Based on the flow regime map developed by Hajal *et al.* (2003), Thome *et al.* (2003) proposed a heat transfer model for condensation inside horizontal smooth tubes assuming the heat transfer within the tube consists of convective condensation and film condensation. This model was developed using the heat transfer data base from Cavallini *et al.* (1999; 2001). The resulting heat transfer coefficient was expressed as:

$$h = \frac{h_f r\theta + (2\pi - \theta) r h_c}{2\pi r} \tag{4}$$

where r is the internal radius of the tube and θ is the falling film angle around the top perimeter of the tube. Therefore, for annular, intermittent and mist flows, θ = 0, and for fully stratified flow, $\theta = \theta_{strat}$. For stratified wavy flow, the stratified angle θ was obtained using a quadratic interpolation between θ_{strat} and 0. The fully stratified angle θ_{strat} was a function of geometry and could be estimated using the following equation:

$$\theta_{strat} = 2\pi - 2\left\{\begin{array}{l} \pi(1-\varepsilon) + \left(\frac{3\pi}{2}\right)^{1/3}\left[1 - 2(1-\varepsilon) + (1-\varepsilon)^{1/3} - \varepsilon^{1/3}\right] \\ -\frac{1}{200}(1-\varepsilon)\varepsilon\left[1 - 2(1-\varepsilon)\right]\left[1 + 4(1-\varepsilon)^2 + \varepsilon^2\right] \end{array}\right\} \tag{5}$$

It should be noted that, in their model, convective condensation refers to the axial flow of the condensate along the tube due to the imposed pressure gradient while the film condensation refers to the flow of condensate form the top of the tube towards the bottom due to gravity.

For convective condensation heat transfer, the authors proposed the following equation:

$$h_c = c\,\mathrm{Re}_l^{\,n}\,\mathrm{Pr}_l^{\,m}\,\frac{k_l}{\delta} f_i \tag{6}$$

where c, n and m are empirical constants (c = 0.003, n = 0.74 and m = 0.5). δ is the liquid film thickness and can be obtained from geometry. f_i is an interfacial roughness correction factor to account for the heat transfer enhancement due to increased interfacial waviness caused by increased vapor shear at high vapor velocities.

$$f_i = 1 + \left(\frac{u_v}{u_l}\right)^{0.5}\left(\frac{[\rho_l - \rho_v]g\delta^2}{\sigma}\right)^{0.25} \tag{7}$$

The interfacial roughness correction factor increases as the vapor-to-liquid velocity ratio increases and tends towards 1.0 as the film becomes very thin. However, the interfacial roughness correction factor decreases as surface tension increases, as the surface tension tends to smooth out the surface waviness.

The authors suggested that, for film condensation, the Nusselt falling-film analysis for circular tubes could be used. It was found sufficient to use the mean value for

condensation around the perimeter from top to bottom instead of integrating from the top of the tube to the liquid level angle θ.

Predictions from the proposed model were compared with the experimental data obtained by Cavallini *et al.* (1999; 2001) and other independent studies and it was found that 85.0% of the data could be predicted with ±20%.

In a recent review paper, Cavallini *et al.* (2003) presented the available experimental data for new ozone-friendly refrigerants with well-established heat transfer prediction models. The authors stated that, according to Cavallini *et al.* (2001), the heat transfer coefficient in stratified flow regime was affected by the wall-saturation temperature difference (T_s-T_w), while the heat transfer coefficient for annular flow only varied with mass flux, quality and saturation temperature. According to their review of the literature, for annular flow, semi-empirical models from Shah (1979), Kosky and Staub (1971), Traviss *et al.* (1973), Tang (1997), Cavallini and Zecchin (1971; 1974) and Boyko and Kruzhilin (1967) are available. For stratified flow, heat transfer through the thin film is often analyzed by Nusselt theory (Nusselt 1916). Jaster and Kosky (1976) suggested that the heat transfer in the liquid pool might be neglected compared to the film condensation. However, as discussed by Dobson and Chato (1998), the convection in the liquid pool might be substantial and could not be neglected at high mass fluxes. Dobson and Chato (1998) and Haraguchi *et al.* (1994) also proposed heat transfer models that cover both annular and stratified-wavy flow. The model proposed by Cavallini *et al.* (2002b) covers all flow regimes: annular, stratified-wavy and slug flow. This model was developed from a large data bank and could be used for in-tube condensation of halogenated refrigerants with $3 < D < 21$ mm, reduced pressure $P_r < 0.75$, and liquid/vapor density ratio $\rho_L/\rho_G > 4$.

The authors also compared the experimental data from Cavallini *et al.* (2001) with the models by Cavallini *et al.* (2002b), Shah (1979), and Dobson and Chato (1998) for R134a, R22, R410A and R32 in a 8 mm smooth tube. It was shown that the model by Cavallini *et al.* (2002b) resulted in lower heat transfer coefficients while the models by Shah (1979) and Dobson and Chato (1998) strongly overpredicted the data. The model by Haraguchi *et al.* (1994) was not applicable for most of the conditions considered.

Pressure drop

Two-phase frictional pressure drops are often expressed in terms of the two-phase multipliers defined as below.

$$\phi_L^{\,2} = \frac{(dP_f / dz)}{(dP_f / dz)_L} \tag{8}$$

$$\phi_G^{\,2} = \frac{(dP_f / dz)}{(dP_f / dz)_G} \tag{9}$$

$$\phi_{LO}^{\,2} = \frac{(dP_f / dz)}{(dP_f / dz)_{LO}} \tag{10}$$

$$\phi_{GO}^{\,2} = \frac{(dP_f / dz)}{(dP_f / dz)_{GO}} \tag{11}$$

where subscripts L, G, LO and GO refer to the flow of the liquid phase alone in the channel, vapor phase alone, total flow having the liquid properties and total flow having vapor properties, respectively. The classical correlation for two-phase frictional pressure drop in tubes is that of Lockhart and Martinelli (1949), who related ϕ_G and ϕ_L to the parameter X, defined in the equation below:

$$X^2 = \frac{(dP_f / dz)_L}{(dP_f / dz)_G} \tag{12}$$

$$\phi_L = \left(1 + \frac{C}{X} + \frac{1}{X^2}\right)^{1/2} \tag{13}$$

$$\phi_G = \left(1 + CX + CX^2\right)^{1/2} \tag{14}$$

where the constant C depends on the flow regimes (laminar or turbulent) associated with the flow of the vapor and the liquid alone in the tube. This model was developed for air, benzene, kerosene, water and various oils in tubes with diameter from 1.49 – 25.83 mm. However, the Lockhart-Martinelli correlations do not closely represent phase-change data and have large systematic errors. Also, they do not adequately represent the physical property effects. Since then, a large number of other correlations have been published. Most of them, such as models by Chisholm (1973) and Friedel (1979), can be regarded as simple data fits. The Chisholm (1973) correlation is :

$$\phi_{LO}^{\ 2} = 1 + [Y^2 - 1][Bx^{\frac{2-n}{2}}(1-x)^{\frac{2-n}{2}} + x^{2-n}] \tag{15}$$

Where n is the power to which Re is raised in the single-phase friction factor (For example, n = 0.25 for Blausius equation). The parameter B is defined as a piecewise function of mass flux and parameter Y given by:

$$Y^2 = \frac{(dP/dz)_{f,GO}}{(dP/dz)_{f,LO}} \tag{16}$$

Based on a data base of 25,000 points, Friedel (1979) proposed a two-phase multiplier correlation for ϕ_{LO} for upward vertical and horizontal flow in circular tubes as a function of vapor quality, mass flux, tube diameter and physical properties.

$$\phi_{LO}^{\ 2} = C_1 + \frac{3.24 C_2}{Fr^{0.045} We^{0.035}} \tag{17}$$

where Fr and We are Froude number and Weber number, respectively.

$$Fr = \frac{G}{gD\rho_{tp}^{\ 2}} \tag{18}$$

$$We = \frac{GD}{\rho_{tp}\sigma} \tag{19}$$

$$C_1 = (1-x)^2 + x^2\left(\frac{\rho_l}{\rho_v}\right)\left(\frac{f_{GO}}{f_{LO}}\right) \tag{20}$$

$$C_2 = x^{0.78}(1-x)^{0.24}\left(\frac{\rho_l}{\rho_v}\right)^{0.91}\left(\frac{\mu_v}{\mu_l}\right)^{0.19}\left(1-\frac{\mu_v}{\mu_l}\right)^{0.7} \tag{21}$$

$$\rho_{tp} = \left(\frac{x}{\rho_v} + \frac{1-x}{\rho_l}\right)^{-1} \tag{22}$$

Despite the complexity of Friedel (1979) correlation, it showed considerable scatter when compared with the data bank he used (Hewitt *et al.* 1993).

Recently, several researchers (Mishima and Hibiki 1996; Tran *et al.* 2000; Ju Lee and Yong Lee 2001; Kawahara *et al.* 2002) have developed pressure drop models for small diameter tubes by modifying the classical pressure drop correlations like Lockhart and Martinelli (1949) and Chisholm (1973). Mishima and Hibiki (1996) studied flow regime, void fraction, rise velocity of slug bubbles and friction pressure loss for air-water flows in

capillary tubes with inner diameters in the range from 1 to 4 mm. They found that the boundaries of the flow regimes were in good agreement with the model by Mishima and Ishii (1984), although flow regimes peculiar to a capillary tube (concentration of bubbles along tube axis, spiral train of small bubbles, etc) were also observed. They also found that, instead of being a constant, as the tube diameter decreases, the parameter C in Lockhart and Martinelli (1949) model (equation 13) decreases. Similar results were obtained by other researchers (Sugawara *et al.* 1967; Mishima *et al.* 1993). Based on this observation, the authors proposed a correlation for C as a function of tube hydraulic diameter. The authors showed that for all the data considered except for those of ammonia-vapor flow, the prediction was within ±12%. For ammonia-vapor flow, the error becomes ±25%. It should also be noted that the parameter C becomes zero when the hydraulic diameter is as small as 0.2 mm.

Lee and Lee (2001) studied two-phase pressure drop for air-water through horizontal rectangular channels with small gaps between 0.4 to 4 mm, while the channel width was constant at 20 mm. The superficial air and water velocities ranged from 0.05-18.7 and 0.03-2.39 m/s, respectively. Atmospheric pressure was maintained throughout the tests. They suggested that the parameter C in the Lockhart and Martinelli (1949) model (equation 13) could be expressed in terms of dimensionless parameters λ, ψ and Re_{LO} as follows:

$$C = A\lambda^{q}\psi^{r}\,\mathrm{Re}_{LO}^{\,s} \tag{23}$$

$$\lambda = \frac{\mu_l^{\,2}}{\rho_l \sigma D} \tag{24}$$

$$\psi = \frac{\mu_l^{\,2} j}{\sigma} \tag{25}$$

where j is the liquid slug velocity. The constants A q, r and s were determined through data regression based on the applicable flow regime (laminar or turbulent) of the liquid and vapor phases. By comparing the model to their own experimental data, the authors concluded that the Lockhart and Martinelli (1949) model with a modified C parameter could cover a wide range of Martinelli parameters ($0.303 < X < 79.4$) and liquid-only Reynolds numbers ($175 < Re_{LO} < 17700$).

Kawahara *et al.* (2002) investigated two-phase pressure drop in a 100 μm diameter circular tube with superficial velocities of water and nitrogen gas at 0.02 – 4 and 0.1 – 60 m/s. They compared their data to a homogeneous flow model (homogeneous friction factor) with various two-phase viscosities available in the literature (McAdams 1954; Cicchitti *et al.* 1960; Owens 1961; Dukler *et al.* 1964; Beattie and Whalley 1982; Lin *et al.* 1991) and found the agreement was generally poor except for the model from Dukler *et al.* (1964) (within ±20%). They also compared their data to the two-phase multiplier models developed by Mishima and Hibiki (1996) and Lee and Lee (2001) and found significant improvement in predictions with an error band of ±10%.

Tran *et al.* (2000) studied pressure drops for R134a, R12 and R113 during phase-change inside three different tubes: two circular, 2.46 and 2.92 mm I.D. and one rectangular channel, 4.06×1.7 mm. The operating pressures ranged from 138 to 856 kPa. They proposed a new two-phase pressure drop model during flow boiling in small channels based on the Chisholm (1973) correlation. The B-coefficient in the Chisholm (1973) correlation was only a function of mass flux and parameter Y, but not the tube dimension and fluid properties. The authors argued that, tube dimension and fluid surface tension were important factors in phase-change pressure drop, especially in refrigerants. Therefore, they suggested that, to better reflect the physics of flow boiling in small tubes, the B-coefficient should be replaced with a dimensionless number – confinement number, introduced by Cornwell and Kew (in (Pilavachi 1993)),

$$N_{conf} = \frac{1}{D}\left[\frac{\sigma}{g(\rho_l - \rho_v)}\right]^{0.5} \tag{26}$$

The authors also included a constant C = 4.3 before the Y parameter to scale the difference in pressure gradient between small and large tubes. A comparison between the model and their own experimental data showed that, most of the data were predicted within ±20% and 93.8% of data were predicted with ±30%.

Cavallini et al. (2001) conducted pressure drop experiments during condensation inside an 8 mm I.D. smooth tube with pure and nearly azeotropic HFC refrigerants R236ea, R134a, R22, R32, R125, R407C and R410A for $30 < T_{sat} < 50^{o}C$ and $100 < G < 750$ kg/m^2-s, over the entire vapor quality range. Using these data, Cavallini et al. (2002b) proposed a new

flow regime-based pressure drop correlation that can be obtained from the momentum equation. They suggested that for gas-phase non-dimensional superficial velocity $J_G \geq 2.5$, a modified version of the Friedel (1979) correlation could be used to compute the frictional pressure gradient, while for $J_G < 2.5$, the original Friedel (1979) correlation should be used.

Prior Investigations of Supercritical Heat Transfer

For conventional single-phase turbulent heat transfer, Gnielinski (1976) proposed a correlation for the range $0.5 < Pr < 2000$, and $3000 < Re < 5\times10^6$. For smooth tubes, the Petukhov (in Irvine and Hartnett (1970)) correlation was suggested for the evaluation of the friction factor needed in the Gnielinski (1976) correlation (Incropera and DeWitt 2002).

Ghajar and Asadi (1986) compared the existing empirical approaches for forced-convective heat transfer in the near-critical region. They concluded that the most significant discrepancy in existing correlations developed for forced convection when applied to the near-critical region may due to the property variations, influences of heat flux and buoyancy, and the differences in properties used by various investigators. Using a data bank they collected from previous literature for water and carbon dioxide heating in the supercritical region, seven different types of forced convective heat transfer correlations were proposed. The experimental data that they collected from the literature were for near-critical and supercritical heating of CO_2 and steam with reduced pressure range from 0.018 to 1.88. The heat fluxes for the database were from 0.8 to 1100 W/cm^2 for CO_2 and 18.7 to 2320 W/cm^2 for steam. The bulk-to-critical temperature ratio ranged from 0.43 to 1.31. The mass fluxes studied were from 1.7 to 300 kg/m^2-s. To compare the correlations based on the same physical property inputs, the constants proposed were determined by curve fitting the experimental data based on correct values of the physical property inputs. Their results showed that convective heat transfer in the supercritical region could be predicted by a Dittus-Boelter type heat transfer correlation combined with property ratio multipliers to account for the large property variations in this region as follows:

$$Nu_b = a\,\mathrm{Re}_b^{\,e}\,\mathrm{Pr}_b^{\,c}\left(\frac{\rho_w}{\rho_b}\right)^d\left(\frac{\overline{C}_p}{C_{pb}}\right)^n \tag{27}$$

where subscript w and b represent wall and bulk temperature, respectively. a, c, d, and e are curve-fitted constants for different fluids. $\overline{C}_p$ is the integrated mean specific heat, defined as a function of and wall and bulk enthalpies and temperatures:

$$\overline{C}_p = \frac{h_w - h_b}{T_w - T_b} \tag{28}$$

The exponent n was proposed by Jackson and Fewster (1975):

$$n = \begin{cases} 0.4 & T_b < T_w < T_{crit} \text{ and } T_w > T_b \geq 1.2T_{crit} \\ 0.4 + 0.2(T_w / T_{crit} - 1) & T_b \leq T_{crit} < T_w \\ 0.4 + 0.2(T_w / T_{crit} - 1)[1 - 5(T_b / T_{crit} - 1)] & T_{crit} \leq T_b \leq 1.2T_{crit} \text{ and } T_b < T_w \end{cases} \tag{29}$$

Ghorbani-Tari and Ghajar (1985) investigated free convection in the near-critical region. They used a data bank for horizontal and vertical free convection of CO_2 and water, with Rayleigh number ranges from 0.2 – 1.04×10^{13}. They found that many free convective heat transfer correlations showed discrepancies when applied in the near-critical region. According to the authors, these discrepancies appeared to be due to 1) the reference temperature used for the evaluation of the physical properties, 2) the physical properties selected in reducing the dimensional experimental data to dimensionless variables, and 3) the differences in values of the physical properties used in the literature. Five different types of free-convection heat transfer correlations were proposed. To compare the correlations based on the same physical property inputs, the constants proposed were determined by curve-fitting the experimental data based on consistent values of the physical property inputs. For horizontal wires and vertical plates with a wide range of Rayleigh numbers, the authors proposed the following correlation.

$$Nu_\infty = a(Gr_\infty \, \mathrm{Pr}_\infty)^b \left(\frac{\rho_w}{\rho_\infty}\right)^c \left(\frac{\overline{C}_p}{C_{p\infty}}\right)^d \left(\frac{k_w}{k_\infty}\right)^e \left(\frac{\mu_w}{\mu_\infty}\right)^f \tag{30}$$

where $\overline{C}_p$ is defined as in equation (28), and a, b, c, d, e and f are curve-fitted constants. The authors also found that when using the free stream temperature to evaluate the fluid properties, the predictions were better. They argued that the effect of tube diameter was reduced if heat transfer coefficients were expressed as $hD^{0.25} = NukD^{-0.75}$.

In a comprehensive review of the literature on in-tube heat transfer and pressure drop characteristics of carbon dioxide in the supercritical region, Pitla *et al.* (1998) concluded that heat transfer was enhanced during supercritical cooling (due to the formation of a higher thermal conductivity liquid-like layer near the wall) and degraded during heating (conversely due to the formation of a gas-like layer near the wall). They also pointed out that much less work had been done in determining the supercritical heat transfer and pressure drop of carbon dioxide during the cooling process, as compared to the heating process. Krasnoshchekov *et al.* (1970) conducted an experimental study of heat transfer during turbulent flow in a horizontal circular tube with carbon dioxide at supercritical pressures under cooling conditions. The bulk fluid temperature and pressure ranges for their study were 30–215°C and 8–12 MPa (0.71 – $1.11\times P_{crit}$), respectively, with Reynolds number ranging from 2.67×10^5 – 8.35×10^5. They suggested that the heat transfer coefficient in supercritical cooling could be evaluated using a single-phase convection correlation evaluated at the inner wall temperature with property ratio multipliers to account for the large property variations in this region.

$$Nu_b = Nu_w\left(\frac{\rho_w}{\rho_b}\right)^n\left(\frac{\overline{C}_p}{C_{pw}}\right)^m \tag{31}$$

where m, and n are constants provided graphically by the authors. They compared the above correlation with their own experimental results and the results of Tanaka *et al.* (1971) and found satisfactory agreement.

More recently, Pitla *et al.* (2001b; 2001a) conducted a combined experimental and numerical study of the heat transfer and pressure drop of in-tube cooling of carbon dioxide. The numerical model was based on the Favre-averaged, parabolized Navier-Stokes equations and an appropriate turbulence model. Favre decomposition was applied to the velocities and the enthalpy, and Reynolds decomposition was applied to thermophysical properties and pressure to account for the highly turbulent flow and large property variations. Both Nikuradse's mixing length model and the *k*-equation turbulence model were used and found to agree within ±1%. Simulations were run for supercritical cooling of CO_2 inside a 4.52 mm tube with a constant wall temperature of 30°C. The length of the test tube was 2 m. The inlet temperature and pressure of the fluid were assumed to be 122°C and 10 MPa, respectively.

The inlet fluid velocity was 9.65 m/s, corresponding to a Reynolds number of 3.2×10^5. The simulations showed that the heat transfer coefficient decreased rapidly in the entrance region, but increased steadily after that. At the temperature corresponding to the pseudo-critical temperature of CO_2 at that pressure, the heat transfer coefficient reached a peak value which mainly due to the peak in the bulk specific heat. Then, the heat transfer coefficient decreased sharply. The simulation also showed that the friction factor decreased as the fluid cools down and finally approaches to a constant value corresponding to that of compressed liquid CO_2.

They also conducted experiments to measure the heat transfer of carbon dioxide inside a 4.72 mm I.D. tube under supercritical cooling at pressures ranging from 8 to 12 MPa ($0.71 - 1.11\times P_{crit}$). The test fluid was cooled from 120°C to 25°C, which was below the thermodynamic critical point. The authors compared the numerical solutions with their experimental results and found they were within ±10% of each other. The comparison therefore verified the accuracy of the numerical model. Based on the numerical solution, Pitla *et al.* (2002) proposed a new correlation for in-tube supercritical cooling of carbon dioxide.

$$Nu = \left(\frac{Nu_{wall} + Nu_{bulk}}{2} \right) \frac{k_{wall}}{k_{bulk}} \tag{32}$$

where Nu_{wall} and Nu_{bulk} are evaluated using the Gnielinski correlation (1976) at wall and bulk temperatures, respectively:

$$Nu = \frac{(f/8)(\mathrm{Re}-1000)\,\mathrm{Pr}}{12.7(f/8)^{0.5}(\mathrm{Pr}^{2/3}-1)+1.07} \tag{33}$$

For smooth tubes, the Petukhov (Incropera and DeWitt 2002) correlation is again used to evaluate the friction factor. The authors found that the best results were obtained by using the inlet velocity to compute the Reynolds number at the wall irrespective of location, and by using the local mean velocity to compute the bulk Reynolds number.

In a two-part paper, Kurganov (1998b; 1998a) investigated the heat transfer and pressure drop of carbon dioxide under supercritical pressures in different tube diameters and orientations based on a series of experimental studies. In part I (Kurganov 1998a), the author suggested that, considering the drastic change in CO_2 properties near the critical region, it

was advisable to divide the temperature (or enthalpy) into three region based on the specific work of thermal expansion (defined below): liquid-like, pseudo-phase transition and gas-like state.

$$E_o = \left(\frac{P\partial V}{\partial h} \right)_P = \frac{P\beta}{\rho c_p} \tag{34}$$

In the liquid-like state, the behavior of the fluid was the same as that of a liquid. The change in properties was gradual and insignificant. In this region, E_q is of the order of 10^{-2}, which was typical for liquids. In the pseudo-phase transition region, the density and viscosity of the fluid decreased sharply, and the specific heat, Prandtl number, and volume expansion coefficient β passed through a maximum. In this region, E_q increased sharply. The steep rise in E_q begins when $E_q > 0.02–0.03$. Therefore, these value could be considered as boundary value when determine the transition from the liquid-like state to the pseudo-phase transition region. The fluid was considered to be in a gas-like state when $E_q > E_q^0 = R/c_p$, which was typical for a substance in an ideal gas state.

The author also found that, for CO_2 under supercritical heating conditions in horizontal tubes, besides the negative pressure gradient due to thermal acceleration of flow, stratification of the liquid density and of the gravity forces in the vertical direction also took place. This stratification was stable near the top portion of the tube, but unstable near the bottom portion of the tube. For supercritical heating with low heat flux, normal heat transfer was observed. As the heat flux exceeded a certain value, the fluid changes to vapor state, deteriorated heat transfer was typical. The author also pointed out that, due to the nonuniform wall temperature distribution along the tube circumference caused by buoyancy, the heat transfer coefficients around the tube circumference were also varying. Near the top of the tube, heat transfer deterioration and wall superheating took place, while near the bottom of the tube, the heat transfer was enhanced, resulting in the wall temperature being lower than average.

Deficiencies in the Literature and Need for Research

The above reviews of the literature on in-tube condensation and supercritical heat transfer are summarized in Tables 2 and 3, respectively.

Table 2. Summary of Literature on In-Tube Condensation

Type	Author	Fluids	D (mm)	G (kg/m2s)	P_r or T_{sat} (°C)	HT and ΔP Models
Pure fluids	Kosky and Staub (1971)	Steam	12.57	2.712 – 149.2		Annular flow heat transfer model
	Traviss et al. (1973)	R-12, R-22	8.0	161 – 1532	$25 < T_{sat} < 58$	Annular flow heat transfer model
	Jaster and Kosky (1976)	Steam	12.57	12.6 – 145		Annular, stratified and transition heat transfer model
	Shah (1979)	R-11, R-12, R-22, R-113, water, methanol, ethanol, benzene, toluene, trichloroethylene	7 – 40	11 – 211	$0.002 < P_r < 0.44$	Empirical heat transfer model for $1 < Pr_l < 13$
Refrigerant blends	Dobson and Chato (1998)	R-134a, R-12, R-22, R-32/R-125	3.14, 4.57, 7.04	25 – 800	$35 < T_{sat} < 45$	Annular and wavy flow heat transfer models
	Sweeney (1996)	R-407C		150 – 400		Modified Dobson and Chato (1998) models
R404A and other fluids	Boissieux, et al. (2000)	R-404A, R-407C, Isceon 59	9.5	150, 300	$15 < T_{sat} < 35$	Dobson & Chato (1998) models recommended
R410A and other pure and refrigerant blends	Ebisu and Torikoshi (1998)	R-410A, R-407C, R-22	6.4	100 – 400	$T_{sat} = 50$	Haraguchi et al. (1994) correlation recommended for R410A for $x \geq 0.4$.
	Han and Lee (2001)	R-410A, R-22	7, 9.52	100 – 400	$T_{sat} = 30, 40$	
	Cavallini et al. (2001)	R-22, R-134a, R-125, R-32, R-410A, R-236ea	8	100 – 750	$30 < T_{sat} < 60$	Kosky and Staub (1971) model for annular flow, Jaster and Kosky (1976) model for stratified flow
	Cavallini et al. (2002a)	Data bank taken from literature	3 – 21		$P_r < 0.75$	Annular, stratified and slug flow heat transfer and pressure drop model, $\rho_l / \rho_v > 4$
	Hajal et al. (2003)	R-22, R-134a, R-125, R-32, R-410A, R-236ea	8	100 – 750	$28 < T_{sat} < 60$	Logarithmic mean void fraction model and flow regime map based on LMε
	Thome et al. (2003)	R-22, R-134a, R-125, R-32, R-410A, R-236ea	8	100 – 750	$27 < T_{sat} < 60$	Annular and stratified wavy flow heat transfer model

Table 2. Summary of Literature on In-Tube Condensation (Continued)

Type	Author	Fluids	D (mm)	P (kPa)	HT and ΔP Models
Adiabatic flow	Lockhart & Martinelli (1949)	Air, benzene, kerosene, water, oils	1.49 – 25.83	110.3 – 358.5	Liquid and vapor two-phase multiplier
	Chisholm (1973)				Liquid only two-phase multiplier
	Friedel (1979)	Data bank in the literature			Liquid only two-phase multiplier pressure drop model
	Mishima and Hibiki (1996)	Air-water mixture	1 – 4		Press drop modified Lockhart and Martinelli (1949) two-phase multiplier
	Lee and Lee (2001)	Air-water mixture	0.4 – 4		Modified Lockhart and Martinelli (1949) two-phase multiplier pressure drop model
	Kawahara *et al.* (2002)	Water-nitrogen mixture	0.1		Mishima and Hibiki (1996) and Lee and Lee (2001) pressure drop model recommended
Phase-change	Tran *et al.* (2000)	R134a, R12 and R113	2.46, 2.92, 4.06×1.7	138 – 856	Modified Chisholm (1973) two-phase multiplier pressure drop model for boiling

Phase-change heat transfer and pressure drop

It is clear from Table 2 that, for condensation heat transfer, most early investigations (Kosky and Staub 1971; Traviss *et al.* 1973; Shah 1979) have focused on heat transfer for pure refrigerants based on the annular flow assumption. Jaster and Kosky (1976) extended Kosky and Staub's (1971) investigation to stratified-wavy flow and proposed flow transition criteria based on the ratio of axial shear force to gravitational body force. However, for stratified-wavy flow, they assumed that the heat transfer in the liquid pool was negligible compared to the film condensation in the upper portion of the tube. This assumption is reasonable for the low mass flux range in his study, but might not be true for higher mass flux, low quality situations where wavy or stratified wavy flow could prevail in the presence of substantial convective heat transfer in the bottom of the tube.

Some recent studies (Sweeney 1996; Dobson and Chato 1998; Ebisu and Torikoshi 1998; Boissieux *et al.* 2000; Cavallini *et al.* 2001; Han and Lee 2001; Cavallini *et al.* 2002a; Hajal *et al.* 2003; Thome *et al.* 2003) have started to investigate condensation heat transfer for pure and refrigerant blends. These studies have yielded correlations that are based on the

Table 3. Summary of Literature on Supercritical Heat Transfer

Type	Author	Fluids	Flow Conditions	P_r or T (°C)	HT and ΔP Models
Single-phase flow	Gnielinski (1976)		Single-phase turbulent flow		Modified Petukov (in Irvine and Hartnett (1970)) correlation
Free convection	Ghorbani-Tari and Ghajar (1985)	CO_2, water	Free convection near critical region data bank from literature	$0.2 < Ra < 1.04\times10^{13}$	Free convection HT correlation with property corrections
Supercritical heating and cooling	Krasnoshchekov (1970)	CO_2	Supercritical **cooling** in horizontal tubes	30 – 215°C	Single-phase turbulent correlation with property corrections
	Ghajar & Asadi (1986)	CO_2, water	Supercritical **heating** data bank from literature	$0.018 < P_r < 1.46$	Dittus-Boelter-type HT correlation with property corrections
	Kurganov (1998a)	CO_2	Supercritical **heating**		Flow regime transition criteria
	Kurganov (1998b)	CO_2	Supercritical **heating**		Generalized Petukhov-Kirillov correlation recommended
	Pitla et al. (2001b)	CO_2	Supercritical **cooling** in horizontal tubes	T_{wall} = 30°C P_{in}= 10 MPa	Numerical heat transfer models
	Pitla et al. (2001a)	CO_2	Supercritical **cooling** in horizontal tubes	$T_{test\ in}$ = 120°C $T_{test\ out}$ = 5°C	Experimentally validate the numerical model in Pitla et al. (2001b)
	Pitla et al. (2002)	CO_2	Numerical predictions from Pitla et al. (2001b)		Average of wall and bulk heat transfer based on Gnielinski (1976) correlation with property corrections

specific flow pattern that exists for the applicable conditions. However, most of these studies on high pressure refrigerant focused on R410A at low reduced pressures (low saturation temperatures). Although the studies by Hajal *et al.* (2003) and Thome *et al.* (2003) were for pure and refrigerant blends at saturation temperatures between 27 and 60°C, the saturation temperature range for high pressure pure and refrigerant blends (R32, R125, R410A) was $28 < T_{sat} < 52$°C. Boissieux *et al.* (2000) studied R404A in a similar tube diameter as in the present study, but the saturation temperature range for their study was $15 < T_{sat} < 35$°C. Cavallini *et al.* (2002a) used a data bank taken from literature for heat transfer in tube diameter range 3 – 21 mm to develop flow regime based heat transfer and pressure models.

But they recommend that their model could be used only for reduced pressures up to 0.75 due to the lack of data at higher reduced pressures.

For pressure drop during condensation, Table 2 shows that many studies have been conducted on air-water or gas-water mixtures instead of refrigerants. Tran *et al.* (2000) studied the pressure drop for pure refrigerants under evaporation and a much lower reduced pressure range.

Thus, there is little literature available on heat transfer and pressure drop at saturation pressures approaching the critical pressure. Many of the commonly used condensation heat transfer correlations result in significant discrepancies when predicting the heat transfer coefficients for the higher pressures of interest in the present study.

Supercritical heat transfer and pressure drop

Table 3 shows that most prior investigations on supercritical heat transfer and pressure drop have been conducted on carbon dioxide or steam. Furthermore, most of these studies have focused on the heating process (Ghorbani-Tari and Ghajar 1985; Ghajar and Asadi 1986; Kurganov 1998b; Kurganov 1998a). Most studies attributed the changes in heat transfer coefficients to the large variation in properties, especially specific heat, near the vicinity of the critical point. Therefore, many researchers developed or recommended heat transfer correlations based on single-phase turbulent flow with property corrections to account for the large property variations near the critical region. There is little literature available on the supercritical cooling process for refrigerant blends. Extrapolating from heat transfer correlations developed for CO_2 mostly under heating conditions may result in significant discrepancies.

Therefore, the present study investigates heat transfer and pressure drop during condensation and supercritical cooling of refrigerant R404A in a horizontal smooth tube (9.4 mm diameter) at pressures from 80 – 120% of P_{crit}. Data are subdivided into categories based on the expected flow regimes predicted from the information available in the literature. Heat transfer and pressure drop models are developed based on appropriate flow regimes using the data obtained in the present study. The following chapter discusses the experimental approach and test facility developed for this study.

CHAPTER 3. EXPERIMENTAL SETUP

This chapter provides a detailed description of the experimental setup and procedures used for both phase-change and supercritical tests. Heat transfer coefficient and pressure drop inside a 9.4 mm-I.D. circular tube were measured for seven different mass fluxes ranging between 200 and 800 kg/m^2-s at five different pressures. $0.8\times P_{crit}$ (2983 kPa), $0.9\times P_{crit}$ (3356 kPa), P_{crit} (3729 kPa), $1.1\times P_{crit}$ (4102 kPa), and $1.2\times P_{crit}$ (4475 kPa). The first two pressures were phase-change (condensation) tests, while the remaining three pressures were quasi single-phase (gas cooling) tests. For each mass flux of the phase change tests, experiments were conducted with nominal local test-section qualities from 0.9 to 0.1. For quasi single-phase tests, at each mass flux, data points were taken with nominal test-section inlet temperatures from 30 to 110°C in nominally 10°C increments. Therefore, the test facility must allow the heat transfer coefficient and pressure drop be measured in small increments over the entire quality or temperature range. Furthermore, the test facility must also withstand the highest pressure under consideration (4475 kPa).

Table 4 shows the test matrix for the current study.

Requirements for Heat Transfer Coefficient Determination

The requirements for heat transfer coefficient determination are discussed here for phase-change tests. The approach developed for addressing these requirements is also applicable for supercritical tests.

To accurately determine the heat transfer coefficient, the test section inlet quality (enthalpy), outlet quality (enthalpy), and heat transfer rate need to be accurately determined. Second, the techniques used must also ensure the establishment of a wide range of quality and temperature for each mass flux. In addition, small condensation (phase-change tests) or cooling (supercritical tests) heat duties, i.e., small quality or temperature increments, are needed to represent local phenomena. Finally, the heat transfer coefficient must be accurately determined from measured heat duty and UA values.

However, in this study, heat transfer rate and heat transfer coefficient determination pose somewhat opposing requirements. Thus, the coolant flow rate and temperature rise

Table 4. Test Matrix

R404A Critical Properties			P_{crit} = **3729 kPa**				T_{crit} = **72.05°C**		
Phase-Change Tests: Test Pressure 10% and 20% Below Critical Pressure									
			P (kPa)= 2983			**3356**			
G (kg/m²-s)	**Nominal Test Section Average Quality**								
200	0.9	0.8	0.7	0.6	0.5	0.4	0.3	0.2	0.1
300	0.9	0.8	0.7	0.6	0.5	0.4	0.3	0.2	0.1
400	0.9	0.8	0.7	0.6	0.5	0.4	0.3	0.2	0.1
500	0.9	0.8	0.7	0.6	0.5	0.4	0.3	0.2	0.1
600	0.9	0.8	0.7	0.6	0.5	0.4	0.3	0.2	0.1
700	0.9	0.8	0.7	0.6	0.5	0.4	0.3	0.2	0.1
800	0.9	0.8	0.7	0.6	0.5	0.4	0.3	0.2	0.1
Critical/Supercritical Tests: Test Pressure Critical, 10% and 20% Above Critical Pressure									
			P (kPa)= 3729			**4102**		**4475**	
G (kg/m²-s)	**Nominal Test Section Inlet Temperature (°C)**								
200	110	100	90	80	70	60	50	40	30
300	110	100	90	80	70	60	50	40	30
400	110	100	90	80	70	60	50	40	30
500	110	100	90	80	70	60	50	40	30
600	110	100	90	80	70	60	50	40	30
700	110	100	90	80	70	60	50	40	30
800	110	100	90	80	70	60	50	40	30

must be measured very accurately to yield the coolant heat duty. While the coolant flow rate can be measured very accurately (± 0.15%) using a Coriolis mass flow meter, an appreciable coolant-side temperature rise is needed for acceptable uncertainties. For the small quality or temperature increments desired in this study to represent local phenomena, the coolant heat duties are very small. Therefore, extremely low flow rates are needed to maintain a measurable coolant temperature rise. However, a low coolant flow rate results in low coolant-side heat transfer coefficients, which make the coolant-side the governing resistance, leading to very poor and even unacceptable uncertainties in the refrigerant-side heat transfer coefficients.

To solve these conflicting constraints, the heat duty determination and resistance ratio issues were decoupled. By introducing a closed, high flow rate primary coolant loop, a high refrigerant-to-coolant resistance ratio could be established easily. The test section heat duty was then determined in an open secondary coolant loop in which the open loop coolant flows at very low flow rates. The low secondary coolant flow rate ensured a large temperature rise, resulting in low uncertainties in the test section heat duty.

Figure 2 shows a schematic of the test facility designed to address all these considerations. In the condensation tests, because the refrigerant enters and exits the test section as a two-phase mixture, the test section heat duty must be deduced indirectly from the coolant side. The inlet and outlet qualities (enthalpies) were determined through pre- and post-cooler energy balance. The procedure for determining the test section inlet and outlet qualities and test section heat duty is described in the following sections.

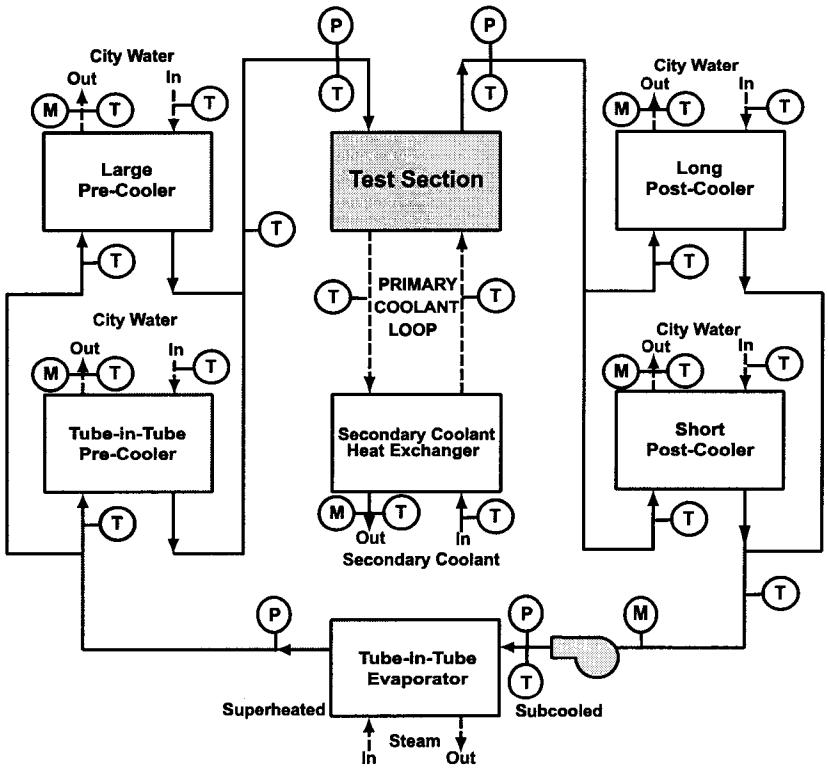

Figure 2 Test Facility Schematic

Experimental Facility

Phase-change tests

Subcooled liquid refrigerant was pumped through a tube-in-tube evaporator, in which steam flows counter-current to the refrigerant to boil and superheat it. The superheated state was ensured by a combination of a sight glass and temperature and pressure measurements. Temperature and pressure measurements at the superheated state enabled determination of the refrigerant enthalpy. The superheated vapor entered one of two pre-coolers, where city water at the desired (variable) flow rate was used to partially condense the vapor. For low mass fluxes ($G < 600$ kg/m^2-s), each pre-cooler was a tube-in-tube heat exchanger, with the long pre-cooler approximately three times longer than the short pre-cooler. All the heat exchanger dimensions are summarized in Tables 5 and 6. For high mass fluxes ($G \geq 600$

Table 5. Tube-in-Tube Heat Exchanger Dimensions

Tube		Material	Length (m)	Tube O.D. (mm)	Wall Thickness (mm)	Manufacturer
Test Section Heat Exchanger						
Inner Tube		Copper	0.292	12.70	1.65	In house
Outer Tube		Stainless Steel		19.05	1.65	In house
Pre-Coolers						
Long	Inner Tube	Stainless Steel	1.47	6.35	0.89	In house
	Outer Tube	Stainless Steel		12.70	0.89	In house
Short	Inner Tube	Stainless Steel	0.56	6.35	0.89	In house
	Outer Tube	Stainless Steel		12.70	0.89	In house
Post-Coolers						
Long	Inner Tube	Stainless Steel	1.47	6.35	0.89	In house
	Outer Tube	Stainless Steel		12.70	0.89	In house
Short	Inner Tube	Stainless Steel	0.56	6.35	0.89	In house
	Outer Tube	Stainless Steel		12.70	0.89	In house
Evaporator						
Inner Tube		Stainless Steel	5.90	12.70	1.65	Exergy Model 00528
Outer Tube		Stainless Steel	5.90	25.40	1.65	

Table 6. Shell-and-Tube Heat Exchanger Dimensions

Length (m)	Material	Shell-Side		Tube-Side		Tube Count	Baffle Count	HT Area (m^2)	Manufacturer
		O.D. (mm)	Wall (mm)	O.D. (mm)	Wall (mm)				
Secondary Heat Exchanger									
0.248	Stainless Steel	28	1.25	3.18	0.32	19	9	0.04	Exergy Model 00540-4
Pre-Cooler									
0.311	Stainless Steel	41	1.65	3.18	0.32	55	7	0.13	Exergy Model 00256-2

kg/m^2-s), the long pre-cooler was replaced by a shell-and-tube heat exchanger (Exergy, model 00256-2). These different pre-coolers, with their different heat transfer surface areas, and variable cooling water flow rates helped establish a wide range of refrigerant conditions at the test section inlet. The heat duty of the pre-cooler was given by:

$$\dot{Q}_{pre} = \dot{m}_{water,pre}\,\Delta h_{water,pre} \tag{35}$$

This heat duty, in conjunction with the refrigerant temperature and pressure measurements at the inlet of the pre-cooler, yielded the test section inlet quality:

$$\begin{aligned} \dot{Q}_{pre} &= \dot{m}_{refg}(h_{refg,in} - h_{refg,out}) \\ x_{test,in} &= x(P, h_{refg,out}) \end{aligned} \tag{36}$$

Refrigerant exiting the pre-coolers entered the test section, which was a counterflow tube-in-tube water-cooled heat exchanger. After flowing through the test section, one of two tube-in-tube post-coolers (similar in design and function to the tube-in-tube pre-coolers) downstream of the test section was used to completely condense and subcool the refrigerant. The subcooled refrigerant enthalpy at the exit of the post-cooler, and an energy balance on the post-cooler, were used to deduce the refrigerant enthalpy and quality at the outlet of the test section as follows:

$$\dot{Q}_{post} = \dot{m}_{water,post}\,\Delta h_{water,post} \tag{37}$$

$$Q_{post} = m_{refg}(h_{refg,in} - h_{refg,out})$$
$$x_{test,out} = x(P, h_{refg,in}) \tag{38}$$

The test section quality was the average of the test section inlet and outlet qualities.

The subcooled refrigerant mass flow rate was measured at the outlet of the post-cooler and then pumped back to the evaporator by a magnetic drive gear pump (Micropump) as specified in Table 7. Two pump heads were used in the present study to obtain the full range of mass flux under consideration in the present study. A bladder-type accumulator (Accumulators Inc., model A1-3100) was located upstream of the evaporator to maintain the system pressure at a desired constant value. A nitrogen tank connected to the accumulator was used to vary the bladder pressure to obtain the desired system pressures.

A 0.292 m-long tube-in-tube heat exchanger (Table 5) was used as the test section. Refrigerant flowed through the inner tube, while being condensed by a "primary closed loop coolant" water stream flowing trough the annulus in counterflow (Figure 2). This primary coolant in turn rejected heat to an open loop city water stream in a shell-and-tube heat exchanger (Table 6). This arrangement of primary and secondary coolant loops satisfied the

Table 7. Refrigerant Pump Specifications

Pump Head					
Model	**Maximum Flow Rate (gpm)**	**Maximum System Pressure (psig)**	**Differential Pressure (psi)**	**Material**	**Manufacturer**
219/56C	0.466	1500	100	Stainless Steel	Micropump
2200/56C	2	1000	75	Stainless Steel	Micropump

Motor						
Frame	**HP**	**Speed (rpm)**	**Voltage (V)**	**Frequency (Hz)**	**Phase**	**Manufacturer**
56C	1/2	1725	230/460	60	3	Reliance

Variable Frequency Drive					
Model	**HP**	**kW**	**Input**	**Output**	**Manufacturer**
Series 15P Mini Inverter	0.5	0.37	115 V/1 Phase	230 V/3 Phase	Baldor Motors and Drives

requirements for the accurate determination of both the test section heat duty, and the refrigerant heat transfer coefficient as follows. Primary coolant flowing at a high flow rate through an annulus with a small gap (1.52 mm) ensured that the dominant heat transfer resistance in the test section was on the refrigerant side. At the required high flow rate of the primary coolant, the temperature rise in this coolant was very small and prone to high uncertainties. Therefore, a secondary coolant flowing at a much lower flow rate was used to obtain a larger temperature rise, and thus measured the test section duty accurately. The secondary coolant flow rate was adjusted as the test conditions changed to maintain a reasonable ΔT and also small condensation duties in the test section. It should be noted that this approach depended upon the minimization of spurious heat losses and gains from/to the primary coolant loop so that the test section heat duty could be calculated accurately from a measurement of the secondary coolant heat load. Thus, it was essential that the primary coolant circulation pump heat dissipation and the ambient heat loss were small fractions of the secondary loop duty, and also that they could be estimated with reasonable accuracy. This ensured that the test section heat load was relatively insensitive to pump heat addition and ambient heat loss, as will be demonstrated in the analysis described in Chapter 4. Low thermal conductivity insulation and small temperature differences between the primary coolant and the ambient minimized the heat loss to the ambient. Similarly, the heat addition to this loop was minimized by using a pump with an extremely low heat dissipation.

Supercritical cooling tests

The test facility developed for phase change tests was also used for the supercritical cooling tests. Two different size pre-coolers, in conjunction with a variable city water flow rate, were used to obtain the test-section inlet temperature range of 30 to 110°C. The large pre-cooler was used to achieve low inlet temperatures at the test section, while the small pre-cooler was used for the high temperature points. The tube-in-tube post-coolers downstream of the test section were again used to cool the refrigerant to a fully liquid state, before it was pumped back to the evaporator. Unlike phase-change tests, for these supercritical experiments, refrigerant enthalpies at the test section inlet and outlet could be directly determined from the corresponding measured temperatures and pressures. Therefore,

temperatures and pressures measured at the test section inlet and outlet were used to directly evaluate the refrigerant enthalpy. In addition, the refrigerant enthalpy at the inlet of the pre-cooler and an energy balance on the pre-cooler were also used to validate independently the enthalpy of the refrigerant at the inlet of the test section obtained from refrigerant-side measurements. Similarly, the refrigerant enthalpy at the exit of the post-cooler and an energy balance on the post-cooler were used to validate the enthalpy of the refrigerant at the outlet of the test section.

The technique of decoupling the determination of heat duty and heat transfer coefficient through thermal amplification described previously enabled accurate test section heat duty measurement. This was particularly important because of the low heat duties involved in the determination of local heat transfer coefficients over small increments of refrigerant temperature needed to capture the sharp variations in heat transfer coefficient near the critical region.

In addition to determining the refrigerant heat transfer coefficients directly from the measured UA, as described above, a redundant method for obtaining the refrigerant heat transfer coefficients was also utilized. Thus, three T-type thermocouples (26 gauge) were soldered to the outer wall of the inner tube through which the refrigerant flowed. The first thermocouple was placed 1.59 mm (1/16 in) from the refrigerant inlet as shown in Figure 3,

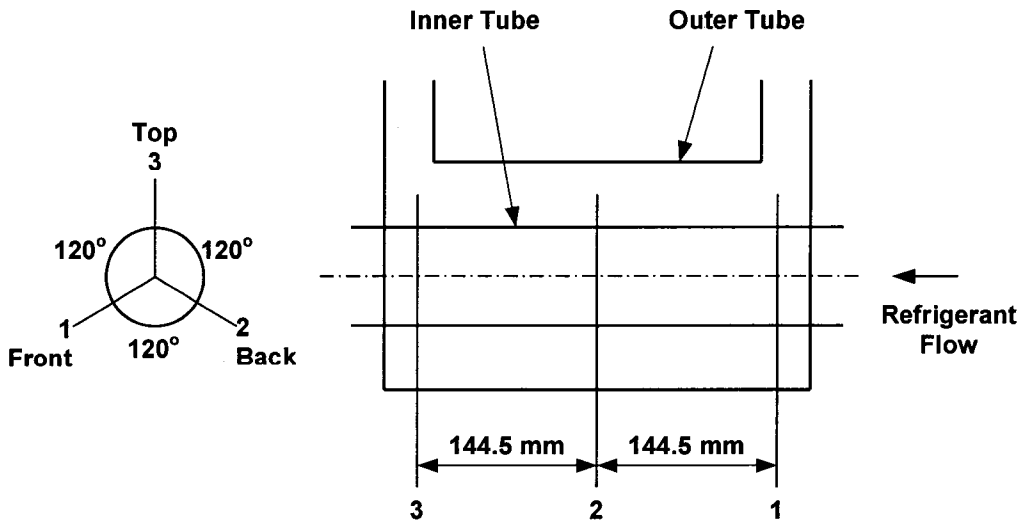

Figure 3. Schematic of Wall-Mounted Thermocouple Locations for the Test Section

with the second and third thermocouples placed further downstream, at intervals of 144.5 mm (5.69 in). In addition, the thermocouples were placed 120° apart from each other in the circumferential direction as shown in Figure 3 to account for temperature variations due to potential stratification. The refrigerant-to-wall temperature difference (after subtracting the ΔT from the inner wall to the outer wall) provided an additional estimate of the refrigerant heat transfer coefficient for the phase-change and supercritical tests. The agreement between these two methods of obtaining the refrigerant heat transfer coefficients is described in the subsequent sections.

Instrumentation and Data Acquisition

The measurement ranges and accuracies of the instrumentation used in this study are summarized in Table 8. The refrigerant and secondary coolant flow rates were measured using Coriolis mass flow meters (Micromotion Elite flow sensor model number CFM025 and Micromotion type D6 sensor), with accuracies of ±0.10% and 0.15% of the reading, respectively. Cooling water flow rates for the pre- and post-coolers were measured using a set of three Gilmont Accucal flow meters, with the flow rate ranges of 0.2 to 4.5 liter per minute, 0.2 to 2.2 liter per minute, and 0.1 to 0.78 liter per minute. The accuracies of these flow meters were ±2% of the reading, or ±1 scale division, whichever was greater. For each data point, the cooling water was routed through the rotameter that yielded the highest accuracy. Integral precision valving with high turndown ratios allowed steady control of the cooling water flow rates. Rosemount model 2088 absolute and gage pressure transmitters with an accuracy of ±0.25% of the calibrated span were used to measure pressures of the refrigerant at various locations. The maximum span for these transducers was 0 to 5,515.8 kPa. Pressure drops were measured using a bank of 3 Rosemount model 3051C differential pressure transmitters with the following spans: 0-248.2, 0-62.27, and 0-6.227 kPa. These differential pressure transducers had an accuracy of ±0.075% of span. For each data point, the measurement was taken using the transducer that yielded the highest accuracy. Temperatures were measured using a combination of Platinum RTDs (Omega PR-13, accuracy: ±0.3°C for 0 – 100°C) and Type-T thermocouples (accuracy: ±1.0°C or ±0.75% of the reading, whichever was greater). The primary coolant volumetric flow rate was initially

Table 8. Instrumentation Specifications

Fluid	Manufacturer	Model	Range	Accuracy
Temperature				
R404A and Water	Omega	Platinum RTD Pr-13	0 – 100°C	±0.3°C
Water	Thermocouple	T		±1.0°C
Mass Flow Rate				
R404A	Micromotion	CFM025	0 – 0.3 kg/s	±0.10% Reading
Secondary Coolant (Water)	Micromotion	D6	0 – 0.015 kg/s	±0.15% Reading
Volumetric Flow Rate				
Pre and Post-Cooler Coolant (Water)	Gilmont	Accucal	0.1 – 0.78 lpm	±2% Reading
	Gilmont	Accucal	0.2 – 2.2 lpm	±2% Reading
	Gilmont	Accucal	0.2 – 4.5 lpm	±2% Reading
Primary Coolant (Water)	Dwyer	RMC-144-SSV	0.8 – 7 gpm	±2% Reading
Primary Coolant (Water)	Rosemount	8711 TSE-30-FS1 Flow Tube and 8712C magnetic Flow Transmitter	0 – 25.02 lpm	±0.5% Reading
Pressure				
R404A	Rosemount	2088 (Absolute)	0 – 5515.8 kPa	±13.79 kPa
R404A	Rosemount	3051C (Differential)	0-248.2 kPa	±0.1862 kPa
R404A	Rosemount	3051C(Differential)	0-62.27 kPa	±0.0467 kPa
R404A	Rosemount	3051C(Differential)	0-6.227 kPa	±0.0047 kPa

measured using a rotameter (Dwyer –144-SSV with an accuracy of ±2% of the full scale reading), and later on a magnetic flowmeter (Rosemount Model 8712C magnetic flow transmitter with Model 8711 magnetic flow tube, with an accuracy of ±0.5%). As explained in Chapter 4, the accuracy of this flow meter was not very significant for the data analysis.

All data were recorded using a TEMPSCAN data acquisition system (Iotech TempScan/1100 High Speed Temperature Measurement system with an expansion chasis Exp/10A. The main system had 16 channels for RTD measurement, while the expansion chasis provided 16 channels for thermocouple and voltage measurements) that could record up to 992 inputs for temperature, pressure, flow rate, and other signal measurements, at

speeds of up to 960 channels per second for real-time data analysis. Measured temperatures, flow rates, and pressures were continuously displayed and plotted as a function of time to ensure that steady state conditions were reached. Once steady state was achieved, the sight glasses, and pressure and temperature readings were inspected to ensure an adequate degree of superheat and subcooling. Two data points were recorded for each case, with each data point representing an average of 120 scans taken every second over a two-minute period.

Experimental Procedures

System charging

The refrigerant-side of the test facility (shown in Figure 2) was initially pressurized with nitrogen gas and a trace amount of R134A. An electronic leak detector (CPS model L-709a) was used to detect any possible leaks around all of the fittings. The test facility was evacuated to a system pressure of 150 microns (20.03 Pa) using a vacuum pump (DV Industries model DV-85N). A Thermal Engineering vacuum gauge (model 14571) with the capability of measuring pressures as low as 10 microns (1.33 Pa) was used to measure the vacuum pressure. The system was charged with approximately 3 kg of R404A immediately after evacuation, and the system pressure was monitored over a 24-hour period to verify system integrity. The system was also charged with cooling water in the primary loop and leak-tested. A relief valve in the primary loop was used to purge the air from this loop.

System start-up

Testing commenced with the pre- and post-condenser water flow, refrigerant flow, primary and secondary water flow, and steam flow being turned on in this order. The desired refrigerant mass flow rate was achieved through a combination of needle valves and a variable frequency drive (Table 7) on the pump. The desired refrigerant testing pressure was maintained through controlling the external pressure to the accumulator by a nitrogen tank.

Based on the mass flux under consideration and the desired test section inlet quality (or temperature for supercritical tests), one of the two available large and small pre-coolers and the coolant flow rate, as well as the volumetric flow meter that yielded the highest accuracy were selected. For example, at low refrigerant mass flux and high test section inlet

quality (or inlet temperature for supercritical tests), the low-range water flow meter and small pre-cooler were selected. For phase-change tests, using the superheated refrigerant inlet enthalpy and mass flow rate, and the measured water-side heat duty, the pre-cooler outlet quality (also the test section inlet quality) was calculated through an energy balance. The test-section primary-coolant flow rate was selected to obtain a low coolant heat transfer resistance and pump heat addition. With the secondary coolant inlet temperature fixed by the city water temperature, the flow rate determined the outlet temperature, and thus the temperature difference available for heat transfer between the primary and secondary coolants. Therefore, secondary flow rate indirectly controlled the cooling duty across the test section, i.e. test section outlet quality for phase-change tests or temperature for supercritical tests. This flow rate was also selected to obtain a large temperature difference across the secondary heat exchanger, which allowed for the test section heat duty to be measured accurately. One out of the two post-coolers and the water flow rate were selected to fully condense and subcool the refrigerant while maintaining a measurable temperature difference at the outlet of the post-cooler. Again, for phase-change tests, an energy balance in the post-cooler was used to derive the post-cooler inlet (also the test section outlet) vapor quality. The subcooled refrigerant was also measured by a coriolis flow meter and pumped back to the evaporator.

For supercritical tests, temperatures and pressures were measured directly at the test section inlet and outlet to evaluate refrigerant enthalpies and ensure that the desired conditions were established. Pre- and post-cooler energy balances were also computed to independently validate these conditions while the test was in progress.

The system pressures, temperatures, and flow rates were constantly monitored during the test. Steady state conditions took between 30 minutes and 3 hours to obtain, depending on the specific test condition under consideration. After steady state was established, the data point was recorded. Water flow rates for the pre- and post-coolers and the primary and secondary coolants (as necessary) were then adjusted to obtain another average test section condition at the same refrigerant flow rate. This process was repeated until all the data points needed in this study (Table 4) were completed.

CHAPTER 4. DATA ANALYSIS

Data taken in this study were analyzed using *Engineering Equation Solver* (EES) software (Klein 2003). In this chapter, sample calculations for both phase change and supercritical tests are provided to show the derivation of the test section quality, heat transfer coefficients and their associated uncertainties from the measured data. The representative phase-change case demonstrated here is for a data point of G = 399 kg/m^2-s, x = 0.4950, and p = 0.8×P_{crit}. For a 9.4 mm I.D. tube, with a flow area of 6.94×10^{-5} m^2, this corresponds to a refrigerant flow rate of 2.77×10^{-2} kg/s. Table 9 shows a summary of the measured data for this case. The detailed calculation procedure is reported in Appendices A – F.

Average Test Section Quality

Test section inlet quality

The measured quantities for required calculations are the inlet and outlet temperatures, as well as the pressure and flow rate of the water-side of the pre-cooler, in addition to refrigerant flow rate, inlet temperature and pressure. The water-side heat duty of the pre-condenser was calculated using the following equation:

$$Q_{pre} = \dot{m}_{water,pre}\,\Delta h_{water,pre} \tag{39}$$

where $\dot{m}_{wter,pre}$ and $\Delta h_{water,pre}$ are the mass flow rate, and enthalpy change of the cooling water in the pre-cooler. The water properties needed to calculate the mass flow rate and the enthalpies were evaluated at the mean water temperature and pressure. Since the refrigerant enters the pre-cooler as a superheated vapor, its enthalpy $h_{refg,pre,i}$ could be calculated using the refrigerant temperature and pressure measurements at the inlet of the pre-cooler. This refrigerant enthalpy, in conjunction with the heat duty obtained from water-side, yielded the test section inlet quality:

$$\begin{aligned} Q_{pre} &= \dot{m}_{refg}\,(h_{refg,in} - h_{refg,out}) \\ x_{test,in} &= x_{pre,out} = x(P_{pre,out}, h_{refg,out}) \end{aligned} \tag{40}$$

Thus, for this representative case, with the pre-cooler water flow rate at 5.33×10^{-5} m^3/s, and

Table 9. Measured Data for Representative Case

Variable	Units	Values	Description
m_{refg}	kg/s	0.0277	Mass flow rate, refrigerant
m_{sec}	kg/s	0.00235	Mass flow rate, secondary coolant
$Vol_{pre\text{-}cooler}$	m^3/s	5.33×10^{-5}	Volumetric flow rate, pre-cooler water
$Vol_{post\text{-}cooler}$	m^3/s	3.25×10^{-5}	Volumetric flow rate, post-cooler water
$Vol_{primary}$	gpm	1.85	Volumetric flow rate, primary coolant water
$P_{pre,in}$	kPa	3098.58	Pressure, pre-cooler inlet
$P_{test,in}$	kPa	3006.59	Pressure, test section inlet
$P_{test,out}$	kPa	3003.58	Pressure, test section outlet
$P_{post,out}$	kPa	2981.89	Pressure, post-cooler outlet
$T_{pre,in}$	°C	103.77	Temperature, pre-cooler inlet
$T_{pre,out}$	°C	62.30	Temperature, pre-cooler outlet
$T_{post,in}$	°C	60.87	Temperature, post-cooler inlet
$T_{post,out}$	°C	51.76	Temperature, post-cooler outlet
$T_{test,in}$	°C	61.76	Temperature, test section inlet
$T_{test,out}$	°C	61.33	Temperature, test section outlet
$T_{w,pre,in}$	°C	13.92	Temperature, pre-cooler water inlet
$T_{w,pre,out}$	°C	26.02	Temperature, pre-cooler water outlet
$T_{w,sec,in}$	°C	17.88	Temperature, secondary loop water inlet
$T_{w,sec,out}$	°C	43.39	Temperature, secondary loop water outlet
$T_{w,post,in}$	°C	13.66	Temperature, post-cooler water inlet
$T_{w,post,out}$	°C	24.43	Temperature, post-cooler water outlet
$T_{w,prim,in}$	°C	45.30	Temperature, primary loop water inlet
$T_{w,prim,out}$	°C	45.51	Temperature, primary loop water outlet
$T_{wall,R}$	°C	46.95	Temperature, outer tube wall of test section
$T_{wall,M}$	°C	46.71	Temperature, outer tube wall of test section
$T_{wall,L}$	°C	N/A	Temperature, outer tube wall of test section
DP	kPa	0.318	Differential pressure, test section refrigerant

measured inlet and outlet temperatures of 13.92 and 26.02°C, the pre-cooler water density was 999.4 kg/m^3, resulting in a mass flow rate of 5.33×10^{-2} kg/s and a heat duty of 2.696 kW. The measured refrigerant temperature and pressure at the inlet of the pre-cooler were 103.8°C and 3099 kPa, respectively, resulting in an enthalpy of 441.3 kJ/kg. From equations (39) and

(40), the refrigerant enthalpy at the pre-cooler outlet (test section inlet) was 343.7 kJ/kg. Here, it was assumed that the heat loss from the pre-cooler outlet to the test section inlet was negligible. For a measured pre-cooler outlet pressure of 3007 kPa, the refrigerant quality at test section inlet was 0.5802.

Test section outlet quality

The test section outlet quality was determined using a similar method as described in the previous section. Instead of the pre-cooler water heat duty, the post-cooler water heat duty was used to calculate the test section outlet quality as follows:

$$Q_{post} = m_{water,post}\,\Delta h_{water,post} \tag{41}$$

$$\begin{aligned} Q_{post} &= m_{refg}\,(h_{refg,in} - h_{refg,out}) \\ x_{test,out} &= x_{post,in} = x(P_{post,in}, h_{refg,in}) \end{aligned} \tag{42}$$

The post-cooler water flow rate was 3.3×10^{-5} m^3/s, with measured inlet and outlet temperatures of 13.66 and 24.43°C, respectively. With a density of 999.5 kg/m^3 and a mass flow rate of 3.25×10^{-2} kg/s, the post-cooler heat duty was calculated to be 1.463 kW. The refrigerant left the post-cooler as subcooled liquid, allowing the refrigerant enthalpy to be determined from the measured temperature and pressure. Thus, with the refrigerant temperature and pressure at the outlet of the post-cooler of 51.76°C and 2982 kPa, the refrigerant enthalpy at the post-cooler outlet was 277.9 kJ/kg. Using equations (41) and (42), the refrigerant enthalpy at the post-cooler inlet (test section outlet) was determined to be 330.8 kJ/kg. For a measured pressure at the post-cooler inlet of 3004 kPa, the refrigerant quality at the test section outlet was 0.4098. Again, it was assumed that the heat loss from the test section outlet to the post-cooler inlet was negligible.

The average test section quality was then determined as follows:

$$x_{test,avg} = \frac{1}{2}\left(x_{test,in} + x_{test,out}\right) \tag{43}$$

which resulted in $x_{test,avg} = 0.4950$.

Test Section Heat Duty

The test section heat duty could be calculated using the energy balance between the

test section and the secondary loop expressed as follows:

$$Q_{w,test} = Q_{w,\sec} + Q_{ambient} - Q_{pump} \tag{44}$$

where $Q_{w,test}$, $Q_{w,sec}$, $Q_{ambient}$, and Q_{pump} are the test section heat duty, secondary water heat duty, ambient heat loss and pump heat addition, respectively. Figure 4 shows a schematic of the relationship between $Q_{w,test}$, $Q_{w,sec}$, $Q_{ambient}$, and Q_{pump}. The secondary water heat duty could be calculated as follows, with the properties evaluated at the mean temperature and pressure:

$$Q_{w,\sec} = \dot{m}_{w,\sec}\, c_{p,w,\sec}(T_{w,\sec,o} - T_{w,\sec,i}) \tag{45}$$

For a measured secondary flow rate of 2.35×10^{-3} kg/s, with inlet and outlet temperatures of 17.88 and 43.39°C, respectively, the secondary water heat duty was 0.251 kW.

The procedures for calculating the pump heat addition and ambient heat loss from the primary loop are discussed below.

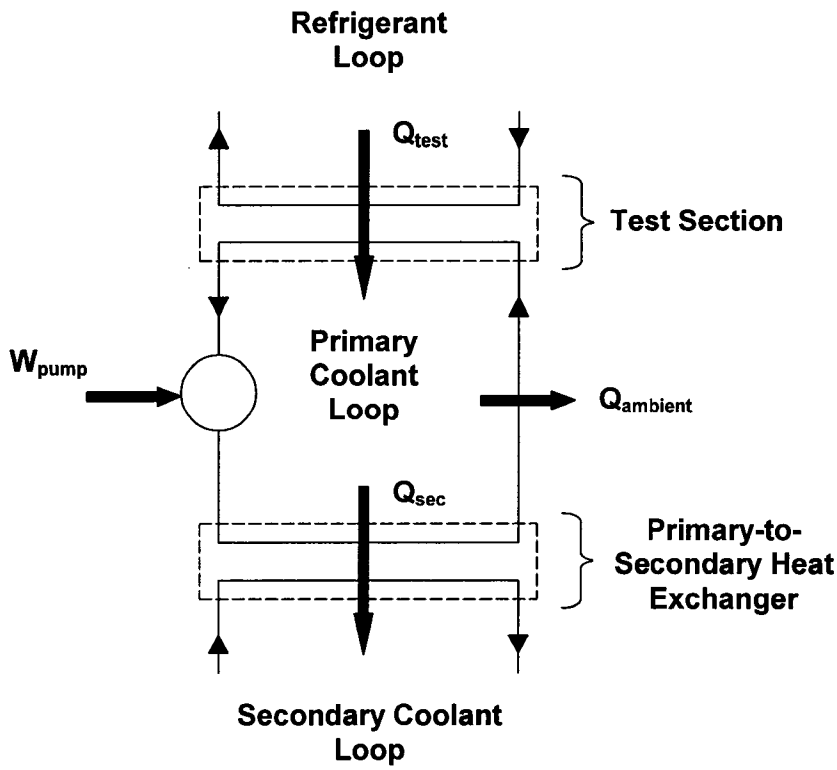

Figure 4. Primary and Secondary Coolant Flows

Pump heat addition

To calculate the pump heat addition, the pressure drop in the primary loop must be calculated first to determine the pumping power required for water circulation. The pressure drop in the primary loop included the pressure drops in the tubing and fittings, primary flow meter, annulus-side pressure drop of the test section, and the shell-side pressure drop of the primary-to-secondary shell-and-tube heat exchanger. The heat exchanger and tubing dimensions, and types of the fittings involved in the discussion below are summarized in Table 10. A detailed calculation is also shown in Appendix B.

Pressure loss in tubing

The pressure loss in the tubing included frictional and minor losses. For the stainless steel tubing with an inner diameter of 10.92 mm (12.70 mm O.D. with wall thickness of 0.89 mm) and a measured volumetric flow rate of 1.17×10^{-4} m^3/s, the velocity of the circulating water in the tube was calculated as 1.25 m/s, resulting a Reynolds number of 22,754 (water properties were evaluated at the average temperature of the circulating fluid). With a roughness for drawn tubing of 0.0015 mm (Munson *et al.* 1998) and the above calculated Reynolds number, the Churchill correlation (Churchill 1977b) yielded a friction factor of 0.025.

The pressure drop in the tubing was calculated as follows:

$$\Delta P_{friction,tube} = \frac{1}{2} \cdot f \cdot \rho \cdot V^2 \cdot \frac{L_{tube}}{(I.D.)_{tube}} \tag{46}$$

For 2.58 m of tubing in the primary loop, the pressure drop was 4.61 kPa.

The minor losses due to fittings were calculated as follows, where K_{total} is the total K-factor of the fittings (Munson *et al.* 1998) (see Table 10).

$$\Delta P_{minor,tube} = \frac{1}{2} \rho V^2 K_{total} \tag{47}$$

Assuming the fluid velocity was the same as in the tubing, the total minor loss was 14.83 kPa. Thus, from equations (46) and (47), the total pressure drop in the tubing due to frictional and minor losses was 19.44 kPa.

Table 10. Tubing Geometry and Fitting Type

Tubing	
Tube O.D. (mm)	$(O.D.)_{tubing} = 12.70$
Tube thickness (mm)	$w_{tubing} = 0.89$
Tube roughness (mm)	Drawn tubing, $\varepsilon = 0.0015$
Tube length (m)	$L_{tube} = 2.58$
Test Section	
Outer Tube O.D (mm)	$(O.D.)_{outer} = 19.05$
Outer tube thickness (mm)	$w_{outer} = 1.65$
Outer tube roughness (mm)	Drawn tubing, $\varepsilon = 0.0015$
Inner Tube O.D. (mm)	$(O.D.)_{inner} = 12.70$
Inner tube thickness (mm)	$w_{inner} = 0.89$
Test section length (m)	$L_{test} = 0.292$
Secondary Heat Exchanger	
Shell O.D. (mm)	$(O.D.)_{shell} = 28.45$
Shell thickness (mm)	$w_{shell} = 1.25$
Heat exchanger length (m)	$L_{test} = 0.2302$
Fittings	
90° threaded elbow, long radius	×7, K = 0.7/each
Tee, line flow, threaded	×2, K = 0.9/each
Tee, branch flow, threaded	×4, K = 2.0/each

Pressure loss in the flow meter

According to manufacturer specifications, the pressure drops at the minimum (0.8 gpm) and maximum (7.0 gpm) flow rates through the volumetric flow meter were 6.22 kPa and 29.7 kPa, respectively. For simplicity, an interpolation between the minimum and maximum flow rates was used to calculate the pressure drop (in kPa) at the test flow rate. Thus, for a 1.85 gpm (1.17×10^{-4} m^3/s) primary coolant flow rate, the pressure loss in the flow meter was 10.20 kPa.

Pressure loss in the test section

The primary water flowed through the annular-side of the test section. The hydraulic diameter of the annulus side could be calculated using the inner tube O.D. and the outer tube

I.D.

$$D_{h,annulus} = \frac{4A_{f,annulus}}{P} = (I.D.)_{outer} - (O.D.)_{inner} \tag{48}$$

where $A_{f,annulus}$ and P are the free flow area and perimeter of the annulus-side, respectively. With an outer tube I.D. of 15.75 mm and a inner tube O.D. of 12.70 mm, the free flow area was 6.81×10^{-5} m^2, the perimeter was 89.38 mm and the hydraulic diameter was 3.05×10^{-3} mm. At a primary coolant flow rate of 1.17×10^{-4} m^3/s, the flow velocity and Reynolds number were 1.71 m/s and 8,736, respectively.

The annulus-side friction factor could be calculated using curvefits for the laminar and turbulent friction factor data of Kays and Leung (1963) by Garimella and Christensen (1995). The transition between laminar and turbulent flow was determined using curve fits to the lower (transition from laminar) and upper (transition to turbulent) critical Reynolds numbers for different annulus radius ratios reported by Walker *et al.* (1957). The transition Reynolds number for annulus was a function of the radius ratio, which was defined as follows:

$$r^* = \frac{(O.D.)_{inner}}{(I.D.)_{outer}} \tag{49}$$

For the current sample conditions, the lower and upper transition Reynolds numbers were 2,643 and 3,233, respectively. The flow in the annulus was therefore in the turbulent region, with a friction factor of 0.03. The annulus-side frictional pressure drop (in the test section) could be calculated as follows:

$$\Delta P_{annulus} = \frac{1}{2} \cdot f_{annulus} \cdot \rho \cdot V_{annulus}^{\ 2} \cdot \frac{L_{test}}{D_{h,annulus}} \tag{50}$$

Thus, the primary water pressure loss in the test section was 4.79 kPa.

Pressure loss in the secondary shell and tube heat exchanger

The primary water flowed through the shell side of the secondary heat exchanger. According to the manufacturer, the shell-side pressure drop (in psi) was a function of the volumetric flow rate (in gpm) as follows:

$$\Delta P_{shell}(\text{in psi}) = 0.49157(\text{Actual Flowrate in gpm})^{1.9} \tag{51}$$

For a primary water flow rate of 1.17×10^{-4} m^3/s (1.85 gpm), the pressure loss on the shell side of the secondary heat exchanger was 10.91 kPa (1.58 psi).

Pump efficiency

From the above calculations, the total pressure loss for the primary water was 45.33 kPa as given by

$$\begin{aligned}\Delta P_{primary} &= \Delta P_{tube} + \Delta P_{flow\,meter} + \Delta P_{annulus} + \Delta P_{shell} \\ &= 19.44 + 10.20 + 4.79 + 10.91\end{aligned} \tag{52}$$

The ideal pump work was a function of the total water pressure drop and was given by:

$$W_{ideal} = \text{Water Flow Rate} \cdot \Delta P_{primary} \tag{53}$$

The operating shaft work was given by:

$$W_{shaft} = \tau \cdot \omega \tag{54}$$

The applied torque and shaft rotational speed were supplied by the manufacturer (Micropump), as shown in Figure 5 for the Micropump Series 5000 H21 pump head model. The applied torque was a function of the primary water loop pressure drop (or pump pressure

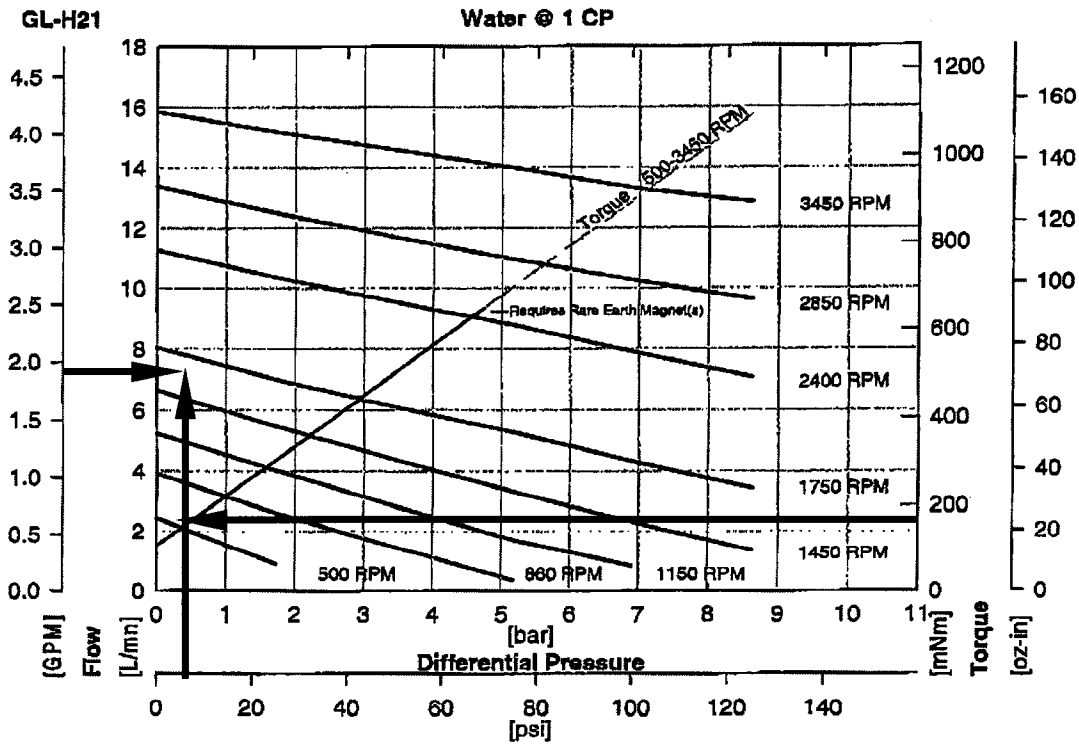

Figure 5. Micropump Series 5000 H21 Pump Curve

rise). The pump shaft rotational speed was a function of the actual flow rate and pressure drop. For a primary water flow rate of 1.17×10^{-4} m^3/s (1.85 gpm) and a total pressure loss in the primary loop of 45.33 kPa (6.58 psi), the ideal pump work was 5.29 W. The applied torque and the shaft rotational speed were 0.165 N-m and 1650 rpm according to the manufacturer's specification, resulting in a shaft work of 28.51 W. The pump efficiency and the pump heat addition could be calculated using the following equations:

$$\eta = \frac{W_{ideal}}{W_{shaft}} \tag{55}$$

$$Q_{pump} = (1-\eta)\cdot W_{shaft} \tag{56}$$

According to the above results, the pump efficiency was 18.6%, and the pump heat addition was 23.22 W (Here, it was assumed that all the pump losses are rejected into the coolant as heat).

Figure 6 shows the pump heat addition as a function of the volumetric flow rate. A

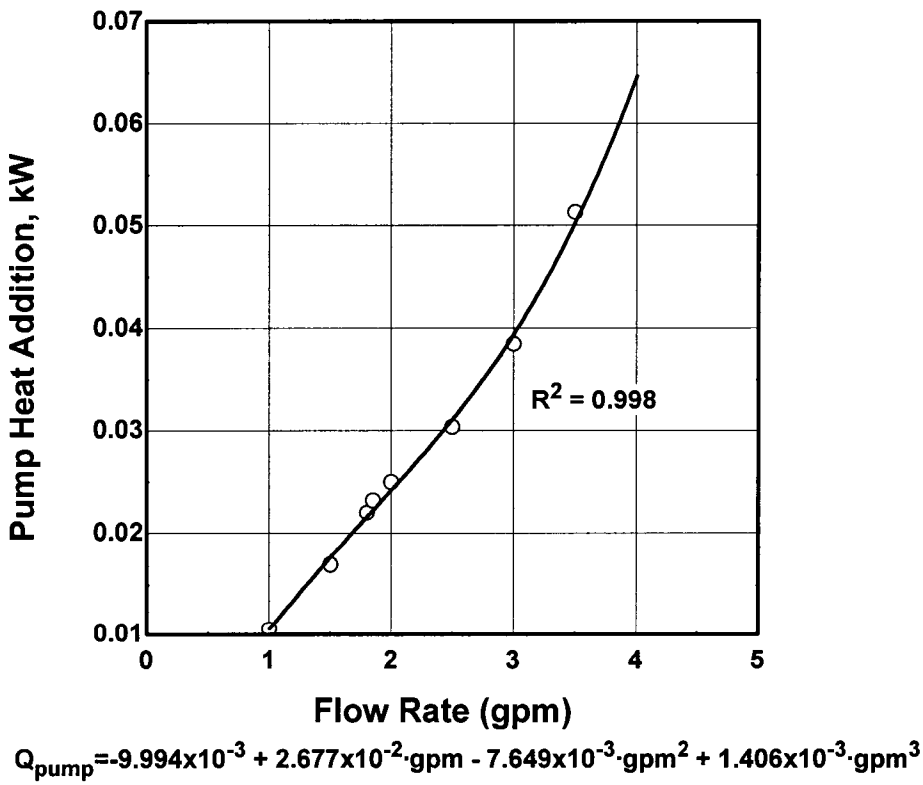

Figure 6. Pump Heat Addition vs. Flow Rate for Micropump Series 5000 H21 Pump

third-order polynomial least square curve fit was developed from the data in Figure 6 as follows:

$$Q_{pump}\ (\text{in KW}) = -9.994\times10^{-3} + 2.677\times10^{-2}\cdot(\text{Flow in gpm}) - 7.649\times10^{-3}\cdot(\text{Flow in gpm})^2 + 1.406\times10^{-3}\cdot(\text{Flow in gpm})^3 \quad (57)$$

For the representative data point, with a primary flow rate of 1.17×10^{-4} m^3/s (1.85 gpm), the pump heat addition calculated from equation (57) was 22.25 W.

Ambient heat loss

Ambient heat losses were minimized by using fiberglass insulation for the test section and the primary and secondary coolant loops. Furthermore, the small temperature differences between the fluid and the ambient (approximately 3°C) led to low heat losses. The heat loss from the primary coolant to the ambient consisted of losses form three locations: test section heat exchanger, secondary heat exchanger, and the rest of the plumbing in the primary loop. The heat was assumed to be lost from the average coolant temperature to the ambient temperature (~23°C). A detailed heat loss calculation is also shown in Appendix C.

Test section heat loss

For the test section, the heat flowed through the following resistances: water-side convection, outer-tube wall, insulation, natural convection, and radiation. Figure 7 shows a schematic of the heat transfer resistance network.

The annulus-side heat transfer coefficient was calculated using curvefits developed by Garimella and Christensen (1995) for laminar and turbulent Nusselt numbers in annuli reported by Kays and Leung (1963). The transition between laminar and turbulent flow was determined using curve fits to the lower and upper critical Reynolds numbers for different annulus radius ratios reported by Walker et al. (1957).

For a primary flow rate of 1.17×10^{-4} m^3/s, the Reynolds number in the annulus of the test section was 8,736. With the lower and upper transition Reynolds numbers of 2,643 and 3,233, respectively, and a radius ratio of 0.807, the heat transfer coefficient in the annulus of the test section was 12,266 W/m^2-K. Thus, the water-side convective heat transfer resistance could be calculated as follows:

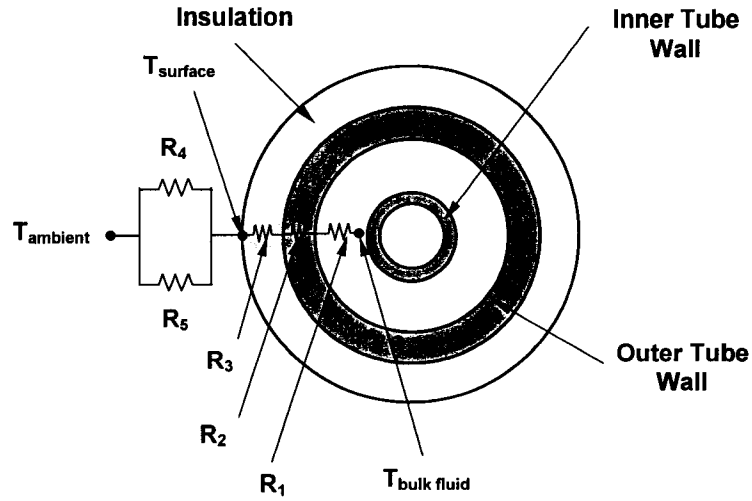

R_1 = Water resistance
R_2 = Tube wall resistance
R_3 = Insulation resistance
R_4 = Natural convection resistance
R_5 = Radiation resistance

Figure 7. Resistance Network for the Ambient Heat Loss Calculation

$$R_{conv} = \frac{1}{h_{annulus} \cdot A_{eff,annulus}} \tag{58}$$

where $A_{eff,annulus}$ is the annulus side heat transfer area:

$$A_{eff,annulus} = \pi (I.D.)_{outer\,tube} L_{test} \tag{59}$$

For a 15.75 mm inner diameter of the outer tube, and a 0.292 m test section, the annulus-side heat transfer area was 1.445×10^{-2} m^2, resulting in a water-side convective heat transfer resistance of 5.702×10^{-3} K/W.

The tube-wall resistance was calculated as follows:

$$R_{wall} = \frac{\ln\left[\frac{(O.D.)_{outer}}{(I.D.)_{outer}}\right]}{2\pi L_{test} k_{wall}} \tag{60}$$

where $(I.D.)_{outer}$ and $(O.D.)_{outer}$ are the inner and outer diameters of the outer tube wall. For the 0.292 m test section of the stainless steel tube (k = 15 W/m-K) with outer and inner diameters of 19.05 mm and 15.75 mm, respectively, the wall resistance was 6.914×10^{-3} K/W.

The resistance of the insulation was calculated in a similar way. With an insulation thickness of 25.4 mm (O.D. = 69.85 mm, I.D. = 19.05 mm) and a thermal conductivity of 0.019 W/m-K, the resistance of the insulation $R_{insulation}$ was 15.39 K/W.

Heat transfer from the insulation to the ambient air was due to natural convection and radiation. The natural convection resistance was based on the Rayleigh number, which is defined as follows:

$$Ra = \frac{g\beta\left(T_{surface} - T_{\infty}\right)D_{insulation}{}^{3}\rho^{2}\,\mathrm{Pr}}{\mu^{2}} \tag{61}$$

where $D_{insulation}$ is the outer diameter of the insulation, g is acceleration due to gravity , β is the volumetric coefficient of thermal expansion, ρ, μ and Pr are dry air properties evaluated at the fluid temperature defined as follows,

$$T_{fluid} = \frac{T_{surface} + T_{\infty}}{2} \tag{62}$$

$T_{surface}$ and T_{∞} are the surface temperature of the insulation and ambient temperature, respectively. Assuming the value of $T_{surface}$, the correlation suggested by Churchill and Chu (1975) could be used to determine the natural convection heat transfer coefficient h_{nc}. Through the following energy balance (equation 63), the surface temperature $T_{surface}$ and thus the ambient heat loss through the test section heat exchanger could be determined iteratively.

$$\begin{aligned} Q_{ambient,test} &= \frac{\left(T_{water} - T_{surface}\right)}{R_{conv} + R_{wall} + R_{insulation}} \\ &= h_{nc}A\left(T_{surface}\text{-}T_{ambient}\right) + \sigma A\left(T_{surface}{}^{4}\text{-}T_{ambient}{}^{4}\right) \end{aligned} \tag{63}$$

where A is the heat transfer area, $A = \pi D_{insulation} L_{test}$.

For a test section length of 0.292 m and an insulation outer diameter of 69.85 mm, the natural convection heat transfer coefficient was 2.681 W/m^2-K. The surface temperature and the test section ambient heat loss from the above equations were 25.35°C and 1.302 W, respectively. Of the 1.302 W from the surface, 0.898 W was attributed to radiation. It was assumed that the insulation has an emissivity of 1.0.

Secondary heat exchanger heat loss

The ambient heat loss through the primary-to-secondary shell-and-tube heat exchanger could be calculated in a manner similar to that for the test section ambient heat loss. The primary water flowed through the shell side of the secondary heat exchanger, and the wall was assumed to be at the bulk temperature. Hence, only the wall and insulation resistances were used in Equation (63). This assumption was reasonable because of the large water-side heat transfer coefficient. With a shell-side outer diameter of 28.45 mm, a wall thickness of 1.25 mm and a heat exchanger length of 0.203 m, for an average water temperature of 47.51°C, the heat lost to the ambient was 1.135 W.

Primary loop tubing heat loss

The ambient heat loss through the rest of the primary loop was also calculated as described above. However, in this case, the water flow is through a single tube instead of an annulus. The Churchill equation (Churchill 1977a) was used to calculate the water-side convection heat transfer resistance.

Thus, for a tube O.D. and wall thickness of 12.70 and 0.89 mm, respectively, and a primary water flow rate of 1.17×10^{-4} m^3/s, the flow velocity was 1.25 m/s. The corresponding Reynolds number and Nusselt number were 22,754 and 132.4, respectively, which yielded a water-side heat transfer coefficient of 7,578 W/m^2-K. The iterative procedure described in previous sections could now be followed to calculate the ambient heat loss in the primary loop plumbing. The total tubing length used here included tubing that connected the primary-to-secondary heat exchanger to the test section heat exchanger, as well as "equivalent" lengths for the pump housing and flow meter, which are defined as follows,

$$L_{equivalent} = \frac{A}{\pi D_{tubing}} \tag{64}$$

Figure 8 shows the outside of the pump housing, which has a total surface area of 0.0513 m^2. The resulting equivalent length of 12.70 mm tubing for the pump housing was 1.286 m. Figure 9 shows the surface of the water flow meter, which has a surface area of 0.102 m^2, resulting in an equivalent length of 2.557 m. Hence, the total length of the primary loop

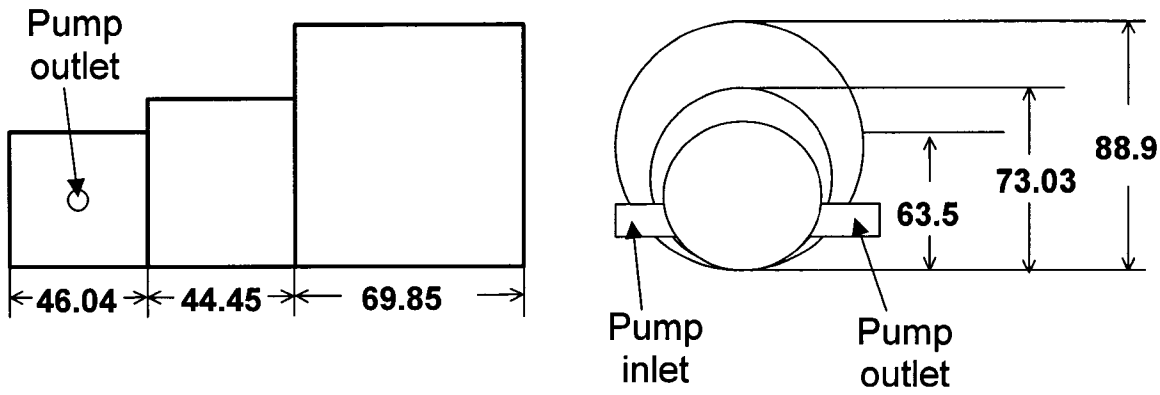

Figure 8. **Side (a) and Front (b) View Sketches of the Micropump Series 5000 Model H21 Pump Housing (Measurements are in mm; Drawing Not to Scale)**

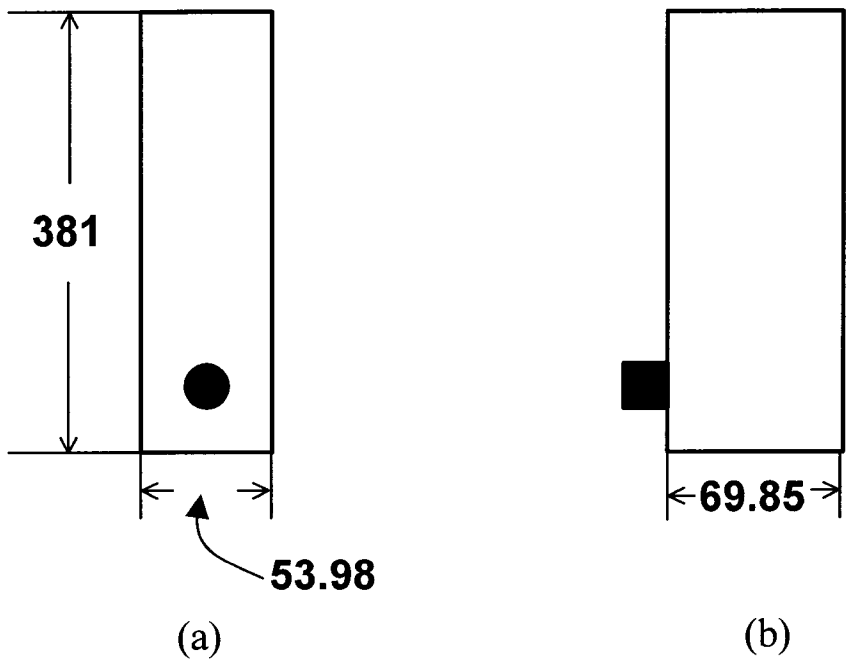

Figure 9. **Side (a) and Front (b) View Sketch of the Dwyer RMC Series Volumetric Flow Meter (Measurements are in mm; Drawing Not to Scale)**

tubing was 6.423 m, with an ambient heat loss of 26.18 W. Therefore, the total heat lost to the ambient from the entire primary loop was 28.61 W.

The test section heat duty could now be readily derived:

$$\begin{aligned} Q_{w,test} &= Q_{w,\sec} + Q_{ambient} - Q_{pump} \\ &= 251 + 29 - 22 = 258\,\mathrm{W} \end{aligned} \tag{65}$$

Heat Transfer Coefficient Calculation

The condensation heat transfer coefficient was determined from the measured test section heat duty (discussed above), the applicable temperature difference, and the other thermal resistances. The calculations are illustrated using the same data point as was used for the explanation of the test section quality and heat duty calculations. A detailed calculation procedure is included in Appendix A.

The primary coolant flows through the annulus side of the test section. For heat transfer from the refrigerant to the water, the annulus side resistance could be calculated as follows:

$$R_{annulus} = \frac{1}{h_{annulus}\left[\pi \cdot (O.D.)_{inner} L_{test}\right]} \tag{66}$$

The wall resistance could be calculated as in the following equation,

$$R_{wall} = \frac{\ln\left[(O.D.)_{inner}/(I.D.)_{inner}\right]}{2\pi \cdot k_{wall} L_{test}} \tag{67}$$

where $(I.D.)_{inner}$ and $(O.D.)_{inner}$ are the inner and outer diameter of the inner tube of the test section, and L_{test} is the length of the test section heat exchanger. The logarithmic temperature difference between the primary water and the refrigerant of the test section heat exchanger was calculated using the following equation,

$$LMTD = \frac{(T_{refg,i} - T_{water,o}) - (T_{refg,o} - T_{water,i})}{\ln[(T_{refg,i} - T_{water,o})/(T_{refg,o} - T_{water,i})]} \tag{68}$$

where all the temperatures were measured quantities. The overall UA and the total heat transfer resistance of the test section could be calculated as

$$UA = \frac{Q_{w,test}}{LMTD} \tag{69}$$

$$R_{total} = \frac{1}{UA} \tag{70}$$

The refrigerant side heat transfer resistance and thus the heat transfer coefficient could be deduced from the total heat transfer resistance.

$$R_{refg} = R_{total} - R_{annulus} - R_{wall} \tag{71}$$

$$h_{refg} = \frac{1}{R_{refg}\left[\pi \cdot (I.D.)_{inner} L_{test}\right]} \tag{72}$$

As reported in the previous sections, the heat transfer coefficient in the annulus for this representative point was 12,266 W/m^2-K, resulting a thermal resistance of 7.00×10^{-3} K/W. The calculated tube-wall resistance was 4.09×10^{-4} K/W. With measured primary coolant and refrigerant inlet and outlet temperatures of the test section at 45.30, 45.51, 61.76 and 61.33°C, respectively, the corresponding LMTD was 16.14°C. The overall UA and thus the total heat transfer resistance were 15.94 W/K and 6.27×10^{-2} K/W. The refrigerant-side resistance was calculated from the measured overall conductance of the test section and the coolant-side and tube-wall resistances, and for this case was 5.53×10^{-2} K/W. This yielded a condensation heat transfer coefficient of 2,095 W/m^2-K.

As mentioned in Chapter 3, outer wall temperatures of the inner tube were measured by three thermocouples and used to derive redundant refrigerant heat transfer coefficients to validate the refrigerant heat transfer coefficients obtained from the above method using water-side, wall and total heat transfer resistances. The average deviation between these thermocouples was 0.94°C, with a range of 0.19°C – 2.06°C over the range of conditions tested. Figure 10 shows the three measured wall temperatures at G = 300, 500 and 700 kg/m^2-s at P_r = 0.8. Thus, by assuming that the wall temperature was the average of the thermocouple measurements, the logarithmic temperature difference between the wall of the test section and the refrigerant was calculated using the following equation,

$$LMTD_{refg-wall} = \frac{(T_{refg,i} - T_{wall}) - (T_{refg,o} - T_{wall})}{\ln[(T_{refg,i} - T_{wall})/(T_{refg,o} - T_{wall})]} \tag{73}$$

The UA and R based on $LMTD_{refg\text{-}wall}$ and the test section heat duty could be calculated as

$$UA_{refg-wall} = \frac{Q_{w,test}}{LMTD_{refg-wall}} \tag{74}$$

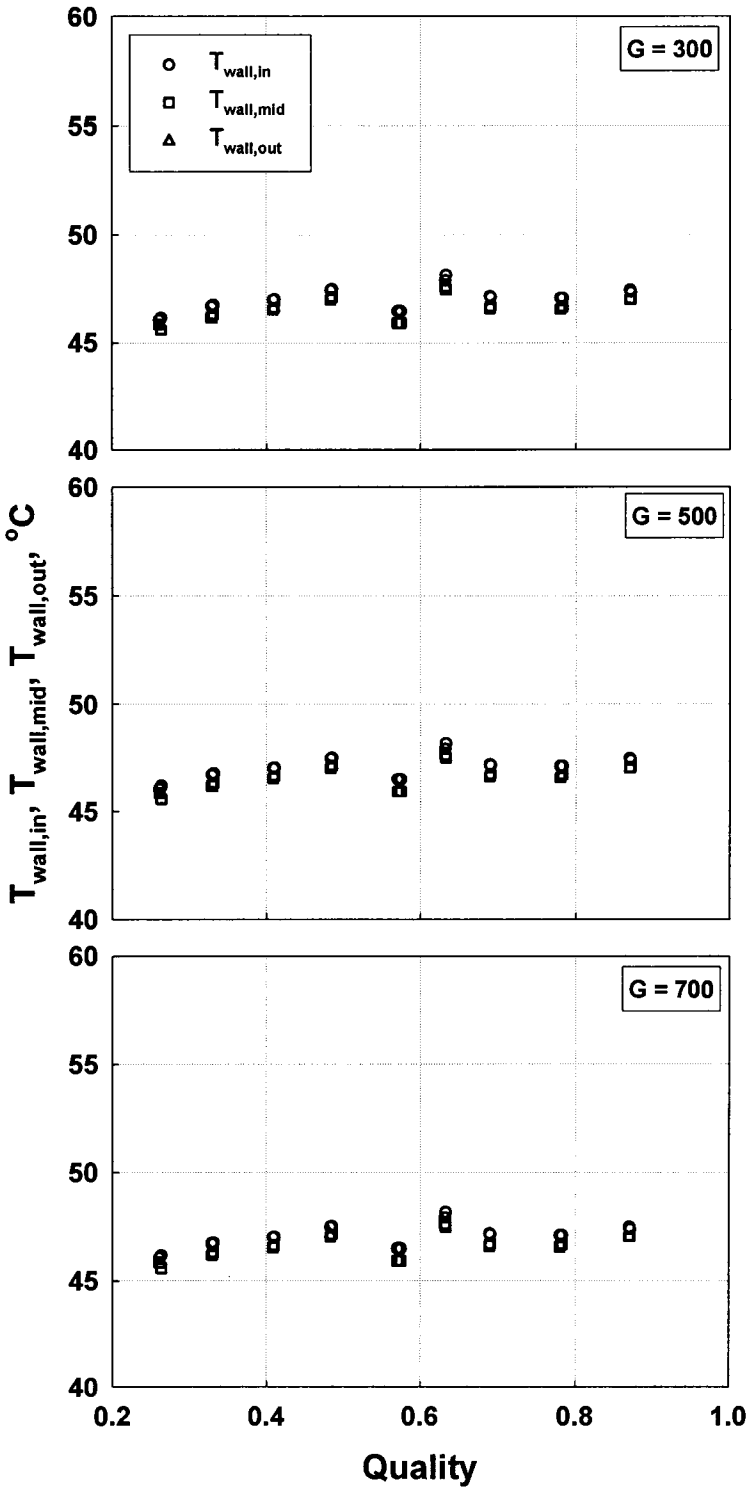

Figure 10. Representative Wall Temperatures (Phase-Change Tests, $P_r = 0.8$)

$$R_{total,refg-wall} = \frac{1}{UA_{refg-wall}} \tag{75}$$

The refrigerant-side heat transfer resistance, and thus the heat transfer coefficient, were calculated from this resistance by subtracting the tube-wall resistance, as follows:

$$R_{refg,wall\ based} = R_{total,refg-wall} - R_{wall} \tag{76}$$

$$h_{refg,wall\ based} = \frac{1}{R_{refg-wall}\left[\pi \cdot (I.D.)_{inner} L_{test}\right]} \tag{77}$$

For this representative data point, with measured wall temperatures of the test section at 46.95 (inlet) and 46.71°C (center) (the thermocouple at the outlet of the test section malfunctioned for this test), respectively, the average wall temperature was 46.83°C. The corresponding $LMTD_{refg\text{-}wall}$ was 14.71°C. The overall $UA_{refg\text{-}wall}$, and thus the total heat transfer resistance, were 17.49 W/K and 5.72×10^{-2} K/W, respectively. The refrigerant-side resistance was calculated from the measured overall conductance of the test section and the tube-wall resistances, and for this case was 5.68×10^{-2} K/W. This yielded a condensation heat transfer coefficient of 2,042 W/m^2-K. Thus, for this data point, the refrigerant heat transfer coefficient based on wall temperature measurements was 2.63% less than the refrigerant heat transfer coefficient of 2,095 W/m^2-K determined from the overall UA.

Uncertainty Analysis

An uncertainty analysis (Taylor and Kuyatt 1994) was conducted to estimate the uncertainty in the refrigerant heat transfer coefficient using the error propagation approach. An Engineering Equation Solver (EES) (Klein 2003) program was developed to evaluate all the uncertainties needed in this study.

Average test section quality

From equation (39), the uncertainty in the test section inlet quality was deduced from the pre-cooler heat duty as follows:

$$U_{Q_{pre}}{}^2 = \left(\frac{\partial Q_{pre}}{\partial Vol_{w,pre}} U_{Vol_{w,pre}}\right)^2 + \left(\frac{\partial Q_{pre}}{\partial h_{w,pre,out}} U_{h_{w,pre,out}}\right)^2 + \left(\frac{\partial Q_{pre}}{\partial h_{w,pre,in}} U_{h_{w,pre,in}}\right)^2 \tag{78}$$

where $Vol_{w,pre}$, $h_{w,pre,in}$ and $h_{w,pre,out}$ are the measured volumetric flow rate, and inlet and outlet enthalpies of the pre-cooler cooling water, respectively. The influence of density

(needed for mass flow rate calculation of cooling water) on uncertainty was neglected in the above calculation. The relative uncertainty in the volumetric flow rate was ±2% of the reading according to the manufacturer (see Table 8). The uncertainty in coolant enthalpy was given by:

$$U_h^2 = \left(\frac{\partial h}{\partial T}U_T\right)^2 = \left(c_p U_T\right)^2 \tag{79}$$

Where the uncertainty in temperature measurements was ±0.3°C (see Table 8), which resulted in an uncertainty in the enthalpy of 0.035 kJ/kg. For the representative data point, the pre-cooler heat duty and the associated uncertainty was 2.696±0.109 kW.

From equation (40), the uncertainty of the refrigerant enthalpy at the pre-cooler outlet could be calculated using the following equation:

$$U_{h_{refg,pre,out}}^2 = \left(\frac{\partial h_{refg,pre,out}}{\partial h_{refg,pre,in}}U_{h_{refg,pre,in}}\right)^2 + \left(\frac{\partial h_{refg,pre,out}}{\partial Q_{pre}}U_{Q_{pre}}\right)^2 + \left(\frac{\partial h_{refg,pre,out}}{\partial \dot{m}_{refg}}U_{\dot{m}_{refg}}\right)^2 \tag{80}$$

The uncertainty in the pre-cooler inlet enthalpy was as follows:

$$U_{h_{refg,pre,in}}^2 = \left(\frac{\partial h}{\partial T}U_T\right)^2 + \left(\frac{\partial h}{\partial P}U_P\right)^2 \tag{81}$$

where

$$\frac{\partial h}{\partial T} = \frac{h_{T+U_T,P} - h_{T-U_T,P}}{2U_T} \tag{82}$$

$$\frac{\partial h}{\partial P} = \frac{h_{T,P+U_P} - h_{T,P-U_P}}{2U_P} \tag{83}$$

With a refrigerant mass flow rate uncertainty of 2.765×10^{-5} kg/s, and a pre-cooler refrigerant inlet enthalpy of 441.3±0.4243 kJ/kg for the representative data point, the uncertainty in the pre-cooler outlet enthalpy was 343.7±3.965 kJ/kg.

The test section inlet quality was a function of enthalpy and pressure, with the corresponding uncertainty given by:

$$U_{x_{test,in}}^2 = \left(\frac{\partial x_{test,in}}{\partial h_{refg,pre,out}}U_{h_{refg,pre,out}}\right)^2 + \left(\frac{\partial x_{test,in}}{\partial P}U_P\right)^2 \tag{84}$$

where

$$\frac{\partial x_{test,in}}{\partial h} = \frac{x_{h+U_h,P} - x_{h-U_h,P}}{2U_h} \tag{85}$$

$$\frac{\partial x_{test,in}}{\partial P} = \frac{x_{h,P+U_P} - x_{h,P-U_P}}{2U_P} \tag{86}$$

For the representative data point, the test section inlet quality and the associated uncertainty was 0.5802±0.0524. Similarly, the test section outlet quality and the associated uncertainty was 0.4098±0.0319, resulting a test section average quality of 0.4950±0.0307.

Test section heat duty

To estimate the uncertainty in the test section heat duty, uncertainties in secondary water heat duty, pump heat addition and ambient heat loss needed to be known as shown in the following equation:

$$U_{Q_{w,test}}{}^2 = \left(\frac{\partial Q_{w,test}}{\partial Q_{w,\sec}} U_{Q_{w,\sec}}\right)^2 + \left(\frac{\partial Q_{w,test}}{\partial Q_{ambient}} U_{Q_{ambient}}\right)^2 + \left(\frac{\partial Q_{w,test}}{\partial Q_{pump}} U_{Q_{pump}}\right)^2 \tag{87}$$

The heat load in the secondary heat exchanger was calculated using the mass flow rate of the coolant (measured using a Coriolis mass flowmeter) and the inlet and outlet temperatures. The thermal amplification provided by the low flow rate of the secondary coolant (2.35×10^{-3} kg/s) was evident from the temperature rise in this fluid. Thus, the secondary coolant temperature rise for this data point was 25.51°C, while the primary coolant ΔT was only 0.21°C. The corresponding primary and secondary water flow rates were 0.116 and 2.351×10^{-3} kg/s respectively. This large temperature rise, coupled with the high-accuracy flow rate measurement, yielded a low uncertainty in the secondary coolant duty, ±1.7%, (250.80±4.19 W). A very conservative uncertainty of ±50% was assumed for pump heat dissipation and ambient heat loss. For this representative case of G = 399 kg/m^2-s, x = 0.4950, and p = $0.8\times P_{crit}$, the pump heat addition and ambient heat loss were estimated using this procedure to be 22.25±11.13 W and 28.61±14.31 W. Because the net contribution of the ambient heat loss (11.4%) and pump heat addition (8.9%) terms was small by design, the relatively high assumed uncertainties in these terms were not very significant in determining the test section heat duty. Thus, the resulting test section heat duty was 257.21±18.60 W.

With a log mean temperature difference of 16.14 ± 0.74°C, the overall heat transfer conductance, UA, was 15.94±1.36 W/K.

Heat transfer coefficient

Neglecting the uncertainties in the heat transfer area and wall resistance, the uncertainty in the refrigerant-side heat transfer coefficient was as follows:

$$U_{h_{refg}}{}^2 = \left(\frac{\partial h_{refg}}{\partial UA} U_{UA} \right)^2 + \left(\frac{\partial h_{refg}}{\partial h_{annulus}} U_{h_{annulus}} \right)^2 \tag{88}$$

With an assumed coolant-side heat transfer coefficient uncertainty of ±25%, the refrigerant-side heat transfer coefficient could be estimated to be 2,095±214 W/m^2-K, i.e., an uncertainty of ±10.2%. It should be noted that for this data point, $R_{refg}/R_{coolant}$ = 7.91, which ensured that the condensation side presents the governing thermal resistance and effectively minimized the sensitivity of the calculated condensation heat transfer coefficient to the coolant-side thermal resistance.

Pressure Gradient

The test section pressure loss was directly measured using a bank of differential pressure transducers with maximum uncertainties of ±0.0047 kPa. The pressure gradient was calculated from this measured pressure drop and the known test section length.

Supercritical Gas Cooling

For each data point, the test section temperature was taken as the average of the measured the inlet and outlet temperatures. The test section heat duty and heat transfer coefficient were derived using the same techniques described above for condensation tests. The detailed procedure of test section heat duty and heat transfer coefficient calculations for this supercritical case is included in Appendix D. Again, an uncertainty analysis was performed on each calculated quantity using the error propagation approach (Taylor and Kuyatt 1994). For the whole set of data points, the uncertainty in the test section average temperature was ± 0.2°C. The heat transfer coefficients and pressure gradients were derived using the technique described in the condensation heat transfer sections. Through the test

matrix, the heat transfer coefficients varied from 670 W/m^2-K at G = 201.7 kg/m^2-s, T = 105.2°C, P = 3790 kPa to 8256 W/m^2-K at G = 800.2 kg/m^2-s, T = 77.49°C, P = 3807 kPa with uncertainties in the range 14.98 to 12.57%. It should be noted that refrigerant properties were evaluated using the property models from the National Institutes of Standards and Technology (REFPROP 7.0, Lemmon *et al.* 2002), which are the most accurate properties available for such fluids. However, uncertainties in the evaluated properties are not provided by REFPROP 7.0. Therefore, in calculating the uncertainties of the heat transfer coefficients and the friction factors, uncertainties in the properties were assumed to be negligible. Thus, in reality, the uncertainties in heat transfer coefficients and Nusselt numbers could be higher, depending on the uncertainties in the properties.

CHAPTER 5. RESULTS AND DISCUSSION

Results

The heat transfer coefficients and pressure gradients obtained using the techniques described in the previous chapters are presented here.

Phase-change tests

For phase change experiments, test conditions investigated in this study, with their respective uncertainties, are shown in Figure 11. Representative uncertainties for the $P = 0.8 \times P_{crit}$ case for the range of mass fluxes and qualities studied are shown below:

$G = 200$ kg/m^2-s:

$x_{avg} = 0.13 \pm 0.05$ $x_{avg} = 0.57 \pm 0.04$ $x_{avg} = 0.78 \pm 0.04$

$G = 400$ kg/m^2-s

$x_{avg} = 0.20 \pm 0.04$ $x_{avg} = 0.50 \pm 0.03$ $x_{avg} = 0.89 \pm 0.03$

$G = 800$ kg/m^2-s:

$x_{avg} = 0.19 \pm 0.06$ $x_{avg} = 0.50 \pm 0.06$ $x_{avg} = 0.89 \pm 0.04$

Heat transfer coefficients (together with the estimated uncertainties) for all phase-change data points taken in this study are shown in Figure 12. For the entire set of data points shown on these graphs, the average uncertainty in heat transfer coefficients was ± 10.21%. The maximum uncertainty was 15.83% at $G = 200.9$ kg/m^2-s, $P = 2966$ kPa, $x = 0.1264$, with a heat transfer coefficient of 1122 W/m^2-K. The minimum uncertainty was 7.89% at $G = 701.6$ kg/m^2-s, $P = 3387$ kPa, $x = 0.1971$, with a heat transfer coefficient of 2978 W/m^2-K. Figure 13 shows the refrigerant-to-coolant resistance ratios for all the data points taken in the phase change tests. It can be seen that this ratio was larger than three for most of the data, ensuring low uncertainties in the heat transfer coefficient determination. Figure 14 shows heat transfer coefficients derived from the wall-mounted thermocouple measurements for $G = 300$, 500 and 700 kg/m^2-s for $P_r = 0.8$. It can be seen that the heat transfer coefficients derived using the two different methods agreed well. For the entire phase-change data set, the average deviation between the two heat transfer coefficients was 7.36%, with maximum and minimum deviations of 17.92% and 0.26%, respectively. The measured pressure gradients (total) for various mass fluxes are shown in Figure 15. The average uncertainty in pressure

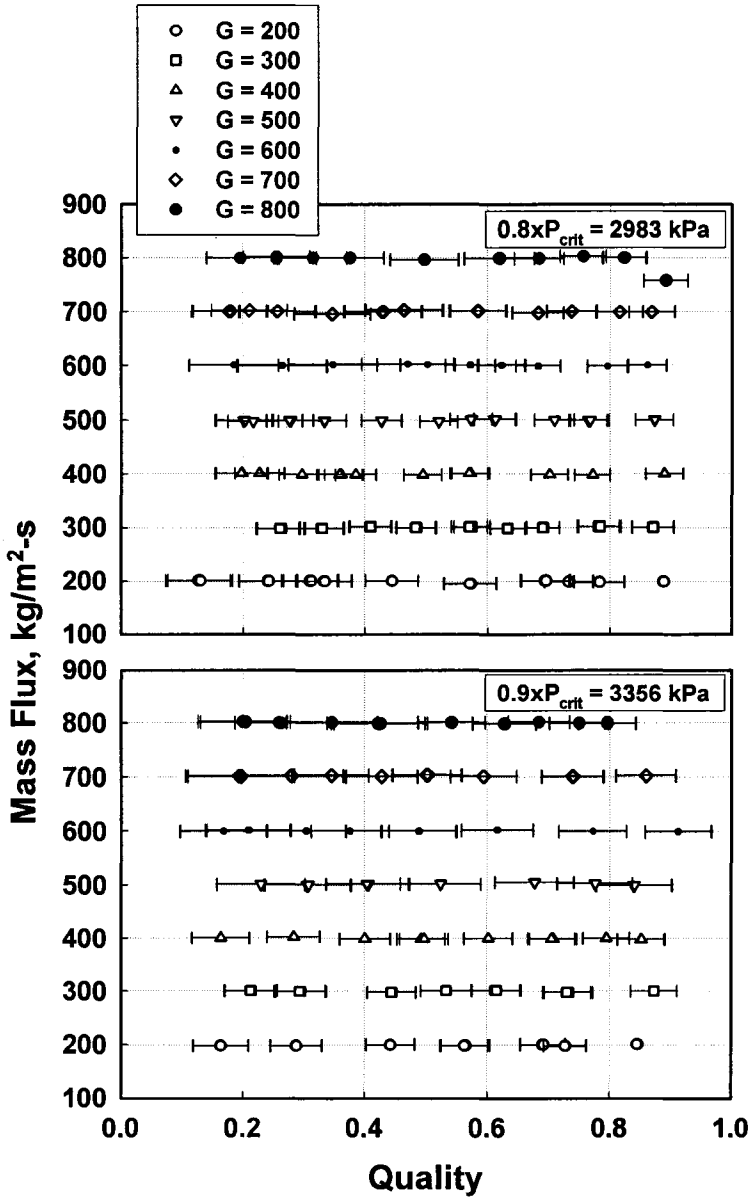

Figure 11. Phase-Change Test Conditions Investigated (with Measurement Uncertainties)

gradient for the entire set of data points was ±1.85%, with a maximum uncertainty of ±8.57% at G = 197.9 kg/m^2-s, P = 3359 kPa, x = 0.1634, and dP/dz = 0.19 kPa/m, and a minimum uncertainty of ±0.28% at G = 757.9 kg/m^2-s, P = 3027 kPa, x = 0.8920, and dP/dz = 5.72 kPa/m, respectively.

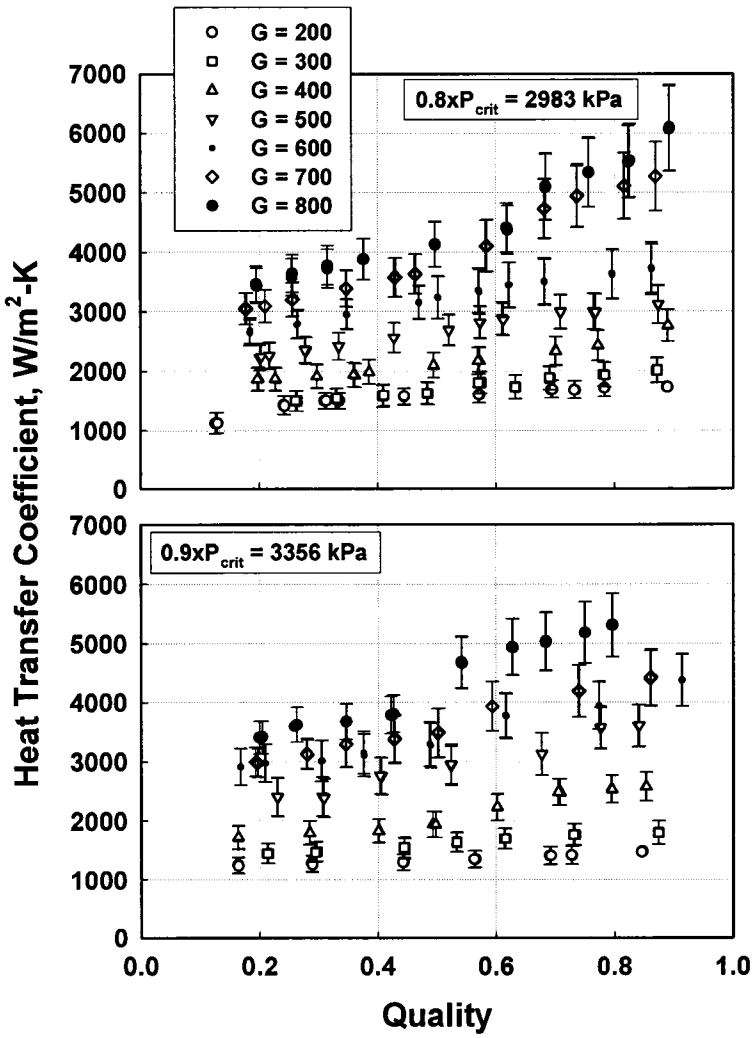

Figure 12. Phase-Change Heat Transfer Coefficients with Uncertainties

Supercritical tests

For supercritical tests, Figure 16 shows the heat transfer coefficients for all the data points taken in this study. For the entire set of data points shown on these graphs, the average uncertainty in the heat transfer coefficients was ±9.68%, with a maximum uncertainty of ±17.36% at G = 303.4 kg/m^2-s, P = 4088 kPa, T = 47.57°C, and heat transfer coefficient of 1125 W/m^2-K, and a minimum uncertainty of ±5.07% at G = 593.4 kg/m^2-s, P = 3734 kPa, T = 110.2°C, and heat transfer coefficient of 2870 W/m^2-K, respectively. The refrigerant-to-coolant resistance ratios for all the data points taken in the supercritical tests

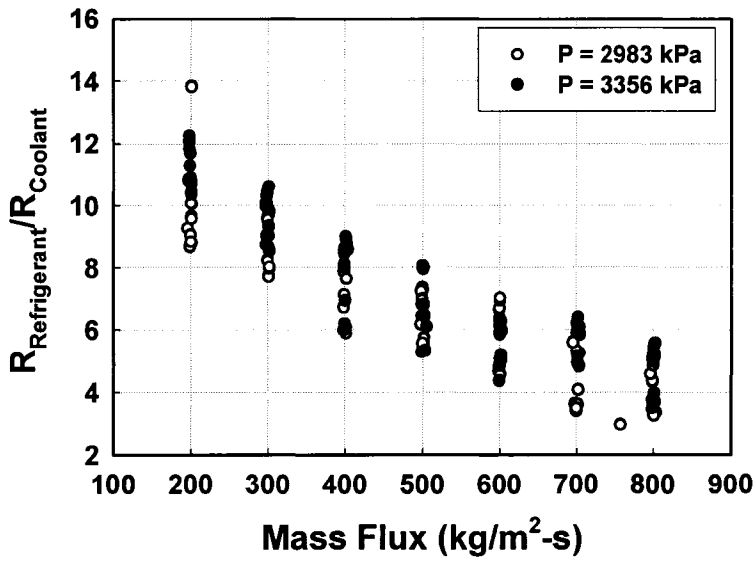

Figure 13. Refrigerant-to-Coolant Resistance Ratio, Phase Change Tests

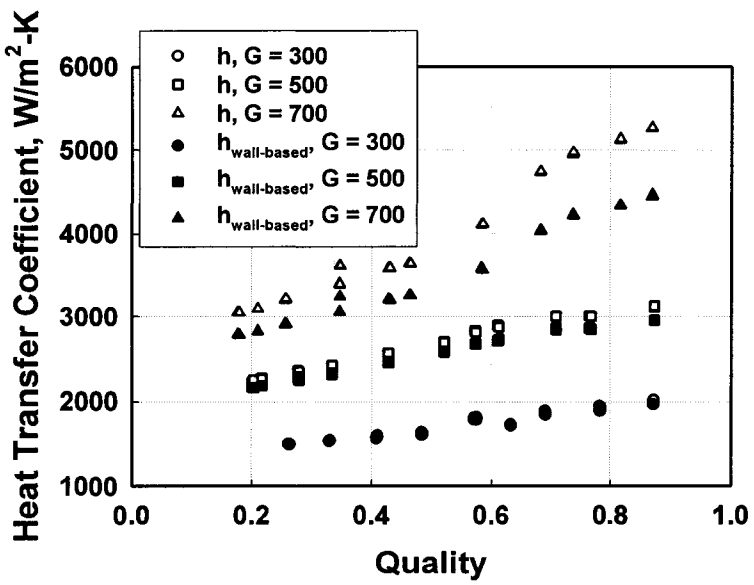

Figure 14. Comparison of Phase-Change Heat Transfer Coefficients Derived from Water-Side Resistance Analysis and Wall-Temperature Measurements

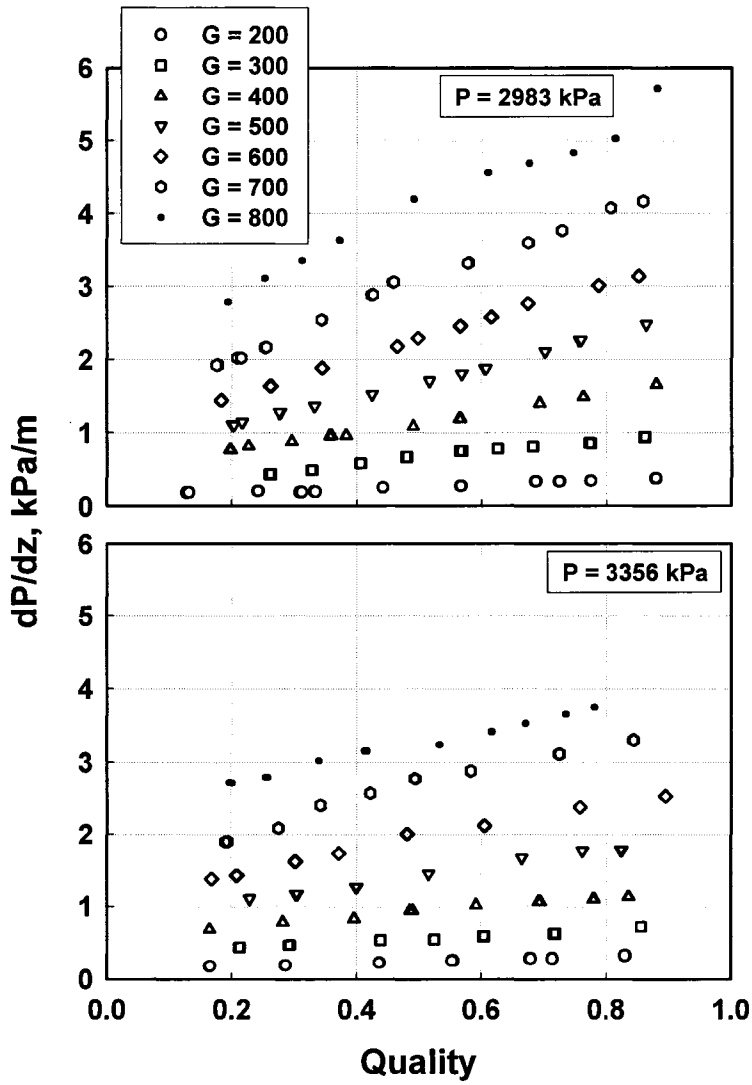

Figure 15. Measured Phase Change Pressure Gradients

are shown in Figure 17. Again, this ratio ranged from 2.30 – 28.34, with only 9 out of 337 data points with resistance ratios between 2.30 and 2.91. These points with lower resistance ratios were all at high mass fluxes (G = 598.0 – 800.2 kg/m^2-s) and with temperature and pressure near the critical point (P_r = 1.0 – 1.1, and T = 77.44 – 79.92°C). The very high heat transfer coefficients (8256 – 5359 W/m^2-K) at these conditions resulted in the somewhat low values of the refrigerant-to-coolant resistance ratios. Figure 18 shows heat transfer coefficients derived from the wall-mounted thermocouple measurements for G = 300, 500 and 700 kg/m^2-s for P_r = 1.1. It can be seen that the heat transfer coefficients derived using

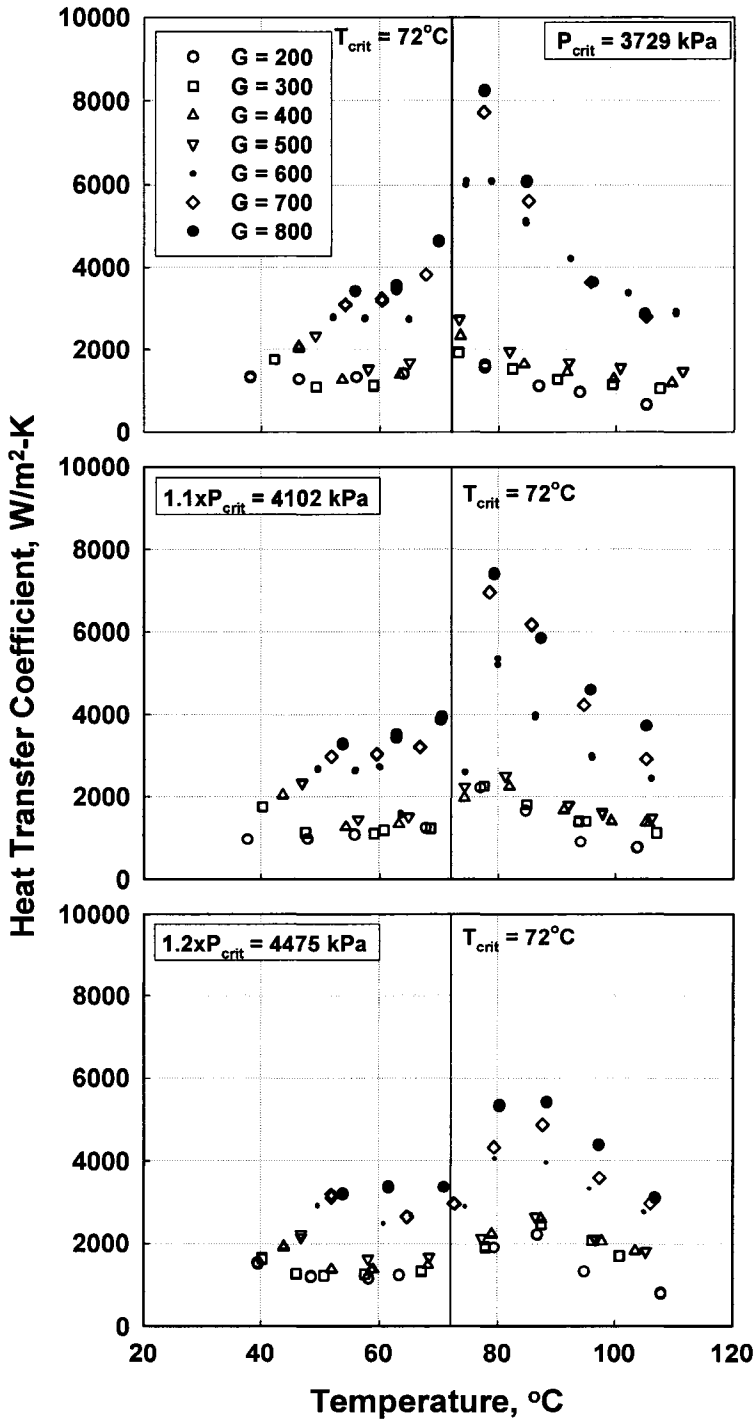

Figure 16. Supercritical Heat Transfer Coefficients

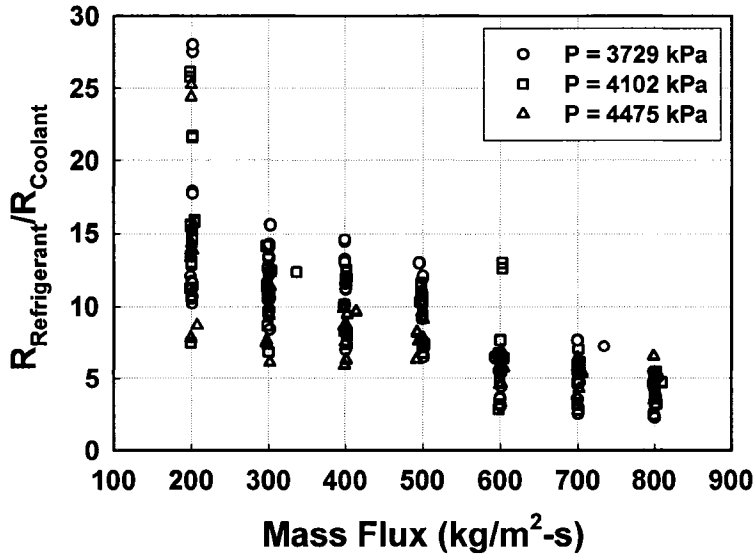

Figure 17. Refrigerant-to-Coolant Resistance Ratio, Supercritical Tests

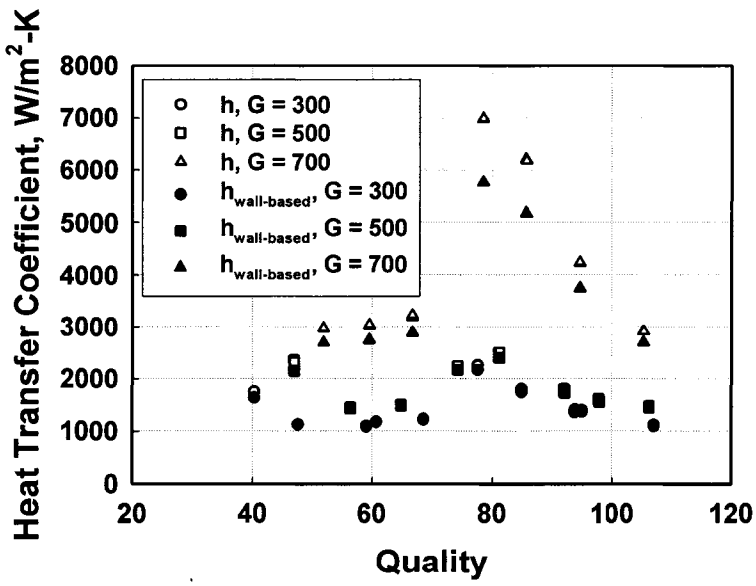

Figure 18. Comparison of Supercritical Cooling Heat Transfer Coefficients Derived from Water-Side Resistance Analysis and Wall-Temperature Measurements

the two different methods agreed well. For the entire phase-change data set, the average deviation between the two heat transfer coefficients was 6.61%, with maximum and minimum deviations of 20.51% and 0.00%, respectively.

Figure 19 shows the pressure gradients for various mass fluxes. The measured pressure gradients were small for G = 200 kg/m^2-s at all critical and supercritical pressures due to the relatively large tube diameter. The measured pressure gradients for G = 200 kg/m^2-s ranged from (-0.011) – 0.134 kPa/m with 71% (34 out of 48) of the data in the range of (-0.011) – 0.039 kPa/m. Since the uncertainty in the differential pressure transducer was constant (0.00467 kPa), the uncertainties in measured pressure gradients for the G = 200 kg/m^2-s were relatively high, i.e. ±3.49% at dP/dz = 0.10 kPa/m and ±1607.20% at dP/dz = 2.91×10^{-4} kPa/m. The average uncertainty in pressure gradient for the entire set of data points for all mass fluxes including the G = 200 kg/m^2-s data was ±9.21%, with maximum and minimum uncertainties of ±1607.20% at dP/dz = 2.91×10^{-4} kPa/m and ±0.22% at dP/dz = 7.25 kPa/m, respectively. For the data set without G = 200 kg/m^2-s, the average uncertainty in pressure gradient was ±1.61%, with maximum and minimum uncertainties of ±6.03% and ±0.22%, respectively. For the data points with G = 200 kg/m^2-s, the average uncertainty in pressure gradient was ±47.26%, with maximum and minimum uncertainties of ±1607.20% and ±3.49%, respectively. For data points with G = 200 kg/m^2-s, high errors occurred at temperatures close to the critical temperature. It is felt that the measured pressure gradients for G = 200 kg/m^2-s should not be used for model development until more accurate data can be obtained.

Separation of Frictional Pressure Drop

The measured pressure drop for phase-change and supercritical tests was composed of pressure drop due to frictional and acceleration/deceleration components. The frictional pressure drops were first obtained from the measured pressure drop for the discussion and interpretation of trends, comparison with the literature and the subsequent model development.

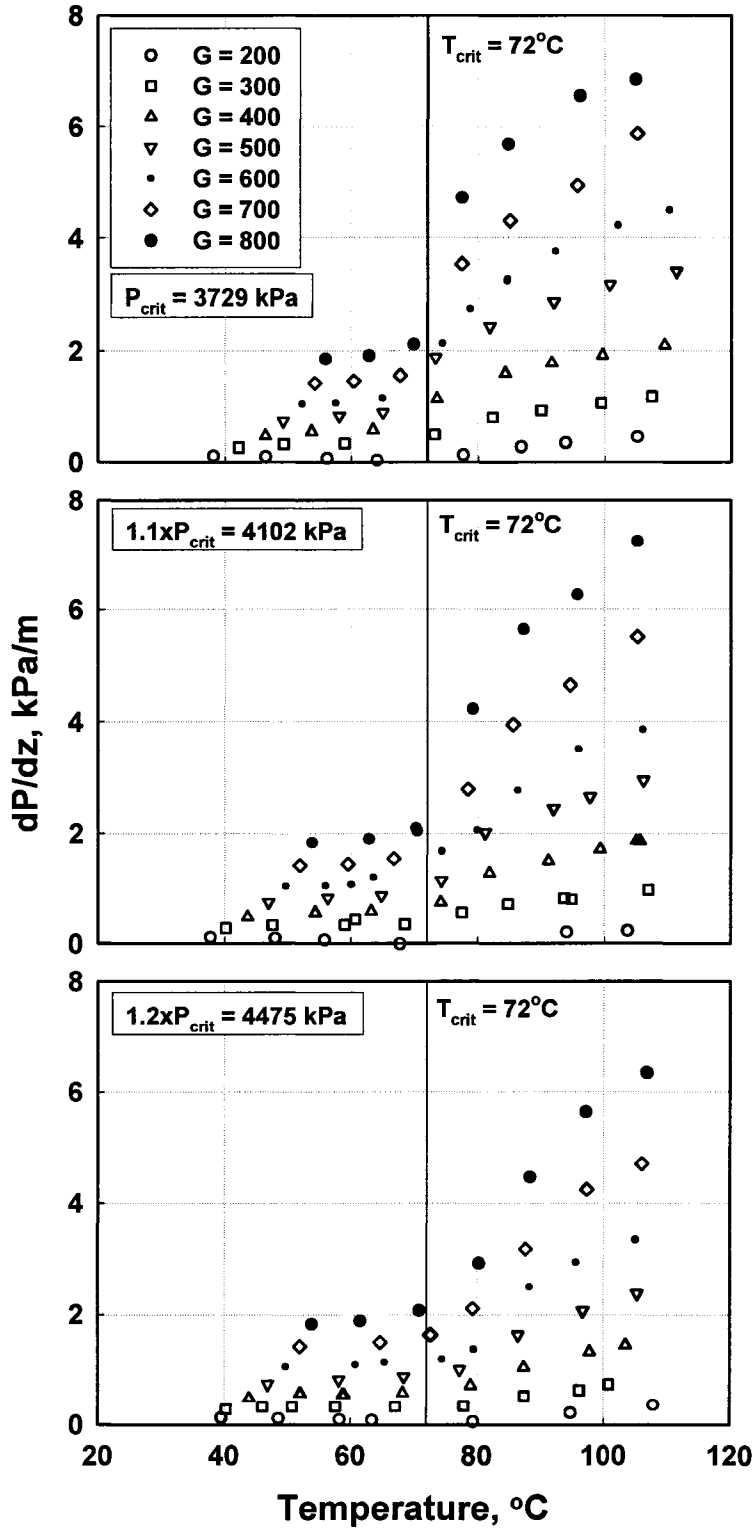

Figure 19. Measured Supercritical Pressure Gradients

Phase-change tests

The frictional pressure drops were computed from the total (measured) pressure drops as follows:

$$(\Delta P)_{total} = (\Delta P)_{frictional} + (\Delta P)_{acceleration/deceleration} \tag{89}$$

For phase-change pressure drop, the acceleration/deceleration component is the pressure loss/gain due to the change in quality and void fraction from the test section inlet to the outlet. For condensation, the changes in quality and void fraction caused pressure recovery (deceleration), and could be calculated as follows (Carey 1992):

$$P_{in} - P_{out} = (\Delta P)_{deceleration} = G^2 \left\{ \left[\frac{x^2}{\rho_v \alpha} + \frac{(1-x)^2}{\rho_l (1-\alpha)} \right]_{out} - \left[\frac{x^2}{\rho_v \alpha} + \frac{(1-x)^2}{\rho_l (1-\alpha)} \right]_{in} \right\} \tag{90}$$

where the void fraction α was calculated using correlation by Baroczy (1965).

Figure 20 shows the measured pressure drop, along with the deceleration and frictional components for G = 300, 500 and 700 kg/m^2-s at a reduced pressure of 0.8. The deceleration component of the pressure drop ranged from 12.5 – 52.2% of the total measured pressure drop, with the high percentage occurring at low total pressure drop. It should be noted that these pressure drops were recorded in tests where the change in quality across the test section varied from $\Delta x = 0.0775$ to $\Delta x = 0.2867$ with 81% (201 out of 249 data points) of the quality change under 0.20. As stated above, the frictional ΔP is used for subsequent discussion and analysis.

Supercritical tests

Frictional pressure drops were also computed from the total pressure drops using equation (89) for the supercritical tests. Here, the acceleration/deceleration component is the pressure loss/gain due to the momentum change in the flow from the test section inlet to outlet due to changes in refrigerant density. For supercritical cooling, the changes in momentum caused pressure recovery (deceleration).

From Newton's Second Law, for a control volume (shown in Figure 21), the momentum balance is as follows:

$$\frac{\partial}{\partial t} \int_{CV} \vec{v} \rho dV + \int_{CS} \vec{v} \rho \vec{v} \cdot \hat{n} dA = \sum F_{CV} = \sum (PA)_{CV} \tag{91}$$

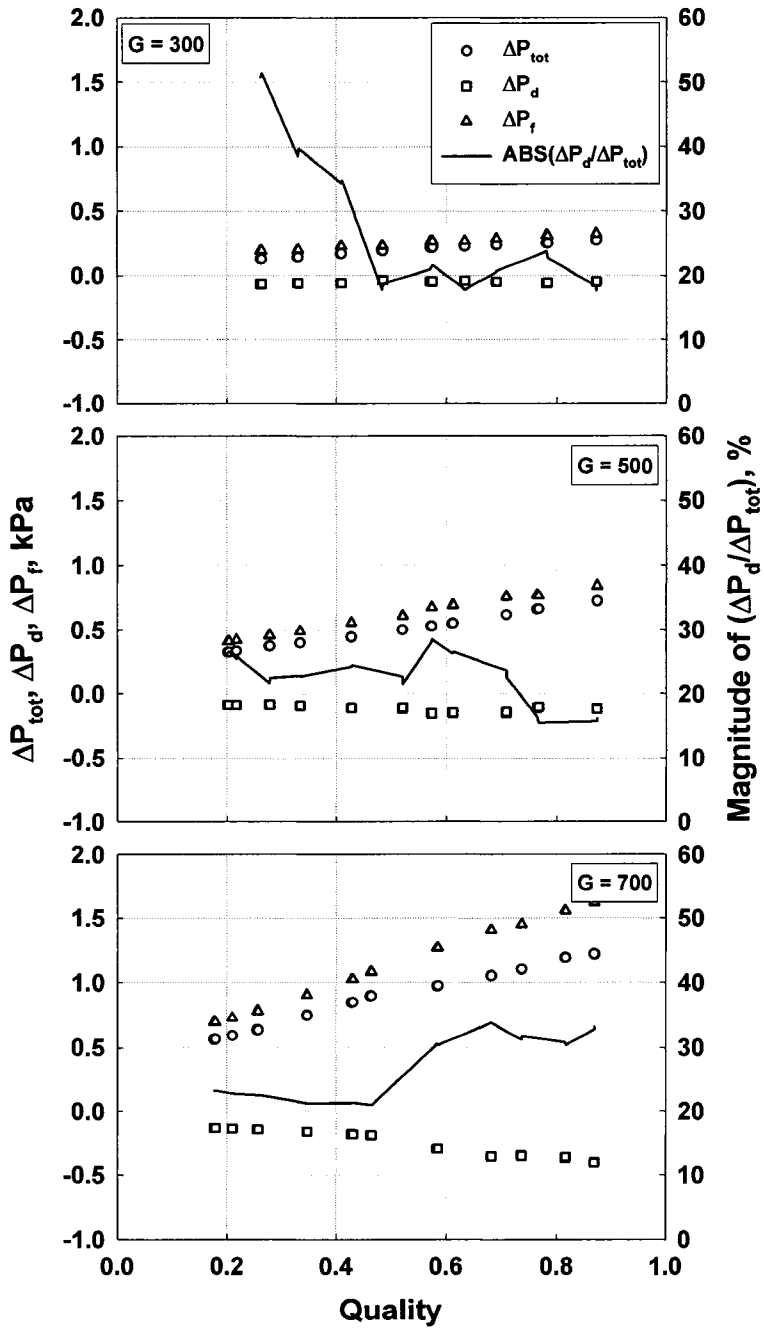

Figure 20. Measured, Deceleration and Frictional Pressure Drops for Phase-Change Tests ($P_r = 0.8$)

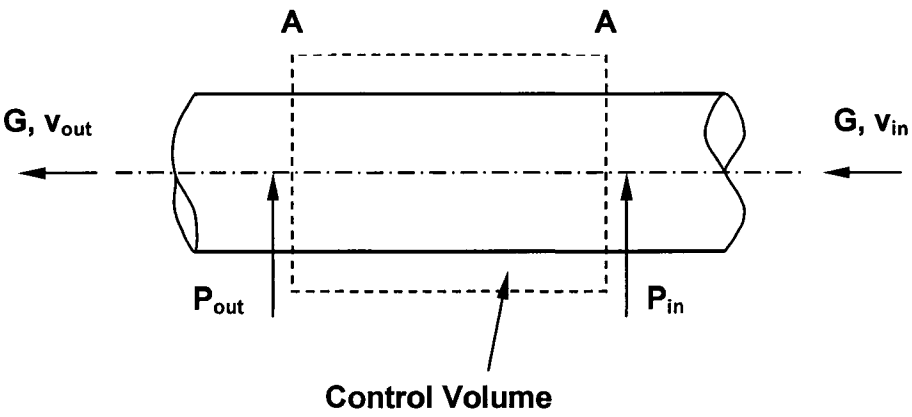

Figure 21. Momentum Balance over A Control Volume

where subscripts CV and CS are control volume and control surface, respectively. Since the flow was steady, the first term on the left hand side of equation (91) is zero. Also, the flow area and the mass flux were constants, resulting in a constant mass flow rate:

$$\dot{m} = GA = \rho \vec{v} A \tag{92}$$

Combining equations (91) and (92), we get:

$$G(v_{out} - v_{in}) = P_{in} - P_{out} = \Delta P_{deceleration} \tag{93}$$

Figure 22 shows the measured pressure drop, along with the deceleration and frictional components for G = 300, 500 and 700 kg/m^2-s at a reduced pressure of 1.0. It should be noted that, for supercritical gas cooling, $(\Delta P)_{deceleration}$ was always negative since the velocity of the flow decreases as fluid density increases (Figure 1 in Chapter 1) when cooled from the inlet to the outlet of the test section. It can be seen that in the gas-like region (high temperature region), the magnitude of $(\Delta P)_{deceleration}$ was small due to the relatively small change in density. Similar results were observed for the liquid-like region (low temperature region). Near the critical region (temperature close to critical value), due to the sudden decrease in fluid density, the $(\Delta P)_{deceleration}$ shows a sudden increase.

Discussion

Trends in phase-change heat transfer and pressure drop

Figure 23 shows the measured heat transfer coefficients as a function of quality for

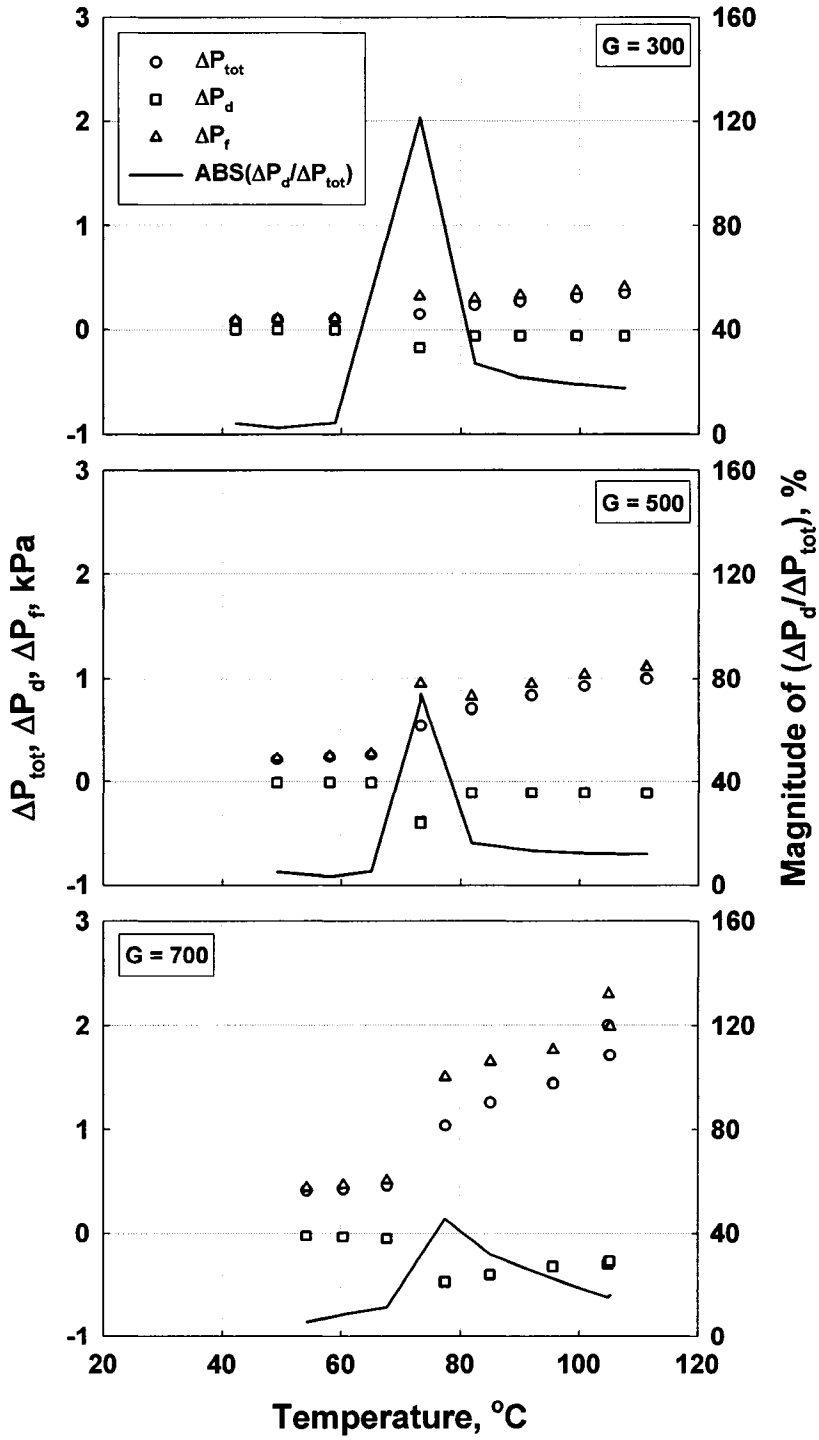

Figure 22. **Measured, Deceleration and Frictional Pressure Drops for Supercritical Tests (P_r = 1.0)**

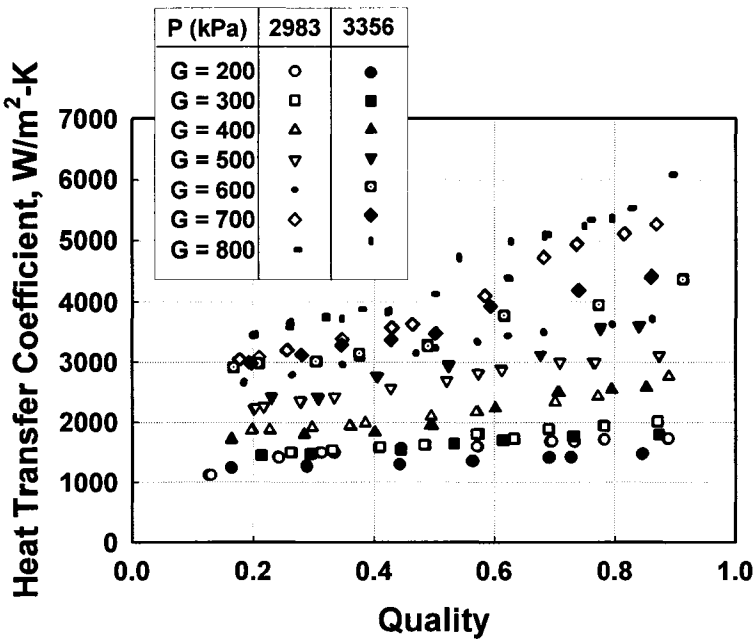

Figure 23. Phase-Change Heat Transfer Coefficient: Effect of Reduced Pressure

both pressures investigated in this study. It can be seen that the heat transfer coefficients increase as the vapor quality and mass fluxes increase, with the effect of vapor quality being more pronounced at the higher mass fluxes. It is also apparent that a change in reduced pressure from 0.8 to 0.9 is not significant enough to cause an appreciable change in the heat transfer coefficient. This is perhaps because, even though the latent heat of condensation decreases from 76.77 kJ/kg at $P_r = 0.8$ to 57.33 kJ/kg at $P_r = 0.9$, the specific heats of both phases increase by a factor of about 1.6-1.9 as the pressure increases. Also, the liquid phase conductivity remains about the same (0.0521 W/m-K at $P_r = 0.8$ to 0.0516 W/m-K at $P_r = 0.9$), whereas the vapor phase conductivity increases by about 23% from $k_v = 0.0312$ W/m-K ($P_r = 0.8$) to $k_v = 0.0386$ W/m-K ($P_r = 0.9$). These compensating variations in properties lead to the minimal effect of reduced pressure on the heat transfer coefficient.

The frictional pressure gradient as a function of vapor quality and mass flux for the two pressures under consideration is presented in Figure 24. As expected, the pressure gradient also increases with the vapor quality and mass flux, and it appears that the effect of reduced pressure is more pronounced than it is for the heat transfer coefficient. Thus, for the same mass flux and vapor quality, the higher the reduced pressure, the lower the pressure

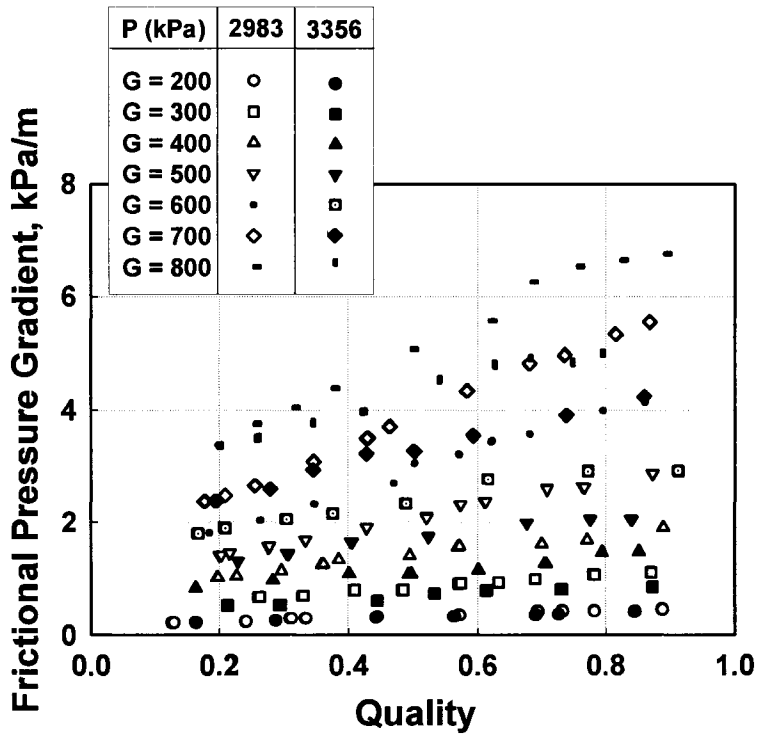

Figure 24. Phase-Change Frictional Pressure Gradient: Effect of Reduced Pressure

gradient, with this effect becoming stronger as the mass flux increases. This is perhaps because as P_r increases, the difference between the vapor and liquid properties such as density and viscosity decreases. At $P_r = 0.8$, $\rho_l/\rho_v = 3.82$, whereas at $P_r = 0.9$, this ratio is 2.69. Similarly, at $P_r = 0.8$, $\mu_l/\mu_v = 3.52$, while at $P_r = 0.9$, this ratio is 2.66. This decrease in the difference between the properties of the two phases reduces the shear between the phases, and therefore the pressure drop. The more pronounced effect of reduced pressure at higher mass fluxes also supports this conclusion because at the higher mass fluxes, the flow would tend toward annular flow, which is governed by vapor shear.

Phase-change flow regime assignment

Coleman and Garimella (2003) map

To further investigate these phenomena based on the prevailing flow regimes, relevant flow regime transition criteria from the literature were considered. It should be noted that there are no flow regime maps in the literature that have been developed or validated for the situation under consideration: condensation of refrigerant blends at high reduced pressures. In the absence of such maps, transition criteria provided in the flow

regime maps proposed by Coleman and Garimella (2003) for the condensation of R134a for circular, square and rectangular shaped tubes (1 mm < d_h < 5 mm) over the mass flux range 150 < G < 750 kg/m^2-s, were used to predict the possible flow regimes for the conditions in the present study. In the annular flow regime, a liquid film coats the circumference of the wall, and the vapor flows through the core with or without liquid droplet entrainment. The wavy flow regime can be subdivided into two categories: discrete-wave flow and disperse-wave flow. For discrete wave flow, the liquid flows primarily on the bottom of the tube while the vapor flows above the liquid with liquid waves at the interface. Similar to annular flow, a thin liquid film exists around the vapor at the top of the tube. Disperse-wave flow is characterized by a large number of secondary waves with no dominant wavelength or amplitude. As the gas velocity increases, the interface becomes more unstable and the intensity of the waves increases until dispersed-wave flow is achieved. For the combination of higher mass fluxes and vapor qualities, flow was mainly annular and mist. The mist flow pattern is characterized by a uniform vapor mist with liquid droplets entrained in the vapor. This flow pattern does not have a clearly discernable film. However, for large tube as in the present study, the mist flow pattern can be classified as annular flow. The intermittent flow regime is characterized by discontinuities in the liquid and vapor phases. In this regime, a continuous stream of intermittent vapor "plugs" or "slugs" surrounded by a liquid film is interrupted by slugs of liquid.

The flow regime transition criteria developed by Coleman (2000) were based on Soliman modified Froude number (Soliman 1982) Fr_{so}, and are shown in Table 11, where

$$Fr_{so} = \begin{cases} 0.025\,\mathrm{Re}_l^{1.59}\left[\dfrac{1+1.09X_{tt}^{0.039}}{X_{tt}}\right]^{1.5}\dfrac{1}{Ga^{0.5}} & \mathrm{Re}_l \le 1250 \\ 1.26\,\mathrm{Re}_l^{1.04}\left[\dfrac{1+1.09X_{tt}^{0.039}}{X_{tt}}\right]^{1.5}\dfrac{1}{Ga^{0.5}} & \mathrm{Re}_l > 1250 \end{cases} \tag{94}$$

It should be noted that the study by Coleman and Garimella (2003) was at low reduced pressures ($P_r \cong 0.34$), thus there may be some differences between these predictions and the actual flow regimes due to this large difference in reduced pressures. However, these criteria were in fact developed for condensation of refrigerants (rather than simulations using air-

Table 11. Phase-Change Flow Transition Criteria (Coleman 2000)

Flow Regime	Transition Criteria
Intermittent	$Fr_{so} < 1.75$
Wavy	$1.75 < Fr_{so} < 18$
Annular	$18 < Fr_{so} < 65$
Mist	$Fr_{so} > 65$

water two-phase flow) and addressed the mass flux range of interest; and are therefore deemed acceptable to provide some guidance. Figure 25 shows the data from the present study plotted on Coleman and Garimella's flow regime map for a 4.91 mm circular tube. According to Coleman's (2000) criteria, the current data points mainly fell in discrete- and disperse-wave flow, and the annular flow pattern. Two data points were identified as being in intermittent flow, while four data points were in the mist flow regime.

Breber et al. (1980) map

The data were also plotted on the Breber et al. (1980) flow regime map (Figure 26), in which transitions occur at constant Martinelli parameters and dimensionless gas velocities.

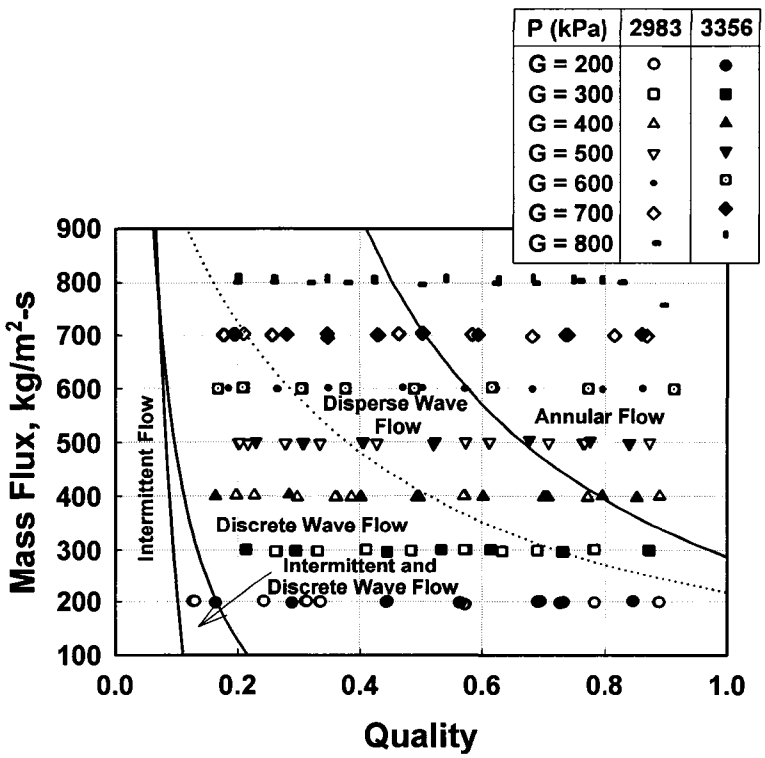

Figure 25. Phase-Change Data Flow Regime Determination (Coleman and Garimella 2003)

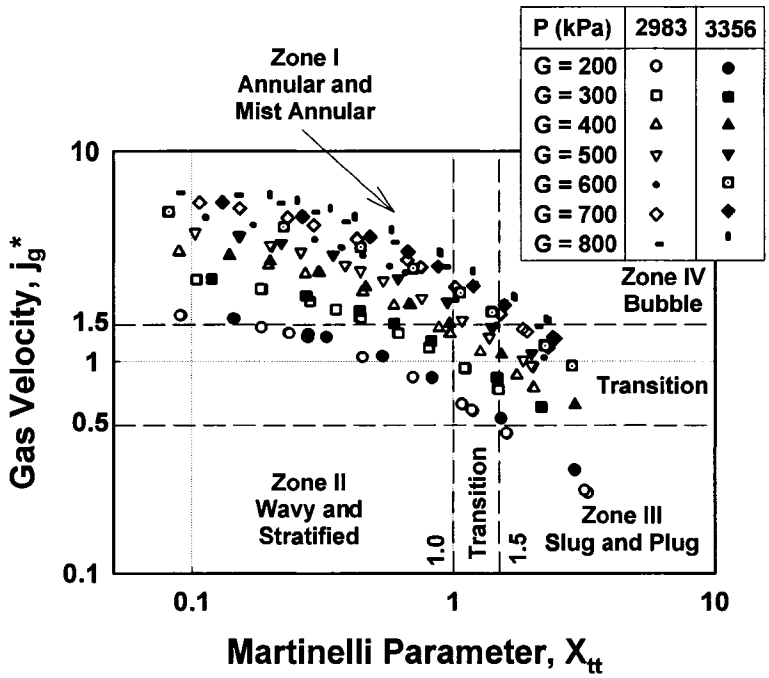

Figure 26. Phase-Change Data Flow Regime Determination (Breber *et al.* 1980)

The map by Breber et al. (1980) (which used the Taitel and Dukler (1976) map as a starting point), was based on the argument that the ratio of shear force-to-gravity force on the condensate film, and the ratio of vapor volume-to-liquid volume are the main factors in establishing transitions between the respective regimes. Using a bank of condensation data for tubes with $8 < d < 50.8$ mm for a variety of fluids, they suggested that the transitions did not occur abruptly, but over regions with some overlap. The data from the present study were primarily in or near the transition region between annular and wavy flows, and the annular flows on this map, with no purely stratified points and a total of three slug and plug flow points. Thus, the subdivision of the data based on transition criteria of these studies result in similar categorizations. It should be noted that differences in definitions and categorizations of different kinds of flows, details of which are available in the respective papers, could be responsible for some of these differences in the assignment of flow regimes.

Hajal et al. (2003) map

Hajal *et al.* (2003) developed a condensation flow pattern map, which used a logarithmic mean (equation 3 in Chapter 2) of void fraction predicted by a homogeneous

void fraction model and Rouhani-Axelsson's void fraction for vertical tubes (Rouhani and Axelsson 1970) to calculate the vapor void fractions from low pressures up to pressures near the critical point. This map was based on the modification of the evaporation and adiabatic flow regime map by Kattan *et al.* (1998) for small diameter horizontal tubes, since dry out does not occur in condensation. The condensation map was validated using other flow regime maps available in literature, i.e. maps by Breber *et al.* (1980), Tandon *et al.* (1982), Sardesai *et al.* (1981), and Cavallini *et al.* (2002b).

The Hajal *et al.* (2003) map is unduly complicated in that, a new map has to be built to check the flow regime for every single point. Figure 27 shows the data from the present study plotted on the Hajal *et al.* (2003) map for G = 200, 500 and 800 kg/m^2-s. The solid and dashed lines are the transition lines for P_r = 0.8 and 0.9, respectively. According to their map, data from the present study were primarily in intermittent and annular flows, with only four data in stratified-wavy flow and no fully stratified flow data. However, the definitions of intermittent and annular flows were not explicitly stated. Since in the following paper (Thome *et al.* 2003), the same heat transfer correlation was used for the intermittent, annular

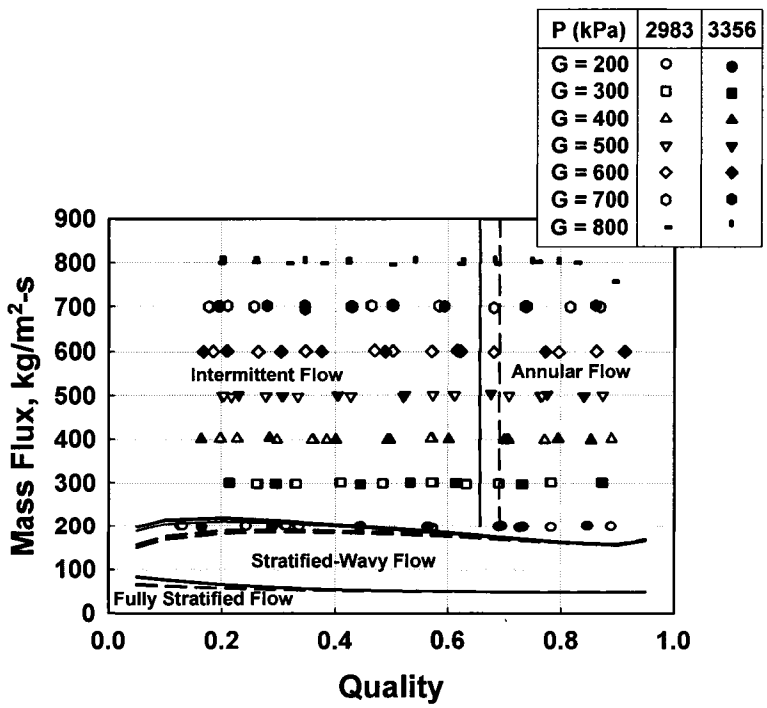

Figure 27. Phase-Change Data Flow Regime Determination (Hajal *et al.* 2003)

and mist flows, one possibility is that the authors considered the intermittent flow to be similar to the annular and mist flows. According to the Hajal et al. (2003) map, the stratified-wavy or fully stratified flow regimes require the mass fluxes to be around or less than 200 kg/m^2-s, which are either at the borderline or beyond the test conditions of the present study.

The flow predictions from Hajal et al. (2003) map were quite different from the predictions from Coleman and Garimella (2003) map, which showed a considerable amount of data from the present study to be in wavy flow regime. The Coleman and Garimella (2003) map, however, results in transitions similar to those predicted by Dobson and Chato (1998) (stratified-wavy flow: $G < 500$ kg/m^2-s and $Fr_{so} < 20$; annular flow: $G < 500$ kg/m^2-s and $Fr_{so} > 20$, or $G > 500$ kg/m^2-s). Since the heat transfer models developed in the present study used an approach similar to that of Dobson and Chato (1998), it is more appropriate to use a flow regime map that is similar to their map. It also should be noted that the Hajal et al. (2003) map requires substantial effort in determining the flow regime before any heat transfer and pressure drop analysis can be conducted. This is not conducive to the implementation of these transition criteria and subsequent heat transfer and pressure drop predictions in heat exchanger design codes. Because the Coleman and Garimella (2003) criteria yielded transitions similar to those predicted by Dobson and Chato (1998), lead to consistency in the heat transfer models, and are easy to implement, they were chosen for the assignment of flow regimes to the data points in this study.

Comparison with the literature

To assess the validity of models in the literature for this high-pressure refrigerant blend when operating at near-critical or supercritical pressures, the heat transfer coefficients from the present study were compared with the predictions of several commonly used correlations, Shah (1979), Traviss et al. (1973), Dobson and Chato (1998), Sweeney (1996) and Cavallini et al. (2002a). Detailed calculations for these models using the representative data point used in Chapter 4 are included in Appendix E.

Shah (1979) and Traviss et al. (1973)

The empirical correlation of Shah (1979) for R-11, R-12, R-22, R-113, water, methanol, ethanol, benzene, toluene, and trichloroethylene, is as follows:

$$\frac{h}{h_{lo}} = (1-x)^{0.8} + 3.8x^{0.76}\frac{(1-x)^{0.04}}{P_r^{0.38}} \tag{95}$$

where P_r is the reduced pressure and

$$h_{lo} = 0.023\left(\frac{k_l}{D}\right)\left(\frac{GD}{\mu_l}\right)^{0.8} \mathrm{Pr}_l^{0.4} \tag{96}$$

This correlation is applicable for $11 < G < 211$ kg/m^2-s for tube diameters between 7 and 40 mm. The reduced pressure of the data ranged from 0.002 to 0.44. The author noted that the application of this model should be restricted to the operating ranges of the data considered for $1 < \mathrm{Pr_l} < 13$ and $\mathrm{Re_l} > 350$. Figure 28 shows the prediction of the data using Shah (1979) correlation.

The momentum-heat transfer analogy based model of Traviss et al. (1973) results in the following expression for Nusselt number:

$$Nu = \frac{0.15\mathrm{Re}_l^{0.9}\,\mathrm{Pr}_l}{F_2}\left[X_{tt}^{-1} + 2.85X_{tt}^{-0.476}\right] \tag{97}$$

where the function F_2 represents the resistance to heat transfer in the laminar sublayer, the buffer layer and the turbulent region in the annular film:

$$F_2 = \begin{cases} 0.707\,\mathrm{Pr}_l\,\mathrm{Re}_l^{0.5}] & \mathrm{Re}_l < 50 \\ 5\mathrm{Pr}_l + 5\ln[1 + \mathrm{Pr}_l(0.09636\mathrm{Re}_l^{0.585} - 1)] & 50 < \mathrm{Re}_l < 1125 \\ 5\mathrm{Pr}_l + 5\ln(1 + 5\mathrm{Pr}_l) + 2.5\ln(0.00313\mathrm{Re}_l^{0.812}) & \mathrm{Re}_l > 1125 \end{cases} \tag{98}$$

The turbulent vapor/turbulent liquid Martinelli parameter is calculated as follows:

$$X_{tt} = \left(\frac{1-x}{x}\right)^{0.9}\left(\frac{\rho_v}{\rho_l}\right)^{0.5}\left(\frac{\mu_l}{\mu_v}\right)^{0.1} \tag{99}$$

Figure 29 shows a comparison of the data from the current study with the predictions of the Traviss et al. (1973) correlation.

It is found that the Shah (1979) and Traviss et al. (1973) models significantly over predict the heat transfer coefficients from the present study. This may be due to the fact that both these correlations were developed for pure refrigerants condensing at much lower reduced pressures or saturation temperatures (Shah (1979): $0.002 < P_r < 0.44$, Traviss et al. (1973): $25 < T_{sat} < 58$). Furthermore, both models were only for annular flow.

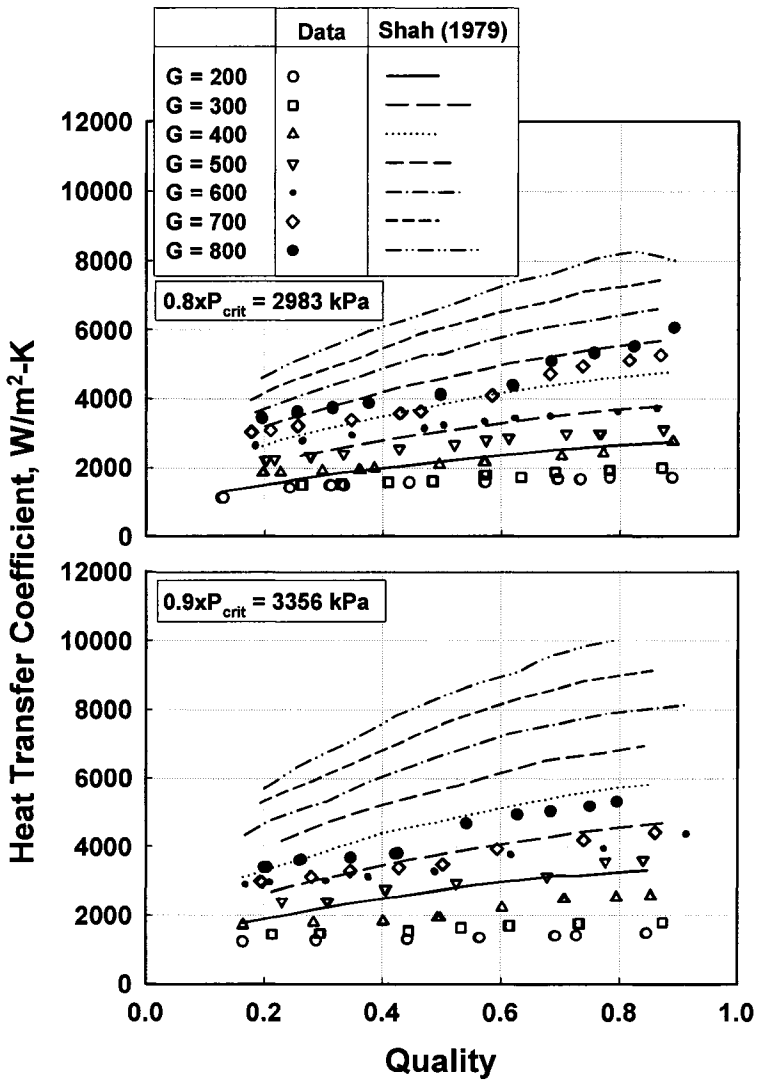

Figure 28. Comparison of the Measured Heat Transfer Coefficients with the Model of Shah (1979)

Dobson and Chato (1998) and Sweeney (1996)

For shear-driven flow ($G < 500$ kg/m^2-s and $Fr_{so} > 20$, or $G > 500$ kg/m^2-s), Dobson and Chato (1998) reduced the Traviss et al. (1973) correlation to a two-phase multiplier type of correlation for $Re_l > 1125$, which is common for annular flow (Dobson *et al.* 1994). Their correlation based on this approach is as follows:

$$Nu_{annular} = 0.023 \mathrm{Re}_l^{0.8} \mathrm{Pr}_l^{0.4} \left[1 + \frac{2.22}{X_{tt}^{0.89}} \right] \tag{100}$$

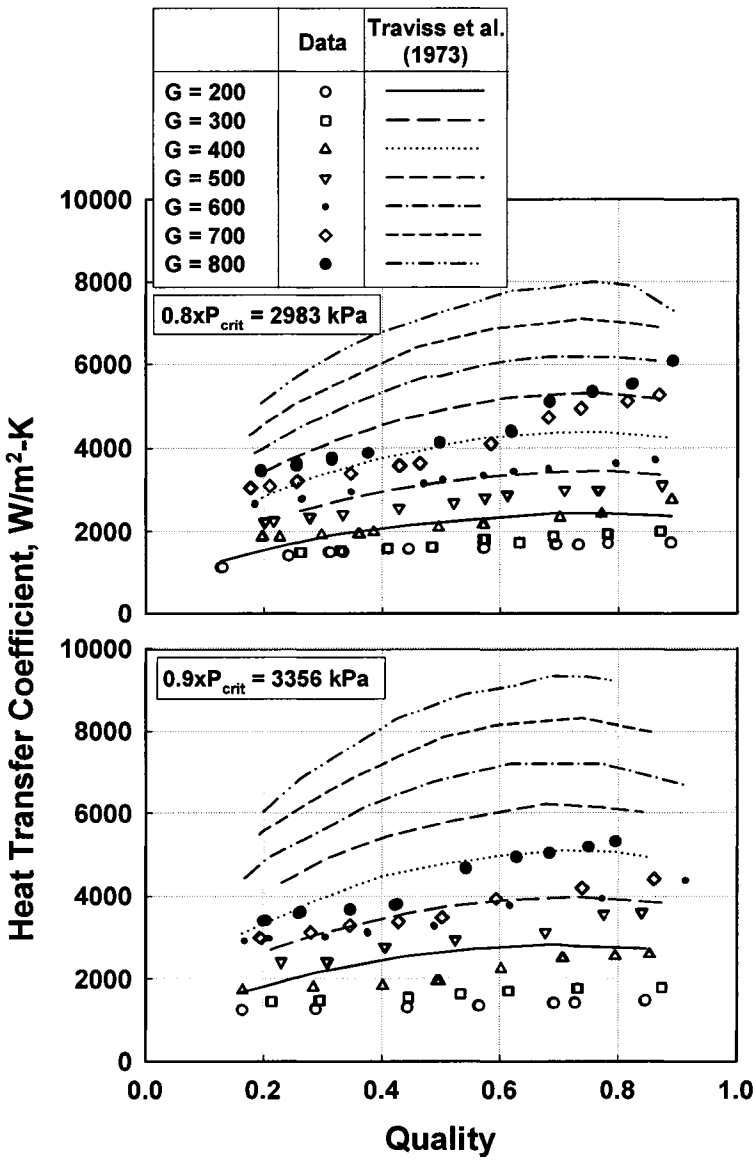

Figure 29. Comparison of the Measured Heat Transfer Coefficients with the Model of Traviss *et al.* (1973)

For the gravity driven correlation (G < 500 kg/m^2-s and Fr_{so} < 20), their additive correlation that accounts for both film condensation and liquid pool forced convection is as follows:

$$Nu_{wavy} = Nu_{film} + (1-\theta_l/\pi)Nu_{forced} \tag{101}$$

The heat transfer model for the forced convection in the liquid pool is as follows:

$$Nu_{forced} = 0.0195\,\mathrm{Re}_l^{0.8}\,\mathrm{Pr}_l^{0.4}\,\phi_l(X_{tt}) \tag{102}$$

where

$$\phi_l(X_{tt}) = \sqrt{1.376 + \frac{c_1}{X_{tt}^{c_2}}} \tag{103}$$

The constants c_1 and c_2 are functions of liquid Froude number. For $0 < Fr_l < 0.7$,

$$c_1 = 4.172 + 5.48Fr_l - 1.564Fr_l^2 \tag{104}$$

$$c_2 = 41.773 - 0.169Fr_l \tag{105}$$

For $Fr_l > 0.7$, $c_1 = 7.424$ and $c_2 = 1.655$, respectively. The heat transfer due to film condensation on the top of the tube was based on a Nusselt type of condensation with a multiplier to account for the enhancement due to interfacial waves.

$$Nu_{film} = \frac{0.23\mathrm{Re}_{vo}^{0.12}}{1 + 1.11X_{tt}^{0.58}}\left[\frac{Ga\,\mathrm{Pr}_L}{Ja_l}\right]^{0.25} \tag{106}$$

The liquid angle θ_l (angle subtended from the top of tube to liquid level) is evaluated using Zivi (1964) void fraction as follows:

$$\left(1 - \frac{\theta_l}{\pi}\right) \cong \frac{\arccos(2\alpha - 1)}{\pi} \tag{107}$$

Comparisons of the current data with the predictions of the Dobson and Chato (1998) model are shown in Figure 30. In general, the experimental values from the present study are between the predictions of the annular and wavy-stratified submodels of Dobson and Chato: their annular model strongly over predicts the current data, while the wavy-stratified model slightly under-predicts the data. This overall result is understandable based on the expectation from the discussion above that the current data are mostly in the discrete and disperse wave regions according to Coleman (2000) or in the transition regions between the annular and wavy region according to Breber et al. (1980). Furthermore, the high reduced pressures in the present study may also contribute to this discrepancy. However, the discrepancies between their model and the current data are substantial; furthermore, the abrupt and unrealistic jump in heat transfer coefficient from the wavy-stratified to the annular region predicted by their model limit its usefulness to the conditions under study here.

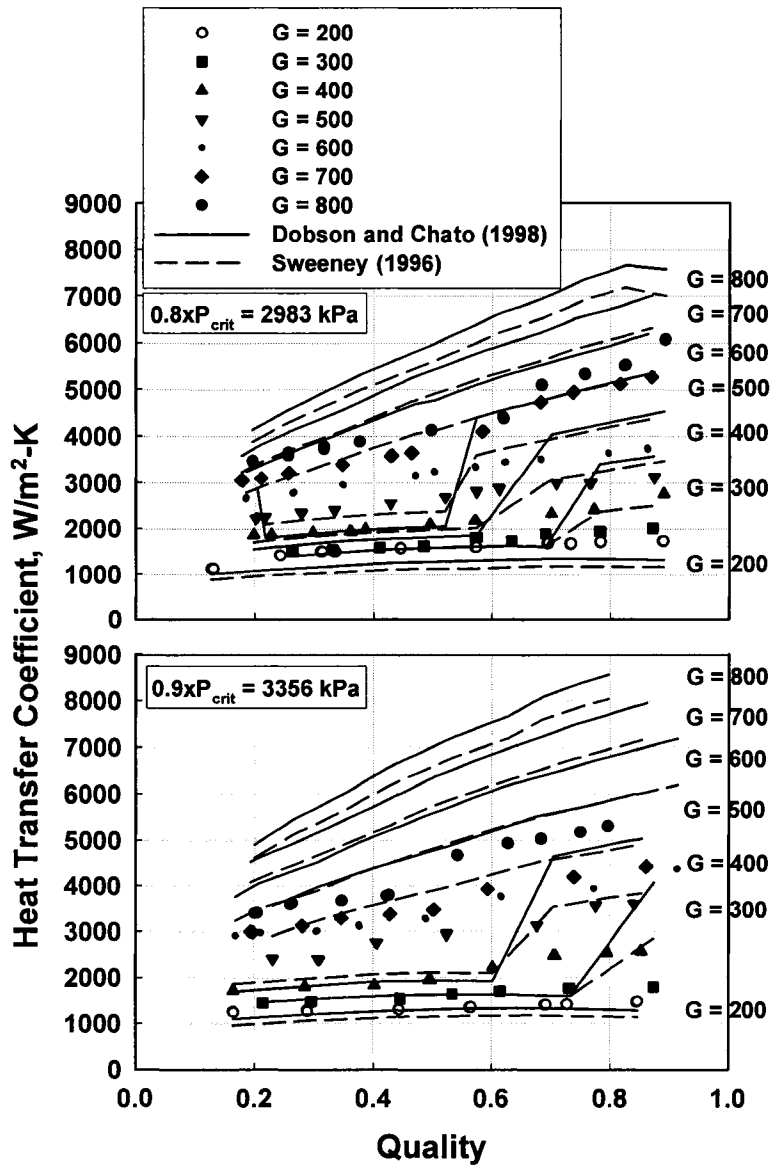

Figure 30. Comparison of the Measured Heat Transfer Coefficients with the Models of Dobson and Chato (1998) and Sweeney (1996)

The mass flux based modification proposed by Sweeney (1996) to the Dobson and Chato (1998) (who used the data from the work of Dobson (1994)) models to allow their usage for R407C are as follows:

$$Nu_{wavy} = \left(\frac{G}{300}\right)^{0.3} Nu_{Dobson\ and\ Chato} \tag{108}$$

$$Nu_{annular} = 0.7\left(\frac{G}{300}\right)^{0.3} Nu_{Dobson\ and\ Chato} \tag{109}$$

Figure 30 also shows the comparison between the Sweeney (1996) model and the data from the current study. It can be seen that, as expected, Sweeney (1996) model shows trends similar to those of Dobson and Chato (1998), except that, perhaps due to these modifications, the annular flow correlation yields somewhat better predictions than those of Dobson and Chato (1998).

Cavallini et al. (2002b; 2002a)

The Cavallini et al. (2002a) models consist of submodels for annular flow, annular-stratified flow transition and stratified flow, and stratified-slug and slug flow. For dimensionless vapor velocity $J_G > 2.5$ and Martinelli parameter $X_{tt} < 1.6$, they used annular flow model, where J_G and X_{tt} are defined as follows:

$$J_G = \frac{xG}{gD\rho_v(\rho_l - \rho_v)^{0.5}} \tag{110}$$

$$X_{tt} = \left(\frac{1-x}{x}\right)^{0.9}\left(\frac{\rho_v}{\rho_l}\right)^{0.5}\left(\frac{\mu_l}{\mu_v}\right)^{0.1} \tag{111}$$

For $J_G < 2.5$, when $X_{tt} < 1.6$, they recommended the annular-stratified flow transition and stratified flow model, while for $X_{tt} > 1.6$, the stratified-slug and slug flow model is recommended.

Based on the theoretical model of Kosky and Staub (1971), their annular flow model is as follows:

$$h_{annular} = \rho_l c_{p,l}(\tau/\rho_l)^{0.5}/T^+ \tag{112}$$

Where τ and T^+ are interfacial shear stress and turbulent temperature, respectively. The turbulent temperature is in turn a function of nondimensional film thickness.

$$\tau = (dP/dz)_f \frac{D}{4} \tag{113}$$

$$T^+ = \begin{cases} \delta^+ \mathrm{Pr}_l & \delta^+ \le 5 \\ 5\{\mathrm{Pr}_l + \ln[1+\mathrm{Pr}_l(\delta^+/5-1)]\} & 5 < \delta^+ < 30 \\ 5[\mathrm{Pr}_l + \ln(1+5\mathrm{Pr}_l) + 0.495\ln(\delta^+/30)] & \delta^+ \ge 30 \end{cases} \tag{114}$$

$$\delta^+ = \begin{cases} (\mathrm{Re}_L/2)^{0.5} & \mathrm{Re}_l \le 1145 \\ 0.0504\,\mathrm{Re}_l^{7/8} & \mathrm{Re}_l > 1145 \end{cases} \tag{115}$$

A modified Friedel (1979) correlation is used to calculate the frictional pressure gradient:

$$\Phi_{LO}^2 = E + \frac{1.262F \cdot H}{We^{0.1458}} \tag{116}$$

$$E = (1-x)^2 + x^2 \frac{\rho_l f_{GO}}{\rho_v f_{LO}} \tag{117}$$

$$F = x^{0.6978} \tag{118}$$

$$H = \left(\frac{\rho_l}{\rho_v}\right)^{0.3278} \left(\frac{\mu_v}{\mu_l}\right)^{-1.181} \left(1 - \frac{\mu_v}{\mu_l}\right)^{3.477} \tag{119}$$

$$We = \frac{G^2 D}{\rho_v \sigma} \tag{120}$$

$$f_{GO} = \begin{cases} 0.046[GD/\mu_v]^{-0.2} & \mathrm{Re}_{GO} > 2000 \\ 16/[GD/\mu_v] & \mathrm{Re}_{GO} \le 2000 \end{cases} \tag{121}$$

$$f_{LO} = \begin{cases} 0.046[GD/\mu_l]^{-0.2} & \mathrm{Re}_{LO} > 2000 \\ 16/[GD/\mu_l] & \mathrm{Re}_{LO} \le 2000 \end{cases} \tag{122}$$

For the annular-stratified flow transition and stratified flow region, the heat transfer model is a linear interpolation between the heat transfer coefficient for annular flow at J_G = 2.5 and the heat transfer coefficient for stratified flow shown as follows:

$$h_{annular-stratified} = (h_{an,J_G=2.5} - h_{strat})(J_G / 2.5) + h_{strat} \tag{123}$$

$$\begin{aligned} h_{strat} &= 0.725\{1 + 0.82[(1-x)/x]^{0.268}\}^{-1}[k_l^3 \rho_l (\rho_l - \rho_G) g h_{fg} / (\mu_l D \Delta T)]^{0.25} \\ &\quad + h_L (1 - \theta_l / \pi) \end{aligned} \tag{124}$$

where the liquid level angle θ_l is again evaluated using Zivi (1964) void fraction.

$$h_L = h_{LO}(1-x)^{0.8} \tag{125}$$

$$h_{LO} = 0.023 \,\mathrm{Re}_{LO}^{0.8} \,\mathrm{Pr}_l^{0.4} \, k_l / D \tag{126}$$

For slug flow (J_G < 2.5 and X_{tt} > 1.6), the heat transfer coefficient is calculated as a linear interpolation between the heat transfer coefficient calculated at X_{tt} = 1.6 and the heat transfer coefficient obtained if the entire flow is liquid flow only.

$$h_{stratified-slug} = h_{LO} + \frac{x(h_{annular-stratified, X_{tt}=1.6} - h_{LO})}{x_{X_{tt}=1.6}} \tag{127}$$

$$x_{X_{tt}=1.6} = \frac{(\rho_v/\rho_l)^{5/9}(\mu_l/\mu_v)^{1/9}}{1.686+(\rho_v/\rho_l)^{5/9}(\mu_l/\mu_v)^{1/9}} \tag{128}$$

Figure 31 shows the comparison of the current data with the predictions of the flow regime-based models by Cavallini et al. (2002a). It can be seen that the predictions of the current data are much better than the other models discussed above. The mean absolute deviations between the data from the current study and their predictions are 17.3% and 10.8% for the 0.80 and 0.90 reduced pressure cases, respectively. The substantially better

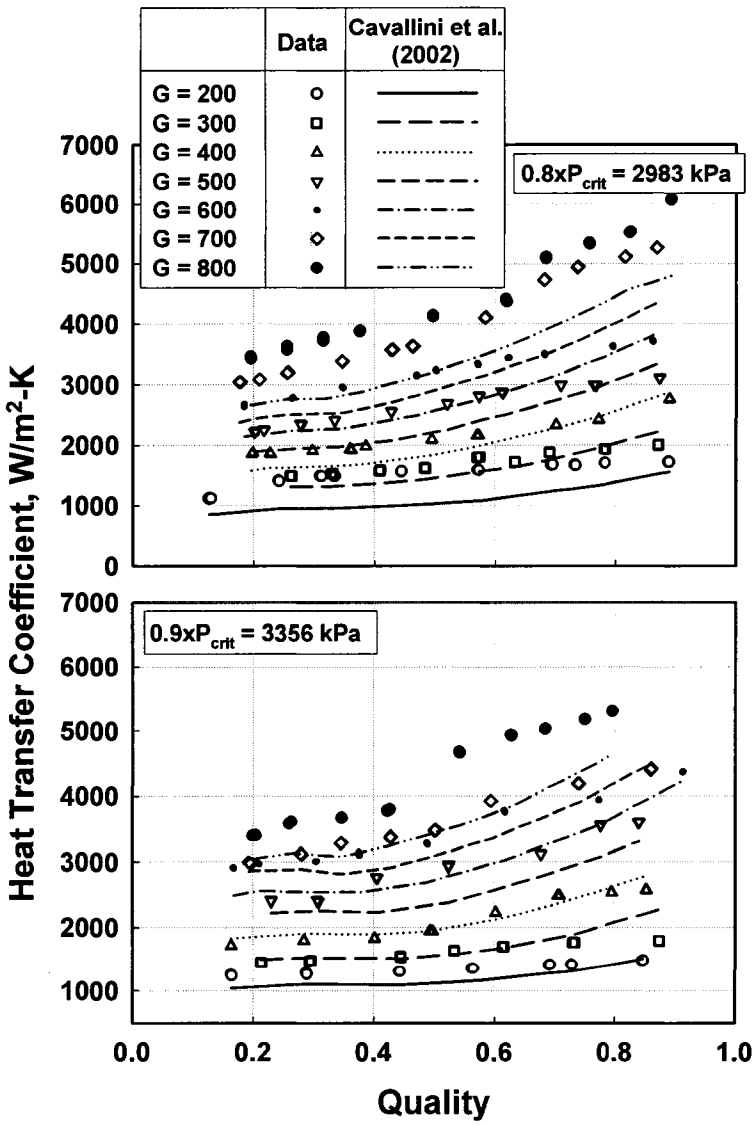

Figure 31. Comparison of the Measured Heat Transfer Coefficients with the Model of Cavallini *et al.* (2002a)

agreement with this model is not surprising when this model's applicable range is considered. The conditions for the present study, P_r = 0.8 and 0.9, and $2.69 < \rho_l/\rho_v < 3.82$, are only slightly outside the range of applicability of their model.

The (total) pressure drop model proposed by Cavallini et al. (2002a) was based on the original (for $J_G < 2.5$) and modified (for $J_G > 2.5$) Friedel (1979) correlation as discussed for the annular flow heat transfer coefficient. Figure 32 shows the comparison of the current (total) pressure gradient data with the predictions of the model by Cavallini et al. (2002a). It can be seen that the agreement between the pressure drop model of Cavallini et al. (2002b) and the current data is not as good as the corresponding agreement of the heat transfer data. Their model under-predicts the experimental values, especially for higher mass fluxes, with mean absolute deviations of 66.3% and 68.6% for P_r = 0.8 and 0.9, respectively. It can also be seen that the original Friedel (1979) correlation for $J_G < 2.5$ yields much better predictions than the modified version of the Friedel (1979) correlation proposed by them. Furthermore, the abrupt transitions between the two correlations are unrealistic. It was discussed above that pressure drop values in the current study are more sensitive to reduced pressure than heat transfer data, which was explained based on the variations in the phase properties. Hence this larger discrepancy in pressure drops between their model and the current data is understandable. Also, the increasing discrepancy as the reduced pressure deviates from their maximum value of 0.75 to 0.9 in this study corroborates this explanation.

Trends in supercritical gas cooling and pressure drop

The variation of measured heat transfer coefficients with temperature for all mass fluxes was shown in Figure 15 earlier in this chapter. It can be clearly seen that there is a sharp peak in the heat transfer coefficients in the vicinity of the critical temperature. A drastic change in thermophysical properties in this region due to a change from gas-like to liquid-like behavior, as shown in Figure 1 (Chapter 1), leads to this peak. Thus, for example, for the G = 300 kg/m^2-s case, for the data point at T = 58.95°C, P = 3732 kPa, the C_p = 1.98 kJ/kg-K, whereas at T = 73.12°C, P = 3729 kPa, C_p = 7.40 kJ/kg-K. The density falls abruptly from 867.9 to 320.3 kg/m^3 across this same temperature, while the viscosity decreases from 8.24×10^{-5} to 2.56×10^{-5} kg/m-s, and the thermal conductivity decreases from

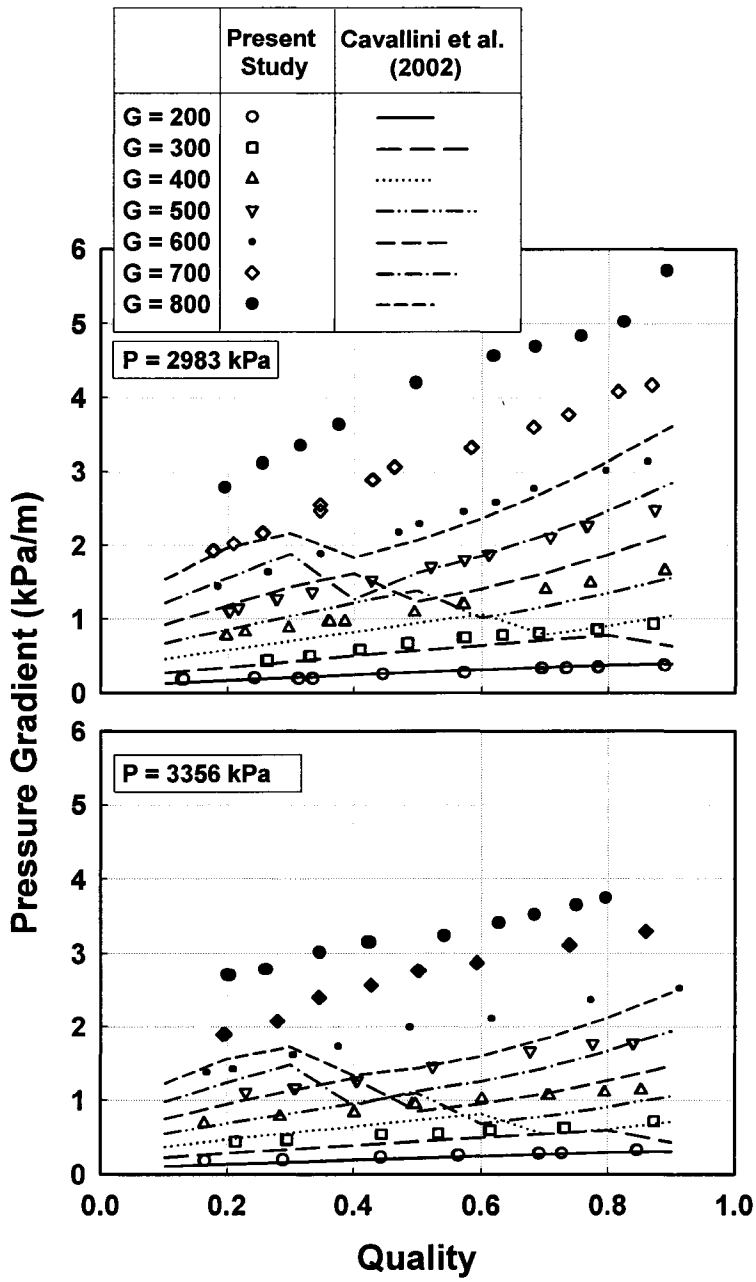

Figure 32. Comparison of the Measured Pressure Gradient with the Model of Cavallini et al. (2002a)

0.0544 to 0.0430 W/m-K. At the same mass flux, the decrease in viscosity leads to an increase in Reynolds number (from 34,233 to 110,999). The combination of property changes leads to an increase in Prandtl number from 3.00 to 4.40. The net effect of these changes is that the Nusselt number increases from 196 to 420, leading to an increase in heat transfer coefficient from 1133 to 1920 W/m^2-K. Similar variations can be seen in the

supercritical ($P = 1.1 \times P_{crit}$) case. For a similar mass flux ($G = 300$ kg/m^2-s), as T increases from 68.54 to 77.56°C, C_p increases from 2.47 to 10.21 kJ/kg-K, the density falls from 781.5 to 409.8 kg/m^3, the viscosity decreases from 6.82×10^{-5} to 3.10×10^{-5} kg/m-s, and the thermal conductivity decreases from 0.0514 to 0.0489 W/m-K. The Reynolds number increases from 41,394 to 90,885, and the Prandtl number increases from 3.28 to 6.47. The resulting effect is to increase the heat transfer coefficient from 1232 to 2260 W/m^2-K. As the temperature increases well beyond the critical temperature (for example, beyond $T > 90$°C), several properties such as C_p, ρ, μ and k gradually approach ideal gas behavior. This approach to ideal gas behavior from quasi two-phase behavior leads to the lower heat transfer coefficients characteristic of gas-phase flow. For example, at critical pressure, T = 107.5°C, h_t = 1062 W/m^2-K, even as the Reynolds number approaches a value of about 139,997 due to the decrease in viscosity ($\mu = 2.03 \times 10^{-5}$ kg/m-s) because of the decrease in k to 0.029 W/m-K. It should also be noted that, as the pressure increases, the variations in properties decreases, resulting less variation in heat transfer coefficients. Furthermore, the heat transfer coefficient maintains high values and peaks at increasingly high temperatures of about 73, 77 and 87°C for $P = P_{crit}$, $1.1 \times P_{crit}$, and $1.2 \times P_{crit}$, respectively. This is because the abrupt change in properties occurs at 72, 76 and 82°C when the pressure increases, as seen in Figure 1 (Chapter 1). Nusselt numbers for these cases are shown in Figure 33. This figure shows that the peaks in Nusselt numbers are at somewhat higher temperatures than those for heat transfer coefficients because of the decrease in thermal conductivity at the higher temperatures. For example, at G = 700 kg/m^2-s, the maximum value in heat transfer coefficient (6979 W/m^2-K) occurs at T = 78.45°C. However, as the temperature increases from 78.45 to 85.57°C, the thermal conductivity decreases from 0.0463 to 0.0342 W/m-K, resulting in an increase in Nusselt number from 1417 to 1706. Similar trends are observed throughout the range of mass fluxes investigated in this study, with the peak being sharper at the higher mass fluxes.

The effect of temperature on heat transfer coefficient is further illustrated by noting that the controlled variation in mass flux in this study was from G = 200 to 800 kg/m^2-s, a factor of 4, while at a representative mass flux of 300 kg/m^2-s, simply changing the

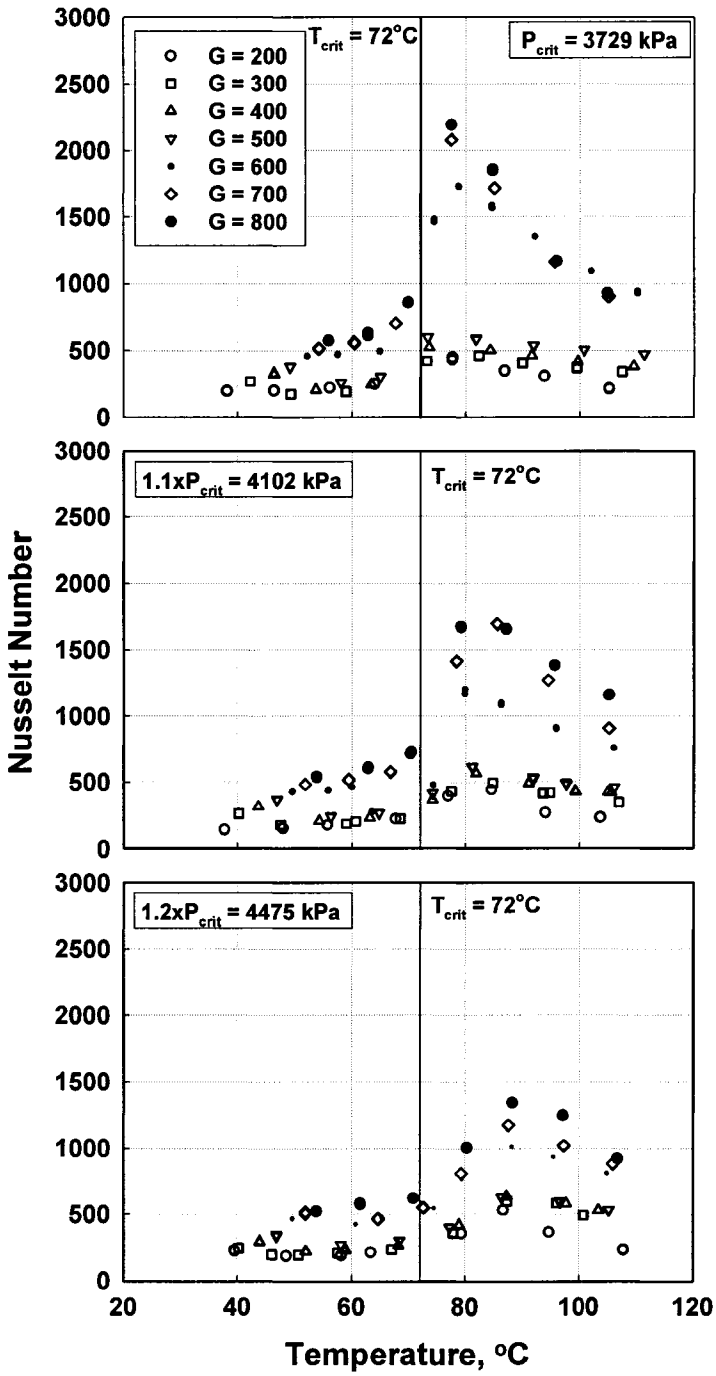

Figure 33. Nusselt Numbers for Supercritical Tests

temperature from about 42 to 108°C, keeping G constant, increases the Reynolds number by a factor of 5.4 (from Re = 25,961 to Re = 139,997). Thus, temperature variation above the vapor-liquid dome has a much more significant effect on heat transfer than the independent variation of mass flux, because it affects thermal properties as well as the flow-related Reynolds number substantially.

The variation in the frictional pressure gradient of the refrigerant with temperature was shown in Figure 34. It can be seen that the variation of pressure drop is not very significant below the transition temperature, i.e., in the liquid-like region. The pressure gradient abruptly drops at the transition temperature due to the sudden change in refrigerant properties from the gas-like to the liquid-like properties. Thus, for example, for the G = 300 kg/m^2-s case, across the transition discussed in connection with the heat transfer results, the large increase in density decreases the velocities from 0.94, 0.73 and 0.91 m/s to 0.36, 0.38 and 0.46 m/s at $P = P_{crit}$, $1.1 \times P_{crit}$ and $1.2 \times P_{crit}$, respectively. It is also observed that for a given mass flux and temperature, the pressure drops in the liquid-like phase are approximately the same at different pressures. In the gas-like phase beyond the transition, however, the pressure drop decreases as the pressure increases. This is because, as the pressure increases, while in the liquid-like phase, the fluid density remains approximately constant (for T = 40°C, ρ = 996.9 kg/m^3 at $P = P_{crit}$ and 1007.1 kg/m^3 at $P = 1.2 \times P_{crit}$), in the gas-like phase, the density increases with increased pressure (for T = 90°C, ρ = 197.8 kg/m^3 at $P = P_{crit}$ and 298.8 kg/m^3 at $P = 1.2 \times P_{crit}$ see Figure 1 in Chapter 1), resulting in velocities of 1.83 m/s (ρ = 165.4 kg/m^3) at 107.5°C at $P = P_{crit}$, 1.54 m/s (ρ = 193.2 kg/m^3) at 107°C ($P = 1.1 \times P_{crit}$), and 1.25 m/s (ρ = 240.2 kg/m^3) at 100.8°C ($P = 1.2 \times P_{crit}$). These progressive decreases in flow velocity in the gas phase lead to the decreases in pressure drop in the gas-like phase seen in Figure 34. The friction factors for these data were plotted versus Reynolds number in Figure 35. The outlier points on the top graph of Figure 35 are friction factors for G = 200 kg/m^2-s, which have large relative uncertainties (average uncertainty in measured pressure gradient was ±47.26%, with maximum and minimum uncertainties of ±1607.20% and ±4.31%, respectively). This figure shows that the measured friction factors following the expected trends based on these Reynolds numbers. It can also be seen that the friction factor

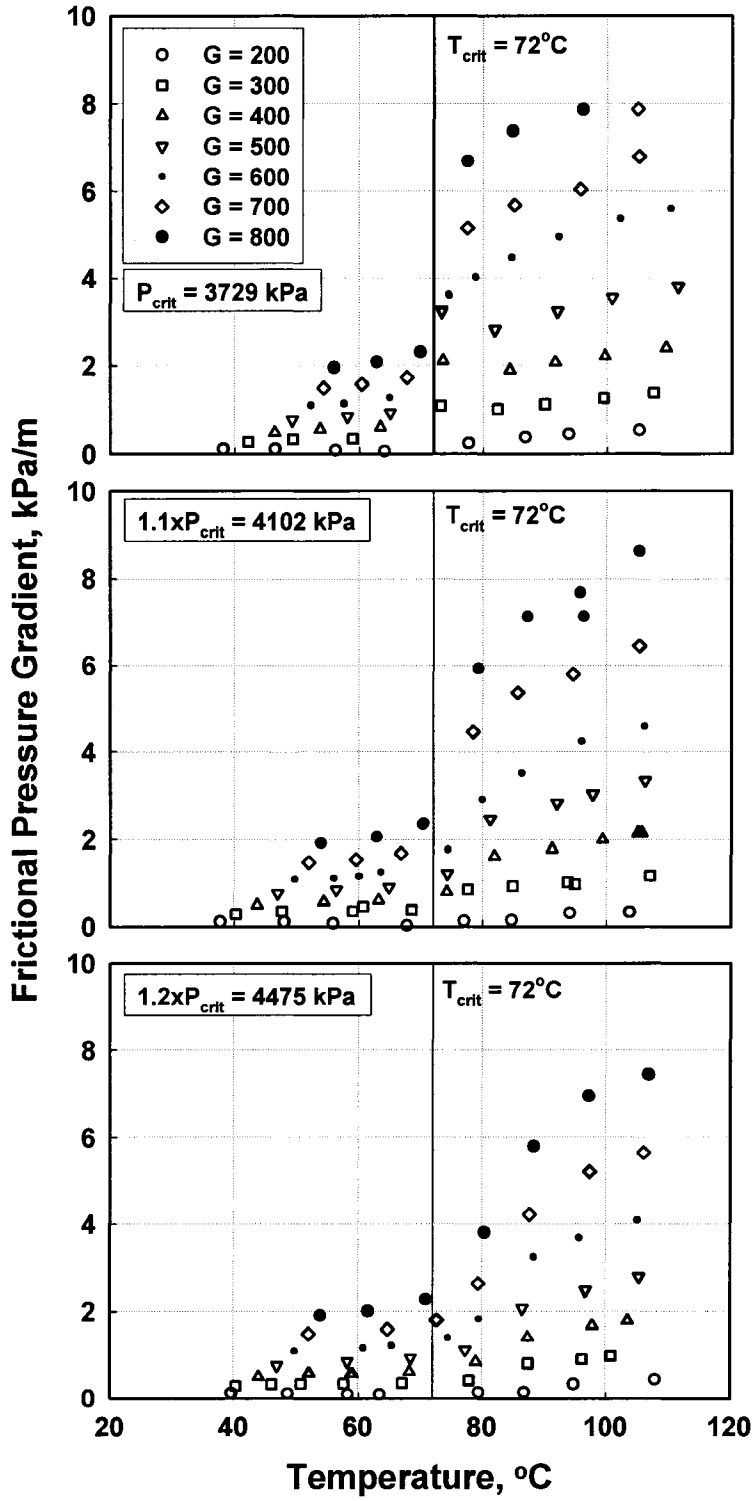

Figure 34. Frictional Pressure Gradients for Supercritical Tests

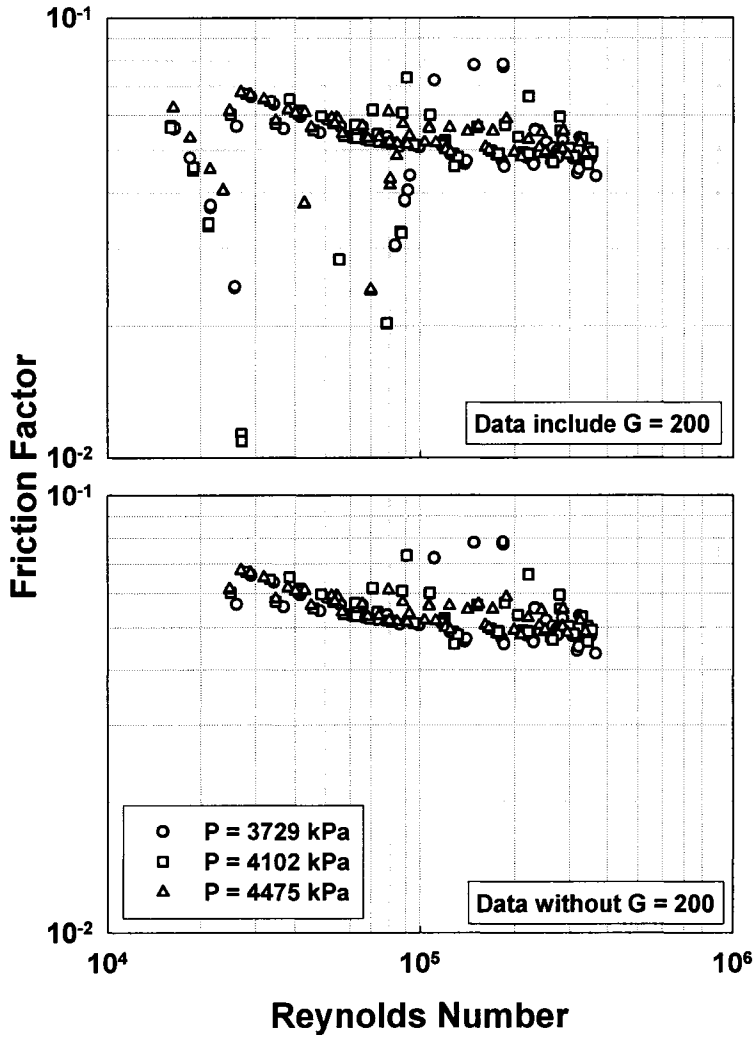

Figure 35. Friction Factors for Supercritical Tests

decreases continuously as the Reynolds number increases, with no significant change around critical temperature. However, it should be noted that the pressure drop is more strongly dependent on the flow velocity than on friction factor.

Supercritical gas cooling flow regime assignment

To further investigate the heat transfer and pressure drop based on the variations in the thermophysical properties, the temperature (or enthalpy) range was divided into three regimes, liquid-like, pseudo-critical transition, and gas-like. In the liquid-like regime, the refrigerant behaves very much like a liquid at subcritical pressures. The viscosity changes the most with the temperature. As the temperature increases, the viscosity decreases

gradually. In the pseudo-critical transition regime, the density and viscosity of the refrigerant decrease sharply with an increase in temperature, while specific heat, volume expansion coefficient and Prandtl number pass through a maximum. In the gas-like regime, the refrigerant properties gradually approach the properties of the perfect gas as the temperature increases.

These flow regime transition criteria are defined quantitatively based on the specific work of thermal expansion (contraction) E_o (Kurganov 1998a), as follows:

$$E_o = \left(P \cdot \frac{\partial V}{\partial h} \right)_p = \frac{P \cdot \beta}{\rho \cdot C_p} \tag{129}$$

E_o is the work done by the refrigerant during cooling or the heat convected out of the system. Figures 36 and 37 show E_o plotted as functions of enthalpy and temperature, respectively. It can be seen that for low temperatures, E_o varies gradually as the enthalpy or temperature increase, but with a further increase in enthalpy or temperature, there is a drastic increase in E_o. This is followed by a peak in E_o, beyond which E_o starts to decline. Therefore, the temperature was classified into three regimes: (a) a liquid-like (low temperature) regime where the change in E_o with temperature (or enthalpy) is not significant, (b) pseudo-critical transition regime where the change in E_o is rapid with temperature (or enthalpy) (although

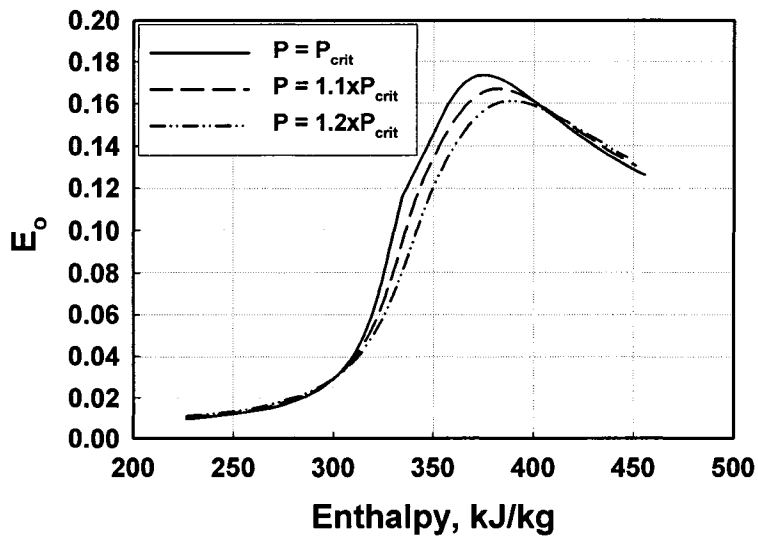

Figure 36. Specific Work of Thermal Expansion as a Function of Enthalpy

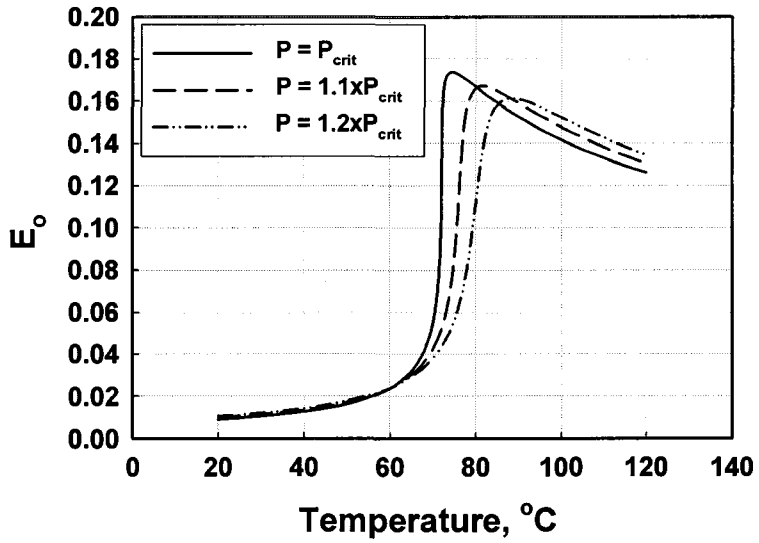

Figure 37. Specific Work of Thermal Expansion as a Function of Temperature

not two-phase flow, this regime has some characteristics of phase-change flow), and (c) the gas-phase regime where the E_o starts to decline as temperature (or enthalpy) increases.

The transition temperatures from the pseudo-critical transition regime to the gas-like regime were found when $dE_o/dh = 0$. For the transition between the liquid-like regime and the pseudo-critical transition regime, since dE_o/dh does not change sign, the transition temperatures were found based on visual inspection to identify the abrupt change in slope. Upon examination of the data, it was found that for a given enthalpy h, E_o was largely independent of pressure. Hence, the corresponding temperatures were used as the basis for dividing the data into liquid-like, pseudo-critical transition and gas-like regimes. Tables 12 and 13 show the transition criteria and the flow regime assignment as a function of temperature.

Table 12. Supercritical Cooling Flow Transition Criteria

Flow Regime	Transition Criteria
Liquid-like	$h = h\ (E_o < 0.03)$
Pseduo-critical transition	$h = h\ (E_o = 0.03)$ to $h = h\ (\partial E_o/\partial h = 0)$
Gas-like	$h > h\ (\partial E_o/\partial h \geq 0)$

Table 13. Supercritical Cooling Flow Regime Assignment

P_r	Liquid-Like Regime	Pseduo-Critical Transition Regime	Gas-Like Regime
1.0	T < 64.25°C	64.25°C < T < 74.45°C	T > 74.45°C
1.1	T < 65.05°C	65.05°C < T < 81.55°C	T > 81.55°C
1.2	T < 65.70°C	65.70°C < T < 88.35°C	T > 88.35°C

Comparison with the literature

The heat transfer coefficients obtained in the present study were compared with the limited literature on heat transfer at supercritical conditions: Krasnoshchekov *et al.* (1970), Pitla *et al.* (2002), and with the well-accepted Gnielinski (1976) correlation for turbulent single-phase heat transfer. Figures 38, 39 and 40 show the comparison for different pressures at G = 300, 500, and 700 kg/m^2-s, respectively.

Gnielinski (1976)

The Gnielinski (1976) single-phase turbulent flow correlation shown below is valid for $0.5 < Pr < 2000$, and $3000 < Re < 5\times10^6$.

$$Nu = \frac{(f/8)(\mathrm{Re}-1000)\,\mathrm{Pr}}{1+12.7(f/8)^{0.5}(\mathrm{Pr}^{2/3}-1)} \tag{130}$$

For smooth tubes, the following correlation by Petukhov is recommended for the evaluation of the friction factor (Incropera and DeWitt 2002).

$$f = [0.790\ln(\mathrm{Re})-1.64]^{-2} \tag{131}$$

From Figures 38, 39 and 40, it can be seen that the Gnielinski (1976) correlation agrees reasonably well with the measured values for lower mass fluxes (G ≤ 500 kg/m^2-s), while the data are considerably underpredicted for higher mass fluxes (G > 500 kg/m^2-s). For the whole set of data, the mean absolute deviations for this correlation are 30.3%.

Krasnoshchekov et al. (1970)

The Krasnoshchekov *et al.* (1970) correlation for single-phase convection uses property ratio multipliers to account for the large property variations in this region as follows:

$$Nu_b = Nu_w\left(\frac{\rho_w}{\rho_b}\right)^n\left(\frac{\bar{c}_p}{c_{pw}}\right)^m \tag{132}$$

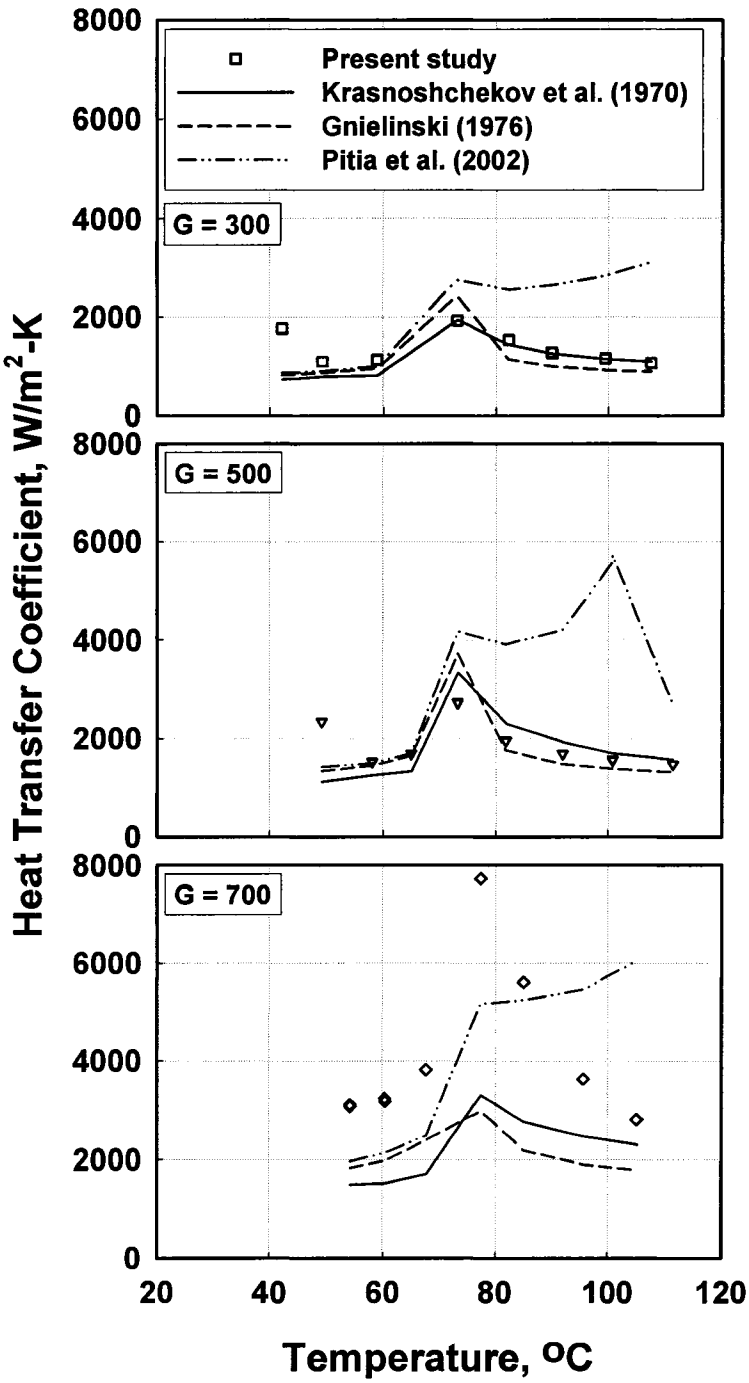

Figure 38. **Comparisons of Measured Heat Transfer Coefficients with the Literature ($P = P_{crit}$)**

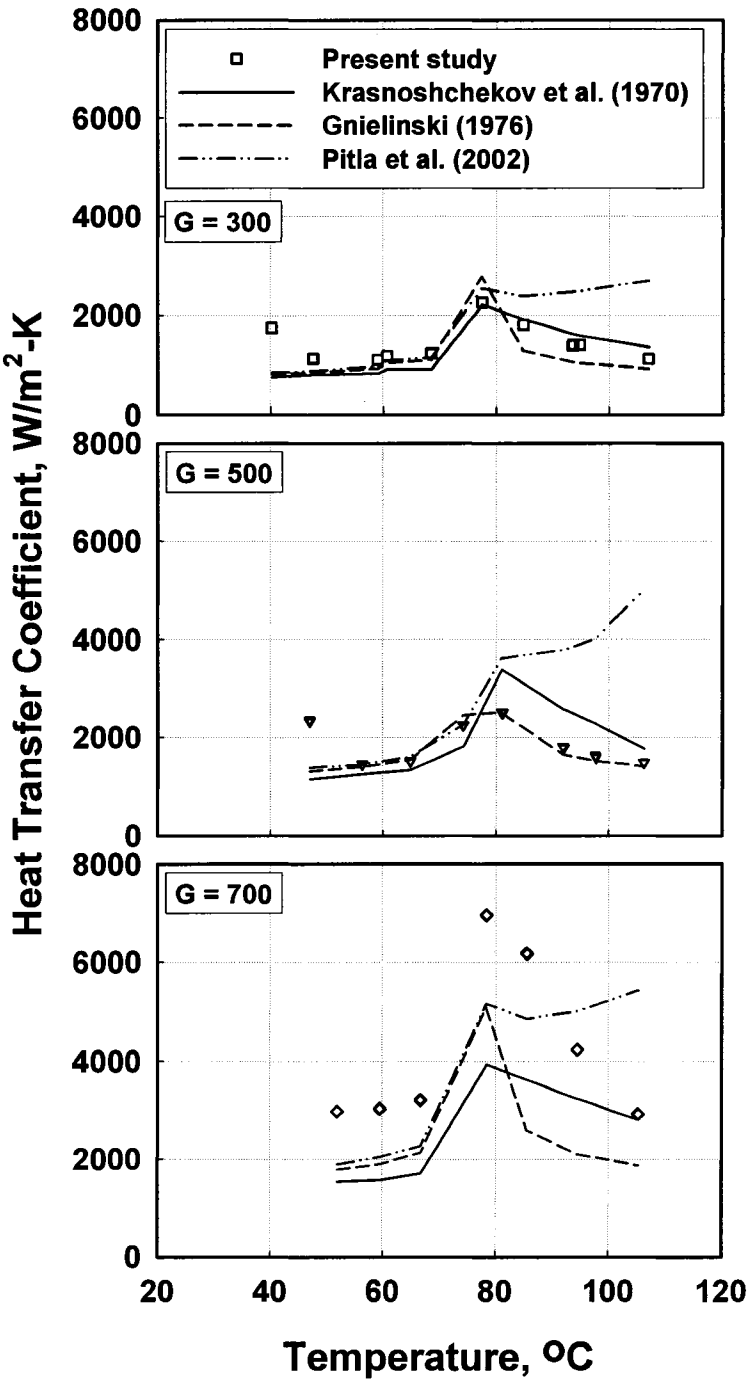

Figure 39. **Comparisons of Measured Heat Transfer Coefficients with the Literature ($P = 1.1 \times P_{crit}$)**

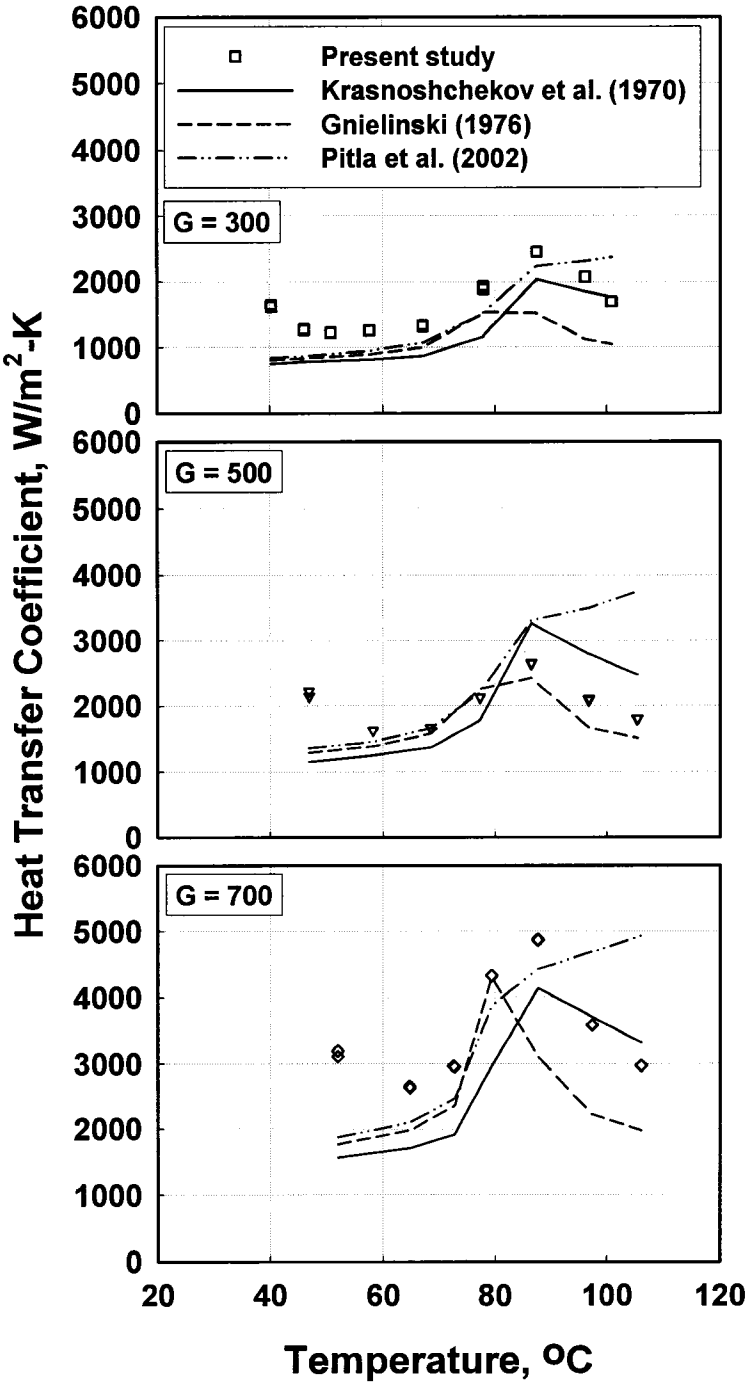

Figure 40. **Comparisons of Measured Heat Transfer Coefficients with the Literature ($P = 1.2 \times P_{crit}$)**

where m, and n are constants provided graphically by the authors. Nu_w is evaluated at the wall temperature using the turbulent heat transfer correlation by Petukhov (Incropera and DeWitt 2002).

$$Nu = \frac{(f/8)\,\mathrm{Re}\,\mathrm{Pr}}{1.07 + 12.7(f/8)^{0.5}(\mathrm{Pr}^{2/3} - 1)} \tag{133}$$

In this correlation also, the friction factor f is evaluated using equation (131).

It can be seen in Figures 38, 39 and 40 that, similar to the Gnielinski (1976) correlation, the Krasnoshchekov (1970) correlation shows good agreement with the measured values for $G \leq 500$ kg/m^2-s, but underpredicts the data considerably for $G > 500$ kg/m^2-s. Also, the Krasnoshchekov *et al.* (1970) correlation, which was developed for supercritical cooling of CO_2, tends to underpredict the data more severely in the liquid-like region. It appears that the correlations developed for CO_2 cannot be extrapolated to refrigerant R404A with an acceptable level of accuracy. For the whole set of data, the mean absolute deviations for this correlation is 31.8%.

Pitla et al. (2002)

The Pitla *et al.* (2002) correlation for in-tube supercritical cooling of carbon dioxide was based on their experimental (Pitla *et al.* 2001a) and numerical (Pitla *et al.* 2001b) studies as follows:

$$Nu = \left(\frac{Nu_{wall} + Nu_{bulk}}{2} \right) \frac{k_{wall}}{k_{bulk}} \tag{134}$$

where Nu_{wall} and Nu_{bulk} are evaluated using the Gnielinski correlation (1976) (Equation 130) at wall and bulk temperatures, respectively. For smooth tubes, the Petukhov correlation (Incropera and DeWitt 2002) is again used to evaluate the friction factor. The authors also noted that the Reynolds number at the wall should be calculated using the inlet velocity irrespective of the location, and the bulk Reynolds number should be evaluated using the local mean velocity.

The agreement between the data and Pitla *et al.* (2002) correlation is not very good (Figures 37, 38 and 39), especially for the gas like region. Again, it underpredicts the data in the low temperature region for higher mass fluxes. Furthermore, the abrupt variation in heat transfer coefficient and the multiple inflection points in the graphs from their predictions

above critical temperature are unrealistic. It appears that these multiple slope changes and peaks occur because Nu_{wall} and Nu_{bulk} in equation (134) above reach peak values at different fluid temperatures, leading to these unrealistic predictions.

Churchill (1977b)

Pressure drops from the present study were plotted in Figure 41 along with the predictions of the single phase Churchill (1977b) correlation. Again, the agreement between the present data and this correlation is not very good. The correlation underpredicts the measured pressure drop at almost all mass fluxes, with this trend being more pronounced at higher mass fluxes and temperatures in the gas-like region.

Summary

The comparisons of the present data with correlations from the literature presented above for both phase change and supercritical heat transfer and pressure drop were selected to represent different modeling approaches. The Shah (1979) and Traviss et al. (1973) models did not predict the data well, indicating that the much higher reduced pressure in this study has a strong influence on the heat transfer coefficient. The wavy flow model by Dobson and Chato (1998) predicts the data reasonably well. However, their annular flow model overpredicts the data. Furthermore, they assumed an abrupt change between the two flow regimes, rather than a gradual transition between annular and wavy flow. The heat transfer coefficients predicted by Cavallini et al. (2002a) are substantially better than the predictions of the other correlations mentioned above. However, their pressure drop model underpredicts the data substantially. It should be noted that this, in turn, could affect the heat transfer results when pressure gradients are used as intermediate steps for the calculation of heat transfer coefficients. In general, the correlations studied above for supercritical heat transfer and pressure drop did not predict the data well, especially for the higher mass fluxes.

Model Development

In this section, both condensation and supercritical heat transfer and pressure drop models are developed and compared with the experimental data. For condensation, models for wavy and annular flow regimes are developed first, followed by an interpolation

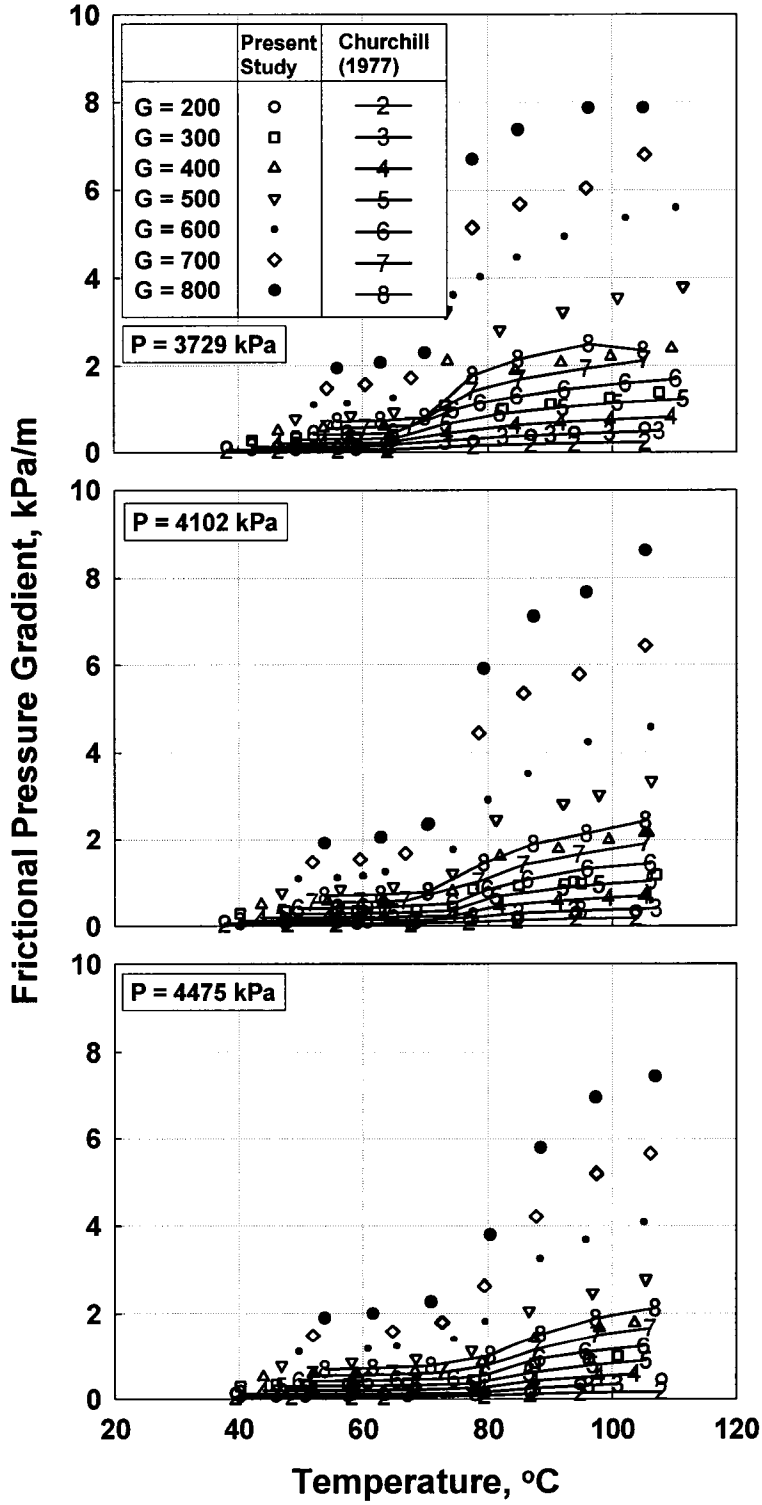

Figure 41. **Comparisons of Measured Pressure Gradient with the Churchill (1977b) Correlation**

technique to predict the data in the transition region between these regimes. For supercritical cooling, heat transfer and pressure drop models are developed based on the specific flow regime, i.e., liquid-like, pseudo-critical transition or gas-like.

It should be noted that a companion study on refrigerant R410A in 6.2 and 9.4 mm diameter tubes is being conducted by another researcher in the same laboratory. The models presented below were developed using data for both fluids. However, the discussion below focuses on the R404A data collected by the author of this dissertation. The models presented below include a diameter ratio, which accounts for the influence of tube diameter deduced from the data collected in the companion study. For the present study on R404A, however, the diameter ratio is unity.

Phase-change heat transfer

Annular flow model

According to Dobson *et al.* (1994), the annular flow model developed by Traviss *et al.* (1973) could be reduced to a two-phase multiplier provided that $Re_l > 1125$. The authors argued that, the Nusselt number could be written in the following form:

$$Nu = \frac{D^+ \mathrm{Pr}_l}{F_2(\mathrm{Re}_l, \mathrm{Pr}_l)} \tag{135}$$

where the term D^+ is the non-dimensional tube diameter scaled by the turbulent length scale, $\nu_l / \sqrt{\tau_w / \rho_l}$. F_2 is a dimensionless heat transfer resistance. This resistance increases as the dimensionless film thickness as well as the liquid Prandtl number increase. Under the assumption of a symmetric annular film with no entrainment, the liquid Reynolds number Re_l uniquely specifies the dimensionless film thickness. Because of the piecewise nature of the universal velocity profile, F_2 is a piecewise function of liquid Reynolds number. For $Re_l < 50$, the annular film is so thin that it is entirely contained in the laminar sublayer. For $50 < Re_l < 1125$ and $Re_l > 1125$, the annular film ends in the buffer layer and fully turbulent region, respectively. Dobson *et al.* (1994) further pointed out that, the liquid film in annular flow was seldom so thin that the fully turbulent region is not reached. With the F_2 confined to values of $Re_l > 1125$, therefore, the piecewise definition of F_2 was generally not necessary. They then proposed a power law function of Re_l and Pr_l for F_2. For the range of Re_l from 1125 to 10,000 and Pr_l from 1 to 10, F_2 can be well approximated by:

$$F_2 \equiv 10.25\,\mathrm{Re}_l^{0.0605}\,\mathrm{Pr}_l^{0.592} \tag{136}$$

By assuming the Lockhart-Matinelli (1949) two-phase liquid multiplier approach for pressure drop correlation, equation (135) was reduced to the following form:

$$Nu = 0.0194\,\mathrm{Re}_l^{0.815}\,\mathrm{Pr}_l^{0.408}\,\phi_l(X_{tt}) \tag{137}$$

which is similar to the approach used by Shah (1979).

For the present study, the liquid Reynolds number $\mathrm{Re_l}$ ranges from 2,991 to 72,623, implying that the film is always in the fully turbulent region. Thus, the two-phase multiplier approach was adopted to correlate the annular flow heat transfer data. The following correlating form was selected:

$$Nu_{annular} = a\,\mathrm{Re}_l^{\,b}\,\mathrm{Pr}_l^{0.3}\left[1+\left(\left(\frac{x}{1-x}\right)\left(\frac{\rho_l}{\rho_v}\right)\right)^{c}\right]\left(\frac{d_{actual}}{d_{baseline}}\right)^{d} \tag{138}$$

Here, $d_{baseline}$ refers to the baseline diameter of 9.4 mm and d_{actual} is the diameter of the tube under consideration in mm. As stated above, for the present case, this ratio is unity. The values of constants a, b, c and d were determined through regression analysis on the measured annular Nusselt numbers to yield the following correlation with $R^2 = 0.90$:

$$Nu_{annular} = 0.013\,\mathrm{Re}_l^{0.84}\,\mathrm{Pr}_l^{0.3}\left[1+\left(\left(\frac{x}{1-x}\right)\left(\frac{\rho_l}{\rho_v}\right)\right)^{0.8}\right]\left(\frac{d_{actual}}{d_{baseline}}\right)^{-0.32} \tag{139}$$

Figure 42 shows this annular flow model compared with the experimental heat transfer coefficients. It can be seen that 85% (76 out of 90) of the data can be predicted within ±15%. The average absolute deviation for the annular model is 7.90%.

Wavy flow model

In wavy flow, heat transfer occurs in the upper portion of the tube by filmwise condensation and in the liquid pool at the bottom of the tube by forced convective condensation, as shown in Figure 43. At low vapor velocities, the liquid pool at the bottom of the tube is relatively quiescent, and heat transfer at the bottom of the tube is much smaller than the heat transfer due to film condensation. In addition, the vapor flow has little effect on the liquid film on the top portion of the tube, and Nusselt-type film condensation on a

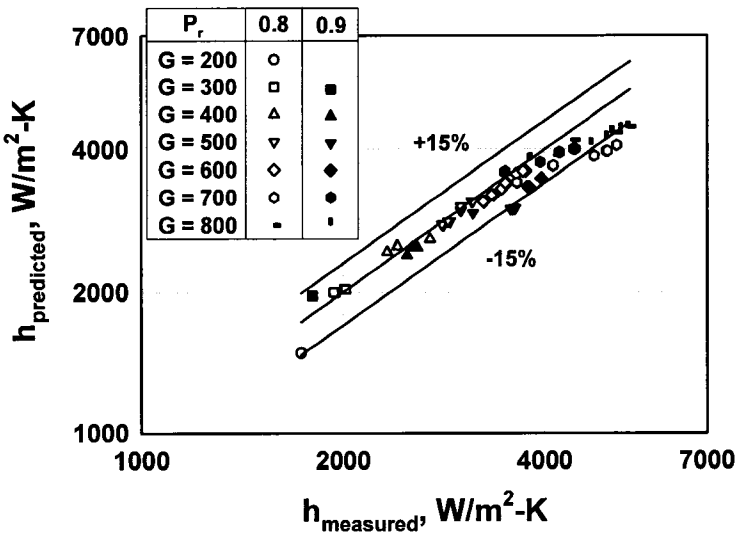

Figure 42. Annular Flow Heat Transfer Model Predictions

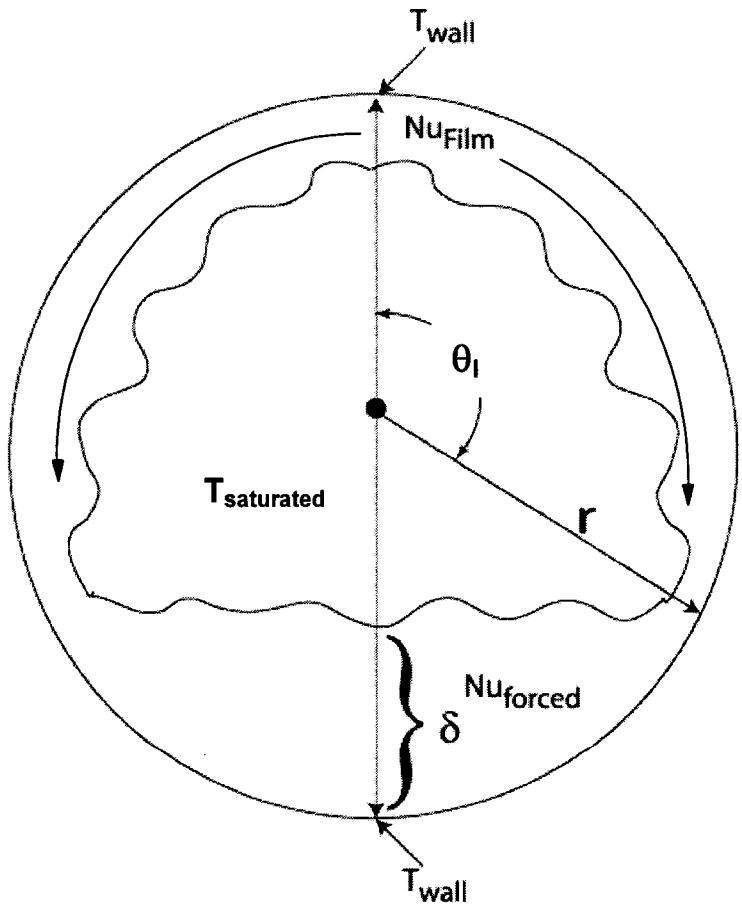

Figure 43. Schematic of Wavy Flow

cylinder can be used to model this process. However, as vapor velocities increase, the heat transfer in the liquid pool also increases due to the increasing waviness of the pool, and may be too significant to be neglect. Furthermore, the interfacial shear exerted by the vapor on the condensate film at the top also increases as the vapor velocities increase. In view of these considerations, an additive model for predicting the local heat transfer coefficient was proposed by combining the heat transfer through film condensation on the top of the tube and forced convection in the liquid pool, as follows:

$$h = \frac{\theta_l}{\pi} h_{film} + \left(1 - \frac{\theta_l}{\pi}\right) h_{forced} \tag{140}$$

where θ_l is the liquid level angle subtended from the top of the tube to the liquid level.

The heat transfer due to film condensation can be calculated using a Nusselt-type analysis over a circular tube. A schematic of the energy balance along the tube curvature is shown in Figure 44. Assuming that the convective terms can be neglected, an energy balance on a differential element of the film requires that

$$h_{fg} \frac{d\dot{m}}{dx} = \frac{k_l [T_{sat}(\rho_v) - T_w]}{\delta} \tag{141}$$

where $\dot{m}$ is the mass flow rate per unit of tube length. x is the coordinate along the curvature. From a simple force balance on the film, one can get

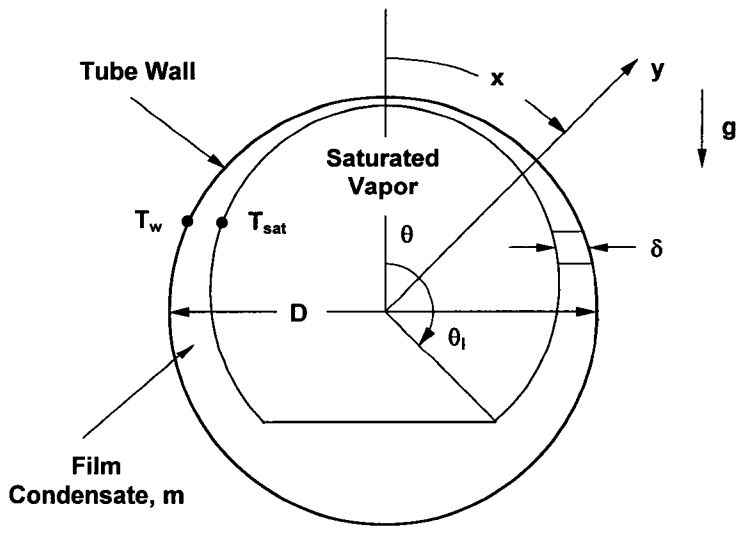

Figure 44. Schematic of Energy Balance on the Film Condensate

$$(\delta - y)dx(\rho_l - \rho_v)g\sin\theta = \mu_l\left(\frac{du}{dy}\right)dx \tag{142}$$

Knowing that u = 0 at y = 0, the velocity profile can be obtained by integrating from y = 0 to y = δ, as follows:

$$u = \frac{(\rho_l - \rho_v)g\sin\theta}{\mu_l}\left(y\delta - \frac{y^2}{2}\right) \tag{143}$$

The condensate mass flow rate per unit of tube length is calculate by integrating the above velocity profile:

$$\dot{m} = \rho_l \int_0^{\delta} u dy = \frac{\rho_l(\rho_l - \rho_v)\delta^3 g\sin\theta}{3\mu_l} \tag{144}$$

By noting that x = θD/2, where D is the inner tube diameter, and combining equations (141) and (144), the following equation is obtained:

$$(\dot{m})^{1/3} d\dot{m} = \frac{Rk_l(T_{sat} - T_{wall})}{h_{fg}}\left[\frac{\rho_l(\rho_l - \rho_v)g}{3\mu_l}\right]^{1/3}\sin^{1/3}\theta d\theta \tag{145}$$

Integrating from θ = 0 to θ = θ_l, we have

$$\dot{m} = \left(\frac{2}{3}\right)^{3/4}\left(\frac{1}{3}\right)^{1/4}\left[\frac{D^3 k_l^{\,3}(T_{sat} - T_{wall})^3}{h_{fg}^{\,3}}\frac{\rho_l(\rho_l - \rho_v)g}{3\mu_l}\right]^{1/4}\left[\int_0^{\theta_l}\sin^{1/3}\theta d\theta\right]^{3/4} \tag{146}$$

From overall energy balance over a control volume (Figure 43) surrounding the inside tube diameter,

$$2h_{fg}\dot{m} = \theta_l D h_{film}(T_{sat} - T_w) \tag{147}$$

and the definition of dimensionless numbers Ga, Pr_l and Ja_l, the Nusselt number for film condensation is obtained as:

$$Nu_{film} = \frac{1.1212}{\theta_l}\left[\frac{Ga\,\mathrm{Pr}_l}{Ja_l}\right]^{1/4}\left[\int_0^{\theta_l}\sin^{1/3}\theta d\theta\right]^{3/4} \tag{148}$$

where $Ga = \frac{\rho_l(\rho_l - \rho_v)gD^3}{\mu_l^{\,2}}$, $\mathrm{Pr}_l = \frac{\mu_l c_{p,l}}{k_l}$ and $Ja_l = \frac{c_{p,l}(T_{sat} - T_{wall})}{h_{fg}}$, respectively.

For the present study, the liquid level angle θ_l was evaluated using the following equation:

$$\left(1-\frac{\theta_l}{\pi}\right)\cong\frac{\arccos(2\alpha-1)}{\pi} \tag{149}$$

where the void fraction α was calculated using correlation by Baroczy (1965):

$$\alpha=\left(1+\left(\frac{1-x}{x}\right)^{0.74}\left(\frac{\rho_v}{\rho_l}\right)^{0.65}\left(\frac{\mu_l}{\mu_v}\right)^{0.13}\right)^{-1} \tag{150}$$

The Baroczy (1965) void fraction correlation was developed using isothermal, two-phase, two-component liquid fraction data from the literature: liquid mercury-nitrogen data from Kiraly and Koestel (1960), and water-air data from Hewitt et al. (1961; 1962). The author recommended that this correlation could be used for all fluids, including liquid metals. For the entire wavy flow data set, θ_l ranges from 1.23 to 2.36 (rad) (70.5 to 135.2°) for G = 195.5 – 802.5 kg/m^2-s, P_r = 0.792 – 0.908 and x = 0.1636 – 0.8464.

For the heat transfer in the liquid pool, a two-phase multiplier type of correlation is proposed:

$$Nu_{forced}=a\,\mathrm{Re}_{liquid}^{\ b}\,\mathrm{Pr}_l^{0.3}\left[1+\left(\frac{x}{1-x}\right)\left(\frac{\rho_l}{\rho_v}\right)\right]\left(\frac{d_{actual}}{d_{baseline}}\right)^c \tag{151}$$

where an actual liquid Reynolds number in the liquid pool Re_{liquid} is used instead of the superficial liquid Reynolds number to better describe the flow in the liquid pool. Thus,

$$\mathrm{Re}_{liquid}=\frac{G\cdot(1-x)\cdot D_{h,liquid\ pool}}{\mu_l} \tag{152}$$

where $D_{h,liquid\ pool}$ is the hydraulic diameter of the liquid pool. The wetted perimeter and flow area of the liquid pool are calculated as follows:

$$P=d_{actual}(\sin\theta_l+\pi-\theta_l) \tag{153}$$

$$A=\frac{(d_{actual})^2}{4}(\sin\theta_l\cos\theta_l+\pi-\theta_l) \tag{154}$$

resulting in the hydraulic diameter of the liquid pool of

$$D_{h,liquid\ pool}=\frac{\left[\sin\theta_l\cos\theta_l+(\pi-\theta_l)\right]}{\left[\sin\theta_l+(\pi-\theta_l)\right]}\times d_{actual} \tag{155}$$

Again, the values of constants a, b and c were determined through regression analysis of R404A data from the present study, and R410A data in the companion study on 9.4 mm and 6.2 mm tube diameters. The resulting correlation ($R^2 = 0.94$) is as follows:

$$Nu_{forced} = 0.005 \mathrm{Re}_{liquid}^{0.97} \mathrm{Pr}_l^{0.3} \left[1 + \left(\frac{x}{1-x} \right) \left(\frac{\rho_l}{\rho_v} \right) \right] \left(\frac{d_{actual}}{d_{baseline}} \right)^{-0.56} \tag{156}$$

Figures 45 shows the present wavy flow model compared with the experimental heat transfer coefficients. It can be seen that 89% (132 out of 148) of the data are predicted within ±15%. The average absolute deviation for the wavy flow model is 7.33%.

Transition region

It is believed that the transitions between different flow patterns are not abrupt but rather gradual in reality. Therefore, a transition region between annular and wavy flow was defined based on the Soliman modified Froude number (Soliman 1982) Fr_{so} (equation 94). For $14 < Fr_{so} < 24$, the heat transfer coefficients can be calculated using an interpolation between the annular and wavy flow heat transfer as follows:

$$Nu = \left(\frac{Fr_{so} - Fr_{so,wavy}}{Fr_{so,annular} - Fr_{wavy}} \right) Nu_{annular} + \left(\frac{Fr_{so,annular} - Fr_{so}}{Fr_{so,annular} - Fr_{so,wavy}} \right) Nu_{wavy} \tag{157}$$

where $Fr_{so,wavy}$ and $Fr_{so,annular}$ corresponding to 14 and 24, respectively.

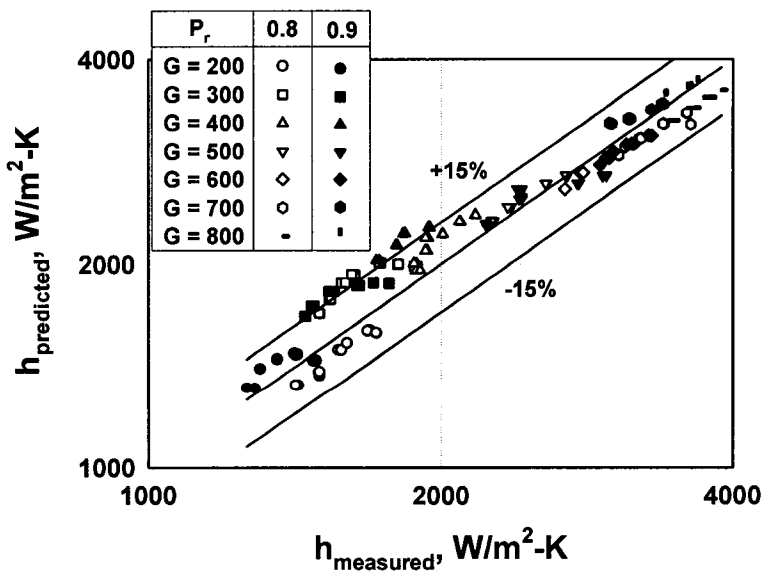

Figure 45. Wavy Flow Heat Transfer Model Predictions

Figure 46 shows the overall prediction and experimental heat transfer coefficients for both annular and wavy flow as a function of quality. Transition region heat transfer coefficients in this figure were calculated according to the interpolation formula shown in equation (157). It can be seen that the transition between annular and wavy flow predictions is smooth due to the interpolation technique used here. Figure 47 shows the comparison of predicted and measured heat transfer coefficients for the entire data set after introducing a transition region between annular and wavy flow. It can be seen that 89% (212 out of 238) of the data can be predicted within ±15%. The average absolute deviation between the data

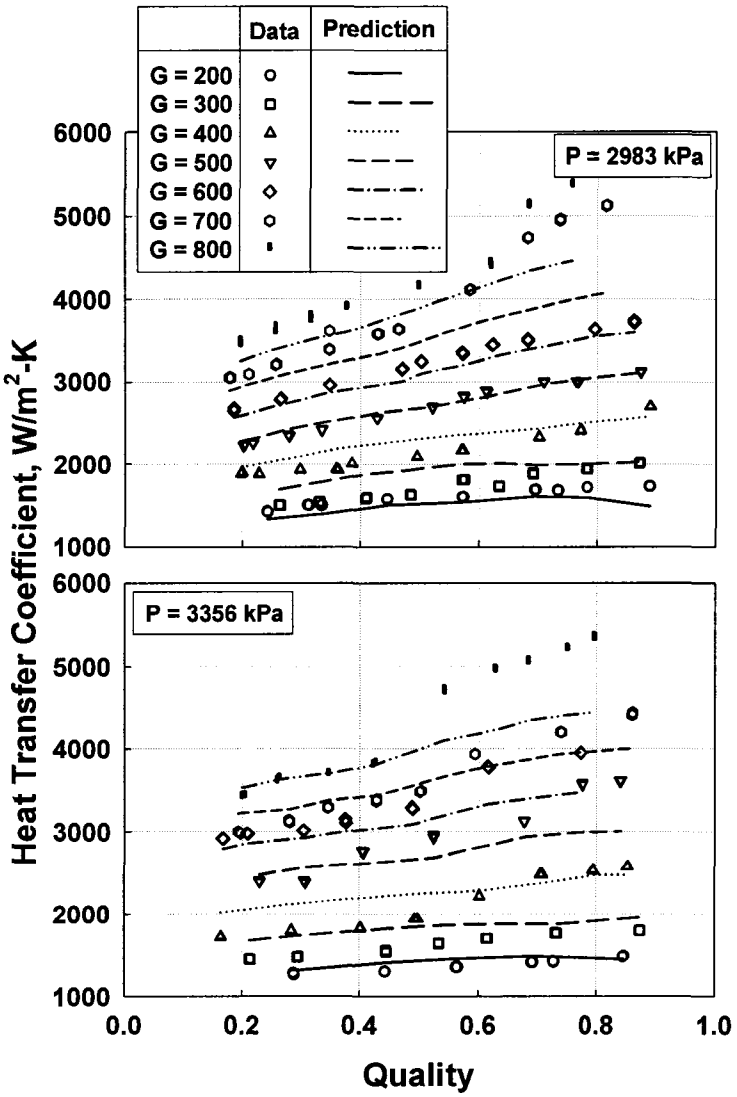

Figure 46. Comparison of Measured Heat Transfer Coefficients with Models Developed in Present Study

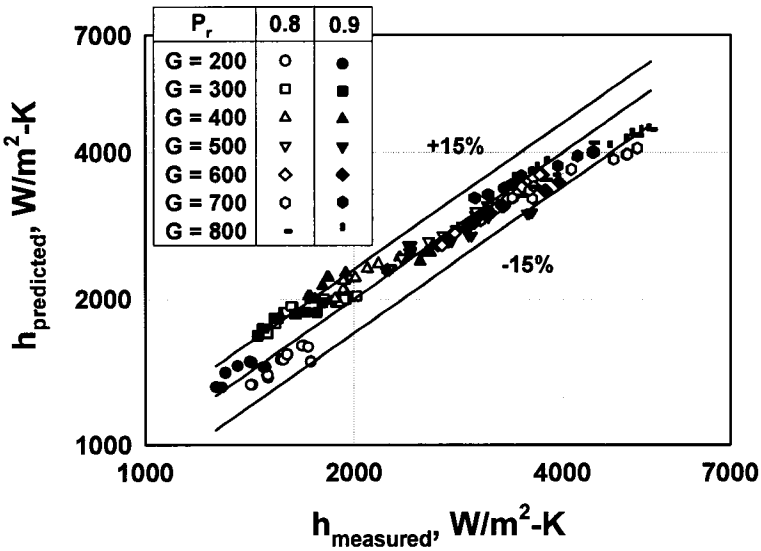

Figure 47. Overall Phase-Change Heat Transfer Model Predictions

and predictions is 7.54%. The detailed calculation of condensation heat transfer models developed in the present study is included in Appendix G.

Phase-change frictional pressure drop

A two-phase multiplier approach was adopted to model the frictional pressure drop in the present study. The Tran *et al.* (2000) two-phase multiplier for boiling in small channels based on the Chisholm (1973) correlation is as follows:

$$\phi_{LO}^{\ 2} = 1 + (CY^2 - 1)[N_{conf} x^{0.875}(1-x)^{0.875} + x^{1.75}] \tag{158}$$

where C is a constant, C = 4.3 and

$$Y^2 = \frac{(dP/dz)_{f,GO}}{(dP/dz)_{f,LO}} \tag{159}$$

$(dP/dz)_{f,GO}$ and $(dP/dz)_{f,LO}$ are the frictional pressure gradients for vapor only and liquid only flows, as follows:

$$(dP/dz)_{f,GO} = 2f_{GO}G^2/(D\rho_v) \tag{160}$$

$$(dP/dz)_{f,LO} = 2f_{LO}G^2/(D\rho_l) \tag{161}$$

where

$$\mathrm{Re}_{GO} = \frac{GD}{\mu_v} \quad \text{and} \quad \mathrm{Re}_{LO} = \frac{GD}{\mu_l} \tag{162}$$

$$f_{GO} = \begin{cases} 16/\mathrm{Re}_{GO} & \mathrm{Re}_{GO} < 2300 \\ 0.079\,\mathrm{Re}_{GO}^{-0.25} & 2300 < \mathrm{Re}_{GO} < 20000 \\ 0.046\,\mathrm{Re}_{GO}^{-0.2} & \mathrm{Re}_{GO} > 20000 \end{cases} \tag{163}$$

$$f_{LO} = \begin{cases} 16/\mathrm{Re}_{LO} & \mathrm{Re}_{LO} < 2300 \\ 0.079\,\mathrm{Re}_{LO}^{-0.25} & 2300 < \mathrm{Re}_{LO} < 20000 \\ 0.046\,\mathrm{Re}_{LO}^{-0.2} & \mathrm{Re}_{LO} > 20000 \end{cases} \tag{164}$$

N_{conf} is the confinement number introduced by Cornwell and Kew (in (Pilavachi 1993)). This confinement number includes density and surface tension terms, and thus accounts for density changes during the condensation of the refrigerant as follows.

$$N_{conf} = \frac{1}{D}\left[\frac{\sigma}{g(\rho_l - \rho_v)}\right]^{0.5} \tag{165}$$

A modified form of ϕ_{LO}^2 was used to correlate the data obtained from the present study as follows:

$$\phi_{LO}^{\ 2} = 1 + [C(x, P_r)Y^2 - 1][N_{conf} x^{\frac{2-n}{2}} (1-x)^{\frac{2-n}{2}} + x^{2-n}] \tag{166}$$

where C may be a function of quality and reduced pressure, and n is the absolute value of the power to which Re_{LO} is raised in the single-phase friction factor as shown in equation (167).

$$n = \begin{cases} 1 & \mathrm{Re}_{LO} < 2300 \\ 0.25 & 2300 < \mathrm{Re}_{LO} < 20000 \\ 0.2 & \mathrm{Re}_{LO} > 20000 \end{cases} \tag{167}$$

Figures 48 and 49 show plots of C as a function of quality and reduced pressure for annular flow regime. From the graphs, it is clear that C is a function of quality but not reduced pressure. Therefore, through regression analysis based on the annular flow data set for R404A (and R410A from the companion study), C was approximated using a second order polynomial of quality as follows:

$$C(x)_{annular} = \left(18.22 - 31.97x + 17.21x^2\right)\left(\frac{d_{actual}}{d_{baseline}}\right)^{-0.34} \tag{168}$$

For the wavy flow regime, as seen in Figures 50 and 51, similar trends are observed for C as

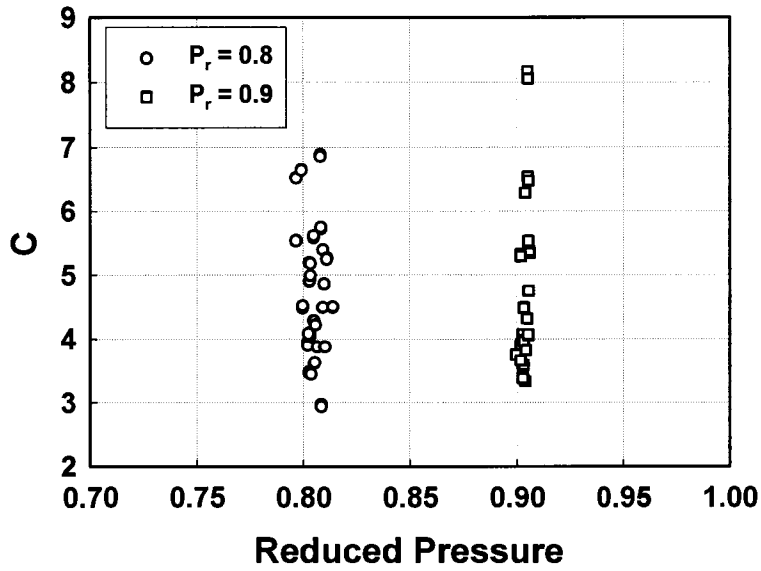

Figure 48. C vs. Reduced Pressure for Annular Flow

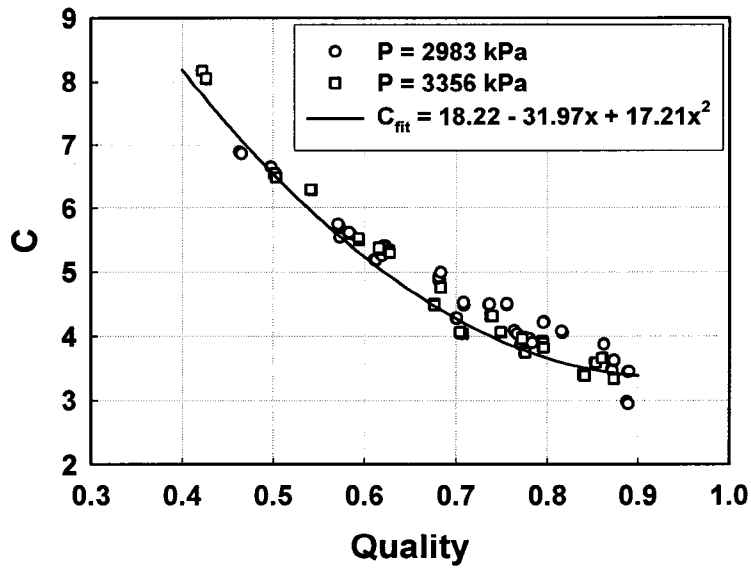

Figure 49. C vs. Quality for Annular Flow

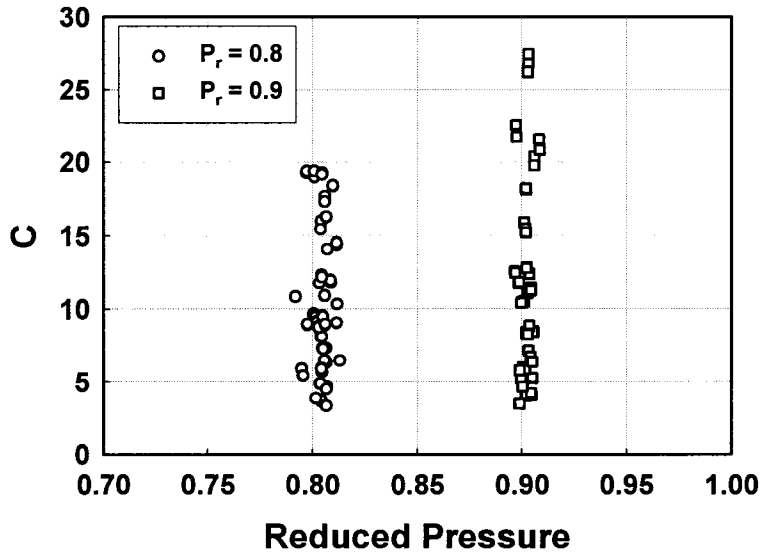

Figure 50. C vs. Reduced Pressure for Wavy Flow

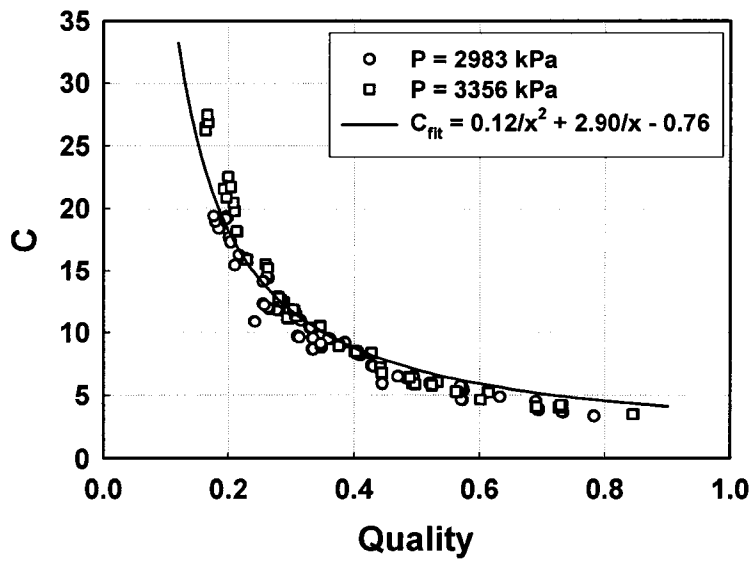

Figure 51. C vs. Quality for Wavy Flow

a function of quality but not reduced pressure. Again through regression analysis based on R404A (and R410A from the companion study) wavy flow data, C was correlated as follows:

$$C(x)_{wavy} = \left(\frac{0.12}{x^2} + \frac{2.9}{x} + 0.76\right)\left(\frac{d_{actual}}{d_{baseline}}\right)^{-0.77} \tag{169}$$

Thus, the resulting correlation for the annular and wavy flow two-phase multiplier is as follows:

$$\phi_{LO}{}^2 = 1 + [C(x)Y^2 - 1][N_{conf} x^{\frac{2-n}{2}} (1-x)^{\frac{2-n}{2}} + x^{2-n}] \tag{170}$$

where

$$C(x) = \begin{cases} \left(18.22 - 31.97x + 17.21x^2\right)\left(\frac{d_{actual}}{d_{baseline}}\right)^{-0.34} & \text{For Annular Flow} \\ \left(\frac{0.12}{x^2} + \frac{2.9}{x} + 0.76\right)\left(\frac{d_{actual}}{d_{baseline}}\right)^{-0.77} & \text{For Wavy Flow} \end{cases} \tag{171}$$

The transition region between annular and wavy flow as defined in the development of the heat transfer model is again used:

$$\begin{cases} \text{Annular Flow Regime} & 24 < Fr_{so} < 65 \\ \text{Annular to Wavy Transition} & 14 < Fr_{so} < 24 \\ \text{Wavy Flow Regime} & 1.75 < Fr_{so} < 14 \end{cases} \tag{172}$$

where $Fr_{so,wavy}$ and $Fr_{so,annular}$ are 14 and 24, respectively. In the transition region, the frictional pressure gradient is calculated using an interpolation between the annular and wavy flow model predictions as follows:

$$\left(\frac{dP}{dz}\right)_f = \left(\frac{Fr_{so_f} - Fr_{so,wavy}}{Fr_{so,annular} - Fr_{wavy}}\right)\left(\frac{dP}{dz}\right)_{f,annular} + \left(\frac{Fr_{so,annular} - Fr_{so}}{Fr_{so,annular} - Fr_{so,wavy}}\right)\left(\frac{dP}{dz}\right)_{f,wavy} \tag{173}$$

Figures 52 shows the comparison between the predicted and experimental frictional pressure gradients for both annular and wavy flow, as well as the transition region. From the graphs, it can be seen that 96% (228 out of 238) of the data are predicted within ±15%. The average absolute deviation between the data and predictions is 8.05%. Figure 53 shows the predicted and experimental frictional pressure gradients as a function of quality for the entire set of R404A data. The predictions show good agreement with the data and the transition

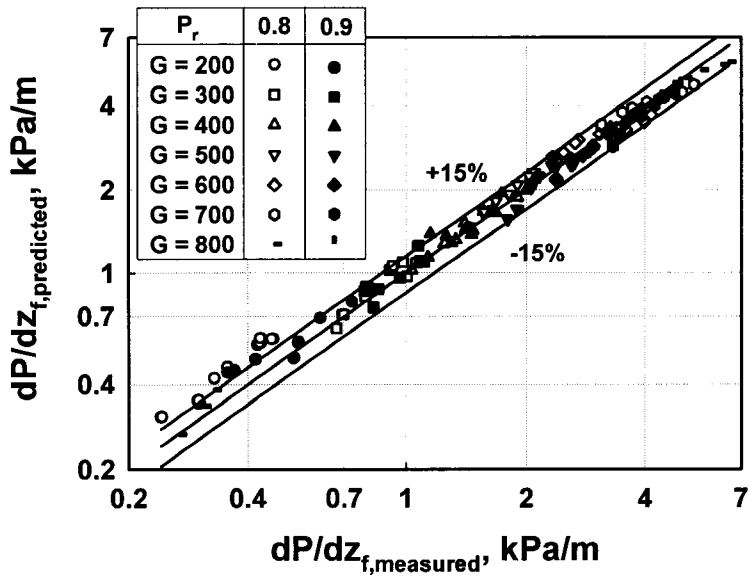

Figure 52. Overall Pressure Gradient Model Predictions

from annular to wavy flow pressure drops is smooth. The detailed calculation of condensation pressure drop models developed in the present study is included in Appendix G.

Supercritical heat transfer and frictional pressure drop

To account for variable-property effects in internal flows, the use of a ratio of fluid properties or the ratio of bulk temperature-to-wall temperature as multipliers to a constant property heat transfer or friction factor correlation is often recommended. For liquids, a viscosity or Prandtl number ratio is used as they vary more significantly, while for gases, a temperature ratio is used since ρ, μ and k are wellbehaved functions of absolute temperature (Mills 1995). In the present study, supercritical heat transfer coefficients and pressure drops were modeled using single-phase correlations with bulk and wall fluid property ratio multipliers to account for the large property variations, based on the specific flow regime, i.e., liquid-like, pseduo-critical transition, and gas-like regimes. However, at pressures close to the critical pressure, the behavior of the fluid properties, i.e., ρ, μ C_p and k, is much different from that of a liquid or a gas. Therefore, these property ratios could have much stronger effects on heat transfer and pressure drop under supercritical conditions than in conventional single-phase flow. Furthermore, these influences could be different in the gas-like, liquid-like and pseudo-phase transition regions.

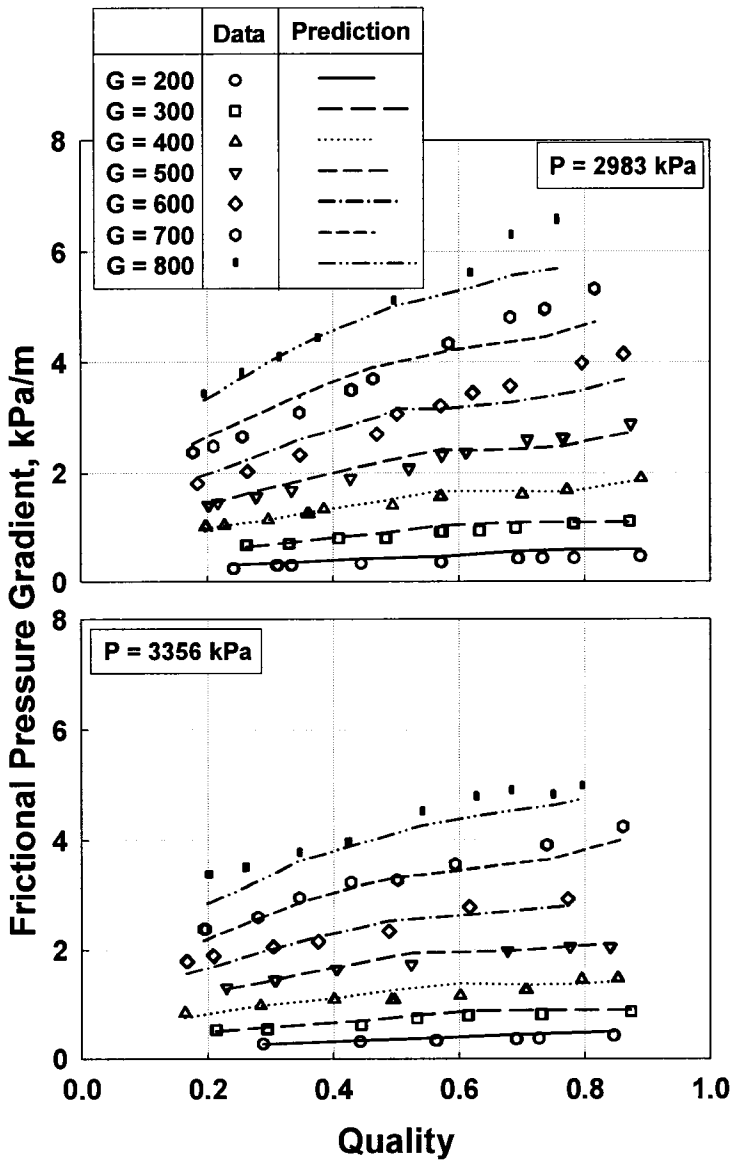

Figure 53. Comparison of Measured Pressure Gradients with Model Predictions

For the liquid-like regime, fluid density and viscosity at wall and bulk temperatures were plotted against the test section average temperature (bulk fluid temperature) in Figures 54 and 55. The wall-to-bulk density ratio (ρ_w/ρ_b) and viscosity ratio (μ_w/μ_b) are a function of bulk fluid temperature, and vary from 1.05 – 1.25 and 1.14 – 1.64, respectively, across the temperature range. Through a regression analysis based on the liquid-like data set for R404A (and R410A from the companion study), the following form for the Darcy friction factor was used:

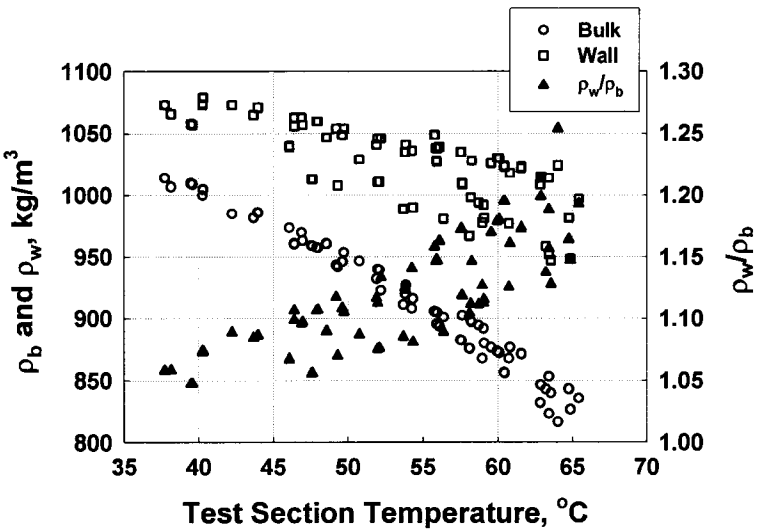

Figure 54. Fluid Density at Bulk and Wall Temperature (Liquid-Like Regime)

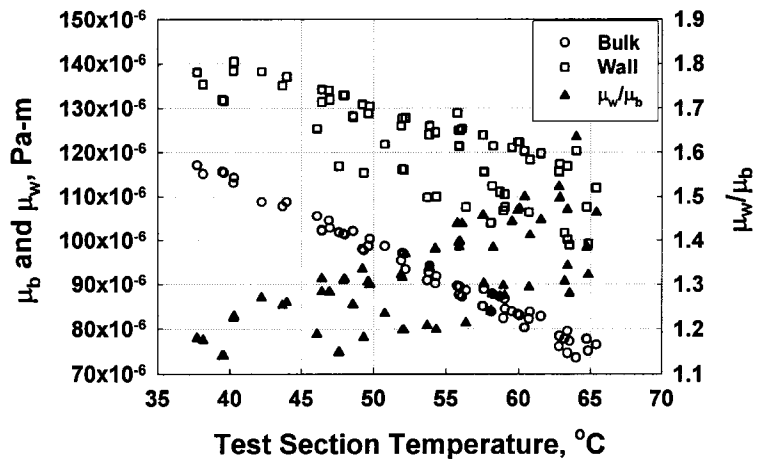

Figure 55. Fluid Viscosity at Bulk and Wall Temperature (Liquid-Like Regime)

$$f_{liquid-like} = a \times f_{Churchill} \left(\frac{\rho_w}{\rho_b} \right)^b \left(\frac{d_{actual}}{d_{baseline}} \right)^c \tag{174}$$

Figure 56 shows the specific heat of the fluid at wall and bulk temperatures as a function of the test section average temperature. From this graph, it can be seen that the wall-to-bulk specific heat ratio ($C_{p,w}/C_{p,b}$) is dependent on the test section average temperature (from 0.68 to 0.95 across the temperature range). The proposed heat transfer correlation for this regime is:

$$Nu_{liquid-like} = aNu_{Churchill-corrected} \left(\frac{c_{p,w}}{c_{p,b}} \right)^b \left(\frac{d_{actual}}{d_{baseline}} \right)^c \tag{175}$$

where $Nu_{churchill-corrected}$ is the Churchill equation (Churchill 1977a) for Nusselt number using the friction factor expression developed in the present study for the liquid-like regime.

The resulting friction factor and heat transfer models for the liquid-like regime ($T < 64.25°C$ at $P_r = 1.0$, $T < 65.05°C$ at $P_r = 1.1$ and $T < 65.70°C$ at $P_r = 1.2$) are as follows:

$$f_{liquid-like} = 2.415 f_{Churchill} \left(\frac{\rho_w}{\rho_b} \right)^{0.507} \left(\frac{d_{actual}}{d_{baseline}} \right)^{-0.184} \tag{176}$$

$$Nu_{liquid-like} = 1.004 Nu_{Churchill-corrected} \left(\frac{c_{p,w}}{c_{p,b}} \right)^{0.455} \left(\frac{d_{actual}}{d_{baseline}} \right)^{-0.283} \tag{177}$$

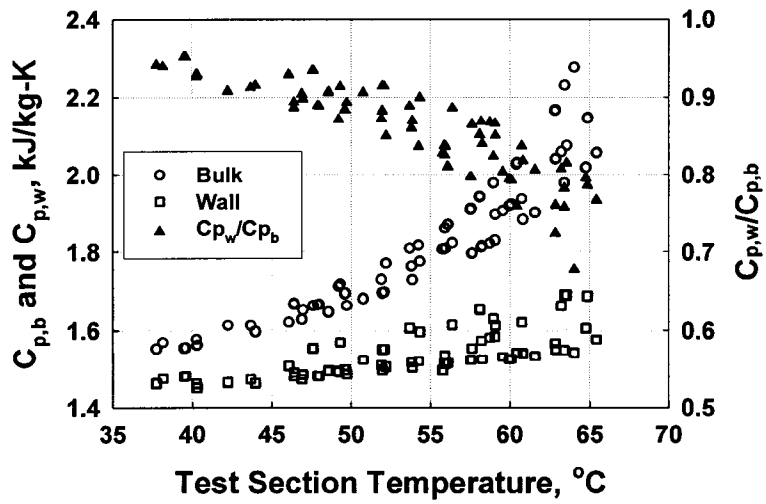

Figure 56. Fluid Specific Heat at Bulk and Wall Temperature (Liquid-Like Regime)

A similar analysis was performed for the pseudo-critical transition regime. Figures 57 through 59 show the fluid density, viscosity and specific heat at wall and bulk temperatures as functions of the test section average temperature, respectively. Similar to the liquid-like regime, the wall-to-bulk density, viscosity and specific heat ratios depend on test section average temperature (ρ_w/ρ_b = 1.16 – 3.10, μ_w/μ_b = 1.35 – 3.75 and ($C_{p,w}/C_{p,b}$ = 0.12 – 0.76 across the temperature range). A regression analysis based on the pseudo-critical transition data set for R404A (and R410A from the companion study) was used to develop the following Darcy form of the friction factor correlation with a density ratio multiplier. The resulting heat transfer and friction factor models for the pseudo-critical transition regime (64.25°C < T < 74.45°C at P_r = 1.0, 65.05°C < T < 81.55°C at P_r = 1.1 and 65.70°C < T < 88.35°C at P_r = 1.2) are as follows:

$$Nu_{pseduo-critical} = 0.928 Nu_{Churchill-corrected}\left(\frac{c_{p,w}}{c_{p,b}}\right)^{0.236}\left(\frac{d_{actual}}{d_{baseline}}\right)^{-0.119} \tag{178}$$

$$f_{pseduo-crtical} = 2.622 f_{Churchill}\left(\frac{\rho_w}{\rho_b}\right)^{0.230}\left(\frac{d_{actual}}{d_{baseline}}\right)^{-0.531} \tag{179}$$

In the gas-like regime, the wall-to-bulk density ratio is between 1.70 and 5.29 (with this ratio between 3.05 and 5.29 for 96% of the data) over the range of test section average temperatures investigated here, as seen in Figure 60. Using a regression analysis on the gas-

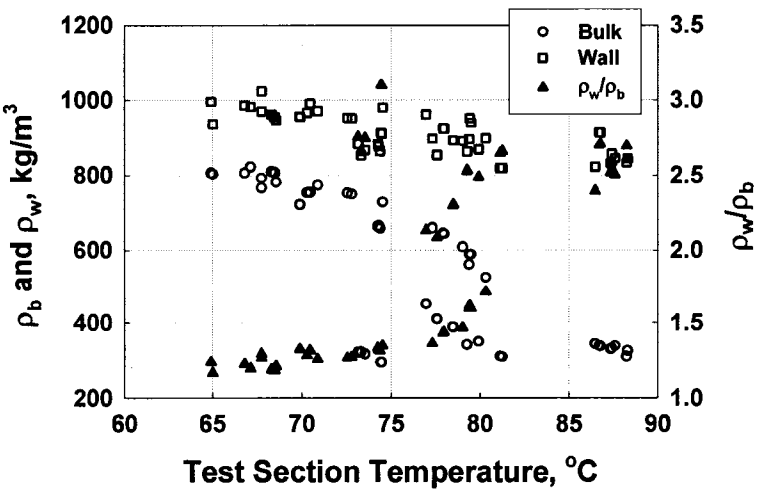

Figure 57. Fluid Density at Bulk and Wall Temperature (Pseudo-Critical Transition)

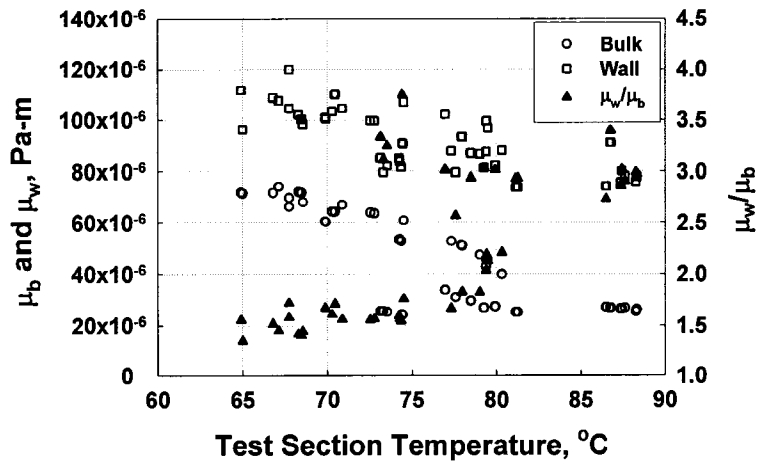

Figure 58. Fluid Viscosity at Bulk and Wall Temperature (Pseudo-Critical Transition)

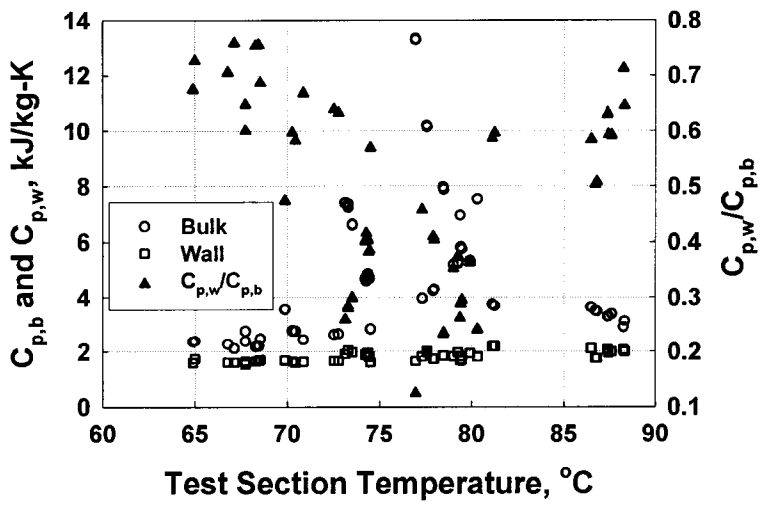

Figure 59. Fluid Specific Heat at Bulk and Wall (Pseudo-Critical Transition)

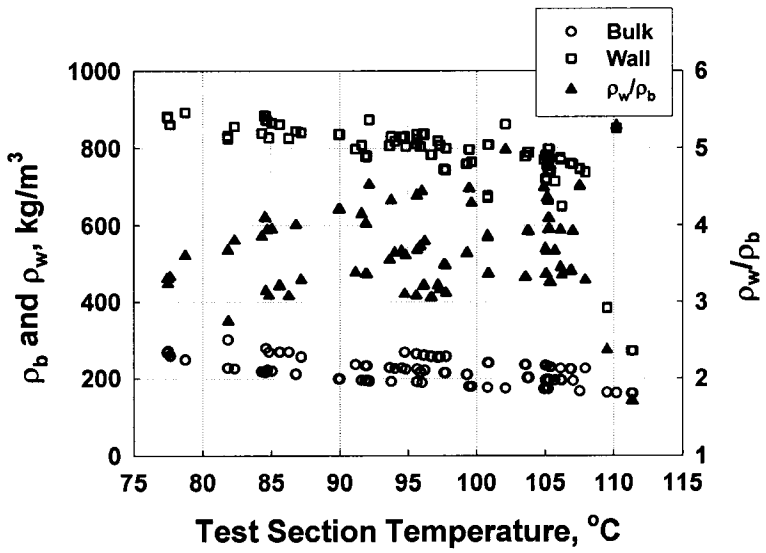

Figure 60. Fluid Density at Bulk and Wall Temperature (Gas-Like Regime)

like region data set for R404A (and R410A from the companion study), a single-phase Darcy friction factor correlation with a simple constant multiplier to the Churchill (1977b) correlation and a diameter ratio term was developed. The wall-to-bulk specific heat ratio varies from 0.59 to 20.24 (with the ratio between 0.59 and 3.87 for 99% of the data) as the test section average temperature varies (Figure 61). The resulting heat transfer and friction factor models for the gas-like regime ($T > 74.45^{\circ}C$ at $P_r = 1.0$, $T > 81.55^{\circ}C$ at $P_r = 1.1$ and $T > 88.35^{\circ}C$ at $P_r = 1.2$) are as follows:

$$Nu_{gas-like} = 1.093 Nu_{Churchill-corrected} \left(\frac{c_{p,w}}{c_{p,b}} \right)^{-0.212} \left(\frac{d_{actual}}{d_{baseline}} \right)^{-0.353} \tag{180}$$

$$f_{gas-like} = 2.872 f_{Churchill} \left(\frac{d_{actual}}{d_{baseline}} \right)^{-0.587} \tag{181}$$

Figures 62 and 63 show a comparison of the measured and predicted heat transfer coefficients and frictional pressure gradients in the supercritical region. It can be seen that the data and predictions are in good agreement with most of the heat transfer data (73%, i.e., 245 out of 337 data points) being predicted within ±25%. The frictional pressure gradients for G = 300 – 800 kg/m^2-s are predicted within ±15% for 90%, i.e., 261 out of 289 data points. Figures 64 and 65 show the variation of heat transfer coefficient and pressure

gradient with temperature. It can be seen that the present models are able to capture the experimental observed characteristics of heat transfer and pressure gradient reasonably well. The detailed calculation of supercritical heat transfer and pressure drop models developed in the present study is included in Appendix H.

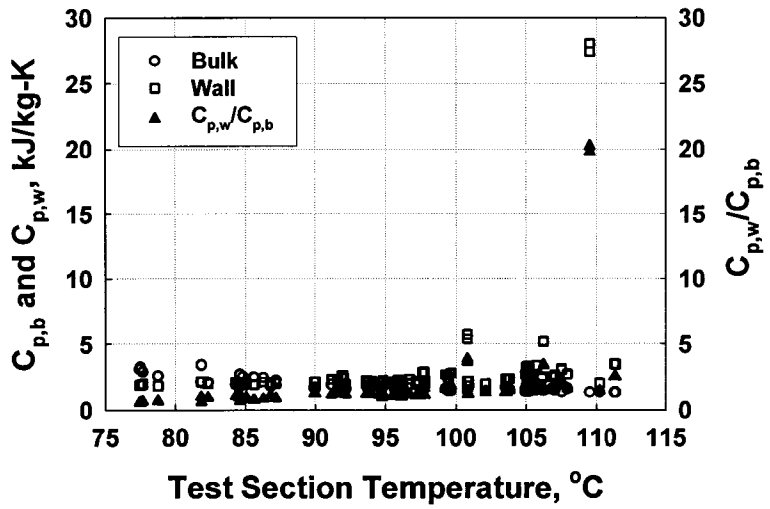

Figure 61. Fluid Specific Heat at Bulk and Wall (Gas-Like Regime)

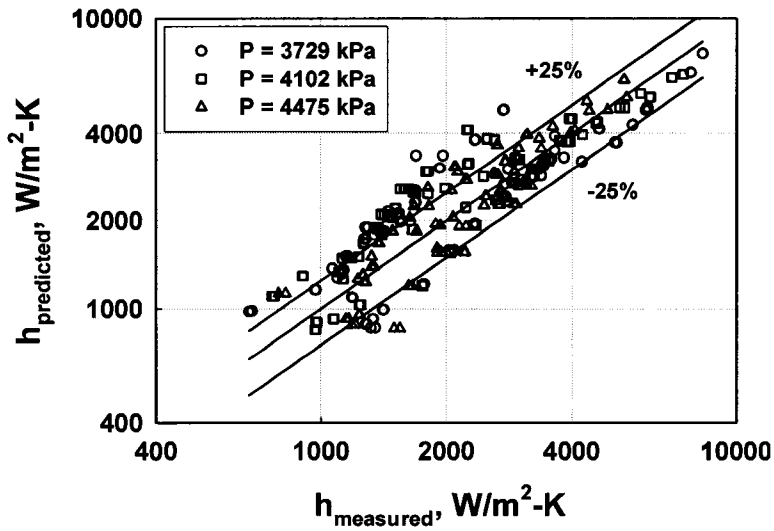

Figure 62. Supercritical Heat Transfer Model Predictions

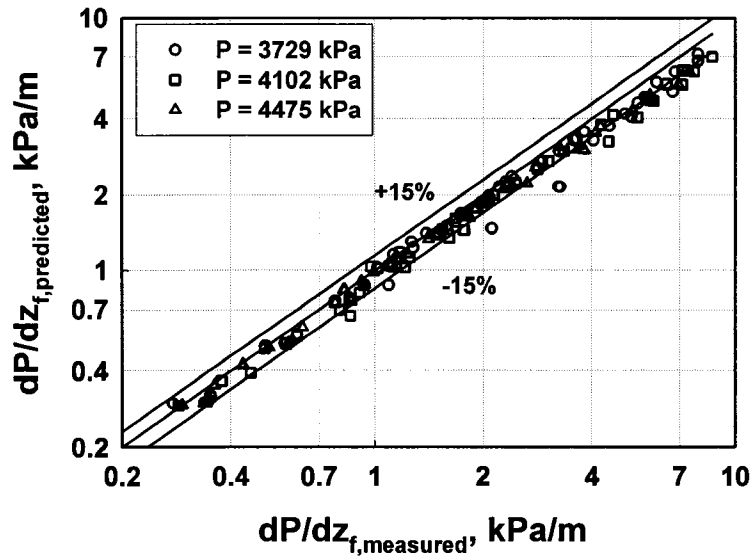

Figure 63. Supercritical Pressure Gradient Model Predictions

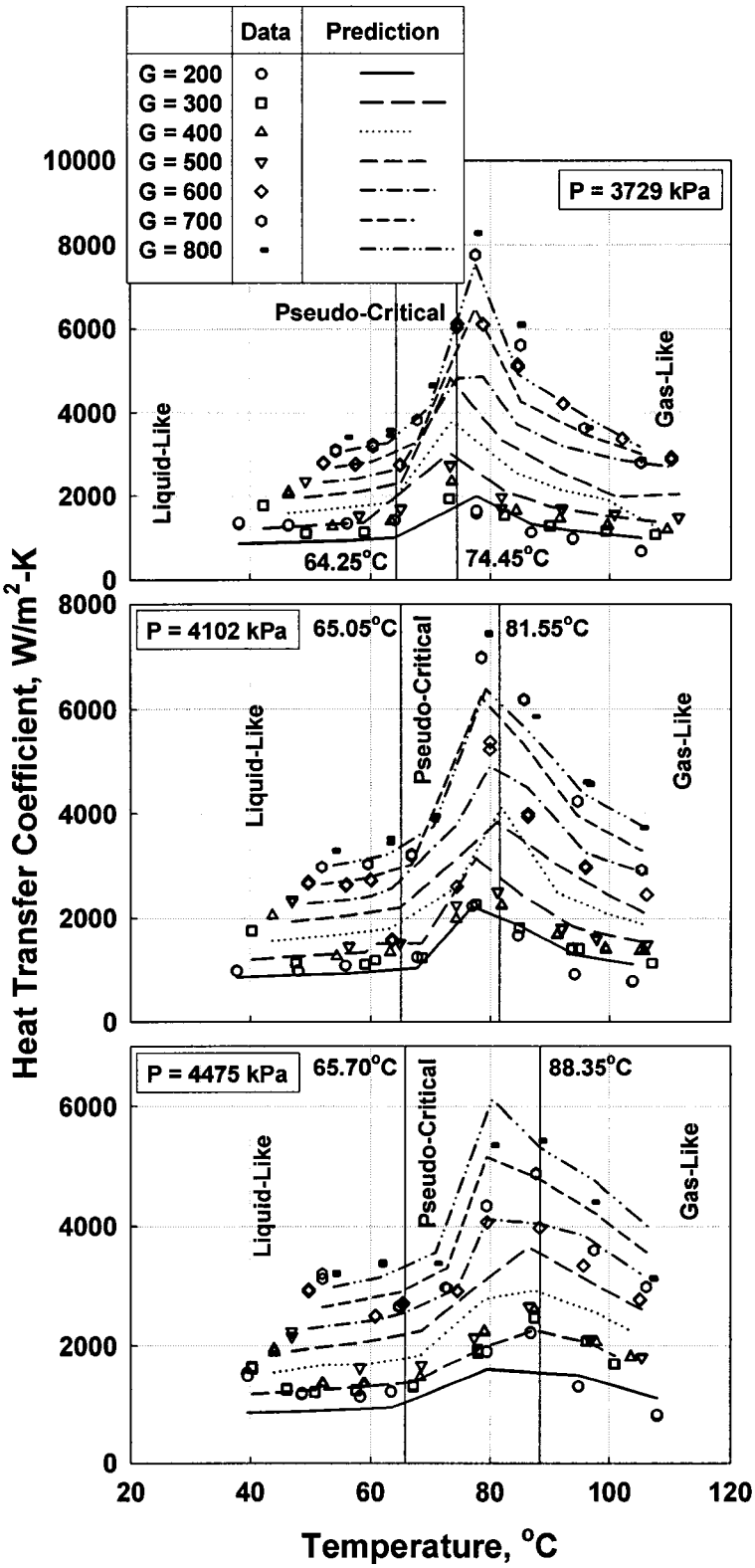

Figure 64. Comparison of Measured Supercritical Heat Transfer Coefficients with Predictions of the Models Developed in the Present Study

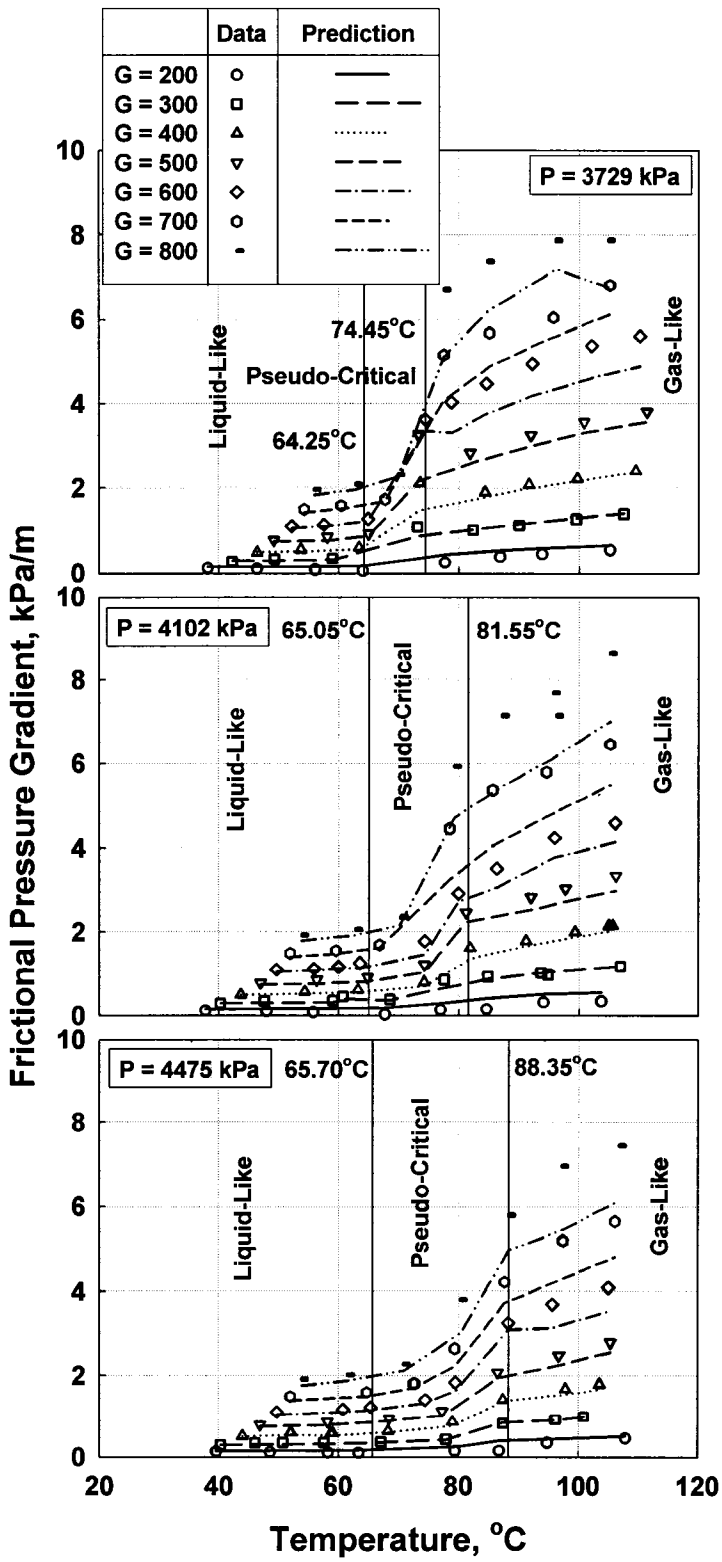

Figure 65. Comparison of Measured Supercritical Pressure Gradients with Predictions of the Models Developed in the Present Study

CHAPTER 6. CONCLUSIONS

Heat transfer and pressure drop during condensation and supercritical cooling of R404A inside a 9.4 mm tube were investigated. The experiments were conducted at five nominal pressures: $0.8\times P_{crit}$ (2983 kPa), $0.9\times P_{crit}$ (3356 kPa), P_{crit} (3729 kPa), $1.1\times P_{crit}$ (4102 kPa), and $1.2\times P_{crit}$ (4475 kPa). Heat transfer coefficients were measured using a thermal amplification technique that measures heat duty accurately while also providing refrigerant heat transfer coefficients with low uncertainties. For condensation tests, local heat transfer coefficients and pressure drops were measured for the mass flux range $200 < G < 800 kg/m^2$-s in small quality increments over entire vapor-liquid region. An uncertainty analysis showed that the average uncertainties in the heat transfer coefficients and pressure gradients were ±10.21% and 1.85%, respectively. For supercritical tests, local heat transfer coefficients and pressure drops were measured for the same mass flux range as in the condensation tests for temperatures ranging from 30 – 110°C. The average uncertainty in these heat transfer coefficients was ±9.68%. For the mass flux range $300 < G < 800$ kg/m^2-s, the average uncertainty in pressure drops for the supercritical conditions was ±1.61%. Accurate pressure drop measurements could not be conducted at $G = 200$ kg/m^2-s due to the relatively small pressure drops compared to the measurement uncertainties of the differential pressure transducer.

For both phase-change condensation and supercritical cooling, frictional pressure gradients were calculated by separating the deceleration component from the measured pressure gradients. The deceleration component was determined from an estimation of the change in fluid velocities (and momentum) due to the change in quality for phase-change condensation, and the change in density for supercritical cooling, respectively.

It is found that, due to the compensating variations in properties at near-critical pressures, a change in reduced pressure from 0.8 to 0.9 is not significant enough to cause an appreciable change in heat transfer coefficients. However, the effect of reduced pressure on the pressure gradient is more pronounced for the two pressures under consideration. The pressure drop is lower at higher reduced pressures because as the reduced pressure increases, the difference between the properties of the two phases decreases, resulting in a reduction in the shear between the phases, and therefore the pressure drop.

It is found that the flow regime maps (or transition criteria) developed by Coleman and Garimella (2003), Breber *et al.* (1980), and Dobson and Chato (1998) all result in similar categorization of the condensation data into applicable flow regimes. Therefore, flow regime transition criteria developed by Coleman (2000) were used to designate the prevailing flow regimes for a given combination of mass flux and quality. The following flow regime classifications were used:

- For Soliman modified Frounde number (Soliman 1982) Fr_{so} <1.75, the flow is considered as intermittent flow.
- For 1.75 < Fr_{so} < 18, the flow is considered in the wavy-stratified regime.
- For 18 < Fr_{so} < 65, the flow is considered as annular flow.
- For Fr_{so} > 65, the flow is in the mist flow regime.

Using these criteria, the data from the present study primarily fell into two flow regimes: wavy-stratified and annular flow. There were only two data points in the intermittent flow regime and four data points in the mist flow regime, respectively.

The condensation heat transfer coefficients and pressure gradients obtained from the present study were compared with several correlations found in the literature. It was shown that many commonly used correlations were not able to predict the heat transfer and pressure drop for condensation of refrigerant blend R404A at such high reduced pressures. Correlations by Shah (1979) and Traviss et al. (1973) were found to significantly over predict the heat transfer coefficient from the present study. The wavy flow model of Dobson and Chato (1998) predicts the data reasonably well; however, their annular flow model overpredicted the data. Furthermore, they assumed an abrupt transition between the annular and wavy flow regimes, resulting in abrupt changes in heat transfer coefficient predictions from annular to wavy flow. The heat transfer coefficient predictions of Cavallini et al. (2002a) are substantially better than those of the other correlations mentioned above. However, their pressure drop model underpredicts the data. This, in turn, affects the heat transfer results when pressure gradients are used as an intermediate step for heat transfer calculation.

For supercritical cooling, the sharp variations in thermophysical properties in the vicinity of the critical temperature were found to have substantial effect on heat transfer

coefficients and led to peaks in the heat transfer coefficients. It was found that temperature variations above the vapor-liquid dome have a much more significant effect on heat transfer than the independent variation of mass flux, because it affects thermal properties as well as the flow-related Reynolds number substantially. Also, as the pressure increases, the peaks in heat transfer shift to higher temperatures. It was also found that, as the pressure increases, the variation in heat transfer coefficients decreases due to a decrease in property variations.

Pressure drop during supercritical cooling drops abruptly at the transition temperature due to the sudden change in refrigerant properties from the gas-like to the liquid-like properties. At temperatures below the transition temperature, pressure does not very significantly due to the small property variation in the liquid-like region. Flow regime designations at the supercritical conditions were based on the characteristics of the specific work of thermal expansion (contraction) E_o as suggested by Kurganov (1998a). Thus, the data from the supercritical tests were grouped into three regimes: liquid-like regime where the change in E_o with temperature (or enthalpy) is not significant, pseudo-critical transition regime where the change in E_o with temperature (or enthalpy) is significant, and gas-like regime where the E_o starts to decline as temperature (or enthalpy) increases. The corresponding temperatures were used as the basis for dividing the data into liquid-like, pseudo-critical transition and gas-like regimes.

The supercritical cooling heat transfer coefficients and pressure gradients obtained from the present study were compared with several correlations available in the literature, including Gnielinski (1976), Krasnoshchekov (1970) and Pitla *et al.* (2002). It was found that the correlations developed for CO_2 could not be extrapolated to refrigerant R404A with an acceptable level of accuracy. The Gnielinski (1976) and Krasnoshchekov (1970) correlations showed good agreement with the heat transfer coefficients from the current study for low mass fluxes ($G \leq 500$ kg/m^2-s) while underpredicting the data considerably for higher mass fluxes ($G > 500$ kg/m^2-s). The agreement between the data from this study and the Pitla *et al.* (2002) correlation generally is not very good, especially for the gas-like region. It underpredicts the data in the low temperature region for higher mass fluxes. Furthermore, because bulk and wall temperatures approach critical temperature at different locations, their

method of arithmetically averaging the bulk and wall Nusselt numbers leads to unrealistic abrupt variations in heat transfer coefficients above the critical temperature.

Flow regime based heat transfer and pressure drop models were developed for both phase-change condensation and supercritical cooling using the R404A data collected by the author and a companion study on R410A by a different researcher in the same laboratory. Tables 14 and 16 show a summary of these models.

Condensation heat transfer and pressure drop models were developed for annular and wavy flow. The annular flow model was based on a two-phase multiplier approach,

Table 14. Summary of Condensation Heat Transfer Models

Wavy Flow
$h_{wavy} = \frac{\theta_l}{\pi} h_{film} + \left(1 - \frac{\theta_l}{\pi}\right) h_{forced}$ $Nu_{film} = \frac{1.1212}{\theta_l}\left[\frac{Ga\,\mathrm{Pr}_l}{Ja_l}\right]^{1/4}\left[\int_0^{\theta_l} \sin^{1/3}\theta d\theta\right]^{3/4}$, $h_{film} = \frac{Nu_{film}\cdot k}{d_{actual}}$ $Nu_{forced} = 0.005\,\mathrm{Re}_{liquid}^{0.97}\,\mathrm{Pr}_l^{0.3}\left[1 + \left(\frac{x}{1-x}\right)\left(\frac{\rho_l}{\rho_v}\right)\right]\left(\frac{d_{actual}}{d_{basline}}\right)^{-0.56}$ $\mathrm{Re}_{liquid} = \frac{G\cdot(1-x)\cdot D_{h,liquid\ pool}}{\mu_l}$, $D_{h,liquid\ pool} = \frac{[\sin\theta_l\cos\theta_l + (\pi - \theta_l)]}{[\sin\theta_l + (\pi - \theta_l)]} \times d_{actual}$ θ_l is evaluated by Baroczy (1965) void fraction model $\left(1 - \frac{\theta_l}{\pi}\right) \cong \frac{\arccos(2\alpha - 1)}{\pi}$, $\alpha = \left(1 + \left(\frac{1-x}{x}\right)^{0.74}\left(\frac{\rho_v}{\rho_l}\right)^{0.65}\left(\frac{\mu_l}{\mu_v}\right)^{0.13}\right)^{-1}$ $d_{baseline} = 9.4\,mm$
Annular Flow
$Nu_{annular} = 0.013\,\mathrm{Re}_l^{0.84}\,\mathrm{Pr}_l^{0.3}\left[1 + \left(\left(\frac{x}{1-x}\right)\left(\frac{\rho_l}{\rho_v}\right)\right)^{0.8}\right]\left(\frac{d_{actual}}{d_{baseline}}\right)^{-0.32}$ $\mathrm{Re}_l = \frac{G(1-x)d_{actual}}{\mu_l}$, $h_{annular} = \frac{Nu_{annular}\cdot k}{d_{actual}}$, $d_{baseline} = 9.4\,mm$
Wavy-Annular Transition
$Nu = \left(\frac{Fr_{so} - Fr_{so,wavy}}{Fr_{so,annular} - Fr_{wavy}}\right) Nu_{annular} + \left(\frac{Fr_{so,annular} - Fr_{so}}{Fr_{so,annular} - Fr_{so,wavy}}\right) Nu_{wavy}$ $Nu_{wavy} = \frac{h_{wavy}\cdot d_{actual}}{k}$

Table 15. Summary of Condensation Pressure Drop Models

Wavy and Annular Flow

$$\left(\frac{dP}{dz}\right)_f = \phi_{LO}^{\,2}\left(\frac{dP}{dz}\right)_{f,LO}$$

$$\phi_{LO}^{\,2} = 1+[CY^2-1][N_{conf}x^{\frac{2-n}{2}}(1-x)^{\frac{2-n}{2}}+x^{2-n}]$$

$$n=\begin{cases}1 & \mathrm{Re}_{LO}<2300\\ 0.25 & 2300<\mathrm{Re}_{LO}<20000\\ 0.2 & \mathrm{Re}_{LO}>20000\end{cases},\quad N_{conf}=\frac{1}{d_{actua}l}\left[\frac{\sigma}{g(\rho_l-\rho_v)}\right]^{0.5},\quad Y^2=\frac{(dP/dz)_{f,GO}}{(dP/dz)_{f,LO}}$$

$$\mathrm{Re}_{GO}=\frac{Gd_{actual}}{\mu_v},\quad \mathrm{Re}_{LO}=\frac{Gd_{actual}}{\mu_l}$$

$$f_{GO}=\begin{cases}16/\mathrm{Re}_{GO} & \mathrm{Re}_{GO}<2300\\ 0.079\mathrm{Re}_{GO}^{-0.25} & 2300<\mathrm{Re}_{GO}<20000\\ 0.046\mathrm{Re}_{GO}^{-0.2} & \mathrm{Re}_{GO}>20000\end{cases},\quad f_{LO}=\begin{cases}16/\mathrm{Re}_{LO} & \mathrm{Re}_{LO}<2300\\ 0.079\mathrm{Re}_{LO}^{-0.25} & 2300<\mathrm{Re}_{LO}<20000\\ 0.046\mathrm{Re}_{LO}^{-0.2} & \mathrm{Re}_{LO}>20000\end{cases}$$

$$(dP/dz)_{f,GO}=2f_{GO}G^2/(d_{actual}\rho_v),\quad (dP/dz)_{f,LO}=2f_{LO}G^2/(d_{actual}\rho_l)$$

$$C(x)=\begin{cases}\left(18.22-31.97x+17.21x^2\right)\left(\frac{d_{actual}}{d_{baseline}}\right)^{-0.34} & \text{For Annular Flow}\\ \left(\frac{0.12}{x^2}+\frac{2.9}{x}+0.76\right)\left(\frac{d_{actual}}{d_{baseline}}\right)^{-0.77} & \text{For Wavy Flow}\end{cases}$$

$$d_{baseline}=9.4\,mm$$

Wavy-Annular Transition

$$\left(\frac{dP}{dz}\right)_f=\left(\frac{Fr_{so\,f}-Fr_{so,wavy}}{Fr_{so,annular}-Fr_{wavy}}\right)\left(\frac{dP}{dz}\right)_{f,annular}+\left(\frac{Fr_{so,annular}-Fr_{so}}{Fr_{so,annular}-Fr_{so,wavy}}\right)\left(\frac{dP}{dz}\right)_{f,wavy}$$

recognizing that the liquid film in the flow almost always exhibited the fully turbulent behavior. In the wavy flow model, it was assumed that the local heat transfer was the sum of film condensation on the top portion of the tube and forced convection in the liquid pool at the bottom. In computing the liquid-phase Reynolds number for the model, proper account was taken of the volume and surface area of the liquid pool, rather than basing it on the tube diameter. The pressure drop models for both annular and wavy flow were modifications of Chisholm (1973) two-phase multiplier approach based on recent work by Tran *et al.* (2000). An appropriate interpolation technique for conditions in the transition region between annular and wavy flow was also defined, which eliminated the abrupt transition in heat transfer coefficients and pressure gradients. For the overall heat transfer model (annular,

Table 16. Summary of Supercritical Heat Transfer and Pressure Drop Models

Heat Transfer Models	
Liquid-Like Region	$Nu_{liquid-like} = 1.004 Nu_{Churchill-corrected}\left(\frac{c_{p,w}}{c_{p,b}}\right)^{0.455}\left(\frac{d_{actual}}{d_{baseline}}\right)^{-0.283}$ $d_{baseline} = 9.4\,mm$ $Nu_{Churchill}^{10} = 4.364^{10} + \left[\frac{\exp\left(\frac{2200-\mathrm{Re}}{365}\right)}{4.364^2} + \frac{1}{\left(6.3 + \frac{0.079(f/8)^{1/2}\,\mathrm{Re}\,\mathrm{Pr}_t}{\left(1+\mathrm{Pr}_t^{4/5}\right)^{5/6}}\right)^2}\right]^{-5}$
Pseudo-Critical Transition	$Nu_{pseudo-critical} = 0.928 Nu_{Churchill-corrected}\left(\frac{c_{p,w}}{c_{p,b}}\right)^{0.236}\left(\frac{d_{actual}}{d_{baseline}}\right)^{-0.119}$
Gas-Like Region	$Nu_{gas-like} = 1.093 Nu_{Churchill-corrected}\left(\frac{c_{p,w}}{c_{p,b}}\right)^{-0.212}\left(\frac{d_{actual}}{d_{baseline}}\right)^{-0.353}$
Pressure Drop Models	
Liquid-Like Region	$f_{liquid-like} = 2.415 f_{Churchill}\left(\frac{\rho_w}{\rho_b}\right)^{0.507}\left(\frac{d_{actual}}{d_{baseline}}\right)^{-0.184}$ $d_{baseline} = 9.4\,mm$ $f_{Churchill} = 8\left[\left(\frac{8}{\mathrm{Re}}\right)^{12} + \frac{1}{\left(\left[2.457\ln\left(\frac{1}{(7/\mathrm{Re})^{0.9}+0.27\varepsilon}\right)\right]^{16} + \left[\frac{37530}{\mathrm{Re}}\right]^{16}\right)^{1.5}}\right]^{1/12}$
Pseudo-Critical Transition	$f_{pseudo-crtical} = 2.622 f_{Churchill}\left(\frac{\rho_w}{\rho_b}\right)^{0.230}\left(\frac{d_{actual}}{d_{baseline}}\right)^{-0.531}$
Gas-Like Region	$f_{gas-like} = 2.872 f_{Churchill}\left(\frac{d_{actual}}{d_{baseline}}\right)^{-0.587}$

wavy and transition), 89% (212 out of 238) of the data were predicted within ±15%, with an average absolute deviation between the data and predictions of 7.54%. For the overall pressure drop model (annular, wavy and transition), 96% (228 out of 238) of the data were predicted within ±15% with an average absolute deviation between the data and predictions of 8.05%. The range of validity for these models is $200 < G < 800$ kg/m^2-s and $0.8 < P_r < 0.9$.

For supercritical cooling, heat transfer and pressure drop (friction factor) models were developed for each flow regime. For pressure drop models, only the data with mass flux range of $300 < G < 800$ kg/m^2-s were used to develop the model due to the large relative uncertainties associated with the $G = 200$ kg/m^2-s pressure drop data. These models were based on single-phase turbulent flow with property ratio multipliers to account for the large property variations between the bulk fluid and wall temperatures. The overall heat transfer model (liquid-like, pseudo-critical transition and gas-like) predicted 73%, i.e., 245 out of 337 data points within ±25%. The applicability range of these models is $200 < G < 800$ kg/m^2-s and $1.0 < P_r < 1.2$. For the overall pressure gradient model (liquid-like, pseduo-critical transition and gas-like), 90%, i.e., 261 out of 289 data points were predicted within ±15%. The applicability range of these models is $300 < G < 800$ kg/m^2-s and $1.0 < P_r < 1.2$.

The above discussion shows that the present study has characterized heat transfer and pressure drop of refrigerant R404A under phase-change condensation at near critical pressure and supercritical cooling above critical pressure through careful measurements and flow regime based models. These results yield insights into the effect of reduced pressure, quality, mass flux, temperature, and property variations at near-critical conditions. It is expected that these experimentally validated models will enable more accurate design of refrigerant condensers and gas-coolers. It is believed that the present study represents one of the first attempts at obtaining these measurements for refrigerants close to and above the critical region. The results from this study will also provide a basis for the validation of further studies on high reduced pressure condensation and supercritical cooling of refrigerant blends, such as numerical simulation of such flows.

The research conducted in this study may be viewed as the beginning of an overall attempt to develop more environmentally benign space-conditioning systems with CFC and HCFC-free refrigerants. A comprehensive experimental research project for the visualization of flow patterns at near-critical pressures over ranges of mass fluxes, qualities (phase-change condition) and temperatures (supercritical condition) will complement the results of the present study. This will help establish any potential fundamental differences in the flow patterns when pressure is close to critical pressure. Void fraction measurements at these conditions would also substantially advance the understanding of these flows and improve

the heat transfer and pressure drop predictions. Similar studies are also recommended for tube diameters much smaller than were investigated in the present study to establish the effect of decreasing diameter at such high reduced pressures. System-level design simulation and optimization and experimental testing would be of further help in the determination of the appropriate trade-offs between capital and operating cost for such space-conditioning systems. This is particularly useful for the development of more thermally efficient and cost effective heat exchangers in view the large heat transfer coefficient variations in the gas-cooler.

APPENDIX A. PHASE-CHANGE HEAT TRANSFER COEFFICIENT DERIVATION

Inputs	Equations	Results	References
Test Section Inlet Quality (Pre-Cooler)			
Water Side $T_{w,in} = 13.92°C$ $T_{w,out} = 26.02°C$ $P_{water} = 413.7$ kPa $Vol_{water} = 5.33\times10^{-5}$ m^3/s	$\Delta T_{water} = T_{w,out} - T_{w,in}$ $h_{w,in} = f(T_{w,in}, P_{water})$ $h_{w,out} = f(T_{w,out}, P_{water})$ $\rho_{water} = f(T_{w,in}, P_{water})$ $Q_{pre-cooler} = Vol_{water}\rho_{water}(h_{w,out} - h_{w,in})$	$\Delta T_{water} = 12.10°C$ $h_{w,in} = 58.81$ kJ/kg $h_{w,out} = 109.4$ kJ/kg $\rho_{water} = 999.4$ kg/m^3 $Q_{pre\text{-}cooler} = 2.696$ kW	
Refrigerant Side $T_{refg,in} = 103.8°C$ $P_{refg,in} = 3{,}099$ kPa $m_{refg} = 0.0277$ kg/s $T_{refg,out} = 62.3°C$ $P_{refg,out} = 3{,}007$ kPa	$h_{pre-cooler,in} = f(T_{refg,in}, P_{refg,in})$ $h_{pre-cooler,out} = h_{pre-cooler,in} - Q_{pre-cooler} / m_{refg}$ $x_{test-section,in} = x_{pre-cooler,out} = f(h_{pre-cooler,out}, P_{refg,out})$ $T_{sat,pre-cooler,in} = f(P_{refg,in}, x = 1)$ $T_{sat,pre-cooler,out} = f(P_{refg,out}, x_{pre-cooler,out})$ $Error_{Tsat,pre-cooler,out} = T_{refg,out} - T_{sat,pre-cooler,out}$ $\Delta T_{sup} = T_{refg,in} - T_{sat,pre-cooler,in}$	$h_{pre\text{-}cooler,in} = 441.3$ kJ/kg $h_{pre\text{-}cooler,out} = 343.7$ kJ/kg $x_{test\text{-}section,in} = 0.5802$ $T_{sat,pre\text{-}cooler,in} = 63.51°C$ $T_{sat,pre\text{-}cooler,out} = 62.02°C$ $Error_{Tsat,pre\text{-}cooler,out} = 0.28°C$ $\Delta T_{sup} = 40.26°C$	
Test Section Outlet Quality (Post-Cooler)			
Water Side $T_{w,in} = 13.66°C$ $T_{w,out} = 24.43°C$ $P_{water} = 413.7$ kPa $Vol_{water} = 3.3\times10^{-5}$ m^3/s	$\Delta T_{water} = T_{w,out} - T_{w,in}$ $h_{w,in} = f(T_{w,in}, P_{water})$ $h_{w,out} = f(T_{w,out}, P_{water})$ $\rho_{water} = f(T_{w,in}, P_{water})$ $Q_{post-cooler} = Vol_{water}\rho_{water}(h_{w,out} - h_{w,in})$	$\Delta T_{water} = 10.77°C$ $h_{w,in} = 57.71$ kJ/kg $h_{w,out} = 102.7$ kJ/kg $\rho_{water} = 999.5$ kg/m^3 $Q_{post\text{-}cooler} = 1.463$ kW	
Refrigerant Side $T_{refg,in} = 60.87°C$ $P_{refg,in} = 3{,}004$ kPa $T_{refg,out} = 51.76°C$ $P_{refg,out} = 2{,}982$ kPa $m_{refg} = 0.0277$ kg/s	$h_{post-cooler,out} = f(T_{refg,out}, P_{refg,out})$ $h_{post-cooler,in} = h_{post-cooler,out} + Q_{post-cooler} / m_{refg}$ $x_{test-section,out} = x_{post-cooler,in} = f(h_{post-cooler,in}, P_{refg,in})$ $T_{sat,post-cooler,in} = f(P_{refg,in}, x_{post-cooler,in})$ $T_{sat,post-cooler,out} = f(P_{refg,out}, x = 0)$	$h_{post\text{-}cooler,out} = 277.9$ kJ/kg $h_{post\text{-}cooler,in} = 330.8$ kJ/kg $x_{test\text{-}section,out} = 0.4098$ $T_{sat,post\text{-}cooler,in} = 61.94°C$ $T_{sat,post\text{-}cooler,out} = 61.53°C$ $Error_{Tsat,post\text{-}cooler,in} = -1.07°C$ $\Delta T_{sub} = 9.77°C$	

Inputs	Equations	Results	References
	$Error_{Tsat,post-cooler,in} = T_{refg,in} - T_{sat,post-cooler,in}$ $\Delta T_{sup} = T_{sat,post-cooler,out} - T_{refg,out}$		
Test Section Heat Duty (Primary-Secondary Loop Balance)			
Secondary Loop $T_{w,in} = 17.88°C$ $T_{w,out} = 43.39°C$ $P_{water} = 137.9$ kPa $m_{water} = 2.35\times10^{-3}$ kg/s	$h_{w,in} = f(T_{w,in}, P_{water})$ $h_{w,out} = f(T_{w,out}, P_{water})$ $Q_{secondary} = m_{water}(h_{w,out} - h_{w,in})$	$h_{w,in} = 75.11$ kJ/kg $h_{w,out} = 181.8$ kJ/kg $Q_{secondary} = 0.251$ kW	
Primary Loop $Q_{secondary} = 0.251$ kW $Q_{ambient} = 28.61\times10^{-2}$ kW $Q_{pump} = 22.25\times10^{-2}$ kW	$Q_{test-section} = Q_{secondary} - Q_{pump} + Q_{ambient}$	$Q_{test-section} = 0.257$ kW	
Test Section Overall UA			
$T_{w,primary,in} = 45.30°C$ $T_{w,primary,out} = 45.51°C$ $T_{test,in} = 61.76°C$ $T_{test,out} = 61.33°C$ $Q_{test-section} = 0.257$ kW	$LMTD = \frac{(T_{test,in} - T_{w,primary,out}) - (T_{test,out} - T_{w,primary,in})}{\ln[(T_{test,in} - T_{w,primary,out})/(T_{test,out} - T_{w,primary,in})]}$ $UA_{test-section} = Q_{test-section} / LMTD$	$LMTD = 16.14°C$ $UA_{test-section} = 15.94$ W/K	
Refrigerant Heat Transfer Coefficient			
Water Side Resistance $T_{w,primary,in} = 45.30°C$ $T_{w,primary,out} = 45.51°C$ $P_{water} = 413.7$ kPa $Vol_{primary} = 1.17\times10^{-4}$ m^3/s $(O.D.)_{inner} = 12.70$ mm $(O.D.)_{outer} = 19.05$ mm $w_{outer} = 1.65$ mm $L_{test} = 0.292$ m	$T_{w,primary,avg} = (T_{w,primary,in} + T_{w,primary,out})/2$ $(\rho, \mu, k, \mathrm{Pr})_{water} = f(T_{w,primary,avg}, P_{water})$ $(I.D.)_{outer} = (O.D.)_{outer} - 2w_{outer}$ $A_{f,annulus} = \frac{\pi}{4}\left[(I.D.)_{outer}^{\ 2} - (O.D.)_{inner}^{\ 2}\right]$ $D_{h,annulus} = \frac{4A_{f,annulus}}{P} = (I.D.)_{outer} - (O.D.)_{inner}$ $V_{annulus} = Vol_{primary} / A_{f,annulus}$ $\dot{m}_{annulus} = \rho_{water} Vol_{primary}$ $\mathrm{Re}_{annulus} = \frac{\rho_{water} V_{annulus} D_{h,annulus}}{\mu_{water}}$	$T_{w,primary,avg} = 45.4°C$ $\rho_{water} = 990.2$ kg/m^3 $\mu_{water} = 5.92\times10^{-4}$ kg/m-s $k_{water} = 0.638$ W/m-K $Pr_{water} = 3.88$ $(I.D.)_{outer} = 15.75$ mm $A_{f,annulus} = 6.81\times10^{-5}$ m^2 $D_{h,annulus} = 3.05$ mm $V_{annulus} = 1.714$ m/s $m_{annulus} = 0.116$ kg/s $Re_{annulus} = 8{,}736$ $r^* = 0.807$ $Re_{CL} = 2{,}643$ $Re_{CU} = 3{,}233$ $Nu_{annulus} = 58.6$ $h_{annulus} = 12{,}266$ W/m^2-K	1. Garimella and Christensen (1995), Kays and Leung (1963) and Walker *et al.* (1957)

Inputs	Equations	Results	References
	[1] $r^* = \frac{(O.D.)_{inner}}{(I.D.)_{outer}}$ [1] $\mathrm{Re}_{CL} = 2089.26 + 686.15r^*$ [1] $\mathrm{Re}_{CU} = 2963.02 + 334.16r^*$ $\mathrm{Nu}_{annulus}$ = Nu(Garimella and Christensen) from the procedure below [1]If $\mathrm{Re}_{annulus} < \mathrm{Re}_{CL}$ $Nu_{annulus} = \frac{1}{0.186 + 0.029 \cdot \ln(r^*) - 0.008 \cdot [\ln(r^*)]^2}$ [1]If $\mathrm{Re}_{annulus} > \mathrm{Re}_{CU}$ $Nu_{annulus} = 0.025 \mathrm{Re}_{annulus}^{0.78} \mathrm{Pr}_{water}^{0.48} (r^*)^{-0.14}$ [1]If $\mathrm{Re}_{CL} \le \mathrm{Re}_{annulus} \le \mathrm{Re}_{CU}$ $\frac{\ln(Nu_{annulus}) - \ln(Nu_{lam}(\mathrm{Re}_{CL}))}{\ln(Nu_{turb}(\mathrm{Re}_{CU})) - \ln(Nu_{lam}(\mathrm{Re}_{CL}))} = \frac{\ln(\mathrm{Re}_{annulus}) - \ln(\mathrm{Re}_{CL})}{\ln(\mathrm{Re}_{CU}) - \ln(\mathrm{Re}_{CL})}$ $h_{annulus} = \frac{Nu_{annulusy} k_{water}}{D_{h,annulus}}$ $A_{s,annulus} = \pi \cdot (O.D.)_{inner} L_{test}$ $R_{annulus} = \frac{1}{h_{annulus} A_{s,annulus}}$	$A_{s,annulus} = 1.17\times10^{-2}$ m^2 $R_{annulus} = 7.00\times10^{-3}$ K/W	
Wall Resistance $(O.D.)_{inner} = 12.70$ mm $w_{inner} = 1.65$ mm $L_{test} = 0.292$ m $k_{wall} = 401$ W/m-K	$(I.D.)_{inner} = (O.D.)_{inner} - 2w_{inner}$ $R_{wall} = \frac{\ln[(O.D.)_{inner}/(I.D.)_{inner}]}{2\pi \cdot k_{wall} L_{test}}$	$(I.D.)_{inner} = 9.40$ mm $R_{wall} = 4.09\times10^{-4}$ K/W	
Refrigerant Heat Transfer Coefficient $UA_{test\text{-}section} = 15.94$ W/K $R_{annulus} = 7.0\times10^{-3}$ K/W $R_{wall} = 4.09\times10^{-4}$ K/W $(O.D.)_{inner} = 12.70$ mm $w_{inner} = 1.65$ mm $L_{test} = 0.292$ m	$R_{total} = \frac{1}{UA}$ $R_{refg} = R_{total} - R_{annulus} - R_{wall}$ $(I.D.)_{inner} = (O.D.)_{inner} - 2w_{inner}$ $A_{s,i} = \pi \cdot (I.D.)_{inner} L_{test}$	$R_{tot} = 6.27\times10^{-2}$ K/W $R_{refg} = 5.53\times10^{-2}$ K/W $(I.D.)_{inner} = 9.40$ mm $A_{s,i} = 8.62\times10^{-3}$ m^2 $h_{refg} = 2095$ W/m^2-K Resistance Ratio = 7.91	

Inputs	Equations	Results	References
	$h_{refg} A_{s,i} = \frac{1}{R_{refg}}$ Resistance Ratio = $R_{refg} / R_{annulus}$		

Note: All references cited in this appendix are included in References of the dissertation.

APPENDIX B. CALCULATION OF PUMP HEAT ADDITION

Inputs	Equations	Results	References
Primary Loop Geometry			
Test Section L_{test} = 0.292 m $(O.D.)_{inner}$ = 12.70 mm $(O.D.)_{outer}$ = 19.05 mm w_{outer} = 1.65 mm	$(I.D.)_{outer} = (O.D.)_{outer} - 2w_{outer}$ $D_{h,annulus} = \frac{4A_{f,annulus}}{P} = (I.D.)_{outer} - (O.D.)_{inner}$ $A_{f,annulus} = \frac{\pi}{4}\left[(I.D.)_{outer}^{\ 2} - (O.D.)_{inner}^{\ 2}\right]$	$(I.D.)_{outer}$ = 15.75 mm $D_{h,annulus}$ = 3.05 mm $A_{f,annulus} = 6.81\times10^{-5}$ m^2	
Primary Loop Tubing L_{tubing} = 2.580 m $(O.D.)_{tubing}$ = 12.70 mm w_{tubing} = 0.89 mm	$(I.D.)_{tubing} = (O.D.)_{tubing} - 2w_{tubing}$ $A_{f,tubing} = \pi(I.D.)_{tubing}^2/4$	$(I.D.)_{tubing}$ = 10.92 mm $A_{f,tubing} = 9.37\times10^{-5}$ m^2	
Primary Loop Pressure Loss			
Test Section $T_{w,primary,in}$ = 45.30°C $T_{w,primary,out}$ = 45.51°C P_{water} = 413.7 kPa $Vol_{primary} = 1.17\times10^{-4}$ m^3/s $D_{h,annulus} = 3.05\times10^{-3}$ mm $A_{f,annulus} = 6.81\times10^{-5}$ m^2	$T_{w,avg} = (T_{w,test,in} + T_{w,test,out})/2$ $(\rho, \mu, k, \mathrm{Pr})_{water} = f(T_{w,avg}, P_{water})$ $V_{annulus} = Vol_{primary} / A_{f,annulus}$ $\mathrm{Re}_{annulus} = \frac{\rho_{water} V_{annulus} D_{h,annulus}}{\mu_{water}}$ [1] $r^* = \frac{(O.D.)_{inner}}{(I.D.)_{outer}}$ [1] $\mathrm{Re}_{CL} = 2089.26 + 686.15r^*$ [1] $\mathrm{Re}_{CU} = 2963.02 + 334.16r^*$ [1] If $\mathrm{Re}_{annulus} < \mathrm{Re}_{CL}$ $f_{annulus} = \frac{96}{\mathrm{Re}_{annulus}}(r^*)^{0.035}$ [1] If $\mathrm{Re}_{annulus} > \mathrm{Re}_{CU}$ $f_{annulus} = 4\left[1.737\ln\left(\frac{\mathrm{Re}_{annulus}}{1.964\ln(\mathrm{Re}_{annulus}) - 3.8215}\right)\right]^{-2}(1 + 0.0925r^*)$ [1] If $\mathrm{Re}_{CL} \le \mathrm{Re}_{annulus} \le \mathrm{Re}_{CU}$	$T_{w,primary,avg}$ = 45.41°C ρ_{water} = 990.2 kg/m^3 $\mu_{water} = 5.92\times10^{-4}$ kg/m-s k_{water} = 0.638 W/m-K Pr_{water} = 3.88 $V_{annulus}$ = 1.71 m/s $\mathrm{Re}_{annulus}$ = 8,736 r^* = 0.81 Re_{CL} = 2,643 Re_{CU} = 3,233 $f_{annulus}$ = 0.034 ΔP_{test} = 4.79 kPa	1. Garimella and Christensen (1995), Kays and Leung (1963), and Walker *et al.* (1957)

Inputs	Equations	Results	References
	$\frac{\ln[f_{annulus}]-\ln[f_{lam}(\mathrm{Re}_{CL})]}{\ln[f_{turb}(\mathrm{Re}_{CU})]-\ln[f_{lam}(\mathrm{Re}_{CL})]}=\frac{\ln[\mathrm{Re}_{annulus}]-\ln[\mathrm{Re}_{CL}]}{\ln[\mathrm{Re}_{CU}]-\ln[\mathrm{Re}_{CL}]}$ $\Delta P_{test}=\frac{1}{2}f_{annulus}\rho_{annulus}V_{annulus}^{\ 2}\frac{L_{test}}{D_{h,annulus}}\cdot\frac{1}{1000}$		
Secondary Heat Exchanger Vol = 1.17×10^{-4} m^3/s = 1.85 gpm	ΔP_{shell}(in psi) = 0.49157(Actual Flowrate in gpm)$^{1.9}$	ΔP_{shell} = 1.58 psi = 10.91 kPa	Shell and tube heat exchanger (Exergy model 00540-4). Pressure drop equation provided by manufacturer
Flowmeter Vol = 1.17×10^{-4} m^3/s = 1.85 gpm	$\Delta P_{flowmeter}$(in psi) = $\frac{29.7-6.22}{7.0-0.8}$(Actual Flowrate in gpm − 0.8)	$\Delta P_{flowmeter}$ = 10.20 kPa	Rotameter (Dwyer RMC series, 0.8 – 7 gpm). Interpolation using maximum and minimum pressure drop provided by manufacturer.
Primary Loop Tubing Vol = 1.17×10^{-4} m^3/s L_{tubing} = 2.58 m $(I.D.)_{tubing}$ = 10.92 mm $A_{f,tubing}$ = 9.37×10^{-5} m^2 ε/D = 0.000137 [3] K_{elbow} = 0.7 N_{elbow} = 7 [3] $K_{Tee,line}$ = 0.9 $N_{Tee,line}$ = 2 [3] K_{elbow} = 2 $N_{Tee,branch}$ = 4 ρ_{water} = 990.2 kg/m^3	$V_{w,tubing}=Vol/A_{f,tubing}$ $\mathrm{Re}_{w,tubing}=\frac{\rho_{water}V_{w,tubing}(I.D.)_{tubing}}{\mu_{water}}$ [2] $f_{w,tubing}=f(Churchill)$ $=8\left[\left(\frac{8}{\mathrm{Re}_{w,tubing}}+\left(\left[2.457\ln\left(\left[\frac{7}{\mathrm{Re}_{w,tubing}}\right]^{0.9}+0.27\varepsilon D\right)\right]^{16}+\left[\frac{37350}{\mathrm{Re}_{w,tubing}}\right]^{16}\right)^{-1.5}\right)\right]^{1/12}$ $K_{minor}=N_{elbow}K_{elbow}+N_{Tee,line}K_{Tee,line}+N_{Tee,branch}K_{Tee,branch}$ $\Delta P_{fric,tubing}=\frac{1}{2}f_{w,tubing}\rho_{water}V_{w,tubing}^{\ 2}\frac{L_{tubing}}{D_{i,tubing}}\cdot\frac{1}{1000}$	$V_{w,tubing}$ = 1.25 m/s $\mathrm{Re}_{w,tubing}$ = 22,754 $f_{w,tubing}$ = 0.025 K_{minor} = 19.3 $\Delta P_{fric,tubing}$ = 4.61 kPa $\Delta P_{minor,tubing}$ = 14.83 kPa ΔP_{tubing} = 19.44 kPa	2. Churchill (1977a) 3. Munson *et al.* (1998)

Inputs	Equations	Results	References
	$\Delta P_{\text{minor,tubing}} = \frac{1}{2}\rho_{water} V_{w,tubing}^{\ 2} K_{\text{minor}} \cdot \frac{1}{1000}$ $\Delta P_{tubing} = \Delta P_{fric,tubing} + \Delta P_{\text{minor,tubing}}$		
Total Primary Loop Pressure loss ΔP_{test} = 4.79 kPa ΔP_{shell} = 10.91 kPa $\Delta P_{flowmeter}$ = 10.20 kPa ΔP_{tubing} = 19.44kPa	$\Delta P = \Delta P_{test} + \Delta P_{shell} + \Delta P_{flowmeter} + \Delta P_{tubing}$	ΔP = 45.33 kPa	
Ideal Pump Work			
ΔP = 45.33 kPa Vol = 1.17×10^{-4} m^3/s	$W_{ideal} = Vol \cdot \Delta P$	W_{ideal} = 5.29×10^{-3} kW	
Pump Shaft Work			
Torque = 0.15 N-m RPM = 1280 rpm	$W_{shaft} = \text{Torque} \cdot \frac{\text{RPM} \cdot 2\pi}{60} \frac{1}{1000}$	W_{shaft} = 2.85×10^{-2} kW	
Pump Efficiency			
W_{ideal} = 5.29×10^{-3} kW W_{shaft} = 2.85×10^{-2} kW	$\eta = \frac{W_{ideal}}{W_{shaft}}$	η = 0.186	
Pump Heat Addition			
W_{shaft} = 2.85×10^{-2} kW η = 0.186	$Q_{pump} = (1-\eta)W_{shaft}$	Q_{pump} = 2.32×10^{-2} kW = 23.22 W	

Note:

1. By applying the above method to flowrates ranging from 1.5 to 4 gpm, a third-order polynomial curvefit (shown below) was developed to calculate the pump heat addition as a function of the volumetric flow rate. For a flow of 1.85 gpm, Q_{pump} = 22.25 W.
   Q_{pump} (in kW) = $-9.994\times10^{-3} + 2.677\times10^{-2} \cdot$(Flow in gpm) $- 7.649\times10^{-3} \cdot$(Flow in gpm)$^2 + 1.406\times10^{-3} \cdot$(Flow in gpm)^3, R^2 = 0.998
2. It is assumed that all the pump losses are rejected into the coolant as heat
3. All references cited in this appendix are included in References of the dissertation.

APPENDIX C. CALCULATION OF AMBIENT HEAT LOSS

Inputs	Equations	Results	References
Primary Loop Geometry			
Test Section L_{test} = 0.292 m $(O.D.)_{inner}$ = 12.70 mm $(O.D.)_{outer}$ = 19.05 mm w_{outer} = 1.65 mm	$(I.D.)_{outer} = (O.D.)_{outer} - 2w_{outer}$ $D_{h,annulus} = \frac{4A_{f,annulus}}{P} = (I.D.)_{outer} - (O.D.)_{inner}$ $A_{f,annulus} = \frac{\pi}{4}\left[(I.D.)_{outer}^{2} - (O.D.)_{inner}^{2}\right]$ $A_{eff,annulus} = \pi(I.D.)_{outer} L_{test}$	$(I.D.)_{outer}$ = 15.75 mm $D_{h,annulus}$ = 3.05 mm $A_{f,annulus} = 6.81\times10^{-5}$ m^2 $A_{eff,annulus} = 1.445\times10^{-2}$ m^2	
Secondary Heat Exchanger L_{sec} = 0.203 m $(O.D.)_{shell}$ = 28.45 mm w_{shell} = 1.25 mm	$(I.D.)_{shell} = (O.D.)_{shell} - 2w_{shell}$	$(I.D.)_{shell}$ = 25.96 mm	
Primary Loop Tubing L_{tube} = 2.580 m $L_{eq,pump\ housing}$ = 1.286 m $L_{eq,flowmeter}$ = 2.557 m $(O.D.)_{tubing}$ = 12.70 mm w_{tubing} = 0.89 mm	$L_{tubing} = L_{tube} + L_{eq,pump\ housing} + L_{eq,flowmeter}$ $(I.D.)_{tubing} = (O.D.)_{tubing} - 2w_{tubing}$ $A_{f,tubing} = \pi(I.D.)_{tubing}^{2}/4$ $A_{eff,tubing} = \pi(I.D.)_{tubing} L_{tubing}$	L_{tubing} = 6.423 m $(I.D.)_{tubing}$ = 10.92 mm $A_{f,tubing} = 9.37\times10^{-5}$ m^2 $A_{eff,tubing}$ = 0.220 m^2	
Insulation			
Test Section $w_{insulation,test}$ = 25.40 mm $k_{insulation,test}$ = 0.046 W/m-K $(O.D.)_{outer}$ = 19.05 mm	$(O.D.)_{insulation,test} = (O.D.)_{outer} + 2w_{insulation,test}$	$(O.D.)_{insulation,test}$ = 69.85 mm	
Secondary Heat Exchanger $w_{insulation,sec}$ = 25.40 mm $k_{insulation,sec}$ = 0.046 W/m-K $(O.D.)_{shell}$ = 28.45 mm	$(O.D.)_{insulation,sec} = (O.D.)_{shell} + 2w_{insulation,sec}$	$(O.D.)_{insulation,sec}$ = 79.25 mm	
Primary Loop Tubing $w_{insulation,tubing}$ = 19.05 mm $k_{insulation,test}$ = 0.046 W/m-K $(O.D.)_{tubing}$ = 12.70 mm	$(O.D.)_{insulation,tubing} = (O.D.)_{tubing} + 2w_{insulation,tubing}$	$(O.D.)_{insulation,tubing}$ = 50.80 mm	
Ambient Conditions			
$T_{ambient}$ = 23°C $P_{ambient}$ = 101.325 kPa			

Inputs	Equations	Results	References
Test Section Heat Loss			
$T_{w,test,in}$ = 45.30°C $T_{w,test,out}$ = 45.51°C $(I.D.)_{outer}$ = 15.75 mm $(O.D.)_{outer}$ = 19.05 mm $(O.D.)_{insulation,test}$ = 69.85 mm $A_{eff,annulus}$ = 1.45×10^{-2} m^2 k_{wall} = 15 W/m-K L_{test} = 0.292 m $k_{insulation,test}$ = 0.046 W/m-K $h_{w,test}$ = 12,266 W/m^2-K (From Table 1)	$T_{w,avg} = (T_{w,test,in} + T_{w,test,out})/2$ $R_{conv,test} = \frac{1}{h_{w,test} \cdot A_{eff,annulus}}$ $R_{wall,test} = \frac{\ln[(O.D.)_{outer}/(I.D.)_{outer}]}{2\pi k_{wall} L_{test}}$ $R_{insulation,test} = \frac{\ln[(O.D.)_{insulation,test}/(O.D.)_{outer}]}{2\pi k_{insulation,test} L_{test}}$ ($T_{surface,test} = 25.35^{o}C$, ***Assumed and verified iteratively***) $Q_{test} = \frac{T_{w,avg} - T_{surface,test}}{R_{conv,test} + R_{wall,test} + R_{insulation,test}}$ $T_{fluid,test} = (T_{surface,test} + T_{ambient})/2$ $(\rho, \mu, k, \alpha, \Pr)_{a,test} = f(T_{fluid,test}, P_{ambient})$ $Ra_{test} = \frac{9.8\beta_{a,test}(T_{surface,test} - T_{ambient})(O.D.)^3_{insulation,tubing}\rho^2_{a,test}\Pr_{a,test}}{\mu^2_{a,test}}$ $^1h_{nc,test} = \frac{k_{a,test}}{(O.D.)_{insulation,test}}\left(0.60 + 0.387\frac{Ra^{1/6}_{test}}{\left[1+\left(\frac{0.559}{\Pr_{a,test}}\right)^{9/16}\right]^{8/27}}\right)^2$ Use energy balance to solve $T_{surface,test}$ and Q_{test} iteratively. Assume black body radiation, ε = 1, $Q_{test} = h_{nc,test}[\pi(O.D.)_{insulation,test}L_{test}](T_{surface,test} - T_{ambient})$ $+ 5.67\times10^{-8}[\pi(O.D.)_{insulation,test}L_{test}](T^4_{surface,test} - T^4_{ambient})$	$T_{w,avg}$ = 45.41°C $R_{conv,test}$ = 5.702×10^{-3} K/W $R_{wall,test}$ = 6.914×10^{-3} K/W $R_{insulation,test}$ = 15.39 K/W $T_{fluid,test}$ = 24.18°C $\rho_{a,test}$ = 1.19 kg/m^3 $\mu_{a,test}$ = 1.85×10^{-5} kg/m-s $k_{a,test}$ = 2.55×10^{-2} W/m-K $\beta_{a,test}$ = 3.36×10^{-3} 1/K $Pr_{a,test}$ = 0.730 Ra_{test} = 79,803 $h_{nc,test}$ = 2.681 W/m^2-K $T_{surface,test}$ = 25.35°C $Q_{nc,test}$ = 0.404 W $Q_{rad,test}$ = 0.898 W Q_{test} = 1.302 W	1. Churchill and Chu (1975)
Secondary Heat Exchanger Heat Loss			
$T_{w,avg}$ = 45.41°C $(I.D.)_{shell}$ = 25.96 mm $(O.D.)_{shell}$ = 28.45 mm	Assume $T_{wall,sec} = T_{w,avg}$	$T_{wall,sec}$ = 45.41°C $R_{wall,sec}$ = 4.781×10^{-3} K/W $R_{insulation,sec}$ = 17.44 K/W	2. Churchill and Chu (1975)

Inputs	Equations	Results	References
$(O.D.)_{insulation,sec}$ = 79.25 mm k_{wall} = 15 W/m-K $k_{insulation,test}$ = 0.046 W/m-K L_{sec} = 0.203 m	$R_{wall,sec} = \frac{\ln[(O.D.)_{shell}/(I.D.)_{shell}]}{2\pi k_{wall} L_{sec}}$ $R_{insulation,sec} = \frac{\ln[(O.D.)_{insulation,sec}/(O.D..)_{shell}]}{2\pi k_{insulation,sec} L_{sec}}$ ($T_{surface,sec} = 25.60^{\circ}C$, ***Assumed and verified iteratively***) $Q_{sec} = \frac{T_{wall,sec} - T_{surface,sec}}{R_{wall,sec} + R_{insulation,sec}}$ $T_{fluid,sec} = (T_{surface,sec} + T_{ambient})/2$ $(\rho, \mu, k, \beta, \Pr)_{a,sec} = f(T_{fluid,sec}, P_{ambient})$ $Ra_{sec} = \frac{9.8\beta_{a,sec}(T_{surface,sec} - T_{ambient})(O.D.)^3_{insulation,tubing}\rho^2_{a,sec}\Pr_{a,sec}}{\mu^2_{a,sec}}$ $^2 h_{nc,sec} = \frac{k_{a,sec}}{(O.D.)_{insulation,sec}}\left(0.60 + 0.387\frac{Ra_{sec}^{1/6}}{\left[1+\left(\frac{0.559}{\Pr_{a,sec}}\right)^{9/16}\right]^{8/27}}\right)^2$ Use energy balance to solve $T_{surface,sec}$ and Q_{sec} iteratively. Assume black body radiation, $\varepsilon = 1$, $Q_{sec} = h_{nc,sec}[\pi(O.D.)_{insulation,sec} L_{sec}](T_{surface,sec} - T_{ambient})$ $+ 5.67\times10^{-8}[\pi(O.D.)_{insulation,sec} L_{sec}](T^4_{surface,sec} - T^4_{ambient})$	$T_{fluid,sec}$ = 24.30°C $\rho_{a,sec}$ = 1.19 kg/m^3 $\mu_{a,sec} = 1.85\times10^{-5}$ kg/m-s $k_{a,sec} = 2.55\times10^{-2}$ W/m-K $\beta_{a,sec} = 3.36\times10^{-3}$ 1/K $\Pr_{a,sec}$ = 0.730 Ra_{sec} = 128,447 $h_{nc,sec}$ = 2.677 W/m^2-K $T_{surface,sec}$ = 25.60°C $Q_{nc,test}$ = 0.352 W $Q_{rad,test}$ = 0.784 W Q_{sec} = 1.135 W	
Primary Loop Tubing Heat Loss			
$T_{w,avg}$ = 45.41°C P_{water} = 413.7 kPa $(I.D.)_{tubing}$ = 10.92 mm $(O.D.)_{tubing}$ = 12.70 mm $w_{insulation,tubing}$ = 19.05 mm $(O.D.)_{insulation,tubing}$ = 50.80 mm $A_{f,tubing} = 9.37\times10^{-5}$ m^2 $A_{eff,tubing}$ = 0.220 m^2	$(\rho, \mu, k, \Pr)_{w,tubing} = f(T_{w,avg}, P_{water})$ $V_{w,tubing} = Vol/A_{f,tubing}$ $\mathrm{Re}_{w,tubing} = \frac{\rho_{w,tubing} V_{w,tubing}(I.D.)_{tubing}}{\mu_{w,tubing}}$ $^3 f_{w,tubing} = f(Churchill)$, see Appendix B	$\rho_{w,tubing}$ = 990.2 kg/m^3 $\mu_{w,tubing} = 5.92\times10^{-4}$ kg/m-s $k_{w,tubing}$ = 0.625 W/m-K $\Pr_{w,tubing}$ = 3.96 $V_{w,tubing}$ = 1.25 m/s $\mathrm{Re}_{w,tubing}$ = 22,754 $f_{w,tubing}$ = 0.0254	3. Churchill (1977a, 1977b) 4. Churchill and Chu (1975) 5. Munson *et al.* (1998)

Inputs	Equations	Results	References
k_{wall} = 15 W/m-K $k_{insulation,tubing}$ = 0.046 W/m-K L_{tube} = 2.580 m $L_{eq,pump\ housing}$ = 1.286 m $L_{flowmeter}$ = 2.557 m L_{tubing} = 6.423 m $Vol_{primary}$ = 1.17×10^{-4} m^3/s [5] ε/D = 0.000137	[3] $Nu_{w,tubing} = Nu(Churchill)$ $= \left[\left(\frac{4.364^{10} + \left(\frac{\exp\left[\frac{2200 - \mathrm{Re}_{w,tubing}}{365}\right]}{4.364^2} \right)^{-5}}{+ \frac{1}{\left[6.3 + 0.079\left(\frac{f_{w,tubing}}{8}\right)^{0.5} \mathrm{Re}_{w,tubing} \frac{\mathrm{Pr}_{w,tubing}}{\left(1+\mathrm{Pr}_{w,tubing}^{0.8}\right)^{\frac{5}{6}}}\right]^2}} \right)^{-5} \right]^{1/10}$ $h_{w,tubing} = \frac{Nu_{w,tubing} k_{w,tubing}}{(I.D.)_{tubing}}$ $R_{conv,tubing} = \frac{1}{h_{w,tubing} \cdot A_{eff,tubing}}$ $R_{wall,tubing} = \frac{\ln((O.D.)_{tubing}/(I.D.)_{tubing})}{2\pi k_{wall} L_{tubing}}$ $R_{insulation,tubing} = \frac{\ln[(O.D.)_{insulation,tubing}/(O.D.)_{tubing}]}{2\pi k_{insulation,tubing} L_{tubing}}$ ($T_{surface,tubing} = 25.84^{o}C$, ***Assumed and verified iteratively***) $Q_{tubing} = \frac{T_{w,avg} - T_{surface,tubing}}{R_{conv,tubing} + R_{wall,tubing} + R_{insulation,tubing}}$ $T_{fluid,tubing} = (T_{surface,tubing} + T_{ambient})/2$ $(\rho, \mu, k, \beta, \mathrm{Pr})_{a,tubing} = f(T_{fluid,tubing}, P_{ambient})$ $Ra_{tubing} = \frac{9.8\beta_{a,tubing}(T_{surface,tubing} - T_{ambient})(O.D.)^3_{insulation,tubing} \rho^2_{a,tubing} \mathrm{Pr}_{a,tubing}}{\mu^2_{a,tubing}}$	$Nu_{w,tubing}$ = 132.4 $h_{w,tubing}$ = 7,578 w/m^2-K $R_{conv,tubing}$ = 5.99×10^{-4} K/W $R_{wall,tubing}$ = 2.49×10^{-4} K/W $R_{insulation,tubing}$ = 0.747 K/W $T_{fluid,tubing}$ = 24.42°C $\rho_{a,tubing}$ = 1.19 kg/m^3 $\mu_{a,tubing}$ = 1.85×10^{-5} kg/m-s $k_{a,tubing}$ = 2.55×10^{-2} W/m-K $\beta_{a,tubing}$ = 3.36×10^{-3} 1/K $Pr_{a,tubing}$ = 0.730 Ra_{tubing} = 36,900 $h_{nc,tubing}$ = 3.028 W/m^2-K $A_{s,insulation,tubing}$ = 1.025 m^2 $T_{surface,tubing}$ = 25.84°C $Q_{nc,tubing}$ = 8.803 W $Q_{rad,tubing}$ = 17.373 W Q_{tubing} = 26.176 W	

Inputs	Equations	Results	References
	[4] $h_{nc,tubing} = \frac{k_{a,tubing}}{(O.D.)_{insulation,tubing}} \left(0.60 + 0.387 \frac{Ra_{tubing}^{1/6}}{\left[1 + \left(\frac{0.559}{\mathrm{Pr}_{a,tubing}} \right)^{9/16} \right]^{8/27}} \right)^2$ Use energy balance to solve $T_{surface,tubing}$ and Q_{tubing} iteratively. Assume black body radiation, $\varepsilon = 1$, $Q_{tubing} = h_{nc,tubing} \left[\pi (O.D.)_{insulation,tubing} L_{tubing} \right] (T_{surface,tubing} - T_{ambient})$ $+ 5.67 \times 10^{-8} \left[\pi (O.D.)_{insulation,tubing} L_{tubing} \right] (T_{surface,tubing}^4 - T_{ambient}^4)$		
Total Primary Ambient Heat Loss			
$Q_{test} = 1.302$ W $Q_{sec} = 1.135$ W $Q_{tubing} = 26.176$ W	$Q_{total} = Q_{test} + Q_{sec} + Q_{tubing}$	$Q_{total} = 28.61$ W	

Note: All references cited in this appendix are included in References of the dissertation.

APPENDIX D. SUPERCRITICAL HEAT TRANSFER COEFFICIENT DERIVATION

Inputs	Equations	Results	References
Test Section Inlet Temperature (Pre-Cooler)			
Water Side $T_{w,in}$ = 15.46°C $T_{w,out}$ = 67.07°C P_{water} = 413.7 kPa Vol_{water} = 6.25×10^{-6} m^3/s	$\Delta T_{water} = T_{w,out} - T_{w,in}$ $h_{w,in} = f(T_{w,in}, P_{water})$ $h_{w,out} = f(T_{w,out}, P_{water})$ $\rho_{water} = f(T_{w,in}, P_{water})$ $Q_{pre-cooler} = Vol_{water}\rho_{water}(h_{w,out} - h_{w,in})$	ΔT_{water} = 51.61°C $h_{w,in}$ = 65.24 kJ/kg $h_{w,out}$ = 281.05 kJ/kg ρ_{water} = 999.2 kg/m^3 $Q_{pre-cooler}$ = 1.348 kW	
Refrigerant Side $T_{refg,in}$ = 109.91°C $P_{refg,in}$ = 4220 kPa m_{refg} = 0.0279 kg/s $T_{refg,out}$ = 84.81°C $P_{refg,out}$ = 4115 kPa	$h_{pre-cooler,in} = f(T_{refg,in}, P_{refg,in})$ $h_{pre-cooler,out} = f(T_{refg,out}, P_{refg,out})$ $h_{pre-cooler,out,calculated} = h_{pre-cooler,in} - Q_{pre-cooler} / m_{refg}$ $T_{pre-cooler,out,calculated} = f(P_{refg,out}, h_{pre-cooler,out,calculated})$ $Error_{T,pre-cooler,out} = T_{refg,out} - T_{pre-cooler,out,calculated}$	$h_{pre-cooler,in}$ = 435.04 kJ/kg $h_{pre-cooler,out}$ = 391.30 kJ/kg $h_{pre-cooler,out,calculated}$ = 386.65 kJ/kg $T_{pre-cooler,out,calculated}$ = 83.15°C $Error_{T,pre-cooler,out}$ = 1.67°C	
Test Section Outlet Temperature (Post-Cooler)			
Water Side $T_{w,in}$ = 13.70°C $T_{w,out}$ = 29.21°C P_{water} = 413.7 kPa Vol_{water} = 3.50×10^{-5} m^3/s	$\Delta T_{water} = T_{w,out} - T_{w,in}$ $h_{w,in} = f(T_{w,in}, P_{water})$ $h_{w,out} = f(T_{w,out}, P_{water})$ $\rho_{water} = f(T_{w,in}, P_{water})$ $Q_{post-cooler} = Vol_{water}\rho_{water}(h_{w,out} - h_{w,in})$	ΔT_{water} = 15.51°C $h_{w,in}$ = 57.87 kJ/kg $h_{w,out}$ = 122.74 kJ/kg ρ_{water} = 999.5 kg/m^3 $Q_{post-cooler}$ = 2.270 kW	
Refrigerant Side $T_{refg,out}$ = 62.40°C $P_{refg,out}$ = 4090 kPa m_{refg} = 0.0279 kg/s $T_{refg,in}$ = 78.71°C $P_{refg,in}$ = 4115 kPa	$h_{post-cooler,out} = f(T_{refg,out}, P_{refg,out})$ $h_{post-cooler,in} = f(T_{refg,in}, P_{refg,in})$ $h_{post-cooler,in,calculated} = h_{post-cooler,out} + Q_{post-cooler} / m_{refg}$ $T_{post-cooler,in,calculated} = f(P_{refg,in}, h_{post-cooler,in,calculated})$ $Error_{T,post-cooler,in} = T_{refg,in} - T_{post-cooler,in,calculated}$	$h_{post-cooler,out}$ = 295.71 kJ/kg $h_{prost-cooler,in}$ = 368.49 kJ/kg $h_{prost-cooler,in,calculated}$ = 377.19 kJ/kg $T_{pre-cooler,in,calculated}$ = 80.40°C $Error_{T,,pre-cooler,out}$ = -1.69°C	

Inputs	Equations	Results	References
Test Section Heat Duty (Primary-Secondary Loop Balance)			
Secondary Loop $T_{w,in}$ = 20.65°C $T_{w,out}$ = 60.38°C P_{water} = 137.9 kPa m_{water} = 1.39×10^{-3} kg/s	$h_{w,in} = f(T_{w,in}, P_{water})$ $h_{w,out} = f(T_{w,out}, P_{water})$ $Q_{secondary} = m_{water}(h_{w,out} - h_{w,in})$	$h_{w,in}$ = 86.68 kJ/kg $h_{w,out}$ = 286.30 kJ/kg $Q_{secondary}$ = 0.278 kW	
Primary Loop $Q_{secondary}$ = 0.278 kW $Q_{ambient}$ = 52 ×10^{-2} kW Q_{pump} = 20×10^{-2} kW	$Q_{test-section} = Q_{secondary} - Q_{pump} + Q_{ambient}$	$Q_{test-section}$ = 0.310 kW	
Test Section Overall UA			
$T_{w,primary,in}$ = 63.25°C $T_{w,primary,out}$ = 63.67°C $T_{test,in}$ = 84.01°C $T_{test,out}$ = 79.69°C $Q_{test-section}$ = 0.257 kW	$LMTD = \frac{(T_{test,in} - T_{w,primary,out}) - (T_{test,out} - T_{w,primary,in})}{\ln[(T_{test,in} - T_{w,primary,out})/(T_{test,out} - T_{w,primary,in})]}$ $UA_{test-section} = Q_{test-section} / LMTD$	LMTD = 18.32°C $UA_{test-section}$ = 16.90 W/K	
Refrigerant Heat Transfer Coefficient			
Water Side Resistance $T_{w,primary,in}$ = 63.25°C $T_{w,primary,out}$ = 63.67°C P_{water} = 413.7 kPa $Vol_{primary}$ = 1.06×10^{-4} m^3/s $(O.D.)_{inner}$ = 12.70 mm $(O.D.)_{outer}$ = 19.05 mm w_{outer} = 1.65 mm	$T_{w,primary,avg} = (T_{w,primary,in} + T_{w,primary,out})/2$ $(\rho, \mu, k, \Pr)_{water} = f(T_{w,primary,avg}, P_{water})$ $(I.D.)_{outer} = (O.D.)_{outer} - 2w_{outer}$ $A_{f,annulus} = \frac{\pi}{4}\left[(I.D.)_{outer}^{\ 2} - (O.D.)_{inner}^{\ 2}\right]$ $D_{h,annulus} = \frac{4A_{f,annulus}}{P} = (I.D.)_{outer} - (O.D.)_{inner}$ $V_{annulus} = Vol_{primary} / A_{f,annulus}$ $\dot{m}_{annulus} = \rho_{water} Vol_{primary}$ $\mathrm{Re}_{annulus} = \frac{\rho_{water} V_{annulus} D_{h,annulus}}{\mu_{water}}$ $^1 r^* = \frac{(O.D.)_{inner}}{(I.D.)_{outer}}$	$T_{w,primary,avg}$ = 63.46°C ρ_{water} = 981.5 kg/m^3 μ_{water} = 4.43×10^{-4} kg/m-s k_{water} = 0.658 W/m-K $\Pr_{water}$ = 2.82 $(I.D.)_{outer}$ = 15.75 mm $A_{f,annulus}$ = 6.81×10^{-5} m^2 $D_{h,annulus}$ = 3.05 mm $V_{annulus}$ = 1.55 m/s $m_{annulus}$ = 0.104 kg/s $\mathrm{Re}_{annulus}$ = 10,472 r^* = 0.81 Re_{CL} = 2,643 Re_{CU} = 3,233 $Nu_{annulus}$ = 57.9 $h_{annulus}$ = 12,496 W/m^2-K $A_{s,annulus}$ = 1.17×10^{-2} m^2	1. Garimella and Christensen (1995), Kays and Leung (1963) and Walker *et al.* (1957)

Inputs	Equations	Results	References
	[1] $Re_{CL} = 2089.26 + 686.15r^*$ [1] $Re_{CU} = 2963.02 + 334.16r^*$ [1] $Nu_{annulus}$ = Nu(Garimella and Christensen), see Appendix A. $h_{annulus} = \frac{Nu_{annulus} k_{water}}{D_{h,annulus}}$ $A_{s,annulus} = \pi \cdot (O.D.)_{inner} L_{test}$ $R_{annulus} = \frac{1}{h_{annulus} A_{s,annulus}}$	$R_{annulus} = 6.87\times10^{-3}$ K/W	
Wall Resistance $(O.D.)_{inner} = 12.70$ mm $w_{inner} = 1.65$ mm $L_{test} = 0.292$ m $k_{wall} = 401$ W/m-K	$(I.D.)_{inner} = (O.D.)_{inner} - 2w_{inner}$ $R_{wall} = \frac{\ln[(O.D.)_{inner}/(I.D.)_{inner}]}{2\pi \cdot k_{wall} L_{test}}$	$R_{wall} = 4.09\times10^{-4}$ K/W	
Refrigerant Heat Transfer Coefficient $UA_{test\text{-}section} = 15.94$ W/K $R_{annulus} = 7.0\times10^{-3}$ K/W $R_{wall} = 4.09\times10^{-4}$ K/W $(O.D.)_{inner} = 12.70$ mm $w_{inner} = 1.65$ mm $L_{test} = 0.292$ m	$R_{total} = \frac{1}{UA}$ $R_{refg} = R_{total} - R_{annulus} - R_{wall}$ $(I.D.)_{inner} = (O.D.)_{inner} - 2w_{inner}$ $A_{s,i} = \pi \cdot (I.D.)_{inner} L_{test}$ $h_{refg} A_{s,i} = \frac{1}{R_{refg}}$ Resistance Ratio = $R_{refg} / R_{annulus}$	$R_{tot} = 5.92\times10^{-2}$ K/W $R_{refg} = 5.18\times10^{-2}$ K/W $(I.D.)_{inner} = 9.40$ mm $A_{s,i} = 8.62\times10^{-3}$ m^2 $h_{refg} = 2235$ W/m^2-K Resistance Ratio = 7.56	

Note: All references cited in this appendix are included in References of the dissertation.

APPENDIX E. PHASE-CHANGE: COMPARISON WITH LITERATURE

Inputs	Equations	Results	References
Refrigerant Properties			
$P_{test,in}$ = 3006.59 kPa $P_{test,out}$ = 3003.58 kPa $x_{test,avg}$ = 0.4950 T_{crit} = 72.05°C P_{crit} = 3728.87 kPa	$P_{test,avg} = (P_{test,in} + P_{test,out})/2$ $T_{sat} = f(P_{test,avg}, x_{test,avg})$ $\rho_l, \rho_v, \mu_l, \mu_v, k_l, k_v, c_{p,l}, c_{p,v}, \mathrm{Pr}_l, \mathrm{Pr}_v, h_{fg} = f(T_{sat})$	$P_{test,avg}$ = 3005.08 kPa T_{sat} = 61.98°C ρ_l = 791.4 kg/m^3 ρ_v = 210.3 kg/m^3 $\mu_l = 7.008\times10^{-5}$ kg/m-s $\mu_v = 2.019\times10^{-5}$ kg/m-s k_l = 0.05198 W/m-K k_v = 0.03142 W/m-K $c_{p,l}$ = 2.790 kJ/kg-K $c_{p,v}$ = 3.189 kJ/kg-K Pr_l = 3.762 Pr_v = 2.049 h_{fg} = 75.64 kJ/kg	
Experimental Heat Transfer Coefficient from the Present Study			
h = 2095 W/m^2-K, G = 398.6 kg/m^2-s, x = 0.4950			
Shah Correlation (1979)			
$P_{test,avg}$ = 3005.08 kPa P_{crit} = 3728.87 kPa G = 398.6 kg/m^2-s $x_{test,avg}$ = 0.4950 $(I.D.)_{inner}$ = 9.40 mm $\mu_l = 7.008\times10^{-5}$ kg/m-s $k_l = 5.198\times10^{-2}$ W/m-K Pr_l = 3.762	$P_r = P_{test,avg}/P_{crit}$ $\mathrm{Re}_l = \frac{G(1-x_{test,avg})(I.D.)_{inner}}{\mu_l}$ $\mathrm{Re}_{lo} = \frac{G(I.D.)_{inner}}{\mu_l}$ $h_{liquid} = \frac{k_l}{(I.D.)_{inner}} 0.023 \mathrm{Re}_{lo}^{0.8} \mathrm{Pr}_l^{0.4}$ $h_{shah} = h_{liquid}\left[(1-x_{test.avg})^{0.8} + 3.8 x_{test.avg}^{0.76} \frac{(1-x_{test,avg})^{0.04}}{P_r^{0.38}}\right]$, $\mathrm{Re}_l > 350$	P_r = 0.806 Re_l = 26,995 Re_{lo} = 53,455 h_{liquid} = 1,309 W/m^2-K h_{Shah} = 3,838 W/m^2-K $h_{Shah} = 1.83\ h_{experimental}$ deviation = 83.20% Overprediction	
Traviss Correlation (1973)			
G = 398.6 kg/m^2-s $x_{test,avg}$ = = 0.4950 $(I.D.)_{inner}$ = 9.40 mm ρ_l = 791.4 kg/m^3 ρ_v = 210.3 kg/m^3	$\mathrm{Re}_l = \frac{G(1-x_{test,avg})(I.D.)_{inner}}{\mu_l}$ If $\mathrm{Re}_l < 50$ $F_2 = 0.707 \mathrm{Pr}_l \mathrm{Re}_l^{0.5}$	Re_l = 26,995 F_2 = 40.04 X_{tt} = 0.5943 F_{Xtt} = 0.80 Nu = 731.5	

Inputs	Equations	Results	References
$\mu_l = 7.008\times10^{-5}$ kg/m-s $\mu_v = 2.019\times10^{-5}$ kg/m-s $k_l = 5.198\times10^{-2}$ W/m-K $Pr_l = 3.762$	If $50 < Re_l < 1125$ $F_2 = 5Pr_l + 5\ln[1 + Pr_l(0.09636Re_l^{0.585} - 1)]$ If $Re_l > 1125$ $F_2 = 5Pr_l + 5\ln(1 + 5Pr_l) + 2.5\ln(0.00313Re_l^{0.812})$ $X_{tt} = \left(\frac{1-x_{test,avg}}{x_{test,avg}}\right)^{0.9}\left(\frac{\rho_v}{\rho_l}\right)^{0.5}\left(\frac{\mu_l}{\mu_v}\right)^{0.1}$ $F_{X_{tt}} = 0.15\left[X_{tt}^{-1} + 2.85X_{tt}^{-0.476}\right]$ $Nu = F_{X_{tt}}\frac{Pr_l Re_l^{0.9}}{F_2}$ $h_{traviss} = \frac{Nu \cdot k_l}{(I.D.)_{inner}}$	$h_{Traviss} = 4{,}046$ W/m^2-K $h_{Traviss} = 1.93\ h_{experimental}$ deviation = 93.13% Overprediction	
Dobson and Chato (1998)			
Wavy point G = 398.6 kg/m^2-s $x_{test,avg} = 0.4950$ $T_{sat} = 61.98$°C $T_{wall,avg} = 46.83$°C $(I.D.)_{inner} = 9.40$ mm $\rho_l = 791.4$ kg/m^3 $\rho_v = 210.3$ kg/m^3 $\mu_l = 7.008\times10^{-5}$ kg/m-s $\mu_v = 2.019\times10^{-5}$ kg/m-s $k_l = 5.198\times10^{-2}$ W/m-K $c_{p,l} = 2.790$ kJ/kg-K $Pr_l = 3.762$ $h_{fg} = 75.64$ kJ/kg $h_{experimental} = 2095$ W/m^2-K ***Annular Point*** G = 500.6 kg/m^2-s $x_{test,avg} = 0.7083$ $T_{sat} = = 61.67$°C $T_{wall,avg} = 47.28$°C	$Re_l = \frac{G(1-x_{test,avg})(I.D.)_{inner}}{\mu_l}$ $Re_{vo} = \frac{G(I.D.)_{inner}}{\mu_v}$ $Ga = \frac{9.8\rho_l(\rho_l - \rho_v)(I.D.)_{inner}^{\ 3}}{\mu_l^{\ 2}}$ $Ja_l = \frac{c_{p,l}(T_{sat} - T_{wall,avg})}{h_{fg}}$ $X_{tt} = \left(\frac{1-x_{test,avg}}{x_{test,avg}}\right)^{0.9}\left(\frac{\rho_v}{\rho_l}\right)^{0.5}\left(\frac{\mu_l}{\mu_v}\right)^{0.1}$ $^1\alpha = \left(1 + \frac{1-x_{test,avg}}{x_{test,avg}}\left(\frac{\rho_v}{\rho_l}\right)^{2/3}\right)^{-1}$ $Fr_l = \frac{G^2}{9.8\rho_l^2(I.D.)_{inner}}$ If $0 < Fr_l < 0.7$,	***Wavy Point*** $Re_l = 26{,}995$ $Re_{vo} = 1{,}855{,}477$ $Ga = 7.618\times10^8$ $Ja_l = 0.5589$ $X_{tt} = 0.5943$ $\alpha = 0.7034$ $Fr_l = 2.755$ $c_1 = 7.242$ $c_2 = 1.655$ $Nu_{forced} = 500.0$ $Fr_{so} = 12.03$ $(1-\theta_l/\pi) = 0.3666$ $Nu = 328.2$ $h_{Dobson} = 1{,}815$ W/m^2-K $h_{Dobson} = 0.87\ h_{experimental}$ deviation = -13.37% Underprediction ***Annular Point*** $Re_l = 19{,}434$	1. Zivi (1964)

Inputs	Equations	Results	References
$(I.D.)_{inner} = 9.40$ mm $\rho_l = 795.0$ kg/m^3 $\rho_v = 207.6$ kg/m^3 $\mu_l = 7.061\times10^{-5}$ kg/m-s $\mu_v = 2.008\times10^{-5}$ kg/m-s $k_l = 5.205\times10^{-2}$ W/m-K $c_{p,l} = 2.745$ kJ/kg-K $Pr_l = 3.724$ $h_{fg} = 76.56$ kJ/kg $h_{experimental} = 2993$ W/m^2-K	$c_1 = 4.172 + 5.48Fr_l - 1.564Fr_l^2$ $c_2 = 1.773 - 0.169Fr_l$ If $Fr_l > 0.7$, $c_1 = 7.242$ $c_2 = 1.655$ $Nu_{forced} = 0.0195 Re_l^{0.8} Pr_l^{0.4} \sqrt{1.376 + \frac{c_1}{X_{tt}^{c_2}}}$ If $Re_l \le 1250$ $Fr_{so} = 0.025 Re_l^{1.59} \left[\frac{1+1.09X_{tt}^{0.039}}{X_{tt}}\right]^{1.5} \frac{1}{Ga^{0.5}}$ If $Re_l > 1250$ $Fr_{so} = 1.26 Re_l^{1.04} \left[\frac{1+1.09X_{tt}^{0.039}}{X_{tt}}\right]^{1.5} \frac{1}{Ga^{0.5}}$ If $G \ge 500\, kg/m^2s$, or $Fr_{so} > 20$ when $G < 500$ kg/m^{2}s, annular flow $Nu = 0.023 Re_l^{0.8} Pr_l^{0.4} \left[1 + \frac{2.22}{X_{tt}^{0.89}}\right]$ If $G < 500$ kg/m^{2}s and $Fr_{so} < 20$, wavy flow $\left(1 - \frac{\theta_L}{\pi}\right) \cong \frac{\arccos(2\alpha - 1)}{\pi}$ $Nu = \frac{0.23 Re_{vo}^{0.12}}{1+1.11X_{tt}^{0.58}} \left[\frac{Ga\, Pr_l}{Ja_l}\right]^{0.25} + \left(1 - \frac{\theta_l}{\pi}\right) Nu_{forced}$ $h_{dobson} = \frac{Nu \cdot k_l}{(I.D.)_{inner}}$	$X_{tt} = 0.2608$ $Fr_{so} = 28.7$ $Nu = 875.6$ $h_{Dobson} = 4{,}850$ W/m^2-K $h_{Dobson} = 1.62\, h_{experimental}$ deviation = 62.04% Overprediction	
Sweeney (1996)			
Wavy Point $G = 398.6$ kg/m^2-s $Nu_{dobson} = 328.2$ $(I.D.)_{inner} = 9.40$ mm	$Nu_{wavy} = \left(\frac{G}{300}\right)^{0.3} Nu_{Dobson}$	***Wavy Point*** $Nu_{wavy} = 357.4$ $h_{Sweeney} = 1977$ W/m^2-K $h_{Sweeney} = 0.94\, h_{experimental}$	

Inputs	Equations	Results	References
$k_l = 5.198\times10^{-2}$ W/m-K $h_{experimental} = 2095$ W/m^2-K ***Annular Point*** G = 500.6 kg/m^2- $Nu_{dobson} = 875.6$ $D_{ti} = 9.40$ mm $k_l = 5.205\times10^{-2}$ W/m-K $h_{experimental} = 2993$ W/m^2-K	$Nu_{annular} = 0.7\left(\frac{G}{300}\right)^{0.3} Nu_{Dobson}$ $h_{sweeney} = \frac{Nu \cdot k_l}{(I.D.)_{inner}}$	deviation = -5.63% Underprediction ***Annular Point*** $Nu_{annular} = 714.7$ $h_{Sweeney} = 3959$ W/m^2-K $h_{Sweeney} = 1.32\ h_{experimental}$ deviation = 32.28% Overprediction	
Cavallini et al. (2002)			
Annular Point G = 398.9 kg/m^2-s $x_{test,avg} = 0.6999$ $(I.D.)_{inner} = 9.40$ mm $T_{sat} = 61.95$°C $T_{wall,avg} = 47.81$°C $\rho_l = 791.7$ kg/m^3 $\rho_v = 210.0$ kg/m^3 $\mu_l = 7.013\times10^{-5}$ kg/m-s $\mu_v = 2.018\times10^{-5}$ kg/m-s $k_l = 5.199\times10^{-2}$ W/m-K $c_{p,l} = 2.786$ kJ/kg-K $Pr_l = 3.759$ $h_{fg} = 75.72$ kJ/kg $\sigma = 6.9105\times10^{-4}$ N/m $h_{experimental} = 2333$ W/m^2-K ***Stratified Point*** G = 398.6 kg/m^2-s $x_{test,avg} = 0.4950$ $(I.D.)_{inner} = 9.40$ mm $T_{sat} = 61.98$°C $T_{wall,avg} = 46.83$°C $\rho_l = 791.4$ kg/m^3 $\rho_v = 210.3$ kg/m^3 $\mu_l = 7.008\times10^{-5}$ kg/m-s $\mu_v = 2.019\times10^{-5}$ kg/m-s $k_l = 5.198\times10^{-2}$ W/m-K	$J_G = \frac{x_{test,avg} G}{9.8 D_{ti} \rho_v (\rho_l - \rho_v)^{0.5}}$ $X_{tt} = \left(\frac{1 - x_{test,avg}}{x_{test,avg}}\right)^{0.9} \left(\frac{\rho_v}{\rho_l}\right)^{0.5} \left(\frac{\mu_l}{\mu_v}\right)^{0.1}$ If $J_G \geq 2.5$ and $X_{tt} < 1.6$, annular model If $J_G < 2.5$ and $X_{tt} < 1.6$, stratified model If $J_G < 2.5$ and $X_{tt} > 1.6$, slug model ***Annular Model*** $Re_l = \frac{G(1 - x_{test,avg})(I.D.)_{inner}}{\mu_l}$ $\delta^+ = \begin{cases} (Re_L/2)^{0.5} & Re_l \leq 1145 \\ 0.0504\, Re_l^{7/8} & Re_l > 1145 \end{cases}$ $T^+ = \begin{cases} \delta^+ Pr_l & \delta^+ \leq 5 \\ 5\{Pr_l + \ln[1 + Pr_l(\delta^+/5 - 1)]\} & 5 < \delta^+ < 30 \\ 5[Pr_l + \ln(1 + 5Pr_l) + 0.495\ln(\delta^+/30)] & \delta^+ \geq 30 \end{cases}$ $f_{GO} = \begin{cases} 0.046[G(I.D.)_{inner}/\mu_v]^{-0.2} & Re_{GO} > 2000 \\ 16/[G(I.D.)_{inner}/\mu_v] & Re_{GO} \leq 2000 \end{cases}$ $f_{LO} = \begin{cases} 0.046[G(I.D.)_{inner}/\mu_l]^{-0.2} & Re_{LO} > 2000 \\ 16/[G(I.D.)_{inner}/\mu_l] & Re_{LO} \leq 2000 \end{cases}$	***Annular Point*** $J_G = 2.63$ $X_{tt} = 0.2722$ $Re_l = 16{,}044$ $\delta^+ = 241.0$ $T^+ = 38.88$ $f_{GO} = 0.004064$ $f_{LO} = 0.005214$ E = 1.5295 F = 0.7796 H = 2.0669 We = 217.1 $\Phi_{LO}^2 = 2.459$ $(dp/dz)_f = 548.2$ Pa/m $\tau = 1.288$ Pa $h_{Cavallini} = 2289$ W/m^2-K $h_{Cavallini} = 0.98\ h_{experimental}$ deviation = -1.89% Underprediction ***Stratified Point*** $J_G = 1.86$ $X_{tt} = 0.5943$ $G_{JG=2.5} = 535.8$ kg/m^2-s $Re_l = 36{,}284$ $\delta^+ = 492.2$ $T^+ = 40.67$ $f_{GO} = 0.003832$	2. Zivi (1964) 3. Cavallini et al. (2002a) 4. Cavallini et al. (2002b)

Inputs	Equations	Results	References
$c_{p,l} = 2.790$ kJ/kg-K $Pr_l = 3.762$ $h_{fg} = 75.64$ kJ/kg $\sigma = 6.9105\times10^{-4}$ N/m $h_{experimental} = 2095$ W/m^2-K ***Slug Point*** $G = 200.9$ kg/m^2-s $x_{test,avg} = 0.1264$ $(I.D.)_{inner} = 9.40$ mm $T_{sat} = 61.31$°C $T_{wall,avg} = 46.62$°C $\rho_l = 799.0$ kg/m^3 $\rho_v = 204.7$ kg/m^3 $\mu_l = 7.123\times10^{-5}$ kg/m-s $\mu_v = 1.995\times10^{-5}$ kg/m-s $k_l = 0.05214$ W/m-K $c_{p,l} = 2.696$ kJ/kg-K $Pr_l = 3.683$ $h_{fg} = 77.61$ kJ/kg $\sigma = 6.9105\times10^{-4}$ N/m $h_{experimental} = 1122$ W/m^2-K	$E = (1-x_{test,avg})^2 + x_{test,avg}^2 \frac{\rho_l f_{GO}}{\rho_v f_{LO}}$ $F = x_{test,avg}^{0.6978}$ $H = \left(\frac{\rho_l}{\rho_v}\right)^{0.3278}\left(\frac{\mu_v}{\mu_l}\right)^{-1.181}\left(1-\frac{\mu_v}{\mu_l}\right)^{3.477}$ $We = \frac{G^2 (I.D.)_{inner\,tl}}{\rho_v \sigma}$ $\Phi_{LO}^2 = E + \frac{1.262F \cdot H}{We^{0.1458}}$ $(dP/dz)_f = \Phi_{LO}^2 \cdot 2 f_{Lo} \frac{G^2}{(I.D.)_{inner}\rho_l}$ $\tau = (dP/dz)_f \frac{(I.D.)_{inner}}{4}$ $h = \rho_l c_{p,l} (\tau/\rho_l)^{0.5} / T^+$ ***Stratified Model*** $h_{LO} = 0.023 \mathrm{Re}_{LO}^{0.8} \mathrm{Pr}_l^{0.4} k_l / (I.D.)_{inner}$ $= [G(I.D.)_{inner}/\mu_l]^{0.8} (c_{p,l}\mu_l/k_l)^{0.8} k_l/(I.D.)_{inner}$ $h_L = h_{LO}(1-x)^{0.8}$ $^2\alpha = \left(1 + \frac{1-x_{test,avg}}{x_{test,avg}}\left(\frac{\rho_v}{\rho_l}\right)^{2/3}\right)^{-1}$ $\left(1-\frac{\theta_L}{\pi}\right) \cong \frac{\arccos(2\alpha - 1)}{\pi}$ $h_{strat} = 0.725\{1 + 0.82[(1-x_{test,avg})/x_{test,avg}]^{0.268}\}^{-1}$ $[k_l^3 \rho_l (\rho_l - \rho_G) g h_{fg} / (\mu_l (I.D.)_{inner} \Delta T)]^{0.25} + h_L(1-\theta/\pi)$ $h_{trans} = (h_{an\,JG=2.5} - h_{strat})(J_G/2.5) + h_{strat}$ ***Slug Model – Cavallini et al. (2002a)*** $h_{LO} = 0.023 \mathrm{Re}_{LO}^{0.8} \mathrm{Pr}_l^{0.4} k_l / (I.D.)_{inner}$ To find the quality at $X_{tt} = 1.6$	$f_{LO} = 0.004914$ $E = 0.9741$ $F = 0.6122$ $H = 2.06$ $We = 392$ $\Phi_{LO}^2 = 1.641$ $(dp/dz)_f = 622.3$ Pa/m $\tau = 1.462$ Pa $h_{ann,JG=2.5} = 2334$ W/m^2-K $h_{LO} = 1309$ W/m^2-K $h_L = 758.1$ W/m^2-K $\alpha = 0.7016$ $h_{strat} = 383.5$ W/m^2-K $h_{Cavallini} = 1835$ W/m^2-K $h_{Cavallini} = 0.88\ h_{experimental}$ deviation = -12.41% Underprediction ***Slug Point (Cavallini et al., (2002a)*** $J_G = 0.24$ $X_{tt} = 3.273$ $h_{LO} = 743.1$ W/m^2-K $x_{1.6} = 0.2427$ $h_{trans,Xtt=1.6} = 956.9$ W/m^2-K $h_{Cavallini} = 854.5$ W/m^2-K $h_{Cavallini} = 0.76\ h_{experimental}$ deviation = -23.84% Underprediction ***Slug Point (Cavallini et al., (2002b)*** $J_G = 0.24$ $X_{tt} = 3.273$ $E_o = 5.373\times10^{-3}$ FE = 0.5344 $G_w = 129.6$ kg/m^2-s	

Inputs	Equations	Results	References
	$x_{1.6} = \frac{(\rho_v/\rho_l)^{5/9}(\mu_l/\mu_v)^{1/9}}{1.686+(\rho_v/\rho_l)^{5/9}(\mu_l/\mu_v)^{1/9}}$ $h_{trans,Xtt=1.6}$ is from stratified model $h_{slug} = h_{LO} + \frac{x_{test,avg}(h_{trans,X_{tt}=1.6} - h_{LO})}{x_{1.6}}$ ***Slug Model – Cavallini et al. (2002b)*** $E_o = 4\sigma/[(\rho_l-\rho_v)gD_{ti}^2]$ $FE = 0.54 - 0.06E_o^2 - 1.05E_o$ $G_W = FE\rho_l[g(I.D.)_{inner\,ti}]^{0.5}$ $G < G_W \quad h = h_{trans} = (h_{an\,J_G=2.5} - h_{strat})(J_G/2.5) + h_{strat}$ $G > G_W \quad h = h_{slug} = h_L\{1+2.87[x^{0.9}(\rho_l/\rho_v)^{0.5}(\mu_v/\mu_l)^{0.1}]^{1.44}\}$	$h_{Cavallini} = 958.3$ W/m^2-K $h_{Cavallini} = 0.85\ h_{experimental}$ deviation = -14.59% Underprediction	
Experimental Pressure Drop from the Present Study			
dP/dz = 1089.7 Pa/m, G = 398.6 kg/m^2-s, x = 0.4950			
Cavallini et al. (2002) Pressure Drop Model			
$J_G < 2.5$ L_{test} = 0.292 m G = 398.6 kg/m^2-s $x_{test,avg}$ = 0.4950 $(I.D.)_{inner}$ = 9.40 mm ρ_l = 791.4 kg/m^3 ρ_v = 210.3 kg/m^3 $\mu_l = 7.008\times10^{-5}$ kg/m-s $\mu_v = 2.019\times10^{-5}$ kg/m-s $c_{p,l}$ = 2.790 kJ/kg-K Pr_l = 3.762 $\sigma = 6.9105\times10^{-4}$ N/m $P_{test,in}$ = 3006.59 kPa $x_{test,in}$= 0.5802 $\rho_{l,in}$ = 790.9 kg/m^3 $\rho_{v,in}$ = 210.6 kg/m^3 $\mu_{l,in} = 7.001\times10^{-5}$ kg/m-s $\mu_{v,in} = 2.020\times10^{-5}$ kg/m-s	***Frictional Pressure Drop*** All properties were evaluated at $P_{test,avg}$ and $x_{test,avg}$ $J_G = \frac{x_{test,avg}G}{9.8(I.D.)_{inner}\rho_v(\rho_l-\rho_v)^{0.5}}$ $Re_l = \frac{G(1-x_{test,avg})(I.D.)_{inner}}{\mu_l}$ $\delta^+ = \begin{cases}(Re_L/2)^{0.5} & Re_L \le 1145\\ 0.0504Re_L^{7/8} & Re_L > 1145\end{cases}$ $f_{GO} = \begin{cases}0.046[G(I.D.)_{inner}/\mu_v]^{-0.2} & Re_{GO} > 2000\\ 16/[G(I.D.)_{inner}/\mu_v] & Re_{GO} \le 2000\end{cases}$ $f_{LO} = \begin{cases}0.046[G(I.D.)_{inner}/\mu_l]^{-0.2} & Re_{LO} > 2000\\ 16/[G(I.D.)_{inner}/\mu_l] & Re_{LO} \le 2000\end{cases}$ If $J_G \ge 2.5$	***$J_G < 2.5$*** J_G = 1.86 Re_l = 26995 δ^+ = 380 f_{GO} = 0.004065 f_{LO} = 0.005214 E = 0.9741 F = 0.4904 H = 2.079 ρ_{tp} = 334.2 kg/m^3 Fr = 15.45 We = 344.9 Φ_{LO}^2 = 3.356 $(dp/dz)_f$ = 747.3 Pa/m $(dp/dz)_{f,in}$ = 829.2 Pa/m τ_{in} = 1.948 Pa $u_{\tau,in}$ = 0.04963 m/s $\delta_{in} = 5.771\times10^{-4}$ m	5. Friedel (1979)

Inputs	Equations	Results	References
$P_{test,out}$ = 3003.58 kPa $x_{test,out}$= 0.4098 $\rho_{l,out}$ = 791.9 kg/m^3 $\rho_{v,out}$ = 209.9 kg/m^3 $\mu_{l,out}$ = 7.015×10^{-5} kg/m-s $\mu_{v,out}$ = 2.018×10^{-5} kg/m-s dP/dz = 1089.7 Pa/m ***$J_G \geq 2.5$*** L_{test} = 0.292 m G = 401.0 kg/m^2-s $x_{test,avg}$ = 0.8889 $(I.D.)_{inner}$ = 9.40 mm ρ_l = 792.0 kg/m^3 ρ_v = 209.8kg/m^3 μ_l = 7.017×10^{-5} kg/m-s μ_v = 2.017×10^{-5} kg/m-s $c_{p,l}$ = 2.783 kJ/kg-K Pr_l = 3.755 σ = 6.9105×10^{-4} N/m dP/dz = 1657.8 Pa/m	$E = (1-x_{test,avg})^2 + x_{test,avg}^2 \frac{\rho_l f_{GO}}{\rho_v f_{LO}}$ $F = x_{test,avg}^{0.6978}$ $H = \left(\frac{\rho_l}{\rho_v}\right)^{0.3278}\left(\frac{\mu_v}{\mu_l}\right)^{-1.181}\left(1-\frac{\mu_v}{\mu_l}\right)^{3.477}$ $We = \frac{G^2 (I.D.)_{inner}}{\rho_v \sigma}$ $\Phi_{LO}^2 = E + \frac{1.262F \cdot H}{We^{0.1458}}$ If $J_G < 2.5$, Friedel (1979) correlation was used $E = (1-x_{test,avg})^2 + x_{test,avg}^2 \frac{\rho_l f_{GO}}{\rho_v f_{LO}}$ $F = x_{test,avg}^{0.78}(1-x_{test,avg})^{0.24}$ $H = \left(\frac{\rho_l}{\rho_v}\right)^{0.91}\left(\frac{\mu_v}{\mu_l}\right)^{0.19}\left(1-\frac{\mu_v}{\mu_l}\right)^{0.7}$ $\rho_{tp} = \left(\frac{x_{test,avg}}{\rho_v} + \frac{1-x_{test,avg}}{\rho_l}\right)^{-1}$ $Fr = \frac{G^2}{9.8(I.D.)_{inner}\rho_{tp}^2}$ $We = \frac{G^2 (I.D.)_{inner}}{\rho_{tp}\sigma}$ $\Phi_{LO}^2 = E + \frac{3.24F \cdot H}{Fr^{0.045} We^{0.035}}$ $(dP/dz)_f = \Phi_{LO}^2 \cdot 2f_{Lo} \frac{G^2}{(I.D.)_{inner}\rho_l}$ ***Acceleration/deceleration term*** All properties were evaluated at $P_{test,in}$ and $x_{test,in}$ $\tau_{in} = (dP/dz)_{f,in} \frac{(I.D.)_{inner}}{4}$	ε_{in} = 0.07695 $(dp/dz)_{f,out}$ = 666.2 Pa/m τ_{out} = 1.565 Pa $u_{\tau,out}$ = 0.04446 m/s δ_{out} = 8.671×10^{-4} m ε_{out} = 0.6650 $(dp/dz)_a$ = -287.1 Pa/m $dp/dz_{cavallini}$ = 460.2 Pa/m $dp/dz_{cavallini}$ = 0.42 $dp/dz_{experimental}$ deviation = -57.76% Underprediction ***$J_G \geq 2.5$*** J_G = 1.86 $(dp/dz)_f$ = 773.4 Pa/m $(dp/dz)_a$ = -233.7 Pa/m $dp/dz_{Cavallini}$ = 539.6 Pa/m $dp/dz_{cavallini}$ = 0.33 $dp/dz_{experimental}$ deviation = -67.45% Underprediction	

Inputs	Equations	Results	References
	$u_{\tau,in} = (\tau_{in} / \rho_{l,in})^{0.5}$ $\delta_{in} = \delta^{+}_{in} \frac{\mu_{l,in}}{\rho_{l,in} u_{\tau,in}}$ $\varepsilon_{in} = [1 - 2\delta_{in} / (I.D.)_{inner}]^2$ Similar procedure was used to calculate ε_{out} using $(dP/dz)_{f,out}$, with all properties evaluated at $P_{test,out}$ and $x_{test,out}$. $(dp/dz)_a = G^2 \left(\frac{\left[\frac{x^2}{\rho_v \varepsilon} + \frac{(1-x)^2}{\rho_l (1-\varepsilon)} \right]_{out} - \left[\frac{x^2}{\rho_v \varepsilon} + \frac{(1-x)^2}{\rho_l (1-\varepsilon)} \right]_{in}}{L_{test}} \right)$ $(dp/dz)_{cavallini} = (dp/dz)_f + (dp/dz)_a$		
Coleman and Garimella Flow Regime Map (2003)			
x = 0.10 x = 0.50 x = 0.90	***Intermittent flow to intermittent and discrete wave flow*** $G_1 = -1097 + 132.1/x$ ***Intermittent and discrete wave flow to discrete wave flow*** $G_2 = -223.2 + 69.9/x$ ***Discrete wave flow to disperse wave flow*** $G_3 = (1340 - 283.6x)/(1 + 3.86x)$ ***Annular film and mist flow to mist flow*** $G_4 = -134.8 + 422.6/x$	G_1(x = 0.1) = 224 kg/m^2-s G_1(x = 0.5): Transition does not occur G_1(x = 0.9): Transition does not occur G_2(x = 0.1) = 475.8 kg/m^2-s G_2(x = 0.5): Transition does not occur G_2(x = 0.9): Transition does not occur G_3(x = 0.1) = 946.3 kg/m^2-s G_3(x = 0.5) = 408.9 kg/m^2-s G_3(x = 0.9) = 242.5 kg/m^2-s G_4(x = 0.1) = 4091 kg/m^2-s G_4(x = 0.5) = 710.4 kg/m^2-s G_4(x = 0.9) = 334.8 kg/m^2-s	
Breber et al. Flow Regime Map (1980)			
G = 398.6 kg/m^2-s $x_{test,avg}$ = 0.4950 $(I.D.)_{inner}$ = 9.40 mm ρ_l = 791.4 kg/m^3	***Transition criteria*** $j_g^*(1) = 0.5$ $j_g^*(2) = 1.5$	X_{tt} = 0.5944 K_p = 0.5502 J_g^* = 2.05	

Inputs	Equations	Results	References
$\rho_v = 210.3$ kg/m^3 $\mu_l = 7.008\times10^{-5}$ kg/m-s $\mu_v = 2.019\times10^{-5}$ kg/m-s $c_{p,l} = 2.790$ kJ/kg-K $Pr_l = 3.762$ $\sigma = 6.9105\times10^{-4}$ N/m	$X_{tt}(1) = 1.0$ $X_{tt}(2) = 1.5$ ***Condensation path*** $X_{tt} = \left(\frac{1-x_{test,avg}}{x_{test,avg}}\right)^{0.9}\left(\frac{\rho_v}{\rho_l}\right)^{0.5}\left(\frac{\mu_l}{\mu_v}\right)^{0.1}$ $K_p = \left(\frac{\rho_v}{\rho_l}\right)^{0.555}\left(\frac{\mu_l}{\mu_v}\right)^{0.111}$ $j_g^* = \frac{G}{\sqrt{\rho_v(\rho_l-\rho_v)(I.D.)_{inner}\,g}}\left(\frac{K_p}{X_{tt}^{1.111}+K_p}\right)$		

Note: All references cited in this appendix are included in References of the dissertation.

APPENDIX F. SUPERCRITICAL COOLING: COMPARISON WITH LITERATURE

Inputs	Equations	Results	References
Refrigerant Properties			
$P_{test,in}$ = 4115.34 kPa $T_{test,in}$ = 84.01°C $P_{test,out}$ = 4111.59 kPa $T_{test,out}$ = 79.69°C $T_{wall,1}$ = 65.32°C $T_{wall,2}$ = 64.72°C P_{crit} = 3729 kPa	$P_{test,avg} = (P_{test,in} + P_{test,out})/2$ $T_{test,avg} = (T_{test,in} + T_{test,out})/2$ $\rho_{bulk}, \mu_{bulk}, c_{p,bulk}, k_{bulk}, \mathrm{Pr}_{bulk}, h_{bulk}, = f(T_{test,avg}, P_{test,avg})$ $\rho_{wall}, \mu_{wall}, c_{p,wall}, k_{wall}, \mathrm{Pr}_{wall}, h_{wall}, = f(T_{wall,avg}, P_{test,avg})$	$P_{test,avg}$ = 4113.47 kPa $T_{test,avg}$ = 81.85°C $T_{wall,avg}$ = 65.02°C ρ_{bulk} = 300.8 kg/m^3 $\mu_{bulk} = 2.481\times10^{-5}$ kg/m-s $k_{bulk} = 3.717\times10^{-2}$ W/m-K $c_{p,bulk}$ = 3.420 kJ/kg-K Pr_{bulk} = 2.283 h_{bulk} = 382.59 kJ/kg ρ_{wall} = 824.4 kg/m^3 $\mu_{wall} = 7.471\times10^{-5}$ kg/m-s $k_{wall} = 5.270\times10^{-2}$ W/m-K $c_{p,wall}$ = 2.161 kJ/kg-K Pr_{wall} = 3.063 h_{wall} = 301.11 kJ/kg	
Experimental Heat Transfer Coefficient			
h = 2235 W/m^2-K, G = 401.6 kg/m2-s, $T_{test,avg}$ = 81.85°C			
Gnielinski correlation (1976)			
G = 401.6 kg/m^2-s $(I.D.)_{inner}$ = 9.40 mm ρ_{bulk} = 300.8 kg/m^3 $\mu_{bulk} = 2.481\times10^{-5}$ kg/m-s $k_{bulk} = 3.717\times10^{-2}$ W/m-K Pr_{bulk} = 2.283	$V = G/\rho_{bulk}$ $\mathrm{Re}_D = \frac{\rho_{bulk}(I.D.)_{inner} V}{\mu_{bulk}}$ [1] $f = (0.790\ln(\mathrm{Re}_D) - 1.64)^{-2}$ [2] $Nu_D = \frac{(f/8)(\mathrm{Re}_D - 1000)\mathrm{Pr}_{bulk}}{1 + 12.7(f/8)^{1/2}(\mathrm{Pr}_{bulk}^{2/3} - 1)}$ $h_{Gnielinski} = \frac{Nu \cdot k_{bulk}}{(I.D.)_{inner}}$	V = 1.335 m/s Re_D = 152,103 $f = 1.649\times10^{-2}$ Nu_D = 499.8 $h_{Gnielinski}$ = 1,977 W/m^2-K $h_{Gnielinski}$ = 0.88 $h_{experimental}$ deviation = -11.54% Underprediction	1. Incropera and DeWitt (2002) 2. Gnielinski (1976)
Krasnoshchekov *et al.* correlation (1970)			
G = 401.6 kg/m^2-s $(I.D.)_{inner}$ = 9.40 mm $T_{test,avg}$ = 81.85°C $T_{wall,avg}$ = 65.02°C	$V = G/\rho_{wall}$ $\mathrm{Re}_{wall} = \frac{\rho_{wall}(I.D.)_{inner} V_{wall}}{\mu_{wall}}$	V = 0.487 m/s Re_{wall} = 50,517 $c_{p,bar}$ = 4.842 kJ/kg-K f = 0.02091	3. Krasnoshchekov *et al.* (1970)

Inputs	Equations	Results	References
h_{bulk} = 382.59 kJ/kg h_{wall} = 301.11 kJ/kg ρ_{bulk} = 300.8 kg/m^3 μ_{bulk} = 2.481×10^{-5} kg/m-s k_{bulk} = 3.717×10^{-2} W/m-K $c_{p,bulk}$ = 3.420 kJ/kg-K Pr_{bulk} = 2.283 h_{bulk} = 382.59 kJ/kg ρ_{wall} = 824.4 kg/m^3 μ_{wall} = 7.471×10^{-5} kg/m-s k_{wall} = 5.270×10^{-2} W/m-K $c_{p,wall}$ = 2.161 kJ/kg-K Pr_{wall} = 3.063	$c_{p,bar} = \frac{(h_{bulk} - h_{wall})}{(T_{test,avg} - T_{wall,avg})}$ $f = (0.790\ln(\mathrm{Re}_{wall}) - 1.64)^{-2}$ $P_r = P_{test,avg} / P_{crit}$ $B = (1.004544 P_r^{10.35729}) / (0.79063 + P_r^{10.35729})$ $k = -0.0066 + 48.0512 e^{-5.1746 P_r}$ $n = (0.87131 P_r^{6.847882}) / (2.312497 + P_r^{6.847882})$ $m = B\left(\frac{c_{p,bar}}{c_{p,wall}}\right)^k$ $Nu_D = \frac{(f/8)\mathrm{Re}_{wall}\,\mathrm{Pr}_{wall}}{1.07 + 12.7(f/8)^{1/2}(\mathrm{Pr}_{wall}^{2/3} - 1)}$ [3] $Nu = Nu_D\left(\frac{\rho_{wall}}{\rho_{bulk}}\right)^n\left(\frac{c_{p,bar}}{c_{p,wall}}\right)^m$ $h_{Krasnoshchekov} = \frac{Nu \cdot k_{bulk}}{(I.D.)_{inner}}$	P_r = 1.103 B = 0.7811 k = 0.1528 n = 0.3998 m = 0.8836 Nu_D = 225.9 Nu = 689.6 $h_{Krasnoshchekov}$ = 2,728 W/m^2-K $h_{Krasnoshchekov}$ = 1.22 $h_{experimental}$ deviation = 22.06% Overprediction	
Pitla *et al.* correlation (2002)			
G = 401.6 kg/m^2-s D_{ti} = 9.40 mm ρ_{in} = 278.8 kg/m^3 ρ_{bulk} = 300.8 kg/m^3 μ_{bulk} = 2.481×10^{-5} kg/m-s k_{bulk} = 3.717×10^{-2} W/m-K $c_{p,bulk}$ = 3.420 kJ/kg-K Pr_{bulk} = 2.283 h_{bulk} = 382.59 kJ/kg ρ_{wall} = 824.4 kg/m^3 μ_{wall} = 7.471×10^{-5} kg/m-s k_{wall} = 5.270×10^{-2} W/m-K $c_{p,wall}$ = 2.161 kJ/kg-K	***Find Nusselt Number at wall temperature*** Use velocity at test section inlet to compute the Reynolds number regardless of the actual location. $V_{in} = G / \rho_{in}$ $\mathrm{Re}_{D,wall} = \frac{\rho_{wall}(I.D.)_{inner} V_{in}}{\mu_{wall}}$ [4] $f_{wall} = (0.790\ln(\mathrm{Re}_{D,wall}) - 1.64)^{-2}$ [5] $Nu_{D,wall} = \frac{(f_{wall}/8)(\mathrm{Re}_{D,wall} - 1000)\,\mathrm{Pr}_{wall}}{1 + 12.7(f_{wall}/8)^{1/2}(\mathrm{Pr}_{wall}^{2/3} - 1)}$ ***Find Nusselt Number at bulk temperature*** $V_{bulk} = G / \rho_{bulk}$	V_{in} = 1.440 m/s $Re_{D,wall}$ = 149362 f_{wall} = 1.655×10^{-2} $Nu_{D,wall}$ = 573.1 V_{bulk} = 1.335 m/s $Re_{D,bulk}$ = 152,103 f_{bulk} = 1.649×10^{-2} $Nu_{D,bulk}$ = 499.8 Nu_D = 760.6 h_{Pitla} = 3,008 W/m^2-K h_{Pitla} = 1.35 $h_{experimental}$ deviation = 34.59% Overprediction	4. Incropera and DeWitt (2002) 5. Gnielinski (1976) 6. Pitla *et al.* (2002)

Inputs	Equations	Results	References
$Pr_{wall} = 3.063$	$Re_{D,bulk} = \frac{\rho_{bulk}(I.D.)_{inner} V_{bulk}}{\mu_{bulk}}$ [4] $f_{bulk} = (0.790\ln(Re_{D,bulk}) - 1.64)^{-2}$ [5] $Nu_{D,bulk} = \frac{(f_{bulk}/8)(Re_{D,bulk} - 1000)Pr_{bulk}}{1 + 12.7(f_{bulk}/8)^{1/2}(Pr_{bulk}^{2/3} - 1)}$ ***Find local heat transfer coefficient*** [6] $Nu_D = \frac{(Nu_{D,wall} + Nu_{D,bulk})}{2}\left(\frac{k_{wall}}{k_{bulk}}\right)$ $h_{Pitla} = \frac{Nu_D \cdot k_{bulk}}{(I.D.)_{inner}}$		

Note: All references cited in this appendix are included in References of the dissertation.

APPENDIX G. PHASE-CHANGE HEAT TRANSFER AND PRESSURE DROP MODELS

Inputs	Equations	Results	References
Heat Transfer Models			
Wavy point $P_{test,in}$ = 3006.59 kPa $P_{test,out}$ = 3003.58 kPa G = 398.6 kg/m^2-s $x_{test,avg}$ = 0.4950 $T_{wall,avg}$ = 46.83°C $(I.D.)_{inner}$ = 9.40 mm $h_{experimental}$ = 2095 W/m^2-K	***Refrigerant Properties*** $P_{test,avg} = (P_{test,in} + P_{test,out})/2$ $T_{sat} = f(P_{test,avg}, x_{test,avg})$ $\rho_l, \rho_v, \mu_l, \mu_v, k_l, k_v, c_{p,l}, c_{p,v}, \mathrm{Pr}_l, \mathrm{Pr}_v, h_{fg} = f(T_{sat})$ $d_{baseline}$ = 9.40 mm $\mathrm{Re}_l = \frac{G(1-x_{test,avg})(I.D.)_{inner}}{\mu_l}$ $X_{tt} = \left(\frac{1-x_{test,avg}}{x_{test,avg}}\right)^{0.9}\left(\frac{\rho_v}{\rho_l}\right)^{0.5}\left(\frac{\mu_l}{\mu_v}\right)^{0.1}$ If $\mathrm{Re}_l \le 1250$ $\mathrm{Fr}_{so} = 0.025\mathrm{Re}_l^{1.59}\left[\frac{1+1.09X_{tt}^{0.039}}{X_{tt}}\right]^{1.5}\frac{1}{\mathrm{Ga}^{0.5}}$ If $\mathrm{Re}_l > 1250$ $\mathrm{Fr}_{so} = 1.26\mathrm{Re}_l^{1.04}\left[\frac{1+1.09X_{tt}^{0.039}}{X_{tt}}\right]^{1.5}\frac{1}{\mathrm{Ga}^{0.5}}$ If $1.75 < \mathrm{Fr}_{so} < 14$, wavy flow model If $14 < \mathrm{Fr}_{so} < 24$, wavy-to-annular transition model If $24 < \mathrm{Fr}_{so} < 65$, annular flow model ***Wavy Flow Model*** θ_l is evaluated by Baroczy (1965) void fraction model $\alpha = \left(1+\left(\frac{1-x_{test,avg}}{x_{test,avg}}\right)^{0.74}\left(\frac{\rho_v}{\rho_l}\right)^{0.65}\left(\frac{\mu_l}{\mu_v}\right)^{0.13}\right)^{-1}$ $\left(1-\frac{\theta_l}{\pi}\right) \cong \frac{\arccos(2\alpha - 1)}{\pi}$ $\mathrm{Ga} = \frac{9.8\rho_l(\rho_l-\rho_v)(I.D.)_{inner}^{3}}{\mu_l^{2}}$	***Wavy Point*** $P_{test,avg}$ = 3005.08 kPa T_{sat} = 61.98°C ρ_l = 791.4 kg/m^3 ρ_v = 210.3 kg/m^3 $\mu_l = 7.008\times10^{-5}$ kg/m-s $\mu_v = 2.019\times10^{-5}$ kg/m-s $k_l = 5.198\times10^{-2}$ W/m-K $c_{p,l}$ = 2.790 kJ/kg-K Pr_l = 3.762 h_{fg} = 75.64 kJ/kg $\sigma = 6.91\times10^{-4}$ Re_l = 26,995 > 1250 X_{tt} = 0.5943 Fr_{so} = 12.03 < 14 ⇒ Wavy flow α = 0.6649 θ_l = 1.907 rad = 109.3° $\mathrm{Ga} = 7.618\times10^{8}$ Ja_l = 0.5589 Nu_{film} = 226.8 h_{film} = 1,254 W/m^2-K $D_{h,liquid\ pool}$ = 3.98 mm Re_{liquid} = 11,442 Nu_{forced} = 301.6 h_{forced} = 3,936W/m^2-K h_{wavy} = 2,308 W/m^2-K $h_{wavy} = 1.10\ h_{experimental}$ deviation = 10.17% Overprediction	1. Baroczy (1965)

Inputs	Equations	Results	References
	$\mathrm{Ja}_l = \frac{c_{p,l}(T_{sat} - T_{wall,avg})}{h_{fg}}$ $Nu_{film} = \frac{1.1212}{\theta_l}\left[\frac{Ga\,\mathrm{Pr}_l}{Ja_l}\right]^{1/4}\left[\int_0^{\theta_l}\sin^{1/3}\theta d\theta\right]^{3/4}$ $h_{film} = \frac{Nu_{film}\cdot k_l}{(I.D.)_{inner}}$ $D_{h,liquid\ pool} = \frac{\left[\sin\theta_l\cos\theta_l + (\pi-\theta_l)\right]}{\left[\sin\theta_l + (\pi-\theta_l)\right]}\times(I.D.)_{inner}$ $\mathrm{Re}_{liquid} = \frac{G\cdot\left(1-x_{test,avg}\right)\cdot D_{h,liquid\ pool}}{\mu_l}$ $Nu_{forced} = 0.005\,\mathrm{Re}_{liquid}^{0.97}\,\mathrm{Pr}_l^{0.3}\left[1+\left(\frac{x}{1-x}\right)\left(\frac{\rho_l}{\rho_v}\right)\right]\left(\frac{(I.D.)_{inner}}{d_{basline}}\right)^{-0.56}$ $h_{forced} = \frac{Nu_{forced}\cdot k_l}{D_{h,kquid\ pool}}$ $h_{wavy} = \frac{\theta_l}{\pi}h_{film} + \left(1-\frac{\theta_l}{\pi}\right)h_{forced}$		
Annular Point $P_{test,in}$ = 3006.59 kPa $P_{test,out}$ = 3003.58 kPa G = 500.6 kg/m^2-s $x_{test,avg}$ = 0.7083 $T_{wall,avg}$ = 47.28°C $(I.D.)_{inner}$ = 9.40 mm $h_{experimental}$ = 2993 W/m^2-K	***Annular Flow Model*** $\mathrm{Re}_l = \frac{G\left(1-x_{test,avg}\right)(I.D.)_{inner}}{\mu_l}$ $Nu_{annular} = 0.013\,\mathrm{Re}_l^{0.84}\,\mathrm{Pr}_l^{0.3}\left[1+\left(\left(\frac{x}{1-x}\right)\left(\frac{\rho_l}{\rho_v}\right)\right)^{0.8}\right]\left(\frac{(I.D.)_{inner}}{d_{baseline}}\right)^{-0.32}$ $h_{annular} = \frac{Nu_{annular}\cdot k_l}{(I.D.)_{inner}}$	***Annular Point*** $P_{test,avg}$ = 2981.93 kPa T_{sat} = = 61.67°C ρ_l = 795.0 kg/m^3 ρ_v = 207.6 kg/m^3 $\mu_l = 7.061\times10^{-5}$ kg/m-s $\mu_v = 2.008\times10^{-5}$ kg/m-s $k_l = 5.205\times10^{-2}$ W/m-K $c_{p,l}$ = 2.745 kJ/kg-K Pr_l = 3.724 h_{fg} = 76.56 kJ/kg $\sigma = 6.91\times10^{-4}$ Re_l = 19,434 > 1250	

Inputs	Equations	Results	References
		$X_{tt} = 0.2608$ $Fr_{so} = 28.7 > 24 \Rightarrow$ annular flow $Nu_{annular} = 536.8$ $h_{annular} = 2973$ W/m^2-K $h_{annular} = 0.99\ h_{experimental}$ deviation = -0.67% Underprediction	
Transition Point $P_{test,in} = 3000.17$ kPa $P_{test,out} = 2997.86$ kPa $G = 497.9$ kg/m^2-s $x_{test,avg} = 0.5208$ $T_{wall,avg} = 47.28$°C $T_{sat} = 61.89$°C $(I.D.)_{inner} = 9.40$ mm $h_{experimental} = 2691$ W/m^2-K	***Wavy-to-Annular Flow Transition*** h_{wavy} = h calculated using wavy flow model $Nu_{wavy} = \frac{h_{wavy} \cdot (I.D.)_{inner}}{k_l}$ $Nu_{annular}$ = Nu calculated using annular flow model $Fr_{so,wavy} = 14$ and $Fr_{so,\ annular} = 24$ $Nu_{transition} = \left(\frac{Fr_{so} - Fr_{so,wavy}}{Fr_{so,annular} - Fr_{wavy}} \right) Nu_{annular} + \left(\frac{Fr_{so,annular} - Fr_{so}}{Fr_{so,annular} - Fr_{so,wavy}} \right) Nu_{wa}$	***Transtion Point*** $P_{test,avg} = 2999.01$ kPa $T_{sat} = 61.89$°C $\rho_l = 792.4$ kg/m^3 $\rho_v = 209.5$ kg/m^3 $\mu_l = 7.023\times10^{-5}$ kg/m-s $\mu_v = 2.016\times10^{-5}$ kg/m-s $k_l = 5.200\times10^{-2}$ W/m-K $c_{p,l} = 2.777$ kJ/kg-K $Pr_l = 3.751$ $h_{fg} = 75.90$ kJ/kg $\sigma = 6.91\times10^{-4}$ $Re_l = 31{,}927 > 1250$ $X_{tt} = 0.5406$ $Fr_{so} = 16.47$ $14 < Fr_{so} < 24 \Rightarrow$ flow in Wavy-annular transition $h_{wavy} = 2708$ W/m^2-K $Nu_{wavy} = 488.48$ $Nu_{annular} = 481.12$ $Nu_{transition} = 486.50$ $h_{transition} = 2697$ W/m^2-K $h_{annular} = 1.00\ h_{experimental}$ deviation = 0.22% Overprediction	

Inputs	Equations	Results	References
Pressure Drop Models			
Wavy point $P_{test,in}$ = 3006.59 kPa $P_{test,out}$ = 3003.58 kPa G = 398.6 kg/m^2-s $x_{test,avg}$ = 0.4950 $T_{wall,avg}$ = 46.83°C T_{sat} = 61.98°C ρ_l = 791.4 kg/m^3 ρ_v = 210.3 kg/m^3 $\mu_l = 7.008\times10^{-5}$ kg/m-s $\mu_v = 2.019\times10^{-5}$ kg/m-s $k_l = 5.198\times10^{-2}$ W/m-K $c_{p,l}$ = 2.790 kJ/kg-K Pr_l = 3.762 h_{fg} = 75.64 kJ/kg $\sigma = 6.91\times10^{-4}$ $(I.D.)_{inner}$ = 9.40 mm $dP/dz_{f,exp}$ = 1.405 kPa/m ***Annular Point*** $P_{test,in}$ = 3006.59 kPa $P_{test,out}$ = 3003.58 kPa G = 500.6 kg/m^2-s $x_{test,avg}$ = 0.7083 $T_{wall,avg}$ = 47.28°C T_{sat} = = 61.67°C ρ_l = 795.0 kg/m^3 ρ_v = 207.6 kg/m^3 $\mu_l = 7.061\times10^{-5}$ kg/m-s $\mu_v = 2.008\times10^{-5}$ kg/m-s $k_l = 5.205\times10^{-2}$ W/m-K $c_{p,l}$ = 2.745 kJ/kg-K Pr_l = 3.724 h_{fg} = 76.56 kJ/kg $\sigma = 6.91\times10^{-4}$ $(I.D.)_{inner}$ = 9.40 mm	If $1.75 < Fr_{so} < 14$, wavy flow model If $14 < Fr_{so} < 24$, wavy-to-annular transition model If $24 < Fr_{so} < 65$, annular flow model $d_{baseline}$ = 9.40 mm $Re_{GO} = \frac{G(I.D.)_{inner}}{\mu_v}$, $Re_{LO} = \frac{G(I.D.)_{inner}}{\mu_l}$ $f_{GO} = \begin{cases} 16/Re_{GO} & Re_{GO} < 2300 \\ 0.079 Re_{GO}^{-0.25} & 2300 < Re_{GO} < 20000 \\ 0.046 Re_{GO}^{-0.2} & Re_{GO} > 20000 \end{cases}$, $f_{LO} = \begin{cases} 16/Re_{LO} & Re_{LO} < 2300 \\ 0.079 Re_{LO}^{-0.25} & 2300 < Re_{LO} < 20000 \\ 0.046 Re_{LO}^{-0.2} & Re_{LO} > 20000 \end{cases}$ $(dP/dz)_{f,GO} = 2 f_{GO} G^2 / (d_{actual} \rho_v)$ $(dP/dz)_{f,LO} = 2 f_{LO} G^2 / (d_{actual} \rho_l)$ $Y^2 = \frac{(dP/dz)_{f,GO}}{(dP/dz)_{f,LO}}$ $n = \begin{cases} 1 & Re_{LO} < 2300 \\ 0.25 & 2300 < Re_{LO} < 20000 \\ 0.2 & Re_{LO} > 20000 \end{cases}$ $N_{conf} = \frac{1}{(I.D.)_{inner}} \left[\frac{\sigma}{g(\rho_l - \rho_v)} \right]^{0.5}$ ***Wavy Flow Model*** $C(x) = \left(\frac{0.12}{x_{test,avg}^{\ 2}} + \frac{2.9}{x_{test,avg}} + 0.76 \right) \left(\frac{(I.D.)_{inner}}{d_{baseline}} \right)^{-0.77}$	***Wavy Point*** Re_{GO} = 185,547 Re_{LO} = 53,457 $f_{GO} = 4.065\times10^{-3}$ $f_{LO} = 5.214\times10^{-3}$ $dP/dz_{f,GO}$ = 653.7 kPa/m $dP/dz_{f,LO}$ = 222.8 kPa/m Y = 1.713 n = 0.2 ($Re_{LO} > 2300$) $N_{conf.} = 3.707\times10^{-2}$ Re_l = 26,995 > 1250 X_{tt} = 0.5943 Fr_{so} = 12.03 < 14 ⇒ Wavy flow C(x) = 7.108 ϕ_{LO}^2 = 6.812 $(dP/dz)_{f,wavy}$ = 1.518 kPa/m $(dP/dz)_{f,wavy}$ = 1.08 $(dP/dz)_{f,exp}$ deviation = 8.04% Overprediction ***Annular Point*** Re_{GO} = 234,324 Re_{LO} = 66,634 $f_{GO} = 3.880\times10^{-3}$ $f_{LO} = 4.989\times10^{-3}$ $dP/dz_{f,GO}$ = 996.6 kPa/m $dP/dz_{f,LO}$ = 334.8 kPa/m Y = 1.725 n = 0.2 ($Re_{LO} > 2300$) $N_{conf.} = 3.687\times10^{-2}$ Re_l = 19,434 > 1250 X_{tt} = 0.2608 Fr_{so} = 28.7 > 24 ⇒ annular flow C(x) = 4.209	

Inputs	Equations	Results	References
$dP/dz_{f,exp}$ = 2.592 kPa/m ***Transition Point*** $P_{test,in}$ = 3000.17 kPa $P_{test,out}$ = 2997.86 kPa G = 497.9 kg/m^2-s $x_{test,avg}$ = 0.5208 $T_{wall,avg}$ = 47.28°C T_{sat} = 61.89°C ρ_l = 792.4 kg/m^3 ρ_v = 209.5 kg/m^3 $\mu_l = 7.023\times10^{-5}$ kg/m-s $\mu_v = 2.016\times10^{-5}$ kg/m-s $k_l = 5.200\times10^{-2}$ W/m-K $c_{p,l}$ = 2.777 kJ/kg-K Pr_l = 3.751 h_{fg} = 75.90 kJ/kg $\sigma = 6.91\times10^{-4}$ $(I.D.)_{inner}$ = 9.40 mm $dP/dz_{f,exp}$ = 2.100 kPa/m	***Annular Flow Model*** $C(x) = \left(18.22 - 31.97x_{test,avg} + 17.21x_{test,avg}^{\ 2}\right)\left(\frac{(I.D.)_{inner}}{d_{baseline}}\right)^{-0.34}$ $\phi_{LO}^{\ 2} = 1 + [CY^2 - 1][N_{conf}x^{\frac{2-n}{2}}(1-x_{test,avg})^{\frac{2-n}{2}} + x_{test,avg}^{\ 2-n}]$ $\left(\frac{dP}{dz}\right)_f = \phi_{LO}^{\ 2}\left(\frac{dP}{dz}\right)_{f,LO}$ ***Wavy-to-Annular Flow Transition*** $(dP/dz)_{f,wavy}$ = $(dP/dz)_f$ calculated using wavy flow model $(dP/dz)_{f,annular}$ = $(dP/dz)_f$ calculated using annular flow model $Fr_{so,wavy}$ = 14 and $Fr_{so,\ annular}$ =24 $\left(\frac{dP}{dz}\right)_{f,transition} = \left(\frac{Fr_{so_f} - Fr_{so,wavy}}{Fr_{so,annular} - Fr_{wavy}}\right)\left(\frac{dP}{dz}\right)_{f,annular} + \left(\frac{Fr_{so,annular} - Fr_{so}}{Fr_{so,annular} - Fr_{so,wavy}}\right)\left(\frac{dP}{dz}\right)_{f,wavy}$	$\phi_{LO}^{\ 2}$ = 7.302 $(dP/dz)_{f,annular}$ = 2.444 kPa/m $(dP/dz)_{f,annular}$ = 0.94 $(dP/dz)_{f,exp}$ deviation = -5.71% Underprediction ***Transtion Point*** Re_{GO} = 232,105 Re_{LO} = 666,34 $f_{GO} = 3.887\times10^{-3}$ $f_{LO} = 4.989\times10^{-3}$ $dP/dz_{f,GO}$ = 978.6 kPa/m $dP/dz_{f,LO}$ = 332.1 kPa/m Y = 1.717 n = 0.2 (Re_{LO} > 2300) $N_{conf} = 3.701\times10^{-2}$ Re_l = 31,927 > 1250 X_{tt} = 0.5406 Fr_{so} = 16.47 14 < Fr_{so} < 24 ⇒ flow in Wavy-annular transition $(dP/dz)_{f,wavy}$ = 2.344 kPa/m $(dP/dz)_{f,annular}$ = 2.177 kPa/m $(dP/dz)_{f,transition}$ = 2.303 kPa/m $(dP/dz)_{f,annular}$ = 1.10 $(dP/dz)_{f,exp}$ deviation = 9.67% Overprediction	

Note: All references cited in this appendix are included in References of the dissertation.

APPENDIX H. SUPERCRITICAL HEAT TRANSFER AND PRESSURE DROP MODELS

Inputs	Equations	Results	References
Heat Transfer and Pressure Drop Models			
Liquid-Like Point $P_{test,in}$ = 4090.91 kPa $P_{test,out}$ = 4086.54 kPa G = 303.4 kg/m^2-s $T_{test,avg}$ = 47.62°C $T_{wall,avg}$ = 37.80°C $(I.D.)_{inner}$ = 9.40 mm $dP/dz_{f,exp}$ = 0.3431 kPa/m h_{exp} = 1132 W/m^2-K ***Pseudo-Critical Point*** $P_{test,in}$ = 4502.52 kPa $P_{test,out}$ = 4504.00 kPa G = 296.5 kg/m^2-s $T_{test,avg}$ = 77.91°C $T_{wall,avg}$ = 54.50°C $(I.D.)_{inner}$ = 9.40 mm $dP/dz_{f,exp}$ = 0.4290 kPa/m h_{exp} = 1933 W/m^2-K ***Gas-Like Point*** $P_{test,in}$ = 3739.54 kPa $P_{test,out}$ = 3735.25 kPa G = 399.1kg/m^2-s $T_{test,avg}$ = 109.5°C $T_{wall,avg}$ = 72.33°C $(I.D.)_{inner}$ = 9.40 mm $dP/dz_{f,exp}$ = 2.401 kPa/m h_{exp} = 1193 W/m^2-K	***Refrigerant Properties*** $P_{test,avg} = (P_{test,in} + P_{test,out})/2$ $T_{test,avg} = (T_{test,in} + T_{test,out})/2$ $P_r = P_{test,avg} / P_{crit}$, P_{crit} = 3729 kPa $\rho_b, \mu_b, c_{p,b}, k_b, \mathrm{Pr}_b, h_b, = f(T_{test,avg}, P_{test,avg})$ $\rho_w, \mu_w, c_{p,w}, k_w, \mathrm{Pr}_w, h_w, = f(T_{wall,avg}, P_{test,avg})$ $d_{baseline}$ = 9.40 mm $\mathrm{Re} = \frac{G(I.D.)_{inner}}{\mu_b}$ $V = G/\rho_b$ $f_{Churchill}$ = f (Churchill), see Appendix B $Nu_{Churchill\text{-}corrected}$ = Nu (Churchill) with f calculated using correlations developed in the present study. ***Liquid-Like Point*** $f_{liquid-like} = 2.415 f_{Churchill}\left(\frac{\rho_w}{\rho_b}\right)^{0.507}\left(\frac{(I.D.)_{inner}}{d_{baseline}}\right)^{-0.184}$ $\left(\frac{dP}{dz}\right)_{f,liquid-like} = \frac{1}{2} f_{liquid-like}\rho_b V^2 \frac{L_{test}}{(I.D.)_{inner}}$ $Nu_{liquid-like} = 1.004 Nu_{Churchill-corrected}\left(\frac{c_{p,w}}{c_{p,b}}\right)^{0.455}\left(\frac{d_{actual}}{d_{baseline}}\right)^{-0.283}$ $h_{liquid-like} = \frac{Nu_{liquid-like}k_b}{(I.D.)_{inner}}$ ***Pseudo-Critical Point*** $f_{pseudo-crtical} = 2.622 f_{Churchill}\left(\frac{\rho_w}{\rho_b}\right)^{0.230}\left(\frac{(I.D.)_{inner}}{d_{baseline}}\right)^{-0.531}$ $\left(\frac{dP}{dz}\right)_{f,pseudo-critical} = \frac{1}{2} f_{gas-like}\rho_b V^2 \frac{L_{test}}{(I.D.)_{inner}}$	***Liquid-Like Point*** $P_{test,avg}$ = 4088.72 kPa P_r = 1.10 ρ_b = 959.0 kg/m^3 μ_b = 1.018×10^{-4} kg/m-s k_b = 5.917×10^{-2} W/m-K $C_{p,b}$ = 1.664 kJ/kg-K Pr_b = 2.862 ρ_w = 1013.2 kg/m^3 μ_w = 1.169×10^{-4} kg/m-s k_w = 6.265×10^{-2} W/m-K $C_{p,w}$ = 1.555 kJ/kg-K Pr_w = 2.900 Re = 28,010 V = 0.316 m/s $f_{Churchill}$ = 0.0238 $f_{liquid-like}$ = 0.0591 $dP/dz_{f,liquid-like}$ = 0.3016 kPa/m $dP/dz_{f,liquid-like}$ = 0.88 $dP/dz_{f,exp}$ deviation = -12.10% Underprediction $Nu_{Churchill-corrected}$ = 206.5 $Nu_{liquid-like}$ = 201.6 $h_{liquid-like}$ = 1266 W/m^2-K $h_{liquid-like}$ = 1.12 h_{exp} deviation = 11.84% Overprediction ***Pseudo-Critical Point*** $P_{test,avg}$ = 4503.26 kPa P_r = 1.21 ρ_b = 645.8 kg/m^3 μ_b = 5.128×10^{-5} kg/m-s k_b = 4.964×10^{-2} W/m-K $C_{p,b}$ = 4.239 kJ/kg-K	

Inputs	Equations	Results	References
	$Nu_{pseudo-critical} = 0.928 Nu_{Churchill-corrected} \left(\frac{c_{p,w}}{c_{p,b}}\right)^{0.236} \left(\frac{d_{actual}}{d_{baseline}}\right)^{-0.119}$ $h_{pseudo-critical} = \frac{Nu_{pseudo-critical} k_b}{(I.D.)_{inner}}$ ***Gas-Like Point*** $f_{gas-like} = 2.872 f_{Churchill} \left(\frac{(I.D.)_{inner}}{d_{baseline}}\right)^{-0.587}$ $\left(\frac{dP}{dz}\right)_{f,gas-like} = \frac{1}{2} f_{gas-like} \rho_b V^2 \frac{L_{test}}{(I.D.)_{inner}}$ $Nu_{gas-like} = 1.093 Nu_{Churchill-corrected} \left(\frac{c_{p,w}}{c_{p,b}}\right)^{-0.212} \left(\frac{d_{actual}}{d_{baseline}}\right)^{-0.353}$ $h_{gas-like} = \frac{Nu_{gas-like} k_b}{(I.D.)_{inner}}$	$Pr_b = 4.379$ $\rho_w = 923.8$ kg/m^3 $\mu_w = 9.339\times10^{-5}$ kg/m-s $k_w = 5.723\times10^{-2}$ W/m-K $C_{p,w} = 1.737$ kJ/kg-K $Pr_w = 2.834$ Re = 54,336 V = 0.4591 m/s $f_{Churchill} = 0.0204$ $f_{pseudo-critical} = 0.0581$ $dP/dz_{f,pseudo-critical} = 0.4204$ kPa/m $dP/dz_{f,pseudo-critical} = 0.98\ dP/dz_{f,exp}$ deviation = -2.00% Underprediction $Nu_{Churchill-corrected} = 485.0$ $Nu_{pseudo-critical} = 364.6$ $h_{pseudo-critical} = 1926$ W/m^2-K $h_{pseudo-critical} = 1.00\ h_{exp}$ deviation = -0.36% Underprediction ***Gas-Like Point*** $P_{test,avg} = 3737.39$ kPa $P_r = 1.00$ $\rho_b = 162.1$ kg/m^3 $\mu_b = 2.025\times10^{-5}$ kg/m-s $k_b = 2.911\times10^{-2}$ W/m-K $C_{p,b} = 1.387$ kJ/kg-K $Pr_b = 0.965$ $\rho_w = 384.4$ kg/m^3 $\mu_w = 2.926\times10^{-5}$ kg/m-s $k_w = 5.863\times10^{-2}$ W/m-K $C_{p,w} = 28.076$ kJ/kg-K $Pr_w = 14.013$ Re = 185,221	

Inputs	Equations	Results	References
		$V = 2.462$ m/s $f_{Churchill} = 0.0158$ $f_{gas\text{-}like} = 0.0453$ $dP/dz_{f,gas\text{-}like} = 2.369$ kPa/m $dP/dz_{f,gas\text{-}like} = 0.99\ dP/dz_{f,exp}$ deviation = -1.33% Underprediction $Nu_{Churchill\text{-}corrected} = 609.8$ $Nu_{gas\text{-}like} = 352.2$ $h_{gas\text{-}like} = 1091$ W/m^2-K $h_{gas\text{-}like} = 0.91\ h_{exp}$ deviation = -8.55% Underprediction	
Heat Transfer Models			

Note: All references cited in this appendix are included in References of the dissertation.

REFERENCES

Akers, W. W., Deans, H. A. and Crosser, O. K. (1959), "Condensing heat transfer within horizontal tubes," *Chemical Engineering Progress Symposium Series* **55**: 171-176.

Akers, W. W. and Rosson, H. F. (1960), "Condensation inside a horizontal tube," *Chemical Engineering Progress Symposium Series* **56**: 145-149.

ASHRAE (1997). ASHRAE handbook - Fundamentals. Atlanta, GA, American Society of Heating, Refrigeration and Air-Conditioning Engineers, Inc.

Baroczy, C. J. (1965), "Correlation of liquid fraction in two-phase flow with applications to liquid metals," *Chemical Engineering Progress Symposium Series* **61** (57): 179-191.

Beattie, D. R. H. and Whalley, P. B. (1982), "A simple two-phase flow frictional pressure drop calculation method," *International Journal of Multiphase Flow* **8**: 83-87.

Boissieux, X., Heikal, M. R. and Johns, R. A. (2000), "Two-phase heat transfer coefficients of three HFC refrigerants inside a horizontal smooth tube, Part II: Condensation," *International Journal of Refrigeration* **23** (5): 345-352.

Boyko, L. D. and Kruzhilin, G. N. (1967), "Heat transfer and hydraulic resistance during condensation of steam in a horizontal tube and in a bundle of tubes," *International Journal of Heat and Mass Transfer* **10**: 361-373.

Breber, G., Palen, J. W. and Taborek, J. (1980), "Prediction of horizontal tubeside condensation of pure components using flow regime criteria," *Journal of Heat Transfer, Transactions ASME* **102** (3): 471-476.

Carey, V. P. (1992). Liquid-Vapor Phase-Change Phenomena : An Introduction to the Thermophysics of Vaporization and Condensation Processes in Heat Transfer Equipment. Washington, D.C., Hemisphere Pub. Corp.

Cavallini, A., Censi, G., Del Col, D., Doretti, L., Longo, G. A. and Rossetto, L. (2001), "Experimental investigation on condensation heat transfer and pressure drop of new HFC refrigerants (R134a, R125, R32, R410A, R236ea) in a horizontal smooth tube," *International Journal of Refrigeration* **24** (1): 73-87.

Cavallini, A., Censi, G., Del Col, D., Doretti, L., Longo, G. A. and Rossetto, L. (2002a), "Condensation of halogenated refrigerants inside smooth tubes," *HVAC and R Research* **8** (4): 429-451.

Cavallini, A., Censi, G., Del Col, D., Doretti, L., Longo, G. A. and Rossetto, L. (2002b), "In-tube condensation of halogenated refrigerants," *ASHRAE Transactions* **108** (1): 146-161.

Cavallini, A., Censi, G., Del Col, D., Doretti, L., Longo, G. A., Rossetto, L. and Zilio, C. (2003), "Condensation inside and outside smooth and enhanced tubes - a review of recent research," *International Journal of Refrigeration* **26** (4): 373-392.

Cavallini, A., Del Col, D., Longo, G. A. and Rossetto, L. (1999), "Condensation heat transfer with refrigerants," *Proceedings of the Two-Phase Flow Modeling and Experimentation Conference*, ETS, Pisa, pp. 71-78.

Cavallini, A. and Zecchin, R. (1971), "High velocity condensation of organic refrigerants inside tubes," *Proceedings of 8th International Congress of Refrigeration*, Washington D.C., pp. 193-200.

Cavallini, A. and Zecchin, R. (1974), "A dimensionless correlation for the heat transfer in forced convective condensation," *5th International Heat Transfer Conference*, Tokyo, pp. 309-313.

Chisholm, D. (1973), "Pressure gradients due to friction during the flow of evaporating two-phase mixtures in smooth tubes and channels," *International Journal of Heat and Mass Transfer* **16**: 347.

Churchill, S. W. (1977a), "Comprehensive correlating equations for heat, mass and momentum transfer in fully developed flow in smooth tubes," *Industrial and Engineering Chemistry, Fundamentals* **16** (1): 109-116.

Churchill, S. W. (1977b), "Friction-factor equation spans all fluid-flow regimes," *Chemical Engineering* **84** (24): 91-92.

Churchill, S. W. and Chu, H. H. S. (1975), "Correlating equations for laminar and turbulent free convection from a horizontal cylinder," *International Journal of Heat and Mass Transfer* **18**: 1049.

Cicchitti, A., Lombardi, C., Silvestri, M., Solddaini, G. and Zavalluilli, R. (1960), "Two-phase cooling experiments - pressure drop, heat transfer and burnout measurement," *Energia Nucl.* **7** (6): 407-425.

Coleman, J. W., 2000, Flow visualization and pressure drop for refrigerant phase change and air-water flow in small hydraulic diameter geometries. Ph.D. dissertation, in *Dept. of Mechanical Engineering*, Iowa State University, Ames, Iowa.

Coleman, J. W. and Garimella, S. (2000), "Two-Phase Flow Regime Transitions in Microchannel Tubes: The Effect of Hydraulic Diameter," *ASME Heat Transfer Division - 2000*, Orlando, FL, American Society of Mechanical Engineers, pp. 71-83.

Coleman, J. W. and Garimella, S. (2003), "Two-phase flow regimes in round, square and rectangular tubes during condensation of refrigerant R134a," *International Journal of Refrigeration* **26** (1): 117-128.

Dobson, M. K., 1994, Heat transfer and flow regimes during condensation in horizontal tubes. Ph.D. Dissertation, in *Dept. of Mechanical and Industrial Engineering*, University of Illinois at Urbana-Champaign, Urbana-Champaign.

Dobson, M. K. and Chato, J. C. (1998), "Condensation in smooth horizontal tubes," *Journal of Heat Transfer, Transactions ASME* **120** (1): 193-213.

Dobson, M. K., Chato, J. C., Wattelet, J. P., Gaibel, J. A., Ponchner, M., Kenney, P. J., Shimon, R. L., Villaneuva, T. C., Rhines, N. L., Sweeney, K. A., Allen, D. G. and Hershberger, T. T., 1994, Heat transfer and flow regimes during condensation in horizontal tubes, *ACRC Technical Report 57*, University of Illinois at Urbana-Champaign, Urbana-Champaign.

Dukler, A. E., Wicks III, M. and Cleveland, R. G. (1964), "Pressure drop and hold-up in two-phase flow," *AIChE Journal* **10** (1): 38-51.

Ebisu, T. and Torikoshi, K. (1998), "Heat transfer characteristics and correlations for R-410A flowing inside a horizontal smooth tube," *ASHRAE Transactions* **104** (2): 556-561.

Friedel, L. (1979), "Improved friction pressure drop correlations for horizontal and vertical two phase pipe flow," *European Two Phase Flow Group Meeting*, Ispra, Italy, paper E2

Friedel, L. (1980), "Pressure drop during gas/vapor-liquid flow in pipes," *Int Chem Eng.* **20** (3): 352-367.

Garimella, S. and Christensen, R. N. (1995), "Heat transfer and pressure drop characteristics of spirally fluted annuli. Part II. Heat transfer," *Journal of Heat Transfer, Transactions ASME* **117** (1): 61-68.

Ghajar, A. J. and Asadi, A. (1986), "Improved forced convective heat -transfer correlations for liquids in the near-critical region," *AIAA Journal* **24** (12): 2030-2037.

Ghorbani-Tari, S. and Ghajar, A. J. (1985), "Improved free convective heat-transfer correlations in the near-critical region," *AIAA Journal* **23** (10): 1647-1649.

Gnielinski, V. (1976), "New equation for heat and mass transfer in turbulent pipe and channel flow," *International Chemical Engineering.* **16** (2): 359-368.

Hajal, J. E., Thome, J. R. and Cavallini, A. (2003), "Condensation in horizontal tubes, part 1: two-phase flow pattern map," *International Journal of Heat and Mass Transfer* **46**: 3349-3363.

Han, D.-H. and Lee, K.-J. (2001), "Experiments on condensation heat transfer characteristics inside a 7mm outside diameter microfin tube with R410A," *35th National Heat Transfer Conference*, Anaheim, CA

Haraguchi, H., Koyama, S. and Fujii, T. (1994), "Condensation of refrigerants HCFC 22, HFC 134a and HCFC 123 in a horizontal smooth tube (2nd report, proposals of empirical expressions for local heat transfer coefficient)," *Nippon Kikai Gakkai Ronbunshu, B Hen/Transactions of the Japan Society of Mechanical Engineers, Part B* **60** (574): 2117-2124.

Hewitt, G. F., King, I. and Lovegrove, P. C., 1961, *AERE Report No. AERE-R 3764.*

Hewitt, G. F., King, I. and Lovegrove, P. C., 1962, *AERE Report No. AERE-R 3921.*

Hewitt, G. F., Shires, G. L. and Bott, T. R. (1993). Process Heat Transfer. CRC Press.

Incropera, F. P. and DeWitt, D. P. (2002). Fundamentals of Heat and Mass Transfer. 5th Ed. New York, J. Wiley.

Irvine, T. F. and Hartnett, J. P., Eds. (1970). Advances in Heat Transfer. New York, Academic Press.

Jackson, J. D. and Fewster, J., 1975, *AERE-R8158*, Harwell.

Jaster, H. and Kosky, P. G. (1976), "Condensation heat transfer in a mixed flow regime," *International Journal of Heat and Mass Transfer* **19** (1): 95-99.

Ju Lee, H. and Yong Lee, S. (2001), "Pressure drop correlations for two-phase flow within horizontal rectangular channels with small heights," *International Journal of Multiphase Flow* **27** (5): 783-796.

Kattan, N., Thome, J. R. and Favrat, D. (1998), "Flow boiling in horizontal tubes. Part I: development of a diabatic two-phase flow pattern map," *Journal of Heat Transfer* **120**: 140-147.

Kawahara, A., Chung, P. M.-Y. and Kawaji, M. (2002), "Investigation of two-phase flow pattern, void fraction and pressure drop in a microchannel," *International Journal of Multiphase Flow* **28** (9): 1411-1435.

Kays, W. M. and Leung, E. Y. (1963), "Heat transfer in annular passages: hydrodynamically developed flow with arbitrarily prescribed heat flux," *International Journal of Heat and Mass Transfer* **6** (7): 537-557.

Kiraly, R. and Koestel, A., 1960, *TRW Report No. ER-4104.*

Engineering Equation Solver, 2003, Klein, S. A., 6.856-3D, F-Chart Software.

Kosky, P. G. and Staub, F. W. (1971), "Local condensing heat transfer coefficients in the annular flow regime," *AIChE Journal* **17** (5): 1037-1043.

Krasnoshchekov, E. A., Kuraeva, I. V. and Protopopov, V. S. (1970), "Local heat transfer of carbon dioxide at supercritical pressure under cooling conditions," *Teplofizika Vysokikh Temperatur* **7** (5): 922-930.

Kurganov, V. A. (1998a), "Heat transfer an pressure drop in tubes under supercritical pressure of the coolant. Part 1: Specifics of the thermophysical properties, hydrodynamics, and heat transfer of the liquid. Regimes of normal heat transfer," *Thermal Engineering* **45** (3): 177-185.

Kurganov, V. A. (1998b), "Heat transfer and pressure drop in tubes under supercritical pressure. Part 2: heat transfer and friction at high heat fluxes. The influence of additional factors. enhancement of deteriorated heat transfer," *Thermal Engineering* **45** (4): 301-310.

Lee, H. J. and Lee, S. Y. (2001), "Pressure drop correlations for two-phase flow within horizontal rectangular channels with small heights," *International Journal of Multiphase Flow* **27** (5): 783-796.

REFPROP, 2002, Lemmon, E. W., McLinden, M. O. and Huber, M. L., NIST Standard Reference Database 23 Version, 7.0 Beta version, National Institute of Standards and Technology.

Lin, S., Kwok, C. C. K., Li, R. Y., Chen, Z. H. and Chen, Z. Y. (1991), "Local frictional pressure drop during vaporization for R-12 through capillary tubes," *International Journal of Multiphase Flow* **17**: 95-102.

Lockhart, R. W. and Martinelli, R. C. (1949), "Proposed correlation of data for isothermal two-phase two-component flow in a pipe," *Chemical Engineering Progress* **45** (1): 39-48.

Martinelli, R. C. (1947), *Transactions of ASME* **69**: 947.

McAdams, W. H. (1954). Heat Transmission. 3rd Ed. New York, McGraw-Hill.

Mills, A. F. (1995). Heat and Mass Transfer. Irwin.

Mishima, K. and Hibiki, T. (1996), "Some characteristics of air-water two-phase flow in small diameter vertical tubes," *International Journal of Multiphase Flow* **22** (4): 703-712.

Mishima, K., Hibiki, T. and Nishihara, H. (1993), "Some characteristics of gas-liquid in narrow rectangular ducts," *International Journal of Multiphase Flow* **19**: 115-124.

Mishima, K. and Ishii, M. (1984), "Flow regime transition criteria for upward two-phase flow in vertical tubes," *International Journal of Heat and Mass Transfer* **27**: 723-737.

Munson, B. R., Young, D. F. and Okiishi, T. H. (1998). Fundamentals of Fluid Mechanics. 3nd. John Wiley & Sons, Inc.

Nusselt, W. (1916), "Die oberflachenkondensation des wasser-dampfes," *Z. Ver. Dt. Ing.* **60**: 541-546, 569-575.

Owens, W. L. (1961). Two-phase pressure gradient, Int. Dev. in Heat Transfer, Pt II. New York, ASME.

Pilavachi, P. A., Ed. (1993). Energy Efficiency in Process Technology. Boiling in small parallel channels. New York, Elsevier.

Pitla, S. S., Groll, E. A. and Ramadhyani, S. (2001a), "Convective heat transfer from in-tube cooling of turbulent supercritical carbon dioxide: Part 2 - Experimental data and numerical predictions," *HVAC&R Research* **7** (4): 367-382.

Pitla, S. S., Groll, E. A. and Ramadhyani, S. (2001b), "Convective heat transfer from in-tube flow of turbulent supercritical carbon dioxide: Part 1 - Numerical analysis," *HVAC&R Research* **7** (4): 345-366.

Pitla, S. S., Groll, E. A. and Ramadhyani, S. (2002), "New correlation to predict the heat transfer coefficient during in-tube cooling of turbulent supercritical CO2," *International Journal of Refrigeration* **25** (7): 887-895.

Pitla, S. S., Robinson, D. M., Groll, E. A. and Ramadhyani, S. (1998), "Heat transfer from supercritical carbon dioxide in tube flow: A critical review," *HVAC&R Research* **4** (3): 281-301.

Rouhani, Z. and Axelsson, E. (1970), "Calculation of void volume fraction in the subcooled and quality boiling regions," *International Journal of Heat and Mass Transfer* **13**: 383-393.

Rufer, C. E. and Kezios, S. P. (1966), "Analysis of two-phase one component stratified flow with condensation," *Journal of heat Transfer* **88** (c): 265.

Sardesai, R. G., Owen, R. G. and Pulling, D. J. (1981), "Flow regimes for condensation of a vapor inside a horizontal tube," *Chemical Engineering Science* **36**: 1173-1180.

Shah, M. M. (1976), "A new correlation for heat transfer during boiling flow through pipes," *ASHRAE Transactions* **82** (2): 66-86.

Shah, M. M. (1979), "A general correlation for heat transfer during film condensation inside pipes," *International Journal of Heat and Mass Transfer* **22** (4): 547-556.

Shao, D. W. and Granryd, E. G. (2000), "Flow pattern, heat transfer and pressure drop in flow condensation, Part 1: Pure and azeotropic refrigerants," *HVAC&R Research* **6** (2): 175-195.

Shitsman, M. E. (1963), "Impairment of the heat transmission at supercritical pressures," *Teplofizika Vysokikh Temperatur* **1** (2): 267-275.

Soliman, H. M. (1982), "On the annular-to-wavy flow pattern transition during condensation inside horizontal tubes," *The Canadian Journal of Chemical Engineering* **60** (4): 475-481.

Steiner, D. (1993). Heat Transfer to Boiling Saturated Liquids, in VDI-warmeatlas (VDI heat atlas), Chapter Hbb. Dusseldorf.

Sugawara, S., Katsuta, K., Ishihara, I. and Muto, T. (1967), "Consideration on the pressure loss of two-phase flow in small-diameter tubes (In Japanese)," *Proceedings of 4th National Heat Transfer Symposium of Japan*, pp. 169-172.

Sweeney, K. A., 1996, The heat transfer and pressure drop behavior of a zeotropic refrigerant mixture in a micro-finned tube. M.S. thesis, in *Dept. Mechanical and Industrial Engineering*, University of Illinois at Urbana Champaign.

Taitel, Y. and Dukler, A. E. (1976), "A model for predicting flow regime transitions in horizontal and near horizontal gas-liquid flow," *AIChE Journal* **22** (1): 47-55.

Tanaka, H., Nishiwaki, N., Hirata, M. and Tsuge, A. (1971), "Forced convection heat transfer to fluid near critical point flowing in circular tube," *International Journal of Heat and Mass Transfer* **14** (6): 739-750.

Tandon, T. N., Varma, H. K. and Gupta, C. P. (1982), "A new flow regime map for condensation inside horizontal tubes," *Journal of Heat Transfer* **104**: 763-768.

Tang, L., 1997, Empirical study of new refrigerant flow condensation inside horizontal smooth and micro-fin tubes. Ph.D. dissertation, University of Maryland at College Park, p. 251.

Taylor, B. N. and Kuyatt, C. E., 1994, Guidelines for Evaluating and Expressing the Uncertainty of NIST Measurement Results, *NIST Technical Note 1297*, National Institute of Standards and Technology.

Thome, J. R., Hajal, J. E. and Cavallini, A. (2003), "Condensation in horizontal tubes, part 2: new heat transfer model based on flow regimes," *International Journal of Heat and Mass Transfer* **46**: 3365-3387.

Tran, T. N., Chyu, M.-C., Wambsganss, M. W. and France, D. M. (2000), "Two-phase pressure drop of refrigerants during flow boiling in small channels: An experimental investigation and correlation development," *International Journal of Multiphase Flow* **26** (11): 1739-1754.

Traviss, D. P., Rohsenow, W. M. and Baron, A. B. (1973), "Forced-convection condensation inside tubes: a heat transfer equation for condenser design," *ASHRAE Transactions* **79** (1): 157-165.

Walker, J. E., Whan, G. A. and Rothfus, R. R. (1957), "Fluid Friction in Noncircular Ducts," *AIChE Journal* **3** (4): 484-489.

Zivi, S. M. (1964), "Estimation of steady state steam void fraction by means of the principle of minimum entropy production," *Journal of Heat Transfer* **86** (c): 247-252.